Bioanalytical Reviews

Frank-Michael Matysik *Editor*

Advances in Chemical Bioanalysis

1
Advances in Chemical Bioanalysis

Series Editors:

Frank-Michael Matysik, Regensburg, Germany
Joachim Wegener, Regensburg, Germany

For further volumes:
http://www.springer.com/series/11663

Aims and Scope

Bioanalytical Reviews is the successor of the former review journal with the same name, and it will complement Springer's successful and reputed review book series program in the flourishing and exciting area of the Bioanalytical Sciences.

Bioanalytical Reviews (BAR) publishes reviews covering all aspects of bioanalytical sciences. It therefore is a unique source of quick and authoritative information for anybody using bioanalytical methods in areas such as medicine, biology, biochemistry, genetics, pharmacology, biotechnology, and the like.

Reviews of methods include all modern tools applied, including chromatography (in its various forms), capillary electrophoresis, biosensors, bioelectroanalysis, fluorescence, mass spectrometry, NMR, IR/Raman, and other optical spectroscopies as well as methods related to bioimaging. In particular the series volumes provide reviews on perspective new instrumental approaches as they apply to bioanalysis, and on the use of micro-/nano-materials such as micro- and nanoparticles. Articles on μ-total analytical systems (μ-TAS) and on labs-on-a-chip also fall into this category.

In terms of applications, reviews on novel bioanalytical methods based on the use of enzymes, DNAzymes, antibodies, cell slices, to mention the more typical ones, are highly welcome. Articles on subjects related to the areas including genomics, proteomics, metabolomics, high-throughput screening, but also bioinformatics and statistics as they relate to bioanalytical methods are of course also welcome. Reviews cover both fundamental aspects and practical applications.

Reviews published in BAR are (a) of wider scope and authoratively written (rather than a record of the research of single authors), (b) critical, but balanced and unbiased; (c) timely, with the latest references. BAR does not publish (a) reviews describing established methods of bioanalysis; (b) reviews that lack wider scope, (c) reviews of mainly theoretical nature.

Frank-Michael Matysik
Editor

Advances in Chemical Bioanalysis

With contributions by

S.M. Borisov • F. Canfarotta • M. Cindric •
F.S. Grünewald • L. Gorton • C. Hägerhäll •
I. Klimant • F.-M. Matysik • S.A. Patil • S.A. Piletsky •
I.M. Perez de Vargas-Sansalvador • M. Quaranta •
T. Riuttamäki (née Rantanen) • T. Soukka

Springer

Editor
Frank-Michael Matysik
Institute of Analytical Chemistry
University of Regensburg
Regensburg
Germany

ISBN 978-3-319-00181-4 ISBN 978-3-319-00182-1 (eBook)
DOI 10.1007/978-3-319-00182-1
Springer Cham Heidelberg New York Dordrecht London

Library of Congress Control Number: 2014941448

Printed on acid-free paper

Springer is part of Springer Science+Business Media (www.springer.com)

Preface

This book is the first volume of a new series of chemistry review books focusing on bioanalytical chemistry. The new series, *Bioanalytical Reviews*, will cover cutting-edge tools used in modern bioanalytical research as well as new solutions to bioanalytical challenges. Methodological developments in bioanalytical chemistry have had an enormous impact on almost all areas of the life sciences. Consequently, *Bioanalytical Reviews* should attract interest from a wide cross section of the scientific community.

The mission of the present volume, *Advances in Chemical Bioanalysis*, is to reflect on the progress of important research within the rapidly growing and diverse area of chemical bioanalysis. Chemical bioanalysis is the scientific discipline of analyzing biological systems by chemical (rather than by purely biophysical or biochemical) methods. It retrieves selective information from complex biological systems. The following contributions have been prepared by experts from an international network in the field of chemical bioanalysis (CHEBANA). Among the methodological approaches in chemical bioanalysis three major areas were singled out for this volume:

- Fluorescence-based methods
- Electrochemistry
- Mass spectrometry

Representative in-depth reviews of research topics in chemical bioanalysis based on at least one of these concepts are as follows:

Quaranta et al. present an overview of recent developments in the field of optical sensing of oxygen providing a guide for selecting suitable oxygen indicators in the context of bioanalytical applications. The important bioelectrochemical research area of electron transfer between microorganisms and electrodes is reviewed by Patil et al.; Perez et al. summarize the progress made in the synthesis of monodisperse polymeric nano- and microparticles and their applications in chemical bioanalysis. New developments in upconverting phosphor labels in the context of bioanalytical assays and associated challenges are reviewed by Riuttamäki and Soukka. The role of periplasmic binding proteins as recognition elements for the

development of optical and electrochemical biosensors and corresponding applications is summarized by Grünewald. The contribution by Cindric and Matysik illustrates the hyphenation of electrochemistry with mass spectrometry and its potential for bioanalytical studies.

I wish to express my appreciation to all of the authors who contributed to this book project with high-quality articles illustrating the current strength and future potential of important bioanalytical approaches. Last but not least, I am deeply indebted to Prof. Otto Wolfbeis for his enthusiasm in forming an international consortium of experts to promote the advances in chemical bioanalysis.

Regensburg, Germany Frank-Michael Matysik
Autumn 2013

Contents

BIOREV (2014) 1: 1–70
DOI: 10.1007/11663_2013_1

Published online: 26 September 2013

Indicators for optical oxygen sensors

Sergey M. Borisov, Michela Quaranta, and Ingo Klimant

Abstract Continuous monitoring of oxygen concentration is of great importance in many different areas of research which range from medical applications to food packaging. In the last three decades, significant progress has been made in the field of optical sensing technology and this review will highlight the one inherent to the development of oxygen indicators. The first section outlines the bioanalytical fields in which optical oxygen sensors have been applied. The second section gives the reader a comprehensive summary of the existing oxygen indicators with a critical highlight on their photophysical and sensing properties. Altogether, this review is meant to give the potential user a guide to select the most suitable oxygen indicator for the particular application of interest.

Keywords Bioanalysis · Oxygen indicators · Luminescence · Metal complexes · Quenching

Contents

Originally published as an article in the journal "Bioanalytical Reviews" (Quaranta M, Borisov SM, Klimant I (2013) Indicators for optical oxygen sensors. Bioanal Rev. doi:10.1007/s12566-012-0032-y).

S.M. Borisov (✉) and I. Klimant
Institute of Analytical Chemistry and Food Chemistry, Graz University of Technology, Graz, Austria
e-mail: sergey.borisov@tugraz.at

M. Quaranta (✉)
Linz, Austria
e-mail: quaranta.michela@gmail.com

1 Introduction

Oxygen is by far one of the most important chemical species on earth since it is essential for life. Measurements of its concentration are of extreme importance in many different research fields such as: medicine, chemistry, environmental and marine analysis, molecular biotechnology, bioprocess control, food packaging, and industrial production monitoring. In the majority of the cases, it would be ideal to monitor oxygen concentration continuously which implies the use of oxygen sensors: a class of chemical sensors and by definition "*a miniaturized device that can deliver real-time and on-line information on the presence of specific compounds or ions in even complex samples*" [234].

Several methods for oxygen detection exist and can be classified on the basis of the principle used in electrochemical (amperometric, potentiometric, or conductometric), optical (absorption changes or photoluminescence), and chemical (Winkler titration).

Since its development, the Clark electrode has been considered the conventional method for the measurement of oxygen concentration because it is quite robust and reliable. However, in the last three decades, optical sensor technology has received increasing attention due to the fact that optical oxygen sensors can be rather inexpensive, are easy to miniaturize, can be used remotely, are virtually noninvasive or minimally invasive and, most of all, do not suffer from electrical interference nor consume oxygen [3].

Optical chemical sensors can be divided in several subgroups depending on the working principle applied; practically all spectroscopic methods have been used (absorption spectroscopy, reflectometry, luminescence, infrared and Raman spectroscopies, interferometry, and surface plasmon resonance). The majority of

the optical sensors developed for oxygen detection rely on quenching of the luminescence of an indicator dye by molecular oxygen [153].

Typical layouts consist of a luminescent dye, whose optical properties are reversibly influenced by the presence of molecular oxygen, which is usually incorporated into a polymeric matrix and deposited on a solid support (planar waveguide, microtitre plate, or optical fiber). Nano- and microparticle-based oxygen probes have also proved to be important analytical tools.

The field of application plays an important role in the choice of the indicator dye and, as a consequence, of the matrix material and detection method. For example, when measuring oxygen in live cells or in tissues, it is necessary to take into account the autofluorescence generated by the presence of biological substances such as proteins, DNA, and melanin. In such cases, in order to minimize absorption and scattering of the excitation and emission light in the tissue, it is preferable to employ indicators that show longwave-shifted absorption (590–650 nm) and emission (730–900 nm) bands [63, 223]. On the other hand, when measuring ultrafast oxygen dynamics, for example in breath monitoring application [33], it is crucial to use optodes with a very fast response time which can be achieved by employing very thin sensing layers and indicator dyes possessing exceptional brightness.

The scope of this review is not only to provide the reader with a selection of recently developed oxygen indicators but also to give a feeling about the area of applicability with a special focus on bioanalysis.

2 Photoluminescence and oxygen quenching schemes

Photoluminescence is the emission of photons produced in certain molecules during de-excitation and is one of the possible physical effects resulting from the interaction between light and matter.

When a luminescent molecule absorbs a photon, it is excited from its ground state (S_0) to some higher vibrational level of either the first or second electronic state (S_1 or S_2). This transition occurs in about 10^{-15} s and the subsequent possible de-excitation processes can be visualized by the Perrin–Jablonski diagram in Fig. 1.

The first process to occur, after absorption, is the internal conversion from the excited vibrational level to the lowest vibrational level of S_1, which takes typically 10^{-12} s or less. Internal conversion is a nonradiative transition and it is generally complete prior emission. From S_1, two major radiative de-excitation processes are possible; the first one is fluorescence emission which is a spin-allowed transition (it happens with no changes in multiplicity) that has a high probability of occurrence; fluorescence lifetimes are typically near 10^{-8} s. The second possible process is phosphorescence emission from the lowest excited triplet state T_1 which requires nonradiative intersystem crossing between two isoenergetic vibrational levels belonging to electronic states of different multiplicities ($S_1 \rightarrow T_1$) and therefore has a lower probability of occurrence. Transition from T_1 to the singlet ground state is forbidden; therefore, the rate constants for triplet emission are several orders of magnitude smaller than those of fluorescence and the lifetimes usually vary from

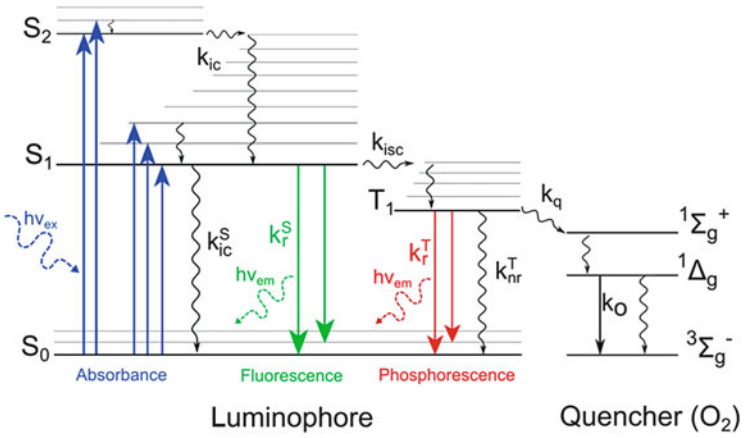

Fig. 1 Perrin–Jablonski diagram

10^{-6} to several seconds. The presence of heavy atom within the indicator, either as the central atom or as a substituent in the ligand, usually greatly increases the probability of intersystem crossing (up to unity). This result can promote highly efficient phosphorescence and shortens the phosphorescent decay time.

When an excited molecule returns to the ground state, it emits light at a longer wavelength and lower energy compared to the absorbed light (Stokes' shift); this phenomenon is more pronounced for phosphorescence emission since it occurs from a lower energy state.

In the presence of molecular oxygen, the photoluminescence of such molecules is quenched via a radiationless deactivation process which involves molecular interaction between the quencher and the luminophore (collisional quenching) and it is therefore diffusion limited. The mechanism by which oxygen quenches luminescence is not yet completely clear, one of the proposed mechanisms suggests that the paramagnetic oxygen causes the luminophore to undergo intersystem crossing to the triplet state while molecular oxygen goes to the excited state (either $^1\Delta_g$, the first excited state or $^1\Sigma_g{}^+$, the second excited state) and then returns to ground state ($^3\Sigma_g{}^-$, the triplet state; Fig. 1) [124]. The formation of singlet oxygen ($^1O_2$) is a direct evidence of the energy transfer mechanism and often the quantum yield of singlet oxygen formation approaches unity. However, quenching mechanism can also occur via electron transfer which was demonstrated to be rather efficient for example in the case of iridium cyclometallated complexes [56].

Independent from the predominant mechanism (energy or electron transfer), the kinetics of collisional quenching by oxygen is very well described by the Stern–Volmer equation (Eq. 1)

$$\frac{I_0}{I} = \frac{\tau_0}{\tau} = 1 + k_q \tau_0 \, pO_2 = 1 + K_{sv} pO_2 \tag{1}$$

Where I and I_0 are the luminescence intensities in the presence and absence of the quencher, τ and τ_0 are the lifetimes of the luminophore in the presence and absence of the quencher, k_q is the bimolecular quenching constant, and K_{sv} is the Stern–Volmer quenching constant.

It is often the case that in microheterogeneous environment (e.g., in polymers) Eq. 1 does not adequately describe the quenching mechanism; in such cases, it is preferable to use a second equation from the so-called two-site model [35] (Eq. 2)

$$\frac{I}{I_0} = \frac{f}{1 + \mathrm{K}^1_{\mathrm{sv}}\mathrm{pO}_2} + \frac{1-f}{1 + \mathrm{K}^2_{\mathrm{sv}}\mathrm{pO}_2} \tag{2}$$

where f represents the fraction of the total emission for the first site and $K_{sv}{}^1$ and $K_{sv}{}^2$ are the Stern–Volmer quenching constants for the two sites. The two-site model assumes the existence of two different environments with substantially different accessibility for oxygen. Although this model is physically meaningful only for luminescence intensities, in most cases it can also be used to fit decay times dependences.

Apart from the two-site model, other models exist that are able to describe the degree of heterogeneity of a sensor; for example the log-Gaussian distribution in τ_0 and k_q [161]. The model assumes that the heterogeneity of an optical oxygen sensor is manifested as a log-Gaussian distribution in rate and therefore is controlled by two kinetic processes: the intramolecular deactivation of the excited state of the luminophore ($1/\tau_0$) and the intermolecular quenching of the excited state by oxygen ($k_q \cdot pO_2$). Such model is able to generate model parameter values which are physically plausible and consistent at all partial pressures of oxygen.

3 Sensing methodologies

Although some of the oxygen sensors in use rely on absorption-based measurements, the majority make use of the luminescence quenching of an indicator dye. Luminescence sensing requires a change in the spectral properties of the indicator in the presence of oxygen. Changes can occur in the form of emission spectrum, luminescence intensity, anisotropy, or lifetime of the sensing probe [124].

The most direct sensing method entails the measurement of changes in luminescence intensity in response to the presence of an analyte. Unfortunately, it is often inconvenient to rely on intensity changes since they can be influenced by a wide variety of factors (e.g., luminophore concentration, photobleaching, light source intensity, scattering, coloration of the probe, etc.) and therefore alter the results of a measurement. Hence, it is important to use alternative methodologies that are independent on these factors, such as ratiometric or lifetime-based measurements. Usually, the choice depends on the cost of the equipment, the availability of indicator dyes, and the field of application.

Ratiometric methods are often preferable for imaging application and typically the sensors contain both an oxygen-sensitive indicator and a reference dye usually incorporated in the same matrix. The latter has to be unquenchable by oxygen and photostable in its presence; the emission spectrum of the reference dye should have little or no overlap with the one of the indicator dye and there should be no energy transfer between the two dyes. Oxygen concentration can then be determined from the ratio of the luminescence intensities of the indicator and the reference dye measured at two different emission wavelengths. This is usually done by using bandpass filters or, alternatively, by attributing the emissions of the components to different color channels of an RGB camera [128, 212, 228]. A more elegant solution is an application of tailor-made indicators which possess dual emission (oxygen-sensitive phosphorescence and oxygen-insensitive fluorescence) but very few examples have been reported so far [244, 254, 256, 258].

Ratiometric oxygen sensors can be applied, for example, for in vitro measurements to image O_2 concentration in cells [43] or for noninvasive real-time monitoring of oxygen levels in live cancer cells under normal and hypoxic conditions [135]. It should be mentioned here that ratiometric imaging is still affected by light scattering because this effect is wavelength dependent.

An alternative property that can be used to monitor oxygen concentration is luminescence lifetime (τ). The lifetime is the average amount of time a luminophore remains in the excited state following excitation and it can be measured either in time domain or in frequency domain [124]. In time domain, the sample is excited with a pulse of light and then the time-dependent intensity is measured; the decay time is calculated from the slope of the a plot of log I(t) versus t (slope $= -1/\tau$). A short delay between the excitation pulse and the measurement allows the complete elimination of short-lived background fluorescence.

In the frequency domain method, the sample is excited with intensity-modulated light. The emission of a luminophore is delayed in time relative to the excitation; the delay is measured as a phase shift (φ) and can be used to calculate the decay time:

$$\tau = \tan\varphi / 2\pi f \tag{3}$$

where f is the modulation frequency.

A two-frequency phase modulation technique can be very practical when measuring intracellular oxygen concentration in plant tissue since it allows discrimination between the luminescent lifetime of the autofluorescence of the plant tissue and the phosphorescence of the indicator dye [198].

Pulse and phase techniques are theoretically equivalent and provide the same kind of information; each has its own advantages and drawbacks. As mentioned earlier, lifetime measurements overcome the disadvantages of the intensity-based measurements. Luminescence lifetime, for example, is an ideal parameter to measure in biological system where the exact concentration of dye after cellular uptake is difficult to determine and replicate accurately [171].

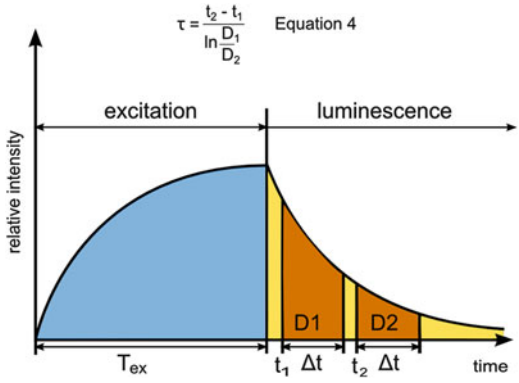

Fig. 2 Schematic representation of RDL measurement

Imaging of oxygen distribution has become a popular technique in different fields of application such as biomedicine [158, 257], marine microbiology [75, 86], and biological systems (intra- and extracellular oxygen distribution) [57, 130].

Luminescence imaging can be performed either through intensity- or lifetime-based measurements. One of the first works on intensity-based phosphorescence imaging was published in 1988 and used to measure oxygen distribution in perfused tissue [192]. Lifetime imaging techniques were developed for the first time two decades ago, and both time-domain (pulsed) [229] and frequency-domain (phase-resolved) [125] have been described; in 1997, the first noninvasive technique to measure oxygen concentration on nonplanar surfaces (e.g., human skin) was described [92].

Lifetime imaging has two major advantages over intensity-based imaging: it consents the enhancement of contrast and it allows the suppression of background fluorescence; also, lifetime imaging does not depend on intensity variation that can derive, for example, from photobleaching or variable indicator concentrations and calibration-free sensing applications are feasible [96]. A frequently used pulsed technique for the determination of fluorescence lifetime is the time-correlated single-photon counting in which the decay time curve is obtained from the integration of many pulses recorded over time [196]. This technique requires complex instrumentation and is less feasible for phosphorescence lifetime imaging because of much longer acquisition times; therefore, a second methodology called rapid lifetime determination (RLD) became rather popular [95, 96, 238].

The principle for image acquisition in RLD is briefly the following: the measurement starts by switching on the excitation source which illuminates the sensing material, the luminescence intensity increases until equilibrium between absorbed and emitted energy of the indicator dye is reached. Then, the light source is switched off and the shutter of the camera is opened to allow luminescence and ambient light to reach the charge-coupled device (CCD) chip at two different time gates (t_1 and t_2) of identical period (Δt); the lifetime is therefore proportional to the ratio of the integrated photon counts D_1 and D_2 (Eq. 4 in Fig. 2) [139].

In recent years, another technique appeared and became rather popular: multiphoton microscopy, which is based on excitation of the dye by simultaneous absorption

of two or more photons. It is usually used with fluorescence dyes to visualize either tissues or cells with high resolution. The advantages of this method rely on the fact that the near-infrared (NIR) light used for excitation penetrates deeply into tissues for which is not harmful, the background fluorescence is absent, the spatial resolution is significantly higher, and the photobleaching is lower than for other techniques such as confocal spectroscopy. As a consequence, some probes using this methodology have been recently developed [74, 131, 195]. Unfortunately, the state-of-the-art luminescence indicators possess very low two-photon absorption cross-sections and that is why rather sophisticated design of new probes are necessary.

4 Application of oxygen sensors in bio-analysis

Optical oxygen sensors have been developed for a wide variety of applications and in this section of the review, the ones inherent to bioanalysis will be highlighted and briefly described. We will focus on the following bioanalytical applications: oxygen content measurements in blood (diagnostics), measurements in bioreactors or in cell cultivating flasks, imaging intra or extracellular oxygen distribution, applications in marine biology, and measurements of photosynthetic and respirometric activity [16]. Finally, the role of oxygen as a transducer for enzymatic biosensors (e.g., for glucose sensors) will be discussed.

4.1 Medical diagnostics

Assessing a patient's need of oxygen is of extreme importance in critical situations such as during surgery, recovery, or while a patient is under intensive care treatment. Sampling of arterial blood and the subsequent analysis suffers from the main disadvantage of not being a continuous method: it is not feasible to sample more than two or three times a minute and oxygen content can fluctuate widely during periods of few seconds.

Back in 1942, Millikan [160] developed the first original oximeter which in concept was very similar to the modern pulse oximeters but suffered from the inability to effectively compensate for the pulsatile variations of arterial blood. Pulse oximetry was developed by Aoyagi in 1972 [203], who had the idea to measure only the pulsatile changes in light transmission through living tissue to compute the arterial saturation.

The role of a pulse oximeter is to determine the "oxygen saturation" in blood which is defined as the ratio of concentrations between oxyhemoglobin and the total hemoglobin; the method is noninvasive and as a typical intrinsic optical sensor, it does not require any indicator. Light at two different wavelengths is allowed to pass through a part of the patient's body (usually the fingertip or the earlobe) to be then measured by a photodetector. Today's oximeters use a pair of light-emitting diodes (LEDs): a red (660 nm) and an infrared (910 or 940 nm) one;

at this two wavelengths, hemoglobin and oxyhemoglobin exhibit a very different absorption, therefore, their concentration's ratio can be calculated from the ratio of the absorptions of the red and infrared lights.

Luminescent oxygen sensors have also been applied in medical diagnostics: for example back in 1994, a portable system for in vitro test blood analysis (OPTI system) was developed and commercialized. The system consists of a disposable cassette containing six different optodes for measurement of pH, oxygen and carbon dioxide partial pressure, sodium, potassium, and calcium, all by fluorescence. Additional cassettes are available for determinations of chloride, glucose, and urea [219].

More recently, additional applications of luminescent oxygen sensor for diagnostics have been emerging such as the control of wound healing processes [200], the measurement of transcutaneous pO_2 [17], and of tumor hypoxia [258], to mention only some.

4.2 Bioreactor and cell cultivating flasks

Continuous measurements of dissolved oxygen (DO) during cell culture are very important not only to control cellular differentiation, viability, and proliferation [79, 215, 248] but also when designing the scale-up from small-scale culture to mass production [89, 255]. DO measurement is particularly important in shake flasks for cell cultivation since, for example, in such devices the oxygen transfer rate is lower than in stirred bioreactors; therefore, accurate measurements are essential to avoid biological misinterpretation [199].

Luminescence-based oxygen sensors are very attractive for biotechnological application for a number of different features such as the fact that they are noninvasive and generally nontoxic since they can be easily incorporated in matrices that are not only biocompatible but also nonreactive and non-irritant to culture media [110].

There are many biotechnological processes such as the synthesis of penicillin or yeast fermentation, which require a sterile environment; therefore, the optical sensor used to continuously measure the oxygen concentration in those bioreactors needs to be autoclavable and to withstand sterilization (e.g., high temperature and humidity). Voraberger et al. [224] developed such sensor which was used to measure oxygen concentration in a fermenter; the results showed good comparison with the ones obtained with a Clark-type electrode, which has the disadvantage to suffer from inadequate signal stability, slow response time, and electrical interferences.

Optical oxygen sensors were also developed for online measurement of the biocatalytic activity of enzymes in microtiter plates by integrating the sensing layer into the bottom of each plate [80]; such devices are of potential interest for the screening of aerobic cell activities, biological degradation of pollutants, and for toxicity tests.

4.3 Intra and extracellular O_2 imaging and DO in tissue

The application of optical oxygen sensors in the measurement of oxygen concentration, particularly in living tissue, has the advantage of being noninvasive and it can be used remotely.

Inter- and intracellular measurements of dissolved oxygen can be potentially performed with the use of a ratiometric fiber optic sensor which was developed and characterized by Park et al. [180]. The described sensor exhibited excellent reversibility, minimal photobleaching, and fast response time which are fundamental qualities to measure oxygen in biological samples. On the other hand, the size of the fibers, with tips ranging from 40 to 200 μm, is too big for noninvasive intracellular measurements. Apart from the size, another disadvantage in using optical fibers is that they allow only single-point acquisition and are therefore unsuitable for microscopic imaging. As previously mentioned, ratiometric methods are often preferable for imaging applications and have been applied to measure oxygen concentration inside cells [43].

Different kinds of sensing probes have been developed for extra- and intracellular microscopic imaging such as dendrimers, dye conjugates, and dyes (non)covalently entrapped in polymeric nanoparticles, which have the characteristic of being small enough to be introduced directly into the medium of interest (e.g., blood or interstitial fluid).

When measuring in biological systems, phototoxicity is a potential concern. The byproduct of the quenching reaction is singlet oxygen which is highly reactive and capable of damaging biological tissue. Several solutions to this problem are currently under investigation some of which are already employed, for example the use of PEGylated dendritic "jackets" to regulate the sensitivity and dynamic range of measurements by controlling the oxygen quenching constant [37]. PEG residues are used to modify dendrimers in order to enhance their solubility, to reduce their toxicity, and to help to prevent interactions between the probe and the biological environment. Such probe was tested for high-resolution microscopic in vivo microscopy of vascular pO_2 in rat's brain [130]. Another approach consists in the encapsulation of an indicator inside an inert nanoparticle, often referred to as probes encapsulated by biologically localized embedding (PEBBLE) [46]; such nano-spheres can have radii as small as 10 nm and therefore occupy only circa 1 ppb of an average mammalian cell's volume which has the advantage of causing a rather negligible mechanical perturbation.

Nanosensors have been successfully used to monitor dissolved oxygen in human plasma [34], to monitor cellular respiration [113], and to measure the real-time oxygen concentration inside tumor cells under normal and hypoxic conditions [135].

Nanosensors can be delivered into cells by different techniques such as pico-injectors, gene guns, liposomal incorporation, and endocytosis. Some oxygen nanosensors can spontaneously penetrate cell's membranes thanks to the presence of positively charged groups on the surface of the particle [69].

Another class of cell-penetrating dyes which rely on an endocytic mechanism of cell entry is represented by the derivative of tetracarboxylic Pt(II)-coproporphyrin I (PtCP) [58, 174]. Such conjugates were successfully tested to measure intracellular O_2 concentration in live cells, giving information-rich data on cellular function and metabolism. The probe has recently being optimized in order to reduce nonspecific bindings and increase intracellular distribution [57].

Measurements of oxygen concentration in tissue entail additional requirements: the probe does not only have to be highly water soluble, but also to be impermeable to biological membranes so that penetration can be avoided. Another important characteristic is to possess an absorption band in the NIR region since the excitation light needs to penetrate the depths of tissue [130].

Accurate measurements of oxygen concentration in tissue not only give information about tissue oxygenation but also about local microcirculation; such information is of clinical interest for example in radiotherapy and chemotherapy of cancer. Continuous monitoring of oxygen partial pressure has also been realized with the use of an optochemical glass capillary oxygen sensor connected to a microdialysis catheter for the extraction of the biological fluid from a subcutaneous adipose tissue [23].

Two-dimensional pO_2 distributions were measured over the cross-section of cultivated tissues which were, for this scope, immobilized on top of an optical sensor foil [101]. The experimental setup used by the authors allowed a continuous, noninvasive measurement of tissue oxygen distribution which correlated well with histological analysis and supports the hypothesis that tissue growth in vitro is limited by oxygen supply.

4.4 Marine biology

The accurate measurement of oxygen concentration in fresh and salty water environments has always solicited the interest of scientists in different fields since monitoring the level of DO is essential to clarify several biological processes. Along with oxygen microelectrodes [119], oxygen micro-optodes have been extensively used in marine biology for over a decade [105, 127, 184].

The study of two dimensional (spatial and temporal) distributions and the dynamics of oxygen in marine sediments is also very important, but it cannot be performed with a fiber optic micro-optode since it allows only single-point measurements and it would require a series of sensors (and recording devices) and therefore render the measurement expensive and impractical. Those problems were overcome with the introduction of planar optode to aquatic sciences [85]. Such systems can be based on either intensity (pure or ratiometric) or lifetime-based measurements and they have been developed and applied in many different habitats [121] like microbial mats [84], marine sediments [112, 202], coastal sands [86, 231], permeable sediments [49], rhizospheres [98], and endolithic algal communities [120].

Monitoring of oxygen on 3D surfaces and in tissues is not yet common in marine biology due to the fact that suitable sensing materials (oxygen-sensitive micro- and nanoparticles) became available only in recent years. A very recent work [67] though suggests that such new analytical tools developed by material chemists will become increasingly important in this field in the future. These tools can provide information which is not accessible by more conventional fiber-optic microsensors and planar optodes.

4.5 Enzymatic biosensors

Optical oxygen sensors can be used as transducers for biosensors when coupled with specific biorecognition elements such as enzymes, antibodies, or oligonucleotides [30]. True biosensors can be defined as analytical devices which comprise the following two elements in spatial proximity: a biological element, which is able to interact specifically with the target analyte and a transducer, which transforms the recognition event into a measurable signal. In addition, true biosensors do not need any additional processing steps such as reagent addition and therefore give a reading when exposed to the sample [214].

The most exploited biosensors that make use of optical oxygen sensors as transducer are glucose sensors since they have a wide application in life science, biotechnology, biology, clinical analysis, and food chemistry. In general, the significant interest in sensing glucose is driven by the fact that 4–5 % of the world population suffers from diabetes mellitus which is a complex disorder and its main characteristic is the chronic shift in glucose concentration in blood [210]. There are several complications related to diabetes which are linked to the duration and severity of hyperglycemia (high blood glucose concentration); therefore, it is of extreme importance to maintain the glucose level near to normal values. This can only be provided by a device that continuously measures glucose concentration in the blood. Ideally, the ultimate implantable glucose sensor (used in artificial pancreas) would constantly monitor glucose concentration and automatically activate the release of insulin when needed; unfortunately, such device is still quite far from being fully developed. Many different types of optical glucose sensor have been successfully assembled and used, but since the focus of this review is on optical oxygen sensors, only those which rely on the measurement of oxygen consumption due to the enzymatic oxidation of glucose by glucose oxidase (GOx; Eq. 5) will be described.

$$D-\text{glucose}+O_2 \rightarrow D-\text{glucono}-1,5-\text{lactone}+H_2O_2 \tag{5}$$

One of the first optical biosensor based on GOx immobilized on a nylon membrane was reported in 1988 [218]. Such sensor was based on the quenchability of decacyclene, allowed a continuous determination of glucose in the physiological range and it was in commercial use for more than 10 years. The sensor had been improved years later to obtain shorter response times within the range of 8–60 s [197].

Among the optical devices developed for continuous glucose detection and measurements in vivo, the miniaturized hybrid fiber optical biosensor presented by Klimant and coworkers [181, 182] should be mentioned. The design of this hybrid sensor allows its implantation in subcutaneous tissue and to compensate for the local pO_2 changes. Two different optodes, one for the determination of glucose and the second one for the determination of local oxygen are placed in close proximity into a polyimide tube; therefore, the final readout which corresponds to glucose can be obtained by the difference between the local oxygen tension (measured by the reference optode) and the reduction of the oxygen level measured by the glucose optode due to the enzymatic reaction [181]. A similar setup has been tested in vitro in a 3-day continuous experiment in glucose-spiked plasma and once coupled with a flow-through cell and commercially available catheter; its ability to measure glucose in humans was also demonstrated in a 24 h test on healthy volunteers [182].

Another fiber-optic dual sensor for the continuous determination of oxygen and glucose was developed by Li et al. [137]. In this approach, the two sensing sites were placed at defined distance between each other on the distal end of an imaging fiber, the changes in fluorescence intensities were therefore captured with a CCD camera. Apart from the instrumental costs, the main drawback of the unit was the dependence of the signal intensity on the dye loading.

Different assemblies of thin film glucose biosensor based on a sol–gel matrix, which are capable of compensating the effect of variable oxygen background, have also been developed by Wolfbeis et al. [236].

Glucose has also been successfully measured online in animal cell cultures with the use of a flow injection analysis system based on fiber optic detection of oxygen consumption using immobilized glucose oxidase [62]. Such system has been tested to be stable for more than 4 weeks in continuous operation withstanding up to 20 analyses per hour and it has been successfully applied to the online monitoring of both glucose and lactate concentrations of an animal cell culture for the production of recombinant human antithrombine III.

Biosensors have also been developed to measure glucose concentration in beverage samples, where the enzyme was either immobilized in eggshell membrane [42] or entrapped in sol–gel [243] and in urine samples where GOx was immobilized in xerogel [240].

Continuous glucose monitoring is of course extremely important, especially for critically ill patients. Many people suffer from diabetes but only one third is aware of it, it is therefore fundamental to have a fast, easy, and cheap way to diagnose diabetes. Wang et al. [230] have developed a new optical biosensor characterized by short response time, lower detection limit, high sensitivity, and stability which can be potentially applied for the fast determination of glucose in human serum. The same group has recently assembled a novel direct readout colorimetric optical glucose sensor strip which can be easily read without instrumental assistance [225]. Such “glucose ruler” was constructed based on a three-layer film which includes a green-emitting CdTe/CdS quantum dots layer as a stable background, a red-emitting platinum–porphyrin oxygen-sensitive layer and

a glucose oxidase layer. Oxygen is consumed when the ruler is exposed to glucose and it results in a color change from green to red depending on the concentration.

Biosensors that make use of oxidase type enzyme combined with an optical oxygen transducer have been also designed for other compounds:

- Phenols in hydrophobic organic solvents (enzyme: tyrosinase) [242]
- Alcohols (methanol and ethanol-biosniffer) in water-miscible solvents and in hydrophobic organic solvents (enzyme: alcohol oxidase) [167, 241]
- Cholesterol, for the continuous detection either in aqueous micelle solution or in hydrophobic organic solvents (enzyme: cholesterol oxidase) [239]
- Aspartame in commercial products such as artificial sweeteners (enzymes: α-chymotrypsin and alcohol oxidase) [247]
- Choline-containing phospholipids in serum samples (enzyme: phospholipase-D) [150]
- Bilirubin in serum samples (enzyme: bilirubin oxidase) [136]
- Glutamine in mammalian cells cultures (enzymes: glutaminase and glutamate oxidase) [36]

5 Classification of indicators for oxygen sensors

The scope of this review is to give the reader an overview on the state-of-the-art indicators available for optical oxygen sensing. Among the different indicators that have been synthesized and used in this area, one can classify them in two main groups: absorption- and luminescence-based indicators. Absorption-based indicators can be further divided in reversible and irreversible while luminescence-based indicators are only reversible.

6 Absorption-based indicators

6.1 Irreversible probes

In general, irreversible absorption-based indicators work by producing a visible color change which is caused by chromogenic chemistry that involves oxidation of the leuco dye by molecular oxygen. Only few of such indicators have been described and their main application can be found in the food and pharmaceutical industries where it is necessary to monitor the headspace gas within packages for meat/fish or for immune reagents, since oxygen is responsible for a variety of food spoiling processes. To be of use for the final consumer, ideal indicators should produce a discernible color change detectable by eyes and should not require specific analytical equipment. Also, an irreversible probe can be preferable to a reversible one in food packaging applications since it can reliably detect the event of the oxygen ingress during the package damage. On the other hand, a reversible

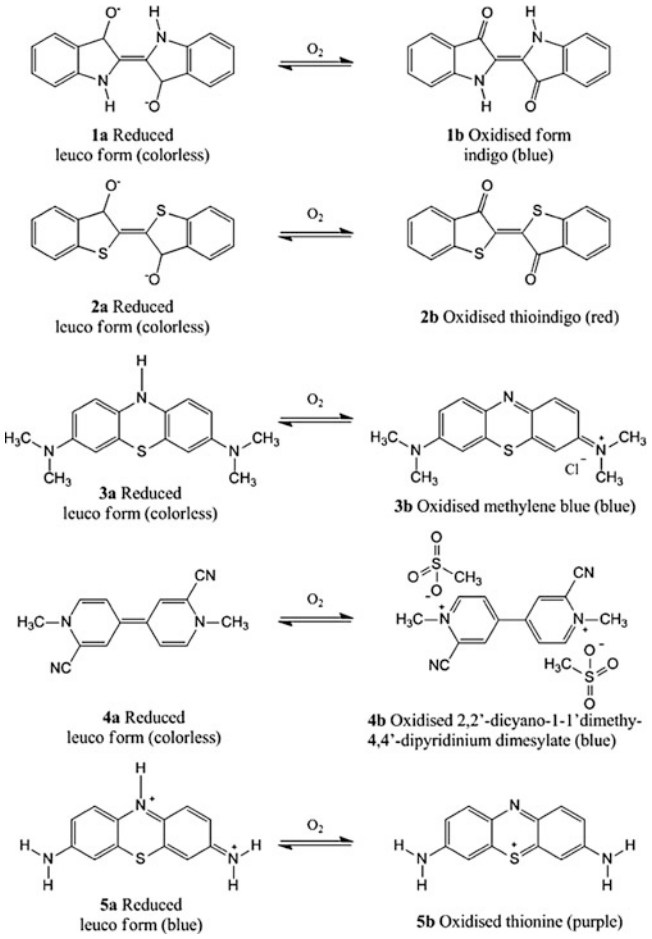

Fig. 3 Chemical structures of irreversible probes

probe may still indicate the absence of oxygen in a damaged package since oxygen, after penetration, can be consumed by growing bacterial species.

Indigo and thioindigo (**1b** and **2b**, respectively, Fig. 3) are vat dyes that can be easily reduced with a suitable reducing agent to become water soluble and colorless. They were incorporated in their reduced form in different polymeric matrices, either moderately or highly oxygen-permeable in order to increase the effective dynamic range [233]. Reaction with oxygen leads to a color change within a few minutes which is quite important when wanting to detect leaks in food packed under modified atmosphere. The authors reported on the possibility to regenerate the sensor immobilized on hydrogel by reduction under inert atmosphere.

Very recently, Mills et al. [162] used a redox dye, methylene blue (MB **3b**, Fig. 3) in combination with a sacrificial electron donor, DL-threitol, and TiO_2 particles to create an oxygen-sensitive pigment that was then incorporated into a

thermoplastic polymer and used as an O_2 smart plastic film. Once the blue-colored indicator is incorporated in the package, it needs to be activated by UVA light (4 mW cm^{-2}) for less than 90 s which causes the MB to be converted to its colorless leuco form that will persist for long time provided that no oxygen is present. It was reported that the indicator can be regenerated in about 4 days. The authors also suggested that the response of the indicator could be increased by depositing Pt nanoparticles onto the TiO_2 surface.

Methylene blue suffers from a slow reduction to its leuco form and a fast subsequent oxidation by oxygen present at low concentration; therefore, Hay et al. [187] have chosen indicators which showed a much faster reduction after UV exposure, namely 2,2′-dicyano-1-1′-dimethy-4,4′-dipyridinium dimesylate and thionine (**4b** and **5b**, respectively, Fig. 3). This class of indicators shows a moderate sensitivity to oxygen and therefore can be used even when the level increases up to 4 kPa.

6.2 *Reversible probes*

In our body, oxygen is efficiently transported from the respiratory organs to the rest of the body by hemoglobin, a metallo-protein which binds oxygen reversibly. The association with oxygen generates a shift in the Soret absorption band of hemoglobin; this absorption change was exploited to build an optical sensor to measure pO_2 from 2.6 to 13.4 kPa, based on immobilized hemoglobin [259]. The main shortcomings of this system are related to the fact that hemoglobin degrades within 2 days when stored at room temperature and 1 week when stored at 4 °C. Therefore, a synthetic, more stable, alternative needed to be found. It is known that some organometallic compounds are able to reversibly bind molecular oxygen [65] and therefore once immobilized on an appropriate support be used as absorption-based oxygen sensors. Among the different organometallic compounds synthesized by Baldini et al. [19], *bis*(histidinato) cobalt(II) [$Co(His)_2$] **6** (Fig. 4) was identified to be the best candidate to work as a transducer for oxygen sensing. Such indicator was adsorbed on a thin layer chromatographic plate which was then coated with a layer of silicon rubber; this additional layer is necessary not only to maintain a wet micro-environment but also to mechanically protect the sensitive layer [54]. The sensor was successfully tested in a series of oxygenation/deoxygenation cycles by monitoring the absorption peak at $\lambda = 408$ nm. It was also found that the response of the indicator is influenced by the pH and it does not give any response at pH lower than 4, since the histidine ligand can exist in different forms depending on pH and a change in the ligand is likely to affect the binding of oxygen.

Another complex that mimics hemoglobin in binding oxygen is the *meso*-tetra (α-α-α-α-*o*-pivalamidophenyl) porphyrinatocobalt(II) **7** [47] which was immobilized on either poly(octylmethacrylate-*co*-1-vinylimidazole) or poly(2,2,3,3,4,4,5,5-octafluoropentylmethacrylate-*co*-1-vinylimidazole) [189]. The complex in the presence of oxygen forms an oxo-adduct (Fig. 4) at the cobalt center which causes a shift in the absorption spectra, monitored at 547 nm. The sensing membranes

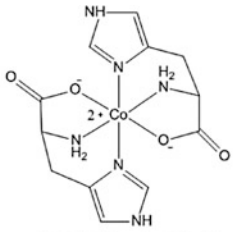

6 Bis(histidinato) cobalt (II)

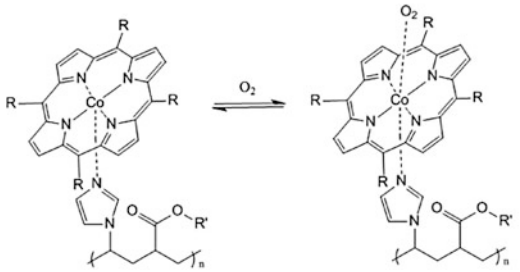

R = $PhNHCOC(CH_3)_2$
R' = **a)** n-octyl or **b)** 2,2,3,3,4,4,5,5-octafluoropenyl

7 *meso*-tetra(a- a- a- a-*o*- pivalamidophenyl) porphyrinatocobalt(II) immobilized on poly(metacrylate-*co*-1-vinylimidazole) (**a**) or on poly(2,2,3,3,4,4,5,5-octafuoropentylmethacrylate-*co*-1-vinylimidazole (**b**)

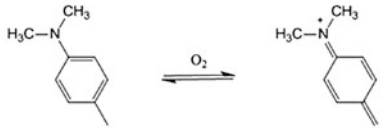

8 *N*,*N*-dimethyl -*p*-toluidine

Fig. 4 Chemical structures of reversible absorption-based indicators

are stable for 1–2 months and possess a useful response range between 0.1 and 100 % of oxygen at atmospheric pressure.

A fiber optic oxygen sensor for gaseous O_2 measurements was successfully developed by Choi and Hawkins [40, 41]. The working principle of this sensor is based on the contact charge–transfer absorption of *N*,*N*-dimethyl-*p*-toluidine **8** (Fig. 4) at 400 nm. The indicator is entrapped inside a poly(tetrafuoroethylene) tubing and inserted into a glass flow though cell. The described sensor can detect O_2 from 4.3 to 100 %, it uses very inexpensive materials and its fabrication is quite simple and fast but it suffers from several drawbacks such as interference from Cl_2 and SO_2, long response time and recovery times (12–26 min).

None of the absorption-based systems presented above became widespread in practice since the resolution provided is quite low as the spectral changes upon oxygen binding are relatively small. It should be mentioned here the existence of another technique for absorption-based oxygen sensors that relies on monitoring of the lifetime change of the triplet–triplet ($T_1 - T_n$) absorption [3]. The triplets of the indicators produced during excitation are dynamically quenched by molecular oxygen. Theoretically, the number of oxygen indicators can be greatly extended

since any luminescent or nonluminescent molecule possessing efficient intersystem crossing is suitable. In practice though, the use of this technique is severely limited by the need of a quite complicated setup and high power light sources to allow an efficient population of triplet states. Two classes of indicators have been reported so far, Zn^{2+} porphyrins, which have a long lifetime of photoexcited triplet state (~100 μs) and fullerene (C_{60} and C_{70}) which have a longer photoexcited triplet state (~20 ms) that is efficiently quenched by oxygen [3].

7 Luminescence-based indicators

To date, the most common and useful types of optical oxygen sensors are those based on the quenching of luminescence of appropriate indicators by molecular oxygen. The ability of oxygen to decrease the luminescence of dyes adsorbed on inorganic surfaces was first observed and published by Kautsky back in 1939 [100] who immobilized organic dyes such as trypaflavin, chlorophyll, porphyrins, eosin, erythrosine on either solid silica gel or aluminum oxide gel and observed that both the fluorescence and the phosphorescence of the adsorbates are reversibly quenched by oxygen.

Since then, different analytical applications of luminescence quenching for the determination of oxygen partial pressure have been reported. In 1944, Pollack et al. [185] described a method to measure oxygen production by exploiting the quenching of phosphorescence of an unspecified dye adsorbed in silica gel. Shaw [204] applied the ability of O_2 to quench the phosphorescence emission of phenanthrene and triphenylene immobilized in acrylic media as a method to measure the diffusion coefficients of oxygen through the polymeric media.

Jones [99] determined the oxygen permeability in thin acrylic films by measuring the quenching rate of the phosphorescence lifetime of naphthalene which was added to the film as an additive. A prototype to measure the atmospheric oxygen tension based on the quenching of fluorescence of fluoranthene adsorbed on porous glass was developed by Bergman in 1967 [22].

The number of luminescent indicators synthesized and exploited in optical oxygen sensing has of course largely increased as researchers started recognizing their potential to measure oxygen concentration in different fields of science as previously described.

The reader will now find the description of luminescent indicators classified in the following groups: polycyclic aromatic hydrocarbons, polypyridyl complexes, metal porphyrins, cyclometallated complexes, and complexes with rarely used central atoms. Indicators for oxygen sensing not belonging to any of these categories can be found in the section called “Miscellaneous”.

1. Polycyclic aromatic hydrocarbons

Polycyclic aromatic hydrocarbons (PAHs), especially pyrene and its derivatives (Fig. 5), have been used as fluorescent indicators as they possess a relative long

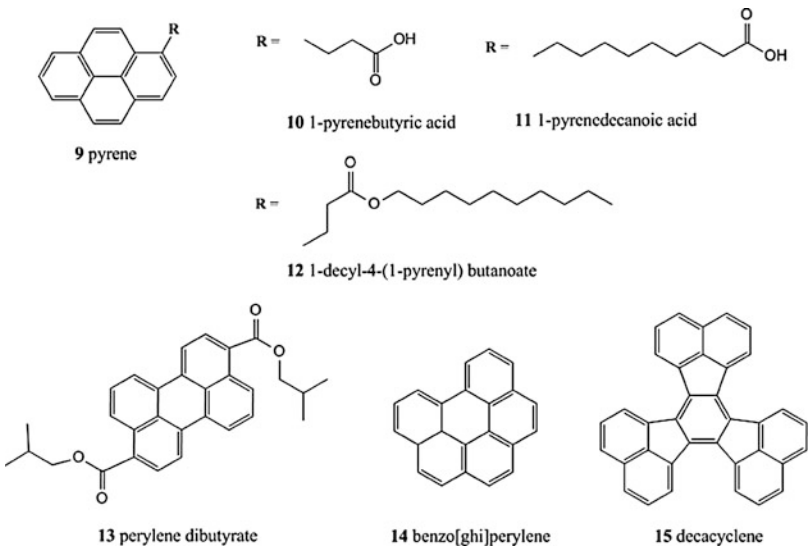

Fig. 5 Chemical structures of polycyclic aromatic hydrocarbons

Table 1 Photophysical properties of polycyclic aromatic hydrocarbons

Dye	λ_{max}^{abs} (nm)	λ_{max}^{em} (nm)	Medium	Φ	τ (ns)	References
9 Pyrene	305/319/335	381/390	Cyclohexane	0.65	450	[252]
10 1-Pyrenebutyric acid	365	376/396/447	Toluene	–	200	[3, 176]
11 1-Pyrenedecanoic acid	340	376/396	Alumina plate			[78]
12 1-Decyl-4-(1-pyrenyl) butanoate	345	480	Toluene	–	–	[21]
13 Perylene dibutyrate	468	514	Toluene	–	–	[183]
14 Benzo[ghi]perylene	386	419	Methanol	0.26[a]	110	[97]
15 Decacyclene	385	510	Toluene	0.29	–	[218, 237]

[a]Taken from [53]

excited-state lifetimes and can be quenched by oxygen in the 0–40 kPa range (Table 1).

Pyrene (**9**) has a relatively high quantum yield (Φ) of circa 0.7, good pressure sensitivity, and low temperature coefficient at ambient temperature; characteristics that can make it a suitable fluorophore for pressure sensitive paint (PSP). On the other hand, studies have demonstrated lack of stability of this indicator which tends to diffuse out of the support and evaporate [20]. Also, low solubility of planar PAHs and their tendency to aggregate in polymer represent another hindrance. Therefore, a number of pyrene derivatives bearing long lipophilic chains were prepared to overcome the above disadvantages. For example, Basu et al. [21] synthesized a pyrene derivative: 1-decyl-4-(1-pyrenyl) butanoate **12** which has a high oxygen quenching sensitivity and lower diffusion coefficient in silicone

polymer. Perylene dibutyrate **13** has been incorporated in an organic polymer adsorbent (amberlite) and deposited on an optical fiber for in vivo oxygen concentration measurements [183].

Among the different PAHs, 1-pyrenebutyric acid **10** possesses longer fluorescence lifetime (0.2 μs) and therefore it is suitable for optical oxygen sensing devices; it has been demonstrated that isolated rat liver cells easily take up 1-pyrenebutyric acid in concentrations up to 0.8 mM and the fluorescence probe can be used to measure intracellular oxygen concentration [108]. In general, PAHs are not very soluble in polymeric matrices; to overcome this problem, Amao et al. [13] fabricated a probe for oxygen sensing based on 1-pyrenebutyric acid adsorbed on the surface of an alumina plate.

1-Pyrenedecanoic acid **11** can also be chemisorbed onto alumina plate through its carboxyl group and the resulting sensor film has rapid response and recovery times. The fluorescence lifetime of benzo[ghi]perylene **14** is longer than 100 ns and its absorption maximum coincided with the wavelength of the second-harmonic emission from a near-infrared semiconductor laser which was used as the light source in an optical fiber setup for the determination of oxygen concentrations [175].

Decacyclene **15** has been used for more than 10 years as the oxygen indicator in a glucose biosensor [218] and it was the indicator of choice in a dual sensor for oxygen and halothane [237]; it can be excited by a blue LED and it has the advantage of not producing singlet oxygen when quenched.

This class of dyes in general suffers from many disadvantages which has limited their application as indicators for oxygen sensors. They have short excitation wavelength (300–390 nm) which causes components of biological media, optical components or polymers to display strong background fluorescence which is emphasized by small Stokes' shifts; despite good emission quantum yields the molar absorption coefficients are rather low which results in moderate brightness; the fluorescence decay times do not exceed several hundred nanoseconds so that sufficient sensitivity can be achieved only in highly gas-permeable polymers; finally, the majority of PAHs is not well soluble in polymeric matrices and therefore suffers from lack of stability due to aggregation.

It can be summarized here that PAHs and other fluorescent oxygen indicators which have been of importance in the early stage of sensor development are nowadays almost completely substituted by more advanced indicators which will be described below.

2. Transition metal polypyridyl complexes

Many luminescent transition metal polypyridyl complexes have been synthesized and some have been used as indicators for oxygen sensing. Within this group of indicators, transition metals used are Ru(II) and Os(II). In general, their complexes are characterized by large Stokes' shifts, possess excitation and emission maxima in the visible region, show good photostability, and their luminescent properties can be tuned as a function of the ligands.

Within this group, Ru(II) polypyridyl complexes have been used more frequently due to their relatively high brightness and relatively long lifetimes;

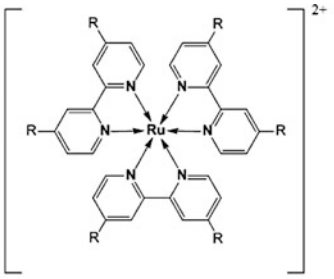

16 R = H, Tris(bipyridine) ruthenium(II)
$[Ru(bpy)_3]^{2+}$
17 R = Ph, Tris(4,4-diphenyl-2,2-bipyridine) ruthenium(II)
$[Ru(dpb)_3]^{2+}$

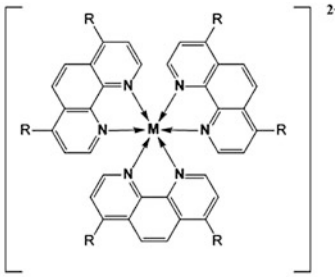

19 M = Ru, R = H, Tris(1,10-phenanthroline) ruthenium(II)
$[Ru(phen)_3]^{2+}$
24 M = Os, R = H, Tris(1,10-phenanthroline) osmium(II)
$[Os(phen)_3]_{2+}$
20 M = Ru, R = Ph, Tris(4.7-diphenyl-1,10-phenanthroline) ruthenium(II)
$[Ru(dpp)_3]^{2+}$
25 M = Os, R = Ph, Tris(4.7-diphenyl-1,10-phenanthroline) osmium(II)
$[Os(dpp)_3]^{2+}$

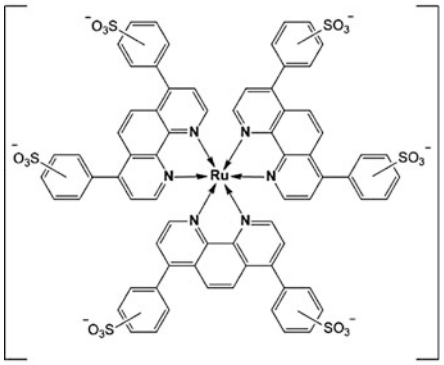

21 Tris(1,10-phenanthroline-4.7-bis(phenylsulphonate)) ruthenium(II)
$[Ru(s2d)_3]^{2-}$

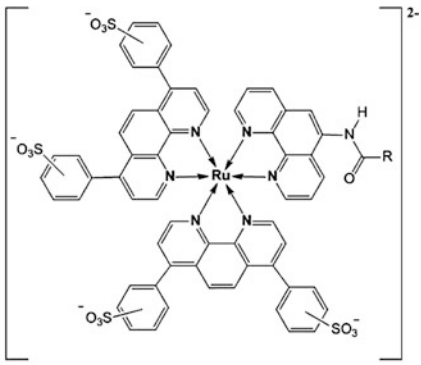

22a R = CH_3, $(s2d)_2$.(5-acetamide-1,10-phenanthroline) ruthenium(II)
$[Ru(s2d)_2(acap)]^{2-}$
22b R = $C_{13}H_{27}$, $(s2d)_2$-(5-tetradecanamide-1,10-phenanthroline) ruthenium(II)
$[Ru(s2d)_2(tdap)]^{2-}$

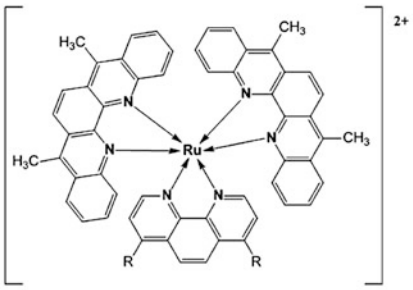

23 R = Ph, ((4,7-diphenyl-1,10-phenanthroline)bis(6.7-dihydro-5,8-dimethyl-dibenzo-[i,j][1,10]penanthroline)) ruthenium(II)
$[Ru(ddp)(DMCH)_2]^{2-}$

Fig. 6 Chemical structures of Ru(II) and Os(II) polypyridyl complexes

this is especially true for the *tris*(4,7-diphenyl-1,10-phenanthroline) ruthenium(II) complex $[Ru(dpp)_3]^{2+}$ **20** (Fig. 6) which has a luminescence lifetime up to 6.4 μs and a quantum yield of 0.3 [2]. Despite the disadvantages which will be described below, this dye is still one of the most popular oxygen indicators in use.

The luminescence of Ru(II) polypyridyl complexes is dominated by the metal to ligand charge transfer (MLCT) process that involves the promotion of an electron from a metal *d* orbit to a ligand π^* orbit; and therefore has been shown to be dependent on the polarity of the microenvironment and on the donor/acceptor character of the surrounding medium because of the significant changes produced on the electronic charge distribution of the molecule upon photoexcitation [166]. Also, both the excitation and the emission bands of the MLCT complexes are very broad which can be viewed as a positive property (higher flexibility in the choice of the excitation sources) but can also be a disadvantage (lower molar absorption coefficients and difficulties in isolating the emission in multi-analyte systems).

Luminescence lifetimes of several microseconds result in rather low oxygen sensitivity in common polymeric matrices such as polystyrene [91]; the resolution of such sensors in the range of 0–21 kPa O_2 is often not sufficient for practical applications. To overcome this problem, the ruthenium(II) polypyridyl complexes have been immobilized in highly oxygen-permeable matrices such as silicon rubbers or organically modified silica (Ormosil). Unfortunately, $[Ru(dpp)_3]^{2+}$, just like the majority of the other ruthenium polypyridyl complexes, is ionic and therefore it displays very poor solubility in silicon rubber which is one of the most common matrices for optical oxygen sensors as it has a high permeability for oxygen, good adhesion to glass fibers, inertness to biological samples, optical transparency, and excellent chemical and mechanical stability. Klimant and Wolfbeis [107] replaced the inorganic counter ion with an organic one to render the dye silicone soluble. Dodecyl sulfate (n-$C_{12}H_{25}SO_3^-$/DS) or trimethylsilylpropanesulfonate ($(CH_3)_3SiCH_2CH_2CH_2SO_3^-$/TSPS) were used. They demonstrated that, thanks to the enhanced solubility, the modified indicators could be used as indicators for oxygen sensors in high concentrations so that very thin but highly luminescent layers could be prepared.

In the same way, Mills [164] incorporated the fluorophore cation into a variety of different plasticized polymeric films (e.g., polymethylmethacrylate (PMMA)/tri-*n*-buthylphospate (TBP)) using a tetraphenylborate anion.

Alternative matrices have been used to immobilize $[Ru(dpp)_3]^{2+}$ to construct a feasible optical oxygen sensor. Examples are sol–gel [147, 152, 154, 249], ethyl cellulose or PVC membranes [61], different types of ORMOSILs [39, 94, 106], polystyrene [91], polysulfones [11, 18], poly(dimethylsiloxane) alone [251] or with different amounts of pendant acrylate groups [168], and a blended fluoropolymer matrix consisting of Nafion® and Aflas® [83]. In another approach, the $[Ru(dpp)_3]^{2+}$ complex was adsorbed onto silica and then dispersed in a silicone rubber support [38, 93]. Finally, the ruthenium indicator can be cross-liked with isobutyl methacrylate and 2,2,3,3-tetrafluoropropyl methacrylate to obtain a porous plastic probe which can be easily coupled with common optic fibers [87].

Table 2 Photophysical properties of transition metals polypyridyl complexes

Dye	λ_{max}^{abs} (nm; $\varepsilon \times 10^{-4}$ M^{-1} cm^{-1})	λ_{max}^{em} (nm)	Medium	Φ	τ	References
16 $[Ru(bpy)_3]^{2+}$	450 (1.43)	630	EtOH-MeOH (4:1 *v*/*v*)	0.089	1.15 μs[a]	[48]
17 $[Ru(dpb)_3]^{2+}$	473 (2.80)	635	EtOH-MeOH (4:1 *v*/*v*)	0.306	1.95 μs	[48]
18 $[Ru(5\text{-}odap)_3]^{2+}$	449 (1.75)	600	MeOH	0.027	0.50 μs	[166]
19 $[Ru(phen)_3]^{2+}$	444 (2.00)	596	MeOH	0.019	0.28 μs	[166]
20 $[Ru(dpp)_3]^{2+}$	463 (2.86)	618	EtOH-MeOH (4:1 *v*/*v*)	0.366	6.40 μs	[2]
21 $[Ru(s2d)_3]^{4-}$	475	620	MeOH	–	0.31 μs	[245]
22a $[Ru(s2d)_2(acap)]^{2-}$	475	616	MeOH	–	0.32 μs	[245]
22b $[Ru(s2d)_2(tdap)]^{2-}$	475	605	MeOH	–	0.30 μs	[245]
23 $[Ru(ddp)(DMCH)_2]^{2+}$	563	738	EtOH	0.009	650 ns	[103]
24 $[Os(Phen)_3]^{2+}$	432/478/660	691	CH_2Cl_2	–	6.0 ns	[250]
25 $[Os(dpp)_3]^{2+}$	454/500/580/650	729	CH_2Cl_2	–	4.6 ns	[250]
26 $[Os(bpy)_2(Nbpy)]^{2+b}$	490	800	Water	0.0096	12 ns	[155]
27 $[Os(dpp)_2(Nbpy)]^{2+}$	450	795	Water	0.013	15 ns	[155]
28 $[ReL(CO)_3CNR]^{+c}$	**a** 338 (0.43)	**a** 448	CH_2Cl_2	**a** 0.59	**a** 1.97 μs	[194]
	b 386 (0.7)	**b** 496		**b** 0.60	**b** 44.4 μs	
29 $Pt(ddp)(CN)_2$	293 (41.3)/375 (5.9)/357 (7.5)	630	Polyethylene glycol	–	1 μs	[122]

[a]Taken from [141]

[b]Nbpy = *N*-(6-aminohexyl)-4′-methyl-2,2′-bipyridine-4-carboxamide

[c]L = 2,2-bipyridine (**a**) or 1,10-phenanthroline (**b**) and R = *tert*-butyl

Optical oxygen sensors have been developed using various Ru(II) polypyridyl complexes such as $[Ru(bpy)_3]^{2+}$ **16** (bpy = bipyridyl) [142, 159, 235], $[Ru(dpb)_3]^{2+}$ **17** (4,4-diphenyl-2,2-bipyridine) [232], $[Ru(5\text{-}odap)_3]^{2+}$ **18** (5-odap = 5-octadecanamide-1,10-phenanthroline) [166], $[Ru(phen)_3]^{2+}$ **19** (phen = phenanthroline) [227], $[Ru(s2d)_3]^{4-}$ **21** (s2d = 1,10-phenanthroline-4,7-*bis*(phenylsulfonate)) also modified with 5-acetamide-1,10-phenanthroline (acap) **22a** or 5-tetradecanamide-1,10-phenanthroline (tdap) **22b** [245] (Fig. 6, Table 2). These indicators have not been as widely used as $[Ru(dpp)_3]^{2+}$ due to their lower quantum yield and shorter luminescent lifetime.

In general, one advantage of Ru(II) polypyridyl complexes is that they are fairly easy to prepare, reason why they are quite popular as indicators for early optical oxygen sensors; on the other hand, though they present many disadvantages they show only moderate molar absorption coefficients and therefore brightness, they possess relatively short lifetimes, their absorption and emission spectra are usually very broad which implies the use of specific filters and more expensive instrumentation and they suffer from pronounced cross talk to temperature since their triplet states are subjected to severe thermal quenching [140].

The absorption of the of Ru(II) complexes is located in the blue part of the spectrum (Table 2) which can be a severe limitation for many applications (particularly for in vivo measurements); thus, Klimant et al. [103] used Ru(II) complexes based on π-extended polypyridyl ligands ($[Ru(ddp)(DMCH)_2]^{2+}$ **23**), whose absorption and emission bands were bathochromically shifted of about 100 nm compared to the conventional Ru(II) complexes. Unfortunately, the brightness of the new indicators was too low (Φ did not exceed 1 %) and the decay times too short (<700 ns).

In an alternative approach, Demas et al. [250] focused their attention on Os(II) complexes which are analogous to the Ru(II) but can be excited in the red part of the spectrum and are therefore compatible with red LEDs and low-cost red lasers diodes. It has also been argued that the Os(II) complexes should be even more photostable and robust than the Ru(II) complexes as they present a larger energy gap between the emitting state and the photochemically destructive upper *dd* states [109]. Optical oxygen sensors have been developed using mainly two indicators: $[Os(phen)_3]^{2+}$ **24** and $[Os(dpp)_3]^{2+}$ **25** (Fig. 6) immobilized in poly (dimethylsiloxane) (PDMS) and in Gp-163 (an acrylate-modified PDMS). The luminescence lifetimes of such indicators in dichloromethane are in the nanosecond range which is much shorter when compared to the Ru(II) analogs; thus, only very highly oxygen-permeable materials can be adequate to obtain measureable responses. It should also be mentioned here that the luminescence quantum yields of the Os(II) are much lower than for the Ru(II) analogs (Table 2) which is a severe disadvantage.

Other two osmium polypyridyl complexes have been used by Bawendi et al. [155] in conjunction with nanocrystals as two-photon oxygen sensors for application in biological microenvironments; namely *bis*(2,2′-bipyridine)(*N*-(6-aminohexyl)-4′-methyl-2,2′-bipyridine-4-carboxamide) osmium(II), $[Os(bpy)_2(Nbpy)]^{2+}$ **26** and *bis*(4,7-diphenyl-1,10-phenanthroline)(*N*-(6-aminohexyl)-4′-methyl-2,2′-bipyridine-4-carboxamide) osmium(II), $[Os(dpp)_2(Nbpy)]^{2+}$ **27** (Fig. 7). The free amine groups of

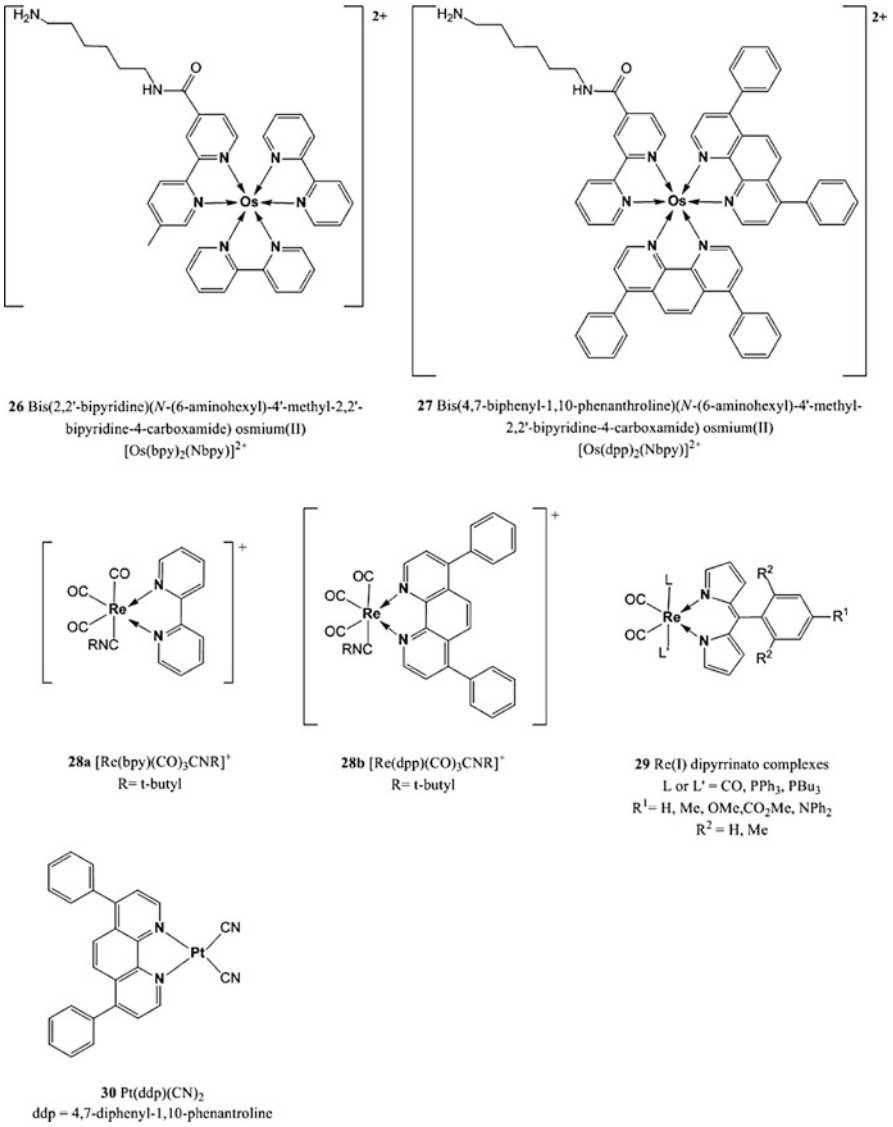

26 Bis(2,2'-bipyridine)(*N*-(6-aminohexyl)-4'-methyl-2,2'-bipyridine-4-carboxamide) osmium(II) $[Os(bpy)_2(Nbpy)]^{2+}$

27 Bis(4,7-biphenyl-1,10-phenanthroline)(*N*-(6-aminohexyl)-4'-methyl-2,2'-bipyridine-4-carboxamide) osmium(II) $[Os(dpp)_2(Nbpy)]^{2+}$

28a $[Re(bpy)(CO)_3CNR]^+$
R= t-butyl

28b $[Re(dpp)(CO)_3CNR]^+$
R= t-butyl

29 Re(I) dipyrrinato complexes
L or L' = CO, PPh_3, PBu_3
R^1= H, Me, OMe,CO_2Me, NPh_2
R^2 = H, Me

30 $Pt(ddp)(CN)_2$
ddp = 4,7-diphenyl-1,10-phenantroline

Fig. 7 Chemical structures of Os(II), Re(I), and Pt(II) polypyridyl complexes

the modified polypyridynes were linked to a carboxylic acid functionality of a semiconductor nanocrystal (NC) to afford a biologically stable amide bond; the resulting compounds possess absorption profiles that extend well into the red spectral region, leading therefore to a good overlap with the emission band of the NCs donors and allowing fluorescence resonance energy transfer from the semiconductor to the osmium complex. Since the NC emission is insensitive to oxygen, it can be used as an internal reference while the enhanced Os(II) emission can be exploited for sensing. However,

the aforementioned disadvantages of the Os(II) complexes are also valid for these indicators.

Also, Re(I) complexes have been used as oxygen indicators, however, their structure is different from the Ru(II) and Os(II) complexes since they contain only a single polypyridyl ligand and additional carbonyl ligands are necessary to obtain sufficient luminescence. $[Re(bpy)(CO)_3CNR]^+$ **28a** and $[Re(dpp)(CO)_3CNR]^+$ **28b** (Fig. 7) can be mentioned as an example. These dyes possess very high quantum yields (~0.7) and long lifetimes (>40 μs) but they lack significant absorption above 400 nm and their molar absorption coefficients are quite low (<7,000 M^{-1} cm^{-1}) [193, 194].

Recently, Telfer et al. [156] reported the first Re(I)-dipyrrinato complexes (**28c**) which in comparison with **28a** and **b**, have higher molar absorption coefficients (2.5–4.2 × 10^4 M^{-1} cm^{-1}) but much lower quantum yields (>0.01; Fig. 7).

Even though platinum complexes do not need extra ligands to increase their luminescence, a Pt(II) complex with a structure similar to **28** has been reported. $Pt(ddp)(CN)_2$ **29** is of interest since it is very soluble and stable in silicone rubber and shows no photochemical degradation (photophysical properties are shown in Table 2) [122]. Complex **29** being neutral can be mixed with silicone rubber quite easily and it does not leach into aqueous solutions. Moreover, $Pt(ddp)(CN)_2$ forms excimer upon irradiation and its emission can be easily monitored, therefore **29** can be used as spectroscopic probe of microenvironments inside polymers.

3. Metalloporphyrins

Among all the indicators that have been used for optical oxygen sensors, Pt(II) and Pd(II) porphyrins are the most popular luminophores since they possess strong phosphorescence at room temperature, moderate to high molar absorption coefficients and large Stokes' shifts. Additionally, phosphorescence lifetimes are rather long (microsecond to millisecond) and can be tuned by varying the nature of the central atom. As it can be noted from Table 3, in general, for each pair of metalloporphyrin complex the one in which M = Pd(II) shows much longer lifetimes with respect to the Pt(II) analog, this can be related to the increase in spin-obit coupling expected in the heavier metal [64]; on the other hand, platinum(II) complexes possess approximately two to three times higher emission quantum yields than the respective palladium(II) derivatives.

A large number of Pt(II) and Pd(II) pophyrin complexes have been synthesized and many have been modified during the years to improve the photophysical properties such as brightness, lifetime, photostability, and to tune the wavelength of absorption, in order to make the indicators suitable for oxygen sensing in different conditions and media.

Platinum and palladium complexes with octaethylporphyrin (PtOEP **30**, PdOEP **31**) remain popular indicators due to their strong room temperature phosphorescence with quantum yields of about 0.5 and 0.2, respectively, and long lifetimes under anoxic conditions (ca. 91 μs and ca. 990 μs, respectively) [177]. These indicators have been widely used as optical oxygen sensors and have been immobilized in various oxygen-permeable polymeric matrices such as polystyrene [104, 178],

Table 3 Photophysical properties of most common metalloporphyrin oxygen indicators

Dye	λ_{max}^{abs} (nm) ($\varepsilon \times 10^{-3}$ M^{-1} cm^{-1})	λ_{max}^{em} (nm)	Medium	Φ	τ	References
30 PtOEP	382/536	649	Toluene	0.41	75 μs	[115]
31 PdOEP	546	670	PS	0.20	990 μs	[177]
32 PtTFPP	390 (323)/504 (23.2)/538 (29.4)	647/710	CH_2Cl_2	0.088	60 μs	[123]
33 PdTFPP[a]	406 (192)/519 (18.2)/552 (15.5)	738	CH_2Cl_2	0.21	1.65 ms	[209]
34 PtTCPP	402 (210)/514 (21)	675	Water	0.01	34 μs	[222]
35 PdTCPP	418/523/556	700	DMF	–	–	[4]
36 PtOEPK[b]	398 (86.2)/592 (55.1)	758	$CHCl_3$	0.12	60 μs	[179]
37 PdOEPK[b]	410 (82.6)/603 (53.5)	789	$CHCl_3$	0.01	455 μs	[179]
38 PtTFPPL	396 (180)/574 (65.5)	733	3-Methyl pentane	–	72 μs	[102]
39 PdTFPPL	412 (120)/584 (39.2)	758	3-Methyl pentane	–	0.8 ms	[102]
40 PtTPTBP	430 (205)/614 (136)	770	Toluene	0.51	47 μs	[27]
41 PdTPTBP	443 (416)/628(173)	800	Toluene	0.21	286 μs	[27]
42 PtTPTBPF	430 (212)/615 (146)	773	Toluene	0.60	50 μs	[27]
43 PdTPTBPF	443 (268)/629 (115)	803	Toluene	0.23	297 μs	[27]
44 Pt1NF	434 (272)/628 (147)/638 (140)	815	Toluene	0.53	44 μs	[172]
45 Pd1NF	450 (202)/641 (74.0)/654 (72.6)	849	Toluene	0.18	203 μs	[172]
46 Pt2NF	438 (106)/652 (108)	835	Toluene	0.27	28 μs	[172]
47 Pd2NF	452 (190)/608 (102)/666 (142)	868	Toluene	0.12	138 μs	[172]
48 Pt3NF	441 (108)/635 (21.9)/667 (83.5)/678 (78.9)	870	Toluene	0.25	21 μs	[172]
49 Pd3NF	456 (138)/630 (17.0)/652 (22.0)/681 (63.8)/691 (60.0)	~882	Toluene	0.07	106 μs	[172]
50 PtTPTNP	436/689	883	Toluene	0.22	8.5 μs	[207]
51 PdTPTNP	465/721	948	Pyridine	0.08	63 μs	[72]
52 PtTBP$(CO_2Bu)_8$	416 (170)/609 (166)	745	Pyridine	0.51	50 μs	[73]
53 PdTBP$(CO_2Bu)_8$	426 (302)/618 (158)	770	DMF	0.23	400 μs	[73]
54 PdPh_4TBP $(CO_2Me)_8$	460 (251)/636 (87)	787	DMF	0.03	62 μs	[73]
55 PtNTBP	406 (106)/606 (61)/630 (137)	844	Toluene	0.22	40 μs	[31]
56 PdNTBP	421 (106)/619 (58)/642 (133)	875	Toluene	0.08	213 μs	[31]

(continued)

Table 3 (continued)

Dye	λ_{max}^{abs} (nm) ($\varepsilon \times 10^{-3}$ M^{-1} cm^{-1})	λ_{max}^{em} (nm)	Medium	Φ	τ	References
57 $PtN_{2\text{-cis}}TBP$	388 (51)/621 (147)	841	Toluene	0.17	20 μs	[31]
58 $PdN_{2\text{-cis}}TBP$	380 (33)/631 (98)	873	Toluene	0.05	101 μs	[31]
61 Oxyphor R2	415/524 (19)	690	Water	0.10	771 μs[c]	[63]
62 Oxyphor G2	442/632 (50)	790	Water	0.12	280 μs[c]	[63]
63 $PdTBP\text{-}(AG^2PEG)_8$	446/635	816	Phosphate buffer	0.03	270 μs	[130]
64 IrOER-CO-Cl	404 (165)/518 (15)/550 (31)	672	Toluene	0.14	97 μs	[115]
65 $Ir\text{-}OEP\text{-}Py_2$	389 (148)/509 (11)/539 (26.6)	655	Toluene	0.195	40 μs	[115]
66 $Ir\text{-}OEP\text{-}n\text{-}butIm_2$	390 (150)/508 (9.7)/541 (15)	655	Toluene	0.20	27 μs	[115]
67 $IR\text{-}OEP\text{-}CarbIm_2$	388 (142)/507 (10)/538 (18)[h]	652[d]	Toluene	0.21[d]	37 μs[e]	[115]

[a]Emission spectra Φ and lifetimes were measured in 3-methylpenthane at 77 K
[b]Emission spectra Φ and lifetimes were measured in a sodium sulfite solution
[c]Measured in deoxygenated condition at 23.5 °C and pH = 6.4
[d]In polystyrene at 25 °C
[e]Measured in EtOH

sol–gels [132, 133], poly(aryl ether ketone) [14], ethyl cellulose, cellulose acetate butyrate and polyvinylchloride [60], styrene-pentafuorostyrene copolymer film [9], and poly(1-trimethylsilyl-1-propyne) [6]. A general disadvantage of these indicators is their rather low photostability.

Platinum tetrakis(pentafuorophenyl)porphyrin (PtTFPP **32**) has received much attention and mostly replaced PtOEP because it shows much less photodeterioration [186]. The higher photostability of **32** compared to **30** is explained by the electron-withdrawing character of the perfluorophenyl substituents which reduces the electron density on the porphyrin ring thus rendering the PtTFPP less reactive toward oxidation by singlet oxygen [134]. PtTFPP possesses similarly long decay time (60 μs) and acceptable brightness when excited in the visible rage; it has been widely used as oxygen indicator in different types of matrices such as polystyrene [5, 134], fluoroacrylic polymer as a component of a pressure-sensitive paint [51, 186], in sol–gel [44, 45], poly(norobornene)s [213], and many other matrices. PtTFPP was also modified to be able to be polymerized and cross-linked with hydrophilic poly(2-hydroxyethyl methacrylate)-co-polyacrylamide or hydrophobic polystyrene to generate highly photostable and biocompatible sensing films [216]. Nucleophilic substitution of the *para*-fluorine atoms of the pentafuorophenyl groups allows covalent coupling to polymeric materials such as polystyrene copolymers [114] and silica gel [25]. Due to its excellent photostability, PtTFPP has been extensively used for those applications in which high light intensities are used, primary in fiber-optic microsensors and microscopy [69], but also in multi-analyte sensors and as components for pressure-sensitive paints [76].

The Pd(II) analogue **33** is characterized by a rather long lifetime (∼1 ms at room temperature); sensors based on this complex covalently attached to the surface of amino-modified silica–gel particles and dispersed in silicon rubber, show higher sensitivity with a dynamic range from 0.02 to 100 Pa and therefore can be used to measure trace level of oxygen. Both PtTFPP and PdTFPP were covalently immobilized on amino-functionalized silica–gel particle to obtain heterogeneous sensing materials which possess high photostability and fast response time [25].

Platinum and palladium tetrakis(4-carboxyphenyl)porphyrin (PtTCPP **34** an PdTCPP **35**) do not possess very high quantum yields or long lifetimes; nevertheless, several sensors using these compounds have been reported [4, 10, 146]. The metal complexes can be chemisorbed on alumina because of the formation of a stable bond between alumina and the carboxyl group of the TCPP.

More exotic oxygen sensors relied on platinum(II) and palladium(II) complexes with cationic water-soluble porphyrins which were electrostatically immobilized in the negatively charged fluorinated Nafion® membrane [221]. The sensors were shown to be suitable for measurements of oxygen in gas phase but their performance in aqueous solutions, evidently, may be compromised by ionic species.

The brightness (defined as the product of the molar absorption coefficient ε and the quantum yield Φ) of the Pt(II) and Pd(II) complexes with OEP and TFPP is very good upon excitation in the Soret band (UV/violet light) due to high molar absorption coefficients for this transition (Table 3). However, excitation in the Q bands located in the green part of the spectrum (which is often more

preferable) is about tenfold less efficient. Therefore, rather thick sensing layers are necessary to insure sufficient absorption and a good S/N ratio. This results in slower dynamic response of the sensors. Also, if used in the form of oxygen-sensitive nanoparticles higher concentration of those is required and this can disturb biological systems. To overcome this drawback, Mayr and co-workers proposed an approach to enhance the brightness of oxygen (and other optical sensors) via light harvesting [151]. Here, excitation is performed via an antenna dye which is added along with an oxygen indicator; the latter becomes excited via the Föster Resonance Energy Transfer.

The indicators described so far efficiently absorb light only in the UV–vis region and therefore suffer from some drawbacks: (1) high level of autofluorescence is produced upon excitation in the UV–vis since many natural compounds which are present in biological samples, such as nucleotides FAD and NAD, are fluorescent, (2) they are poorly suitable for measurements in scattering media such as marine sediments or tissues, (3) they cannot be used in implantable sensors since blood efficiently absorbs in visible region.

Excitation in the red part of the spectrum is strongly preferred not only because it allows sensing in highly scattering media and in tissue but also because it can be combined with cheaper optical components; for example, the sensitivity of cheap and compact Si photodiodes increases at wavelengths longer than 600 nm and reaches a maximum at 850–900 nm [27]. For these reasons, red-excitable and NIR-emitting indicators are becoming increasingly popular for the development of optical oxygen sensors to be used in marine sediments, in blood, in cells, or in tissues.

Compared to the metalloporphyrins described above, platinum(II) and palladium(II) complexes with porphyrin ketones (PtOEPK **36**, PdOEPK **37**) and porphyrin lactones (PtTFPPL **38**, PdTFPPL **39**) possess bathochromically shifted absorption peaking at 570–600 nm. Unfortunately, these dyes have only moderate emission in the NIR (Table 3).

The Pt(II) and Pd(II) porphyrin ketones which were obtained via oxidation of the porphyrin macrocycle and displayed high photochemical stability [177]. PtOEPK and PrOEPK display room temperature phosphorescence with reasonable quantum yield, particularly the Pt(II) complex ($\Phi_P > 0.1$), and long lifetimes (60 μs for the Pt(II) and 455 μs for the Pd(II) complexes) but only moderate to low brightness; they have been used in different matrices such as polystyrene and polyvinylchloride which influenced the dynamic range of the sensors [104, 111, 217].

Recently, Nock et al. [173] applied the platinum(II) octaethylporphyrinketone/polystyrene probe for measurements of both gaseous and dissolved oxygen in microfluidic devices. Platinum(II) and palladium(II) tetra(pentafluorophenyl)porpholactone are similar in their spectral properties to the complexes of porphyrin–ketones and show phosphorescence lifetimes that are about 60 % that of the unmodified TFPP complexes (~70 μs for PtTFPPL and ~1 ms for PdTFPPL). The lactone ring was produced from the parent free-base porphyrin via oxidation and it is responsible for a shift in the emission spectra toward longer wavelengths; also, the lactone functionality makes this indicators even more stable toward photo-oxidation [102].

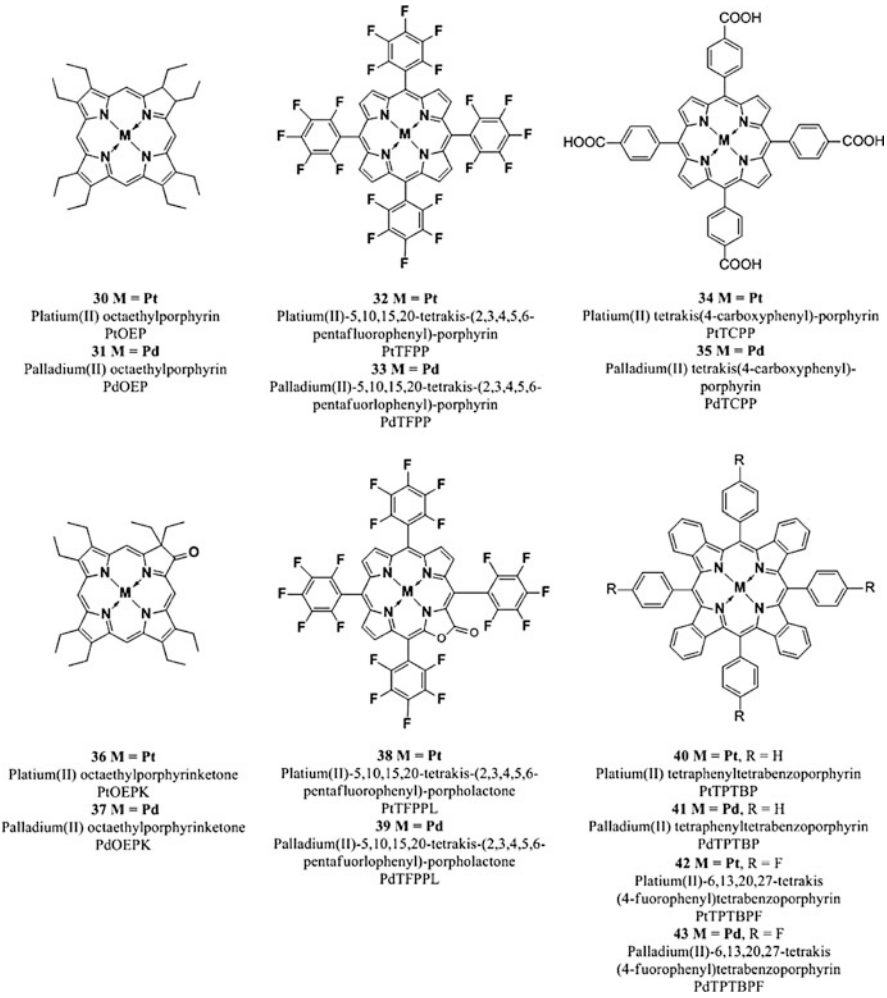

Fig. 8 Chemical structures of Pt(II) and Pd(II) porphyrin complexes

Palladium(II) and platinum(II) complexes with benzo- [188] and naphthoporhyrins [73, 188, 191] represent another group of the NIR oxygen indicators. These dyes belong to the class of π-extended porphyrins which are characterized by an extended aromatic fragment fused on the porphyrin core; this feature is responsible for the bathochromic shift of the absorption and emission bands.

The complexes possess excellent brightness upon excitation both in the blue and red region due to very high molar absorption coefficients and quantum yields. For example, molar absorption coefficients for the platinum(II) and palladium(II) complexes with tetraphenyltetrabenzoporphyrin PtTPTBP **40** and PdTPTBP **41** (Fig. 8), respectively, exceed 200,000 M^{-1} cm^{-1} for the blue region and 130,000 M^{-1} $cm^{-1}$for the red region, and the emission quantum yields are about 0.50 and 0.20, respectively. The Pd(II) complexes with

tetraphenyltetrabenzoporphyrin are water insoluble and not cell penetrating, but once incorporated into polystyrene nanoparticle, functionalized with polyethylene glycol (PEG) and an antibody, they were successfully used for in vivo imaging [170].

PtTPTBPF **42** and PdTPTBPF **43** (Fig. 8) are obtained by substitution of the hydrogen to fluorine in the *meso*-phenyl rings, which slightly improves the luminescence quantum yield of both Pt(II) and Pd(II) complexes (Table 3) and enhances their photostability [27].

Solubility of an indicator in polymeric matrices is an important parameter for its application in optical sensors; planar π-extended porphyrins were shown to aggregate readily, but substituents in the *meso*-position of the porphyrin ring significantly improve their solubility. For example, *meso*-substituted benzoporphyrins as **40**, **41**, **42**, and **43** show a low tendency to aggregate in nonpolar polymers such as polystyrene [28].

In general, when dissolved in polystyrene, the Pt(II) *meso*-substituted benzoporphyrins are ideally suitable for measurements from 0 to 100 % air saturation while the analog Pd(II) dyes, as they show a significantly higher sensitivity to oxygen with decay times in the order of 300 μs, are more adequate for trace oxygen sensing because their luminescence is almost completely quenched at air saturation. However, the Pd(II) complexes could be used to measure oxygen up to air saturation when incorporated into polymers with lower oxygen permeability such as poly(styrene-*co*-acrylonitrile).

NIR indicators efficiently absorb light at wavelengths higher than 600 nm; therefore, they have the potential to be used in the so called "smart tattoos". These are sensors that are implanted into subcutaneous tissues and can be exploited for continuous noninvasive monitoring of vital analytes like oxygen or glucose [28]. Further, bathochromic shifts of the absorption and emission can improve the performance in such applications even more. This can be realized by further extension of the π-system as for tetranaphthoporphyrins TNP (Fig. 9). Compared to the benzoporphyrins, the absorption (for the Q bands) and emission of these dyes shift bathocromically by about 80 nm (Table 3). Unfortunately, this is accompanied by the decrease in the phosphorescence quantum yields ($\Phi_P = 0.22$ for PtTPTNP **50** and $\Phi_P = 0.079$ for PdTPTNP **51**) [71, 73]. Even more importantly, the photostability of these dyes decreases dramatically [148] in comparison with the corresponding tetrabenzoporphyrins; which can compromise potential application in oxygen sensing, organic light-emitting diodes (OLEDs) [207], and photovoltaics [52].

Lower solubility of the *meso*-tetraphenyltetranaphthoporphyrins is another drawback, but other more soluble derivatives are known and will be discussed below. It should be mentioned here that a synthetic way to render halogenated naphthoporphyrins significantly more photostable and better soluble have been recently described [70]. However, the multistep synthesis of precursors and the porphyrins is not unchallenging.

Hybrid benzo- and naphthoporphyrin complexes of platinum(II) and palladium(II) with tunable spectral properties were reported by Niedermair et al. [172] The photophysical properties of the platinum(II)-*meso*-tetra-(4-fluorophenyl)-mononaphthotribezoporphyrin (Pt1NF **44**), the *cis*-platinum(II)-*meso*-tetra-(4-fluorophenyl)

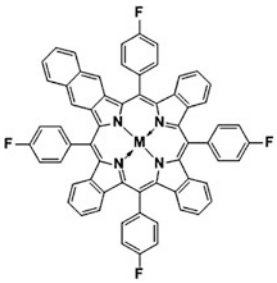

44 M = Pt
Platinum(II)-*meso*-tetra-(4-fuorophenyl) mononaphthotribenzoporphyrin
Pt1NF
45 M = Pd
Palladium(II)-*meso*-(4-fluorophenyl) mononaphthotribenzopophyrin
Pd1NF

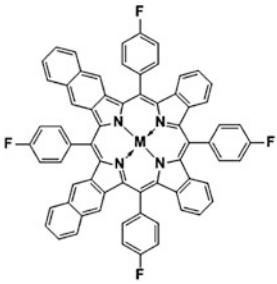

46 M = Pt
cis-Platinum(II)-*meso*-tetra-(4-fluorophenyl) dibenzodinaphthoporphyrin
*cis*Pt2NF
47 M = Pd
cis-Palladium(II)-*meso*-tetra-(4-fluorophenyl) dibenzodinaphthoporphyrin
*cis*Pd2NF

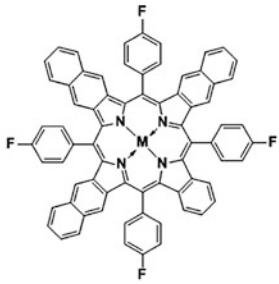

48 M = Pt
Platinum(II)-*meso*-tetra-(4-fluorophenyl) monobenzotrinaphthoporphyrin
Pt3NF
49 M = Pd
Palladium(II)-meso-tetra-(4-fluorophenyl) monobezotrinaphthoporphyrin
Pd3NF

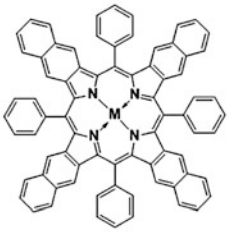

50 M = Pt
Platinum(II) tetraphenyl tetranaphthoporphyrin
PtTPTNP
51 M = Pd
Palladium(II) tetraphenyl tetranaphthoporphyrin
PdTPTNP

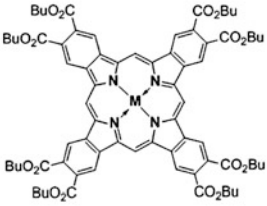

52 M = Pt
Platinum(II) tetrabenzoporphyrin octabutylester
$PtTBP(CO_2Bu)_8$
53 M = Pd
Palladium(II) tetrabenzoporphyrin octabutylester
$PdTBP(CO_2Bu)_8$

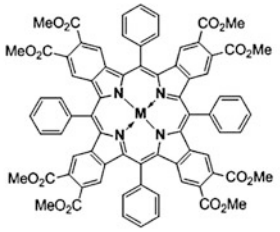

54 M = Pd
Palladium(II) tetraphenyltetrabenzoporphyrin octamethylester
$Pd\text{-}Ph_4TBP(CO_2Me)_8$

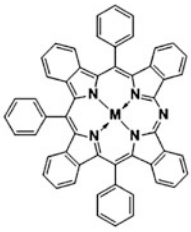

55 M = Pt
Platium(II)-6-aza-13,20,27-triphenyltetrabenzoporphyrin
PtNTBP
56 M = Pd
Palladium(II)-6-aza-13,20,27-tetraphenyltetrabezoporphyrin
PdNTBP

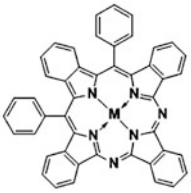

57 M = Pt
Platium(II)-6,13-diaza-20,27-triphenyltetrabenzoporphyrin
$PtN_{2\text{-}cis}TBP$
58 M = Pd
Palladium(II)-6,13-diaza-20,27-tetraphenyltetrabezoporphyrin
$PdN_{2\text{-}cis}TBP$

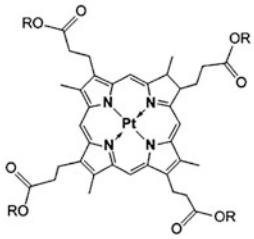

59 M = Pt
Platium(II) coproporphyrin
PtCP
60 M =Pd
Palladium(II) coproporphyrin
PdCP

R = peptide

Fig. 9 Chemical structures of Pt(II) and Pd(II) porphyrin complexes

dibenzodinaphthoporphyrin (*cis*-Pt2NF **46**) and the platinum(II)-*meso*-tetra-(4-fluorophenyl)monobenzotrinaphthoporphyrin (Pt3NF **48**) and the corresponding palladium(II) complexes (Pd1NF **45**, cis-Pd2NF **47**, Pd3NF **49**; Fig. 9) are reported in Table 3. These complexes absorb intensively in the near-infrared region between 628 and 691 nm (the higher the number of the naphtha moieties annealed to the porphyrin system, the higher the bathochromic shift) and emit at room temperature between 815 and 882 nm. The phosphorescence quantum yields decrease with the number of naphtha moieties and they range from 0.53 to 0.25 for the Pt(II) complexes and from 0.18 to 0.07 for the Pd(II) complexes. The luminescence decay times follow the same trend decreasing from 44 to 21 μs for the Pt(II) complexes and from 203 to 106 μs for the analog Pd(II) complexes; therefore, it can be stated that the sensitivity to oxygen is affected and gradually reduces upon substitution. It has been reported that the decrease in photostability of these indicators correlates well with the number of naphtho moieties annealed to the porphyrin system. Thanks to their tunable properties, the described chromophores are good candidates for different multiplexing applications as for example the simultaneous measurement of glucose and oxygen in enzymatic sensors [172].

Platinum(II) and palladium(II) tetrabenzoporphyrin-octabutylester ($PtTBP(CO_2Bu)_8$ **52**, $PdTBP(CO_2Bu)_8$ **53**; Fig. 9) and the palladium(II) tetraphenyltetrabenzo-porphyrin-octamethylester ($(Pd\text{-}Ph_4TBP)CO_2Me)_8$ **54** (Fig. 9) represents another variation in the class of π-extended porphyrins which were synthesized and characterized by Vinogradov and co-workers [73].

The absorption bands of the *meso*-unsubstituted tetrabenzoporphyrins (**52** and **53**) are blue shifted by about 10–30 nm when compared to the corresponding bands of the TPTBP analog (**40–41**; Table 3) while the emission decay times and quantum yields are comparable.

Another class of red excitable dyes for optical oxygen sensing is the platinum(II) and palladium(II) complexes with azatetrabenzoporphyrins recently reported by Borisov et al. [31]. These compounds can be viewed as hybrids between tetrabenzoporphyrins and phthalocyanines and combine the advantages of both. Pt(II) and Pd(II) phthalocyanines are characterized by extremely good chemical, thermal, and photostability but their phosphorescence quantum yields are very poor ($\Phi_P < 0.01$) [190] which makes them hardly feasible for optical sensing or imaging of oxygen. The photophysical properties of platinum(II) 6-aza-13-20-27-triphenyltetrabenzo-porphyrin (PtNTBP **55**), platinum(II) 6-aza-13-20-27-triphenyltetrabenzoporphyrin ($PtN_{2\text{-}cis}TBP$ **57**) and the corresponding palladium(II) analog (PdNTBP **56**, $PdN_{2\text{-}cis}$ TBP **58**) are reported in Table 3. When compared to the respective TPTBP complexes, they show a hypsochromic shift of the Soret band and a bathochromic shift of the Q bands. In general, the decay times and the emission quantum yields of complexes **55–58** are lower when compared to the ones of the respective *meso*-tetraphenyltetrabenzoporphyrins; but despite this, the brightness of such indicators is quite adequate for practical applications and the lower sensitivity can be exploited in application where the oxygen partial pressure is higher than 21 kPa (e.g., in photosynthetic systems). Importantly, the aza-modified complexes were shown to possess a much higher photostability than the corresponding TPTBP complexes.

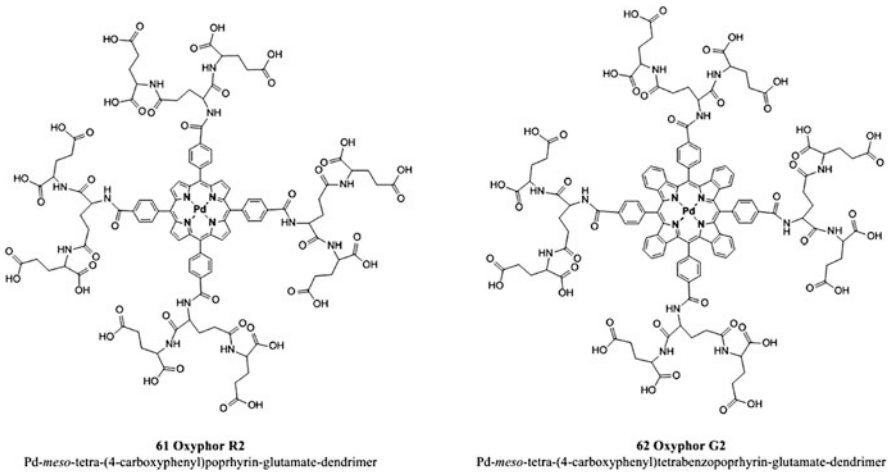

Fig. 10 Chemical structure of Oxyphor R2 and Oxyphor G2

Porphyrin conjugates and dendrimers represent another group of oxygen probes and have been reported both for non-extended and π-extended porphyrins. Usually, the aim of the synthetic modifications is to provide additional functionality (water solubility, partial shielding from oxygen and other species, cell penetration, recognition of specific cells or cellular components, etc.).

Recently, Papkovsky and co-workers [57] reported on a panel of phosphorescent oligoarginine conjugates of tetracaboxylic Pt(II) and Pd(II)-coproporphyrin I (PtCP **59** and PdCP **60**; Fig. 9) mono or tetra-substituted, which were successfully used for sensing intracellular oxygen thanks to their ability to penetrate cells. The authors showed that all the Pt(II)-tetra-substituted conjugates displayed absorption spectra that were similar to those of the free PtCP; on the other hand, it was reported that the conjugation with peptides had a significant decreasing effect on the emission quantum yield (see Supporting Information of [57]) while all the PtCP conjugates displayed very similar phosphorescence lifetimes (20–23 μs in air saturated and ~80 μs in deoxygenated media).

The corresponding PdCP conjugates, as expected, showed significantly longer unquenched phosphorescence lifetimes (~1 ms) and therefore are better suited to measure oxygen at very low concentrations.

Metalloporphyrins are generally hydrophobic and therefore insoluble in water or in physiological fluids; they therefore need to be modified by addition of "molecular coats" in order to enhance their interactions with the environment when used, for example, to measure the oxygenation of tumors in vivo [63]. Oxyphors R2 **61** and G2 **62** (Fig. 10) have been constructed by modification of Pd(II)-*meso*-tetra (4-carboxyphenyl)-porphyrin and Pd(II)-*meso*-tetra (4-carboxyphenyl)-tetrabenzoporphyrin, respectively, and are the second generation of polyglutamic dendrimers. The outer layers of the dendrimers have 16 carboxylate groups which are responsible for both their solubility in biological fluids and their inability

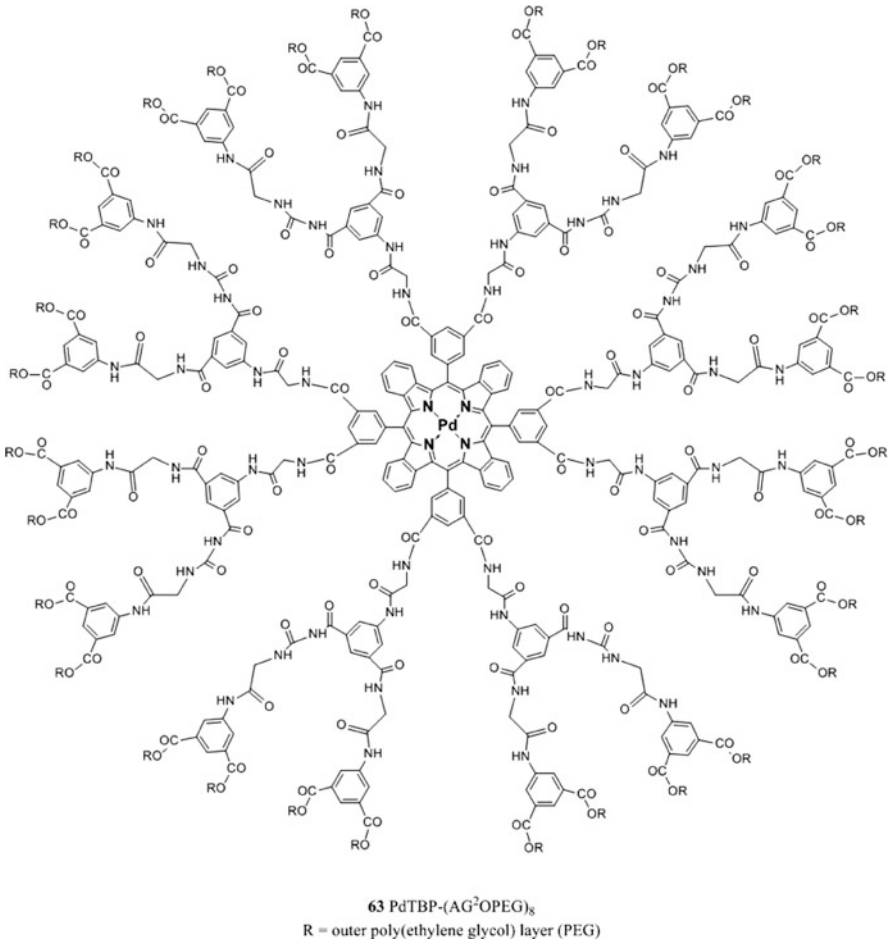

Fig. 11 Schematic structure of PEG modified PdTBP-dendrimer

to pass through biological membranes. The photophysical properties of the two dendrimers are shown in Table 3 and it can be highlighted that Oxyphor **G2** could be the indicator of choice when measuring tissue oxygenation that require light penetration into the depths of tissue since it has an absorption band near 632 nm.

The same phosphor **G2** was incorporated into nanoparticles (PEBBLES) modified with peptides to be used for intracellular oxygen measurements [135]. Metalloporphyrins of palladium(II) and platinum(II) have been also encapsulated into poly(arylglycine) dendrimers modified with poly(ethyleneglycol) residues in order to enhance the dye's solubility, diminish its toxicity and help preventing its interaction with the biological environment when used in vivo [130]. The dendrimer folds in aqueous environments and creates a diffusion barrier for oxygen which can be exploited to regulate the sensitivity and the dynamic range

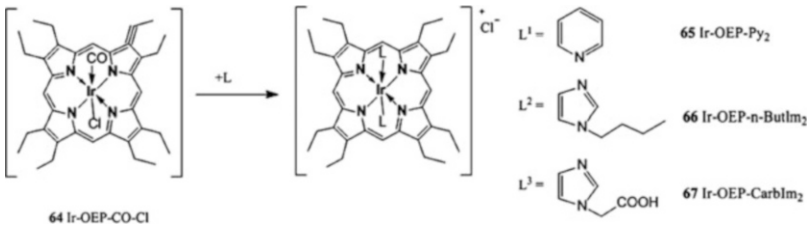

Fig. 12 Chemical structures of Ir(III) porphyrins complexes

of the probe. The photophysical properties of such a probe PdTBP-$(AG^2OPEG)_8$ **63** (Fig. 11) are reported in Table 3. Several other water-soluble dendrimers were reported recently by the same group [66]. Vinogradov and co-workers have also reported dendrimeric oxygen probes bearing coumarin antennas along with a porphyrin core [32, 74]. These probes were found useful for application in two-photon microscopic imaging of oxygen distribution in tissues due to the fact that the coumarin antennas increased the efficiency of the two-photon excitation compared to the dendrimers solely based on the benzoporphyrin complexes.

It should be mentioned here that lipophilic porphyrins encapsulated into water-dispersible nanoparticles represent an alternative to dendrimeric oxygen probes and often perform similarly despite their significantly larger dimensions (typically tens of nanometer). The polymer of the particle provides necessary protection for the indicator dye from the environment and helps to tune oxygen sensitivity. The functional groups on the surface of the particles not only render them water-dispersible but also can enable, e.g., cell penetration [69].

Recently, Koren et al. [115] reported the synthesis and characterization of new Ir(III) porphyrin complexes. In contrast to the square planar Pt(II) and Pd(II) porphyrins, the new hexa-coordinating complexes showed quite interesting photophysical properties which could be tuned by modification of the axial ligands, modifications that demonstrated to have an influence also on the solubility of the complexes. Three different indicators were synthesized from the same parent complex (Ir-OEP-CO-Cl **64** - Fig. 12) by ligand exchange and their photophysical properties are reported in Table 3 together with the ones of the parent complex **64**. The positively charged complexes Ir-OEP-Py_2 **65**, Ir-OEP-*n*-$butIm_2$ **66**, and Ir-OEP-$CarbIm_2$ **67** with two similar axial ligands show similar properties, in contrast to the neutral Ir-OEP-CO-Cl; they all have relatively high phosphorescence quantum yields (up to 21 %) but shorter decay times. The absorption and emission spectra of **65–67** are bathochromically shifted compared to the Pt(II) complexes and therefore they can be excited with visible light directly in the Soret band (Fig. 12).

The axial ligands can be used not only to modify the solubility of the complexes but also to introduce functional groups to enable, for example, covalent coupling. For example, very recently, Koren et al. [116] directly attached short peptides to

Table 4 Photophysical properties of cyclometallated complexes of Ir(III) and Pt(II)

Dye	λ_{max}^{abs} (nm) ($\varepsilon \times 10^3$ M^{-1} cm^{-1})	λ_{max}^{em} (nm)	Medium	Φ	τ	References
68 $Ir(ppy)_3$	376	512	THF	0.90	1.5 μs	[7]
69 $Ir(ppy\text{-}NPh_2)_3$	405	527	2-MeTHF	0.70	4.3 μs	[149]
70 $Ir(btpy)_3$	292 (67.6)/366 (20.4)/408 (21.8)	596	$CHCl_3$	–	8.6 μs[a]	[77]
		645				
71 N-948[b]	494	665	CH_2Cl_2	0.58[b]	102 μs[c]	[157]
72 $Ir(C_N)_2(acac)$	450 (57.1)/421 (86.9)	545	$CHCl_3$	0.53	8.5 μs	[24]
73 $Ir(C_O)_2(acac)$	467 (53.7)/443 (47)	552	$CHCl_3$	0.34	10.7 μs	[24]
74 $Ir(C_{S\text{-}Me})_2(acac)$	471 (75.4)/441 (77.8)	564	$CHCl_3$	0.44	11.3 μs	[24]
75 $Ir(C_S)_2(acac)$	472 (92.8)/444 (86.8)	563	$CHCl_3$	0.54	11.3 μs	[24]
76 $(C_N)_2Ir(\mu\text{-}Cl)_2Ir(C_N)_2$	463 (87.6)/433 (133.6)	568	$CHCl_3$	0.30	9.7 μs	[24]
77 $(C_S)_2Ir(\mu\text{-}Cl)_2Ir(C_S)_2$	482 (136.5)/457 (136.9)	587	$CHCl_3$	0.21	13.1 μs	[24]
78 $Ir(C6)_2(vacac)$	445[d] (77.9)/474[d] (86.9)	568	Toluene	0.22	6.0 μs	[55]
80 $Pt(thpy)_2$	470 (2)	~590	Acetonitrile	0.36	4.8 μs	[59]
81 $C\hat{}N_1Pt(acac)$	459 (13.0)	502	Toluene	0.95[e] 0.22[e]	0.06 ns 1.53 μs	[143]
		535				
		683				
		753				
82 $C\hat{}N_2Pt(acac)$	474 (21.7)	521	Toluene	3.03[e]	0.14 ns	[143]
		556				
		692		0.57[e]	3.74 μs	
		762				
83 $C\hat{}N_3Pt(acac)$	243 (52.0) 390 (33.7)	455	CH_2Cl_2	1.1[e]	3.2 ns	[244]
		638			6.6 μs	
84 $C\hat{}N_4Pt(acac)$	357 (1.73) 400 (0.41)	386 538	CH_2Cl_2	18.2[e]	25 ns	[244]
					25.5 μs	
85 $C\hat{}N_5Pt(acac)$	292 (2.76) 396 (0.51)	536	CH_2Cl_2	32.3[e]	5.4 μs	[244]
86 $C\hat{}N_6Pt(acac)$	234 (38.1) 339 (25.1)	575	CH_2Cl_2	9.1[e]	15.8 μs	[244]
87 $C\hat{}N_7Pt(acac)$	335 (2.68) 400 (0.63)	560	CH_2Cl_2	4.5[e]	0.86 μs	[244]
88 dppe-Pt2P	344[d] (12.4)/496[d] (3.2)	677	DMSO	0.002	0.2 ns	[220]
		732		0.01	8.66 μs	

[a]Measured at 50 mbar air pressure and 1 °C

[b]*N*-948 = Ir(2-phenylpyridine)$_2$(4,4′-*bis*(2-(4-*N*,*N*-methylhexylaminophenyl)ethenyl)-2,2′-bipyridine)

[c]When incorporated in polystyrene (PS)

[d]Measured in dichloromethane

[e]Obtained in toluene with $Ru(byp)_2(phen)[PF_6]_2$ as the standard

the Ir(III) complex via a hystidine unit at the *N*-terminus of the peptide and used the new probes for oxygen imaging in mammalian cells.

Very recently, an oxygen probe based on a copolymer of a Pt(II) porphyrin and 9,9-dioctylfluorene has been reported [246]. The conjugated polymer combines the properties of a luminescent indicator and a polymeric matrix and, more importantly, possesses dual emission under UV/violet excitation which originates from the fluorene (oxygen-independent fluorescence) and Pt(II) porphyrin (oxygen-dependent phosphorescence). Thus, ratiometric sensing and imaging becomes possible; the authors also demonstrated that the ratio of the emission intensities can be adjusted by varying the ration of fluorene/Pt(II) porphyrin units.

4. Cyclometallated complexes

Another class of indicators which have been exploited for oxygen sensing is represented by the cyclometallated complexes of Ir(III) and Pt(II). The last decade has seen an enormous progress in the field of luminescent cyclometallated complexes which was driven by the development of OLED technology. Some of these dyes were also applied as oxygen indicators.

In general, thesee complexes show high luminescence quantum yields, have large Stokes' shift and are photostable. However, their luminescence decay times are in order of several microseconds; therefore, usually much shorter than the one of metalloporphyrins, also their absorption in the visible region is not efficient (ε rarely exceeds 10,000 M^{-1} cm^{-1}).

The *tris*(2-phenylpyridine) iridium(III) [Ir(ppy)$_3$] **68** displays a very strong green luminescence with high quantum yield (0.90) and relatively long lifetime (1.5 μs; Table 4). The molar absorption coefficient in the visible region is comparable to other cyclometallated compound and is rather low (<10,000 M^{-1} cm^{-1}) [126]. This indicator has been used as oxygen sensor immobilized in different matrices such as: poly(styrene-*co*-trifluoroethylmetacrylate (TFEM)) in which it showed quite good photostability [7], Ormosil where it was used as a transducer for the detection of uric acid [201], and poly(dimethylsiloxane) which was functionalized with the Ir(III) complex and blended with polystyrene [117]. Very recently, complex **68** has been modified to be suitable for imaging living cells; to enable cellular uptake the phenylpyridine ligands were functionalized with three different amino acids (lysine, alanine, and glycine) [211]. The modified complexes were shown to possess relatively high cellular uptake but, compared to **68**, their quantum yields were only moderate (< 0.2).

A substitution of the ppy ligands in complex **68** with ppy-NPh_2 leads to the formation of a new cyclometalated indicator: [Ir(ppy-NPh_2)$_3$] **69** which has the advantage of being less sensitive to self-quenching and is even better soluble in organic solvents and organic polymers [149]. Complex **69** has a high phosphorescence quantum yield (∼70 %), lifetime in the order of several microseconds (Table 4), can be excited at 405 nm and therefore is compatible with low-cost LED as excitation source and its excitation and emission spectra are well shifted. A third complex possessing the same skeleton as **68** has been used as red-emitting dye: the *tris*{2-(benzo[b]thiophene-2-yl)pyridinato-C^3,N}iridium(III) **70**; which

is characterized by large Stokes' shift and a lifetime of 8.6 μs that is suitable for lifetime imaging application. However, similarly to other cyclometallated complexes the absorption is very efficient only in the UV region (ε as high as 60,000 M^{-1} cm^{-1} at 292 nm Table 4). $Ir(btpy)_3$ has been used, along with a green-emitting iridium dye, in a dual pressure and temperature sensitive paint [77]. The barometric dye **70** was incorporated in a cellulose acetate butyrate film and the cross-sensitivity to temperature was efficiently corrected by simultaneous optical determination of the temperature.

The [Ir(2-phenylpyridine)2(4,4′-*bis*(2-(4-N,N-methylhexylaminophenyl)ethyl)-2,2′-bipyridine)Cl] **71** which for convenience was given the name N-948 possesses luminescent emission at a wavelength higher than 650 nm (665 nm; Table 4). N-948 was shown to have quite good quantum yields ($\Phi_P > 0.50$), extraordinary long decay time (102 μs when incorporated in polystyrene) and high lipophilicity which increase its retention in rather apolar polymeric films. N-948 was incorporated in both polystyrene and a nanostructured metal oxide matrix which increased its photostability and resistance to heat and γ-irradiation during sterilization.

As was mentioned above, rather low molar absorption coefficients of the cyclometallated complexes represent a serious disadvantage for their application as oxygen indicators. Cyclometalated iridium(III) complexes with coumarins overcome this drawback [24, 126]. Such indicators are characterized by efficient visible absorption in the blue part of the spectrum (ε as high as 90,000 M^{-1} cm^{-1}; Table 4) and very strong phosphorescence ($\Phi_P \sim 0.50$) which results in an exceptionally high brightness and makes them attractive for application in thin films to monitor fast processes and different types of nano- and microparticles. The photophysical properties of cyclometalated Ir(III) coumarin complexes of general formula $Ir(C_X)_2(acac)$ where $X = N$ (**72**), O (**73**), S-Me (**74**) and S (**75**) are reported in Table 4 and their chemical structures shown in Fig. 13. The coumarin substituent represents a rather flexible system in respect to fine-tuning of spectral properties of the complexes, which depend on the X substituent of the coumarin: the bathochromic shift increases when $X = N > O > S$ [24]. As already mentioned, these indicators show high luminescence brightness ($\varepsilon \times \Phi_P$ exceeds 50,000 for $Ir(C_S)_2(acac)$ and it is as high as 46,000 for $Ir(C_N)_2(acac)$). It should be also mentioned that all the complexes **72–75** can be efficiently excited with 425, 435, and 450 nm LEDs and possess relatively sharp excitation and emission bands therefore are suitable for multi-analyte sensing. The phosphorescent decay times for this class of ultrabright indicators are of ~10 μs for all the complexes which insures good sensitivity in polystyrene-based materials [24].

The dimeric coumarin complexes of general formula $(C_X)_2Ir(\mu\text{-}Cl)_2Ir(C_X)_2$ were also investigated (**76–77**, Fig. 13). However, the emission quantum yields are lower than the respective monomeric complexes (Table 4). The absorption and emission maxima of the dimeric complexes shift bathochromically and in general the shift in the emission maxima is more pronounced.

De Rosa et al. presented a derivative of a coumarin complex, $Ir(C6)_2(vacac)$ **78** (Fig. 13) which was covalently bound to a polymeric support (silicone rubber) to eliminate dye aggregation. Unfortunately, the indicator in this case exhibited lower

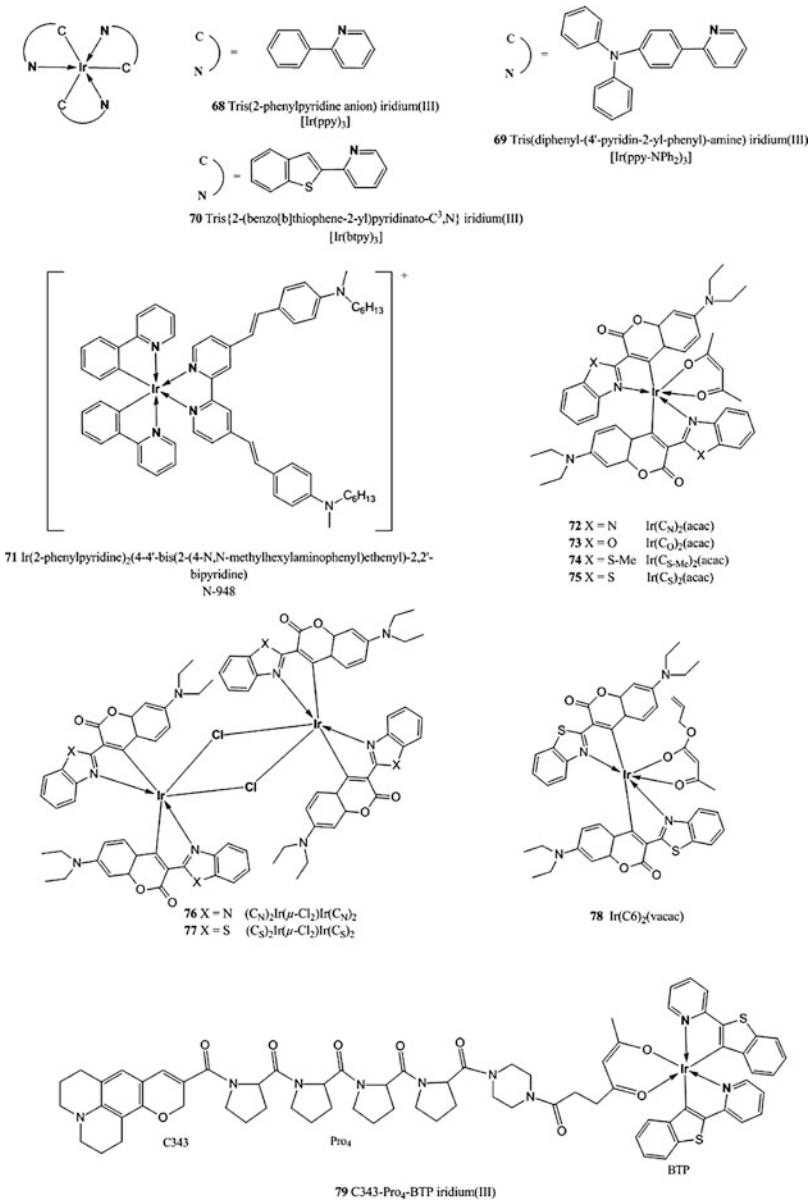

Fig. 13 Chemical structures of selected Ir(III) cyclometallated complexes

brightness in respect to the unbounded derivative. Nevertheless, complex **78** displayed good quantum yields and luminescence lifetime (Table 4) and was suggested as a good candidate for PSP studies [55].

Very recently, Yoshihara et al. [254] presented a novel intrinsic ratiometric molecular probe, the C343-Pro$_4$-BTP **79** (Fig. 13) which consists of an oxygen-sensitive phosphor (Ir(III)BTP, BTP = *bis*(2-(2′-benzothienyl)-pyridinato-N,C^3)) connected to an oxygen-insensitive fluorophore (coumarin C343) by a tetraproline linker. Ideally, this probe was designed to measure local oxygen levels in living cells and tissue but currently cellular uptake is too low to perform quantitative analysis but the proline linker can be modified to enhance the delivery to cells.

As previously mentioned, also Pt(II) cyclometalated complexes have been used as indicators for oxygen sensors and a selection is reported here. *Cis-bis* [2-(2′-thienyl)pyridine]platinum(II), Pt(thpy)$_2$ **80** was selected as a luminophore for sensing O_2 concentration in seawater [59]. This indicator can be easily excited with blue LED as it absorbs light up to 500 nm, it possesses high luminescence quantum yield ($\Phi_P = 0.36$) and an excited-state lifetime of 4.8 μs. The non-ionic character makes it basically insoluble in water and therefore it is not susceptible to leaching in presence of water. Similarly to the analogous Ir(III) complexes, cyclometallated Pt(II) indicators possess moderate to low absorption in the visible part of the spectrum. It should be mentioned here that as recently demonstrated by Hanson et al. [90], the visible absorption of the cyclometallated complexes can be enhanced by introducing a highly absorbing ligand in addition to the cyclometallated one. Although this approach has not yet been applied in oxygen sensors, it represents an elegant solution.

As mentioned earlier in this review, it would be highly desirable to design a ratiometric sensor for imaging which uses a single molecule. Only few examples of such indicators were found in the literature, which is understandable since such probes are not easy to design, it is in fact difficult to predict if a molecule will show both fluorescent and phosphorescent emissions and in comparable quantum yields. Some examples of such indicators were recently reported by Zhao et al. [143, 244]. They entailed cyclometalated Pt(II) complexes of general formula CˆNPt(acac), some of which show dual fluorescence and phosphorescence emission. The structures of complex **81–87** are shown in Fig. 14 and their photophysical properties, which mainly depend on the CˆN cyclometallating ligand, are reported in Table 4. Some of the complexes show enhanced absorption in the visible region due to the presence of naphthalimide chromophore and **81- 84** presented well-separated dual emission bands.

CˆN$_1$Pt(acac) **81** gives fluorescence emission bands at between 500 and 650 nm with a quantum yield of 0.95 and a lifetime of 0.06 ns, this bands are basically unaffected by the presence of O_2. On the other hand, the phosphorescence emission bands at 650–850 nm with quantum yields of 0.22 and lifetime of 1.53 μs are quite sensitive toward variation of oxygen concentration. Similar behavior was shown by CˆN$_2$Pt(acac) **82** which was found to be more sensitive due to its longer phosphorescence lifetime (3.75 μs).

CˆN$_3$Pt(acac) **83** is the first of a series of (ppy)Pt(acac) complexes which differ from each other by the R substitution in the ppy ligand (Fig. 14). Complex **83** is the only one showing deep NIR emission (638 nm) with and emission lifetime of 6.6 μs. CˆN$_4$Pt(acac) **84**, which has the same subunit as **83** but attached to the ppy ligand

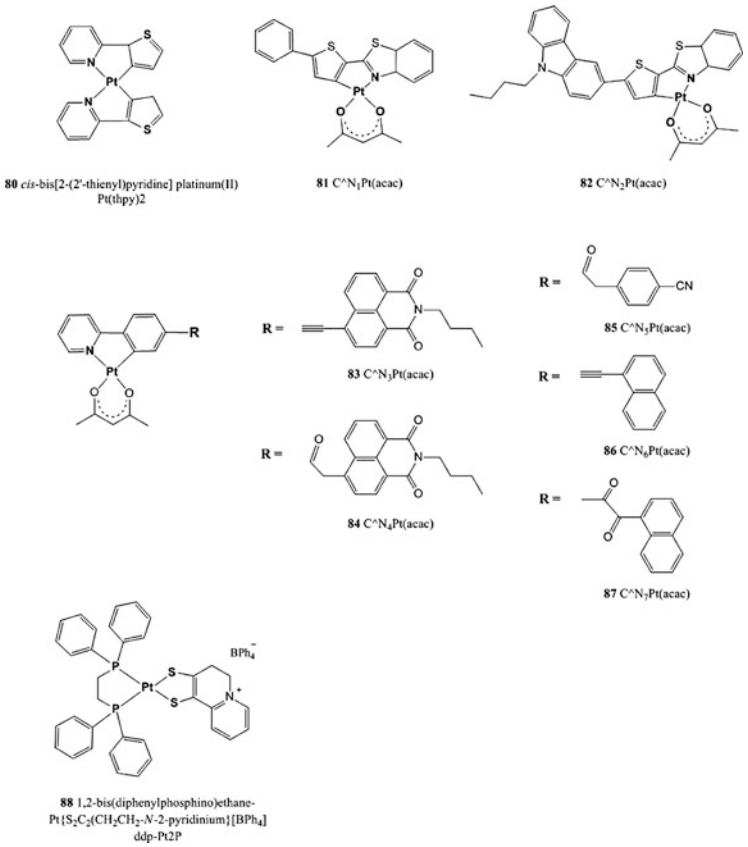

Fig. 14 Chemical structures of selected Pt(II) cyclometallated complexes

via a methylene-keto group, has a blue-shifted emission at 538 nm and a longer luminescent lifetime (25.5 μs). Minor emission bands for both **83** and **84** could be exploited for ratiometric dual emission measurements.

C^N_5Pt(acac) **85**, C^N_6Pt(acac) **86**, C^N_7Pt(acac) **87** emit roughly at the same wavelength range (530–570 nm) but show different sensitivities towards oxygen quenching as they show quite different decay times, with C^N_6Pt(acac) **86** having the longer one (15.8 μs).

Another complex belonging to the same class of dual emitters for oxygen ratiometric measurements is the 1,2-*bis*(diphenylphosphino)ethane-Pt{S_2C_2(CH_2CH_2-*N*-2-pyridinium)}[BPh_4], ddpePtP2 **88** [220]. Excitation of **89** leads to a dual emission: a fluorescent one at 677 nm with a quantum yield of 0.002 and lifetime of 0.2 ns and a phosphorescent one at 732 nm with a quantum yield of 0.01 and lifetime of 8.66 μs. The triplet intensity decreases approximately 2.5-fold on changing from nitrogen to oxygen while the singlet intensity is basically unaffected; this feature can be therefore used for ratiometric measurement [118].

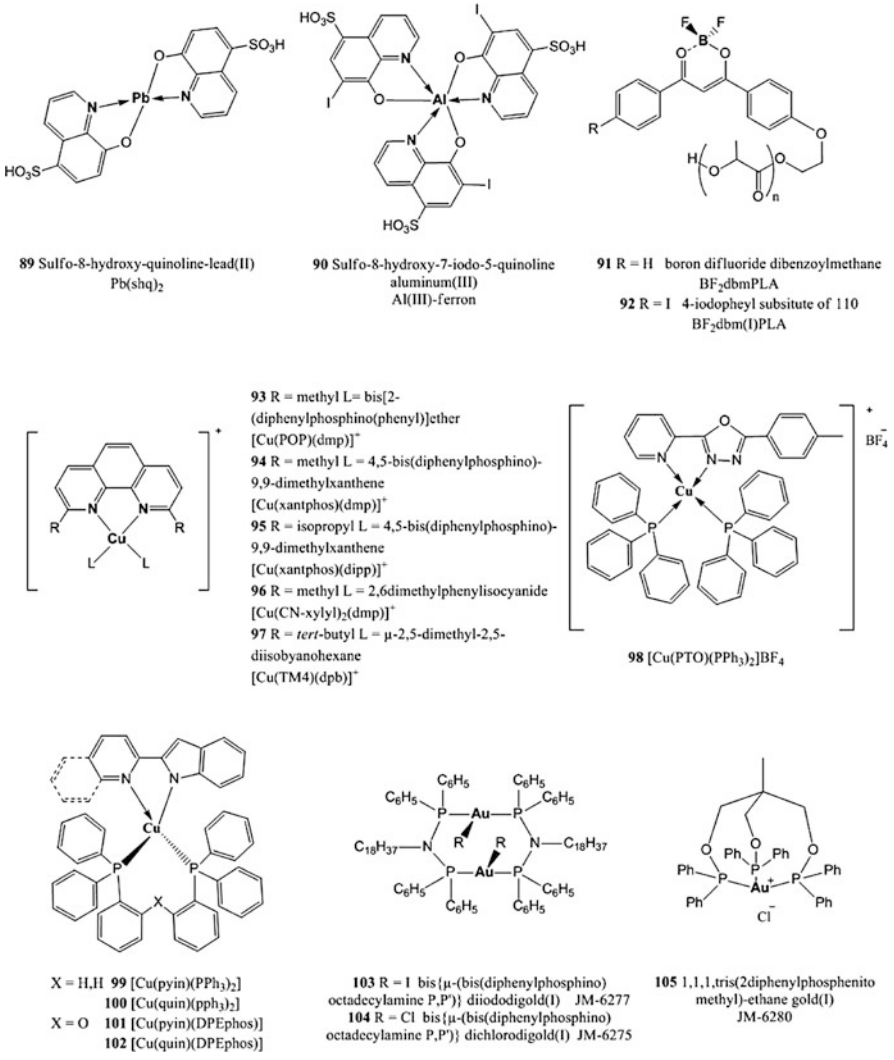

Fig. 15 Chemical structures of selected Al(III), Pb(II), Cu(I), Au(III), and boron complexes

A complication arises from a significant overlap between the peaks of excitation and emission spectra; to overcome this problem the authors utilized a method that switches between two frequencies of excitation modulation and excludes any overlapping effects. Unfortunately both emissions are rather weak, which is a very serious drawback.

5. Complexes with rarely used central atoms

Under this section, the reader can find those indicators for optical oxygen sensing which possess a central atom that has been used less commonly (Figs. 15 and 16).

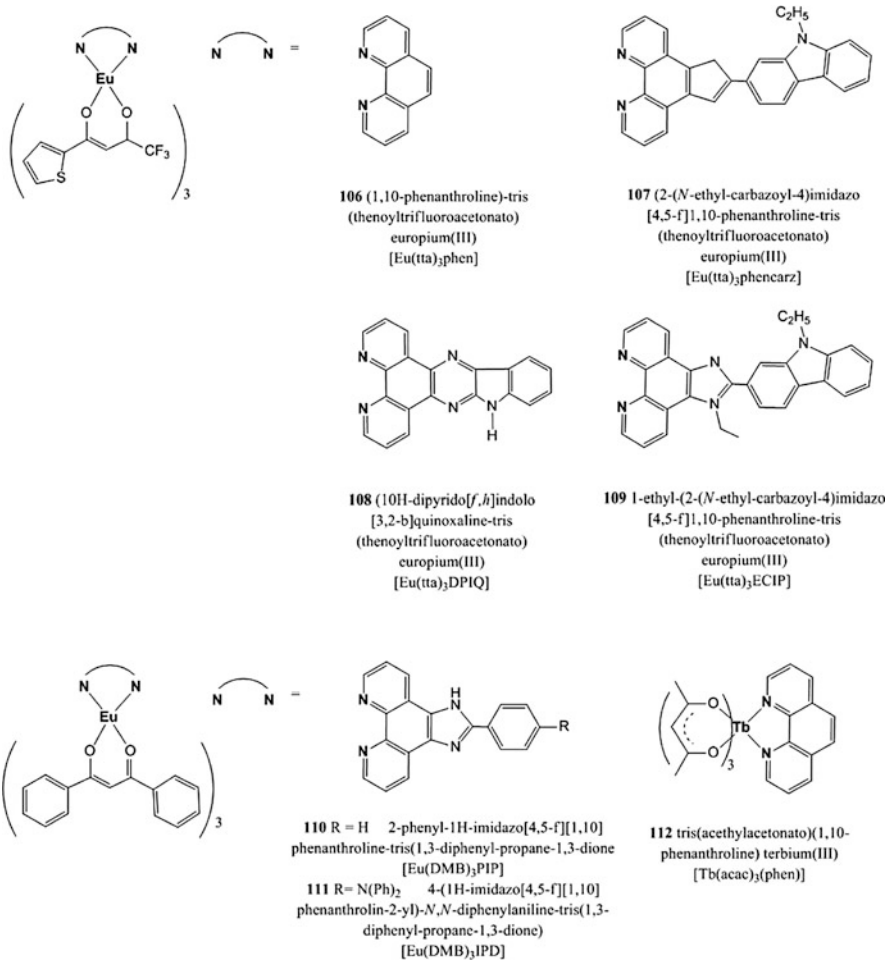

Fig. 16 Chemical structures of selected Eu(III) and Tb(III) complexes

The primary motivation behind the research of different materials is to provide an alternative to rather expensive platinum group metals as central atoms which can be of relevance for certain applications (e.g., food packaging where the price of the sensing material is one of the most important parameters to be considered).

Similar to the Ru(II) polypyridyl complexes, the luminescence of Pb(II) complexes is dominated by the metal-to-ligand charge transfer process that involves the promotion of an electron from a metal *d* orbit to a ligand π^* orbit.

When the lead(II) complex of 8-hydroxy-5-quinolinesulfonic acid (**89**) is retained on the surface of anion-exchange resin beads, it exhibits room temperature phosphorescence in suspensions of both aqueous and organic solutions [1]. This complex is characterized by long emission lifetime (Table 5) and very good photostability.

Table 5 Photophysical properties of complexes with rarely used central atoms

Dye	λ_{max}^{abs} (nm) ($\varepsilon \times 10^3$ M^{-1} cm^{-1})	λ_{max}^{em} (nm)	Medium	Φ	τ	References
89 $Pb(shq)_2$	450	638	Toluene	–	0.16 ms	[1]
90 Al(III)-ferron	390	600	Water	–	460 μs[a]	[144]
91 BF_2dbmPLA	396[b] (50.1)	440 509	Thin film	0.89[c]	1.2 ns 170 ms	[256]
92 BF_2dbm(I)PLA	406[b] (33)	485 535	Powder	0.41[c]	0.37 ns 4.06 ms	[258]
93 [Cu(POP)(dmp)]tfbp	–	517	Solid state	0.88[d]	26.0 μs	[205]
94 [Cu(xantphos)(dmp)] tfbp	–	540	Solid state	0.66[d]	30.2 μs	[205]
95 [Cu(xantphos)(dipp)] tfbp	–	513	Solid state	0.95[d]	38.5 μs	[205]
96 [Cu(CN-xylyl)$_2$ (dmp)] tfbp	~270[e]	520	Solid state	0.228[d]	309 μs	[206]
97 [Cu(TM4)(dmp)]$_2$ (tfbp)$_2$	~270[e]	530	Solid state	0.226[d]	1.2 ms	[206]
98 [Cu(PTO)(PPh_3)$_2$]BF_4	220/340	515	CH_2Cl_2	–	64.4 μs[b]	[88]
99 [Cu(pyin)(PPh_3)$_2$]	232[f] (40.5) 324[f] (15.5)	562 474	PMMA film	0.08	1.17 μs 4.66 ns	[145]
100 [Cu(quin)(PPh_3)$_2$]	231[f] (53.1) 354[f] (15.6)	608 550	PMMA film	0.042	1.32 μs 5.04 ns	[145]
101 [Cu(pyin)(DPEphos)]	231[f] (32.4) 324[f] (14.9)	566 475	PMMA film	0.05	1.20 μs 4.78 ns	[145]
102 [Cu(quin)(DPEphos)]	231[f] (38.1) 354[f] (13.9)	610 550	PMMA film	0.044	1.59 μs 4.89 ns	[145]
103 JM-6277	418[g]	530	PS	–	9.8 μs[d]	[163]
104 JM-6275	405[g]	525	PS	–		[165]
105 JM-6280	283[g]	501	PS	–	3.1–12.2 μs[b]	[163]
106 [Eu(tta)$_3$phen]	268/341	612	PS-*co*-TFEM film	/	340–420 μs[h]	[12]
107 [Eu(tta)$_3$phencarz]	287/326	610	CH_2Cl_2	0.24–0.31[i]	0.15–0.53 ms[i]	[226]
108 [Eu(tta)$_3$DPIQ]	225/279	610	CH_2Cl_2	–	300 μs	[260]

109 [$Eu(tta)_3ECIP$]	260/350	610	PS film	–	380–440 μs[l]	[208]
110 [$Eu(DMB)_3PIP$]	256/293/353	610	CH_2Cl_2	0.18	215 μs	[138]
111 [$Eu(DMB)_3IPD$]	352	610	CH_2Cl_2	–	400 μs	[68]
112 [$Tb(acac)_3(phen)$]	228/268	546	Alumina film	–	–	[8]

[a]Measured in argon media and taken from [50]
[b]Absorption measured in CH_2Cl_2
[c]Fluorescence lifetime
[d]Under pure nitrogen
[e]In methanol
[f]In dichloromethane
[g]$\lambda_{max}{}^{exc}$
[h]Range of lifetimes of the PS nanofibrous membranes doped with different amounts of complex **106** [253]
[i]Percentage of quantum yield and lifetimes of complex **107** in 1, 2, 3, and 4 wt% in PS in DMF solution
[l]Range of lifetimes of the nanofibrous membranes doped with different amounts of complex **109**

An analogous aluminum complex was shown to possess phosphorescence at room temperature once a heavy atom (iodine) was introduced in the ligand to promote intersystem crossing. The Al(III)-ferron complex **90** was either retained on the surface of anion exchange resin beads [144] or immobilized in sol–gel matrix to monitor oxygen in the gas phase, in water, and in organic solvents [50]; in both cases, the sensor was found to be very photo- and mechanically stable: no bleaching or leaching of the metal–chelate in either aqueous or organic solvent solutions was observed.

Strong room temperature phosphorescence under deoxygenation was also shown by boron difluoride dibenzoylmethane (BF_2dbm) when coupled with poly (lactic acid) (PLA). This is rather surprising since virtually all boron complexes are known to be fluorescent but not phosphorescent (e.g., BODIPY dyes). In dichloromethane solution, BF_2dbmPLA **91** showed a maximum absorption at 396 nm with a quite high molar absorption coefficient of about 50,000 M^{-1} cm^{-1} (Table 5), and an emission maximum at 436 nm with fluorescence quantum yield of 0.89 [256]. In solid state, on the other hand, BF_2dbmPLA exhibits both delayed fluorescence and long-lived green room temperature phosphorescence, optical properties that can be exploited for single-component oxygen sensors.

In a more recent report, the same group modified the dually-emissive compound **91** to obtain the iodide-substituted difluoroboron dibezoylmethane-poly(lactic acid) compound **92** [258]. The addition of a heavy atom had the effect of enhancing the spin-orbit coupling and therefore increasing the rate of intersystem crossing, rendering **92** more practical for sensing applications. In fact, as shown in Table 5, the phosphorescence room temperature lifetime decreased from 170 to 4.06 ms. The sensitivity to oxygen of this boron biomaterials was demonstrated by fabricating both thin films and nanoparticles.

Recently, it has been shown that copper(I) complexes in crystalline form can be used as solid-state oxygen gas sensors and their sensing ability correlates well with the amount of void space contained within their lattice structures [205].

An advantage of these indicators is that they replace precious metals such as ruthenium, iridium, or platinum with copper which is significantly cheaper and oxygen-sensitive materials can be synthesized in few steps from commercially available starting material.

Copper complexes **93–95** (Fig. 15) are based on the same basic structure but differ by the substituent on the phenanthroline ligand (denoted with R) and by the other two ligands to the copper central atom (denoted with L).

[Cu(POP)(dmp)]tfbp **93** exhibits reasonable oxygen sensitivity but suffers from rapid photochemical degradation [205]; when the POP ligand (POP = *bis* [2-(diphenylphosphino)phenyl]ether) was substituted with the more rigid xantphos ligand (xantphos = 4,5-*bis*(diphenylphosphino)-9,9-dimethylxanthene), the stability of the resulting indicators increased. Complexes **93–95** possess good quantum yields (0.60–0.90) in the rigid matrices and lifetime in a range between 26–32 μs (Table 5).

Mann et al. [206] have recently shown that [Cu(CN-xylyl)$_2$(dmp)] tfbp **96** and [Cu(TM4)(dmp)]$_2$(tfbp)$_2$ **97** can also be used as efficient crystalline oxygen sensors. These complexes showed much longer excited-stated lifetimes (in the order of ms)

when compared to the previously reported [205] and therefore higher sensitivity to oxygen. It has been also reported that complex **97** shows higher stability under continuous illumination when compared to **96**.

Haitao et al. [88] recently constructed an optical sensor based on the sensitivity to oxygen of a novel Cu(I) complex: $[Cu(PTO)(PPh_3)_2]BF_4$ **98**, which was embedded in mesoporous silica matrix. The photo-hysical properties of the complex are reported, in dichloromethane solution, in Table 5; the lifetime under pure nitrogen was found to be 64.4 μs which sharply decreases to 2.5 μs under 100 % O_2 suggesting quite good sensitivity. When grafted onto silica matrix, the probe showed a red shift in the emission spectra from 515 to 554 nm due to a breakdown of the rigid structure of **98** when dispersed in the matrix; it was also demonstrated that the doping concentration has an influence on the sensitivity of the probe.

Very recently, a series of Cu(I) complexes based on indole derivatives (**99–102**; Table 5), were shown to possess dual emission—a feature that can be exploited for ratiometric fluorescence oxygen sensing [145].

All of these complexes, when in their solid state at room temperature did not show any emission because of triplet–triplet annihilation, but once dispersed in a rigid matrix like PMMA they showed quite good emission. The maximum emission peak of complexes **99**, **100**, **101**, and **102** are 562, 566, 608 and 610 nm, respectively, and can be assigned to the emission from the MLCT-excited states, which have a lifetime in the range of 1.10–1.50 μs. The second weaker emissions at lower wavelengths were found to have a much longer lifetime in the order of ms. Further developments of this new neutral Cu(I) complexes are currently under progress.

Generally, the main drawback of the Cu(I) complexes as oxygen indicators is their inefficient absorption in the visible part of the spectrum. In fact, most of the complexes can be efficiently excited only with the UV light.

Binuclear and polynuclear complexes of Au(I) were shown to exhibit strong visible luminescence when excited in the UV; this luminescence is associated with the Au–Au interaction which is thought to give rise to a metal-centered emission with excited state lifetime, in the absence of oxygen, between 4 and 200 μs [163]. Three different gold compounds are reported here: two containing two gold metal centers, the *bis*{μ-(*bis*(diphenylphosphino)octadecylamine-P,P′)} diiododigold(I) referred as JM6277 **103** and *bis*{μ-(*bis*(diphenylphosphino)octadecylamine-P,P′)} dichlorodigold(I) referred as JM6275 **104**, and one possessing a tripod structure containing only one gold metal center, the 1,1,1,-*tris*(2-diphenylphosphenitomethyl)-ethane gold(I) referred as JM6280 **105** (Fig. 16). Once incorporated in polystyrene, complex **103** showed an excitation maximum at 418 nm, an emission maximum at 530 nm, and an excited-state lifetime under nitrogen of 9.8 μs; the films showed good sensitivity to oxygen but their photostability was rather low since sunlight exposure caused complete photobleaching within 5 days [163]. When the iodine ligand of complex **103** was changed with chlorine, photobleaching was slightly reduced but still present especially after prolonged exposure to strong sunlight. Complex **104** was incorporated in both polystyrene ($\lambda_{max}^{ex} = 405$ nm and $\lambda_{max}^{em} = 525$ nm) and Ormosil matrices ($\lambda_{max}^{ex} = 360$ nm and $\lambda_{max}^{em} = 525$ nm)

with latter showing a higher sensitivity to oxygen. The encapsulation in Ormosil resulted in a hypsochromic shift in the excitation maximum of 45 nm which suggests that the luminescence of the gold complex is affected by molecular interactions with the host matrix [165].

The mono gold(I) complex **105** showed strong luminescence not only in solid state but also in nonaqueous solvents like dichloromethane and tetrahydrofuran. Once incorporated in polystyrene, **105** showed an excitation maximum at 283 nm, an emission maximum at 501 nm and non-monoexponential decay curves with a short and a long lifetime components of 3.1and 12.2 μs, respectively.

Europium(III) complexes, thanks to their strong luminescence which is attributed to the 4*f*–4*f* transitions, have been widely applied in optical amplification, light conversion molecular devices, OLEDs, and their luminescence properties have been exploited for oxygen sensing [260]. Very narrow luminescence bands are of particular interest for oxygen sensing because of the potential for multiplexing applications where emission of other probes or labels can be used in different spectral windows.

A series of europium(III) complexes bearing similar structure have been recently reported and studied to be used as oxygen probes; complex **106–109** differ from each other by the diaza ligand as show in Fig. 15.

Amao et al. [12] immobilized [Eu(thenoyltrifluoroacetonato (tta))$_3$phen] **106** in polystyrene-*co*-2,2,2-TFEM and characterized the resulting oxygen-sensitive film (Table 5). The [Eu(tta)$_3$phen] films were shown to be sensitive to oxygen and possessed good photostability (no spectral changes after continuous irradiation using a 150 W tungsten lamp for 12 h). It has been reported that complex **106** suffers from photobleaching when used as powder but its photostability greatly increases once immobilized in rigid matrix [253]. Another group, in fact, used the same Eu(III) dye to dope a polystyrene nanofibrous membrane which resulted in a sensor for oxygen. Interestingly, the sensitivity increases with the weight percent of dopant up to 3 % [253].

Despite rather long luminescence lifetimes (several hundred microseconds), the sensitivity of the Eu(III) complexes is rather low. The luminescence of Eu(III) complexes is influenced by the energy gap between the Eu^{3+} ions and the antenna ligand and it is supposed to be more sensitive to the presence of oxygen when this energy gap is less than 1,500 cm^{-1} [129]. Therefore, a good way to increase the sensitivity of such complexes to oxygen is to change the nature of the ligand in order to modulate this energy gap.

Recently the group of Li and Su [226] reported the preparation of an optical oxygen sensor based on [Eu(tta)$_3$phencarz] **107**, which has a metal-ligand energy gap of 721 cm^{-1}. The complex was electrospun in polymer nanofibrous membrane. In this case as well, the sensitivity of the sensor showed a dependence on the amount of dye (weight percent) used to dope the nanofibrous membrane (lifetimes were in order of ms) and the best performances were obtained with 3 % of **107** in the matrix.

Two further complexes featuring three tta ligands and an additional antenna ligand have been reported: [Eu(tta)$_3$DPIQ] **108** and [Eu(tta)$_3$ECIP] **109** which were

respectively incorporated in a mesoporous matrix and in polystyrene nanofibrous membrane [208, 260]. The sensitivity to oxygen of these two complexes was lower than the one of complex **107**; the photophysical properties can be found in Table 5.

Complexes **110** and **111** (Fig. 16) possess the same basic structure (the tta ligands are changed with DMB (1,3-diphenyl-propane-1,3-dione)) but differ from each other by the diaza ligand. [$Eu(DMB)_3PIP$] **110** was electrospun into poly (vinypyrrolidone) [138] while [$Eu(DMB)_3IPD$] **111** was used to dope silica matrix [68]. Both were shown to have good sensitivity toward oxygen and to be potentially useful, once incorporated into the matrix, as optical oxygen sensors.

The strong luminescence of another lanthanide complex has been exploited by Amao et al. [8] to fabricate optical oxygen sensing material: the *tris*-(acethylacetonato)(1,10-phenanthroline) terbium(III) complex **112**.

The luminescence lifetime of Tb(III) complexes are usually quite long (up to several ms) and the quantum yields often about 50 %, but the actual values for **112** were not reported by the authors. The major drawback of this indicator is that it cannot be excited in the visible light but only in the UV region because the main resonance level of terbium $^5D_4$ is located at rather high energies ($\sim$20,400 cm^{-1}).

It should be mentioned here that for the similar reasons, the excitation of most Eu(III) complexes is also located in the UV region which is a serious drawback. Additionally, it should be noted that the luminescence of the Eu(III) complexes is usually strongly affected by temperature, which enabled their application as optical thermometers and their use for simultaneous luminescent sensing of temperature and oxygen [29].

Very recently, an oxygen indicator based on a gadolinium(III) complex was reported [26]. The acridone antenna was covalently bound to a polystyrene backbone to enable excitation with violet light. Gadolinium(III) *tris*-thenoyltrifluoroacetonate complex was used as an energy acceptor and showed rather strong phosphorescence ($\Phi = 14$ %) at room temperature in the absence of oxygen which is attributed to efficient intersystem crossing due to the heavy atom effect and paramagnetism of Gd(III). Quenching by oxygen was rather efficient due to a long decay time of about 900 μs, but Stern–Volmer plots showed pronounced nonlinearity indicating high heterogeneity of the material. Nevertheless, the work demonstrated for the first time the potential of Gd(III) complexes as new phosphorescent indicators for oxygen sensors.

6. Miscellaneous indicators

In this section, the reader will find all those indicators that do not belong to any specific class but still have been successfully used for optical oxygen sensing.

The thermally activated E-type delayed fluorescence (DF) of fullerene C_{70} **113** (Table 6) has been exploited by Nagl et al. [169] to make an optical oxygen sensor that is especially suited for sensing oxygen down to the ppb range. High sensitivities are explained by exceptionally long decay time of the delayed fluorescence (20 ms). The DF quantum yield of **113** increases from 0.01 at 20 °C to 0.08 at temperatures around 150 °C. Fullerene C_{70} was incorporated into

Table 6 Photophysical properties of miscellaneous indicators

Dye	λ_{max}^{abs} (nm) ($\varepsilon \times 10^3$ M^{-} cm^{-1})	λ_{max}^{em} (nm)	Medium	Φ	τ	Reference
113 Fullerene C_{70}	470 (20)	650–725	Organosilica	0.01	20 ms	[169]
114 $[Mo_6Cl_8]Cl_4L_2$	300–400	600–900	PTMSP[a]	–	100 μs	[82]

[a]Poly[1-trymethylsilyl-1-propyne]

highly oxygen-permeable matrices such as organically modified silica and ethyl cellulose to enable good sensitivity. Another feature is high chemical and photochemical stability of the material; on the other hand, moderate luminescence brightness (particularly at room temperatures) is a clear disadvantage.

The photophysical properties of molybdenum cluster **114** (Table 6) were shown to be well suited for oxygen sensing, as the red luminescence of the Mo cluster in PTMSP (poly[1-trymethylsilyl-1-propyne]) can be efficiently quenched by oxygen. The luminescence intensity can be easily detected by integration over the broad emission band as the cluster exhibits quite a long lifetime (>100 μs) and a large Stokes' shift (300 nm) [82]. The advantage of Mo cluster is that they and show exceptional thermal stability with no sign of decomposition even at temperatures higher than 600 °C.

Mo clusters were modified to be used for aqueous applications: $K_2Mo_6Cl_{14}$ clusters were caged in a hydrophobic oxygen polymer matrix, the [(acryloxypropyl)-methylsiloxane-dimethylsiloxane copolymer] [81]. A fiber optic sensor based on the phosphorescence quenching of $K_2Mo_6Cl_{14}$ clusters has been developed and if showed no photobleaching after more than 13,000 measurements and it gave a linear response in the temperature range between 10 and 37 °C.

The dependence of the fluorescent spectra of poly(9,9-dioctylfluorene) (PF8) on the oxygen content has been recently exploited to create an optical oxygen gas sensor [15]. It has been shown that in addition to the irreversible oxidation of PF8, which results in the formation of Keto defects, reversible fluorescence quenching is also observed when the PF8 thin films are excited with a He–Cd laser at 325 nm. The sensitivity of the conjugated polymer was only moderated and unfortunately, the sensors based on PF8 degrade irreversibly after 12 h of continuous laser exposure.

8 Criteria for selection of indicators

As it has been highlighted, numerous classes of oxygen indicators exist and feature significantly different photophysical and sensing properties. After giving an overview of the available indicators for optical oxygen sensing, in order to help the reader to choose the most suitable one for his/her needs, useful criteria for selection will be given in this session.

8.1 Absorption and emission spectra

In general, excitation in the UV part of the spectrum should be avoided due to high levels of background fluorescence originating from many biological substances, sensor supports, optical components etc. Additionally, UV light can be often disturbing for many biological systems. These are among the reasons why indicators excitable in the visible part of the spectrum are strongly preferable. Oxygen monitoring in tissues is more demanding and requires indicators that can be excited in the red or NIR part of the spectrum; this ensures deeper penetration depth of the excitation light and minimizes the loss of the emission light. As was demonstrated above, Pt(II) and Pd(II) complexes with π-extended benzonaphthoporphyrins as well as azabenzoporphyrins represent an excellent choice for such applications.

Generally, large Stokes' shifts are strongly preferable since the emission can be easily separated from the excitation light by means of optical filters. Fortunately, this requirement is almost always fulfilled for luminescent indicators. Compatibility with the available excitation sources and detectors is another important issue. Depending on the application the excitation sources of choice can be LEDs, laser diodes, lasers or, e.g., a mercury lamp. For example, bright LEDs are now available for virtually all parts of the spectrum; however, there is a gap between 540 and 580 nm. Compatibility with the detector can be another critical issue. For example, oxygen imaging with NIR-emitting dyes can be critical because of the lower sensitivity of the CCD chips in this region. The same is even more crucial for the photomultipliers as most devices (e.g. confocal microscopes) are still equipped with cheaper models which become almost insensitive at $\lambda > 700$ nm. Finally, compatibility with other optical components can be important for some particular sensors. For instance, the attenuation of cheap plastic optical fibers peaks at about 740 nm and then further increases above 820 nm, which can represent a certain problem when using NIR dyes. Fortunately, benzoporphyrin complexes emit between 770 and 800 nm, where the attenuation is lower.

8.2 Luminescence brightness of the probe

The luminescent brightness is defined as the product of the molar absorption coefficient (ε) and the luminescence quantum yields (Φ). Therefore, an indicator possessing a quantum yield close to unity but a molar absorption coefficient of only several thousand moles per centimeter can still not be bright enough for some applications. This situation is typical for most cyclometallated complexes of Ir(III) and Pt(II).

Generally, an advantage of indicators with high luminescence brightness is that they can be used in lower concentration within the polymeric matrix (thus avoiding aggregation) and therefore enable the preparation of fast responding thin-film

planar optodes or optical fibers. Nanoparticle sensors based on bright indicators can be used in lower concentration thus providing less interference to the biological systems. High luminescence brightness is of particular importance for measurements in tissues since the loss of excitation and the emission light due to absorption and scattering is very significant.

Clearly, the oxygen indicators with the highest brightness reported are the orange light-emitting Ir(III) coumarin complexes and NIR emitting Pt(II) benzoporphyrins. In fact, these dyes possess both very high molar absorption coefficients ($>$80,000 M^{-1} cm^{-1}) and luminescence quantum yields ($>$0.5). The brightness of the not extended Pt(II) porphyrins (e.g., octaethylporphyrin) is also very high but only upon excitation in the Soret band located in the UV region.

8.3 Luminescence decay times

The luminescence decay time of an indicator is also a very important parameter since the sensitivity of an optical oxygen sensor is proportional to both the decay time of the indicator and the gas permeability of the polymer. Thus, indicators with moderately long decay times (several microseconds) will show sufficient sensitivity only in highly gas-permeable matrices (silicone rubber, fluorinated polymers, or Ormosils) but in many common polymers used for the preparation of planar optodes, fiber-optic sensors, and nanoparticles (e.g., polystyrene) they will not show adequate sensitivity. On the other hand, long decay times ($>$1 ms) are often too long to design sensors which can operate between 0 and 21 kPa pO_2. In fact, the luminescence of such indicators will be almost completely quenched at low pO_2; in these cases, a solution could be to use polymers with low gas permeability even though it should be considered that the dynamic response of such materials will be negatively affected. Conversely, indicators with long decay times are indispensible when designing trace oxygen sensors. In fact, the sensors for moderately low oxygen concentrations can be designed on the basis of Pd(II) porphyrins (decay times about 1 ms) but ultratrace oxygen sensors require indicators with even longer decay times. Fullerene C70 (τ = 20 ms) was found to be useful for such applications. On the other hand, Pt(II) porphyrins with their phosphorescence decay times of 40–80 μs represent the most popular class of indicators for designing oxygen sensors operating in physiologically relevant concentrations.

8.4 Chemical stability and photostability

In general, the chemical stability of the majority of the indicators used for oxygen sensing is acceptably good. However, their stability in harsh conditions

(high temperature and humidity during sterilization, presence of oxidizing species such as hypochlorite, etc.) can be poor.

On the other hand, the photostability of different dyes can vary a lot even among compounds that are chemically closely related. This property is not critical for indicators used in disposable systems but it is fundamental for those applications where high light intensities are used and/or prolonged measurements are performed. Photosensitized singlet oxygen is often responsible for the photodegradation of indicator dyes through oxidation; therefore the introduction of electron-withdrawing substituents (such as halogens) in the indicator molecule usually helps to improve their photostability. For this reason, the complexes of Pt(II) and Pd(II) with highly fluorinated tetra(pentafluorophenyl)porphyrin are known to be one of the most photostable indicators reported. Unfortunately, very little data comparing the photostabilities of different classes of oxygen indicators is available.

8.5 Cross-sensitivity to other parameters

The luminescence of an indicator can be affected by the presence of ionic species and water. This can be critical for water-soluble indicators but it is of less relevance for the lipophilic ones since they are incorporated in polymers which can act as permeation-selective membrane for ionic species.

The phosphorescence of all luminescent dyes is prone to thermal quenching; however, the extent of this process varies dramatically for different indicator groups. Particularly, MLCT indicators (e.g., Ru(II) polypyridyl complexes) and luminescent Eu(III) complexes show a much higher degree of thermal quenching than, for example, Pt(II) metalloporphyrins (0.05–0.2 % of the decay time change per 1 K). The temperature cross-sensitivity of oxygen-sensing materials does not only depend on the nature of the compound but mostly is dominated by the temperature dependence of the diffusion and solubility of oxygen in polymers.

8.6 Solubility in the polymeric matrices/analyzed media

Low solubility of an indicator in the polymeric matrix can result in either aggregation or migration to other components (e.g., the material of the sensor support). Aggregation is of particular concern in case of planar π-extended molecules such as, e.g. unsubstituted porphyne, tetrabenzoporphyrin or phthalocyanine. The solubility in apolar polymers can usually be enhanced by introducing bulky substituents in the indicator molecule (e.g., alkyl chains). In case of porphyrins, it is efficiently suppressed by introducing phenyl rings in the *meso*-position of the porphyrin macrocycle. On the contrary, polar groups (e.g., charged groups, polyethylene glycol chains, peptides or proteins, etc.) can be introduced to enable/

enhance the solubility of an indicator in water. An alternative method to suppress dye migration and leaching is to covalently grafting the indicator into the matrix. However, often tedious modification of the indicator is necessary to achieve this goal. It should be mentioned here that the solubility in the analyzed media can also be obtained by immobilizing lipophilic indicators in the core of amphiphilic polymeric nanoparticles bearing polar groups on their surface. In this case modification of an indicator is not necessary.

8.7 Toxicity

Toxicity of an indicator is of main concern for biological and medical applications. Usually, encapsulation of the indicator into a polymeric matrix greatly reduces its toxicity. However, the phototoxicity caused by the production of singlet oxygen cannot be eliminated completely. This is especially true for water-soluble indicators and nanoparticles since the diffusion ways are short enough for the singlet oxygen to damage the cells despite its relatively short lifetime (about 3 μs) in aqueous media. Here, indicators with exceptional brightness are very useful since the loading of the probe (and consequently damage for the live cells) can be substantially reduced without compromising the S/N ratio.

8.8 Commercial or synthetic availability

Commercial availability is very important for numerous researchers who do not have enough facilities/experience to prepare the oxygen indicators by themselves. Unfortunately, only few oxygen indicators are commercially available at acceptable prices, such as, for example, the Ru(III) polypyridyl complexes and Pt(II) and Pd(II) complexes with some porphyrins including OEP and TFPP. If the synthesis of the indicators cannot be avoided the simplicity of the method is often of crucial significance. Price and/or simplicity of the synthetic pathway are of much less importance if the indicators are used in microscopic imaging or in fiber-optic microsensors because the amount of dye needed is usually very small. On the other hand, some emerging applications (e.g., food packaging) would require high quantities of the indicators at very competitive price. In this case, the less conventional indicators such as copper(I) or lanthanide(III) complexes can be very promising providing that they possess efficient absorption in the visible or NIR part of the spectrum and acceptable luminescence quantum yields.

9 Concluding remarks

To summarize, there is no perfect indicator which would be suitable for all oxygen-sensing applications. An adequate indicator should rather be carefully chosen according to the above mentioned criteria. Among different dye classes, Pt(II) and Pd(II) complexes with benzoporphyrins can be considered the most promising due to the high flexibility in tuning their spectral properties but also because of excellent luminescent brightness and photo-stability of some representatives.

These dyes are also suitable for further synthetic modification to provide additional functionalities. However, certain representatives of other classes possess interesting photophysical and sensing properties, such as for example ultrabright emission (iridium(III) coumarin complexes), dual emission (some platinum(II) complexes) which makes them particularly promising for ratiometric imaging. Despite the significant progress in the field of oxygen indicators that has been achieved in the last decade, there is still work to be done particularly in designing tailor-made dyes for many vital applications where state-of-the-art systems may not be fully adequate.

Acknowledgments Financial support from the European Commission (Grant Agreement number 264772 – ITN CHEBANA) and European Research Council (Project "Oxygen", N 207233) is gratefully acknowledged.

References

1. Alava-Moreno F, Valencia-Gonzalez MJ, Sanz-Medel A, Diaz-Garcia ME (1997) Oxygen sensing based on the room temperature phosphorescence intensity quenching of some lead-8-hydroxyquinoline complexes. Analyst 122:807–810
2. Alford PC, Cook MJ, Lewis APMGSG, Skarda V, Thomson AJ, Glasper JL, Robbins DJ (1985) Luminescent metal complexes. Part 5. Luminescence properites of ring-substituted 1,10-phenanthroline *tris*-complexes of ruthenium (II). J Chem Soc Perkin Trans 2:705–709
3. Amao Y (2003) Probes and polymers for optical sensing of oxygen. Mikrochim Acta 143(1): 1–12
4. Amao Y, Asai K, Okura I (1999) Photoluminescent oxygen sensing using palladium tetrakis (4-carboxyphenyl)porphyrin self-assembled membrane on alumina. Anal Commun 36(5): 179–180
5. Amao Y, Asai K, Okura I (2000) Oxygen sensing based on lifetime of photoexcited triplet state of platinum porphyrin-polystyrene film using time-resolved spectroscopy. J Porphyrins Phthalocyanines 4:292–299
6. Amao Y, Asai KOI, Shinohara H, Nishide H (2000) Platinum porphyrin embedded in poly(1-trimethylsilyl-1-propyne) film as an optical sensor for trace analysis oxygen. Analyst 125:1911–1914

7. Amao Y, Ishikawa Y, Okura I (2001) Green luminescent iridium(III) complex immobilized in fluoropolymer film as optical oxygen-sensing matrial. Anal Chem Acta 445:177–182
8. Amao Y, Ishikawa Y, Okura I, Miyashita T (2001) Optical oxygen sensing material: terbium(III) complex adsorbed thin film. Bull Chem Soc Jpn 74:2455–2449
9. Amao Y, Miyashita T, Okura I (2000) Optical oxygen sensing based on the luminescence change of metalloporphyrins immobilized in styrene-pentafuorostyrene copolymer film. Analyst 125:871–875
10. Amao Y, Okura I (2000) An oxygen sensing system based on the phosphorescence quenching of metalloporohyrin thin film on allumina plates. Analyst 125:1601–1604
11. Amao Y, Okura I (2003) Optical oxygen sensing materials: chemisorption film of ruthenium(II) polypyridyl complexes attached to anionic polymer. Sens Actuators B 88:162–167
12. Amao Y, Okura I, Miyashita T (2000) Optical oxygen sensing based on the luminescence quenching of Europium(III) complex immobilized in fluoropolymer film. Bull Chem Soc Jpn 73:2663–2668
13. Amao Y, Okura I, Miyashita T (2001) Pyrene chemisorption film on an alumina plate as an optical oxygen-sensing material. Bull Chem Soc Jpn 74:1159–1160
14. Amao Y, Tabuchi Y, Yamashita Y, Kimura K (2002) Novel optical oxygen sensing material: metalloporphyrin dispersed in fluorinated poly(aryl ether ketone) films. Eur Polym J 38: 675–681
15. Anni M, Rella R (2010) Oxygen optical gas sensing by reversible fluorescence quenching in photo-oxidized poly(9,9-dioctylfluorene) thin films. J Phys Chem B 114:1559–1561
16. Arain S, Gernot JT, Krause C, Gerlach J, Wolfbeis OS, Klimant I (2006) Characterization of microtiterplates with integrated optical sensors for oxygen and pH, and their applications to enzyme activity screening, respirometry, and toxicological assays. Sensors Actuators B Chem 113(2):639–648
17. Babilas P, Lamby P, Prantl L, Schreml S, Jung EM, Liebsch G, Wolfbeis OS, Landthaler M, Szeimies R-M, Abels C (2008) Transcutaneous pO2 imaging during tourniquet-induced forearm ischemia using planar optical oxygen sensors. Skin Res Technol 14(3):304–311
18. Badocco D, Mondin A, Pastore P, Voltolina S, Gross S (2008) dependence of calibration sensitivity of a polysulfone/Ru(II)-*tris*(4,7-diphenyl-1.10-phenanthroline)-based oxygen optical sensor on its structural parameters. Anal Chem Acta 627:239–246
19. Baldini F, Bacci M, Cosi F, Bianco ADB (1992) Absorption-based optical-fibre oxygen sensor. Sens Actuators B 7:752–757
20. Basu BJ, Anandan C, Rajam KS (2003) Study of the mechanism of degradation of pyrene-based pressure sensitive paints. Sens Actuators B 94(3):257–266
21. Basu BJ, Thirumurugan A, Dinesh AR, Anandan C, Rajam K (2005) Optical oxygen sensor coating based on the fluorescence quenching of a new pyrene derivative. Sens Actuators B 104(1):15–22
22. Bergman I (1968) Rapid-response atmospheric oxygen monitor based on fluorescence quenching. Nature 218:396
23. Bizzarri A, Koehler H, Cajlakovic M, Pasic A, Schaupp L, Klimant I, Ribitsch V (2006) Continuous oxygen monitoring in subcutaneous adipose tissue using microdialysis. Anal Chim Acta 573–574:48–56
24. Borisov SM, Klimant I (2007) Ultrabright oxygen optodes based on cyclometalated iridium(III) coumarin complexes. Anal Chem 79:7501–7509
25. Borisov SMLP, Klimant I (2011) Novel optical trace oxygen sensors based on platinum(II) and palladium(II) complexes with 5,10,15,20-meso-tetrakis-(2,3,4,5,6-pentafluorphenyl)-porphyrin covalently immobilized on silica-gel particles. Anal Chim Acta 690(1):108–115
26. Borisov S, Klimant I (2012) New luminescent oxygen-sensing and temperature-sensing materials based on gadolinium(III) and europium(III) complexes embedded in an acridone/polystyrene conjugate. Anal Bioanal Chem. doi:10.1007/s00216-012-6244-8
27. Borisov SM, Nuss G, Haas W, Saf R, Schmuck M, Klimant I (2009) New NIR-emitting complexes of platinum(II) and palladium(II) with fuorinated benzoporphyrins. J Photochem Photobio A 201:128–135

28. Borisov SM, Nuss G, Klimant I (2008) Red light-excitable oxygen sensing materials based on platinum(II) and palladium(II) benzoporphyrins. Anal Chem 80(24):9435–9442
29. Borisov SM, Wolfbeis OS (2006) Temperature-sensitive europium(III) probes and their use for simultaneous luminescent sensing of temperature and oxygen. Anal Chem 78 (14):5094–5101
30. Borisov SM, Wolfbeis OS (2008) Optical biosensors. Chem Rev 108(2):423–461
31. Borisov SM, Zenkl G, Klimant I (2010) Phosphorescent platinum(II) and palladium(II) complexes with azatetrabenzoporphyrins-new red laser diode-compatible indicators for optical oxygen sensing. ACS App Mater Interfaces 2(2):366–374
32. Brinas RP, Troxler T, Hochstrasser RM, Vinogradov SA (2005) Phosphorescent oxygen sensor with dendritic protection and two-photon absorbing antenna. J Am Chem Soc 127(33): 11851–11862
33. Burke CS, Moore JP, Wencel D, McEvoy AK, MacCraith BD (2008) Breath-by-breath measurement of oxygen using a compact optical sensor. J Biomed Opt 13(no. 1):014027
34. Cao Y, Koo Y-EL, Kopelman R (2004) Poly(decyl methacrylate)-based fluorescent PEBBLE swarm nanosensors for measuring dissolved oxygen in biosamples. Analyst 129(8):745–750
35. Carraway ER, Demas JN, DeGraff BA (1991) Luminescence quenching mechanism for microheterogeneous systems. Anal Chem 63(4):332–336
36. Cattaneo MV, Male KB, Luong JHT (1992) A chemiluminescence fiber-optic biosensor system for the determination of glutamine in mammalian cell cultures. Biosens Bioelec 7(8):569–574
37. Ceroni P, Lebedev AY, Marchi E, Yuan M, Esipova TV, Bergamini G, Wilson DF, Busch TM, Vinogradov SA (2011) Evaluation of phototoxicity of dendritic porphyrin-based phosphorescent oxygen probes: an in vitro study. Photochem Photobiol Sci 10(6):1056–1065
38. Chan C-M, Chan M-Y, Zhang M, Lo W, Wong K-Y (1999) The performance of oxygen sensing films with ruthenium-adsorbed fumed silica dispersed in silicone rubber. Analyst 124:691–694
39. Chang G, Morigaki K, Tatsu Y, Hikawa T, Goto T, Imaishi H (2011) Vertically integrated human P450 and oxygen sensing film for the annays of P450 metabolic activity. Anal Chem 83:2956–2963
40. Choi MF, Hawkins P (1995) A novel oxygen and/or carbon dioxide-sensitive optical transducer. Talanta 42(3):483–492
41. Choi MF, Hawkins P (1996) A fibre-optic oxygen sensor based on contact charge-transfer absorption. Sens Actuators B 30(3):167–171
42. Choi MMF, Pang WSH, Xiao D, Wu X (2001) An optical glucose biosensor with eggshell membrane as an enzyme immobilization platform. Analyst 126:1558–1563
43. Choi NW, Verbridge SS, Williams RM, Chen J, Kim J-Y, Schmehl R, Farnum CE, Zipfel WR, Fischbach C, Stroock AD (2012) Phosphorescent nanoparticles for quantitative measurements of oxygen profiles in vitro and in vivo. Biomaterials 33(9):2710–2722
44. Chu C-S, Lo Y-L (2010) 2D full-field measurement of oxygen concentration based on the phase fluorometry technique that uses the four-frame integrating-bucket method. Sens Actuators B 147(1):310–315
45. Chu C-S, Lo Y-L (2011) Highly sensitive and linear calibration optical fiber oxygen sensor based on Pt(II) complex embedded in sol–gel matrix. Sens Actuators B 155(1):53–57
46. Clark HA, Barker SL, Brasuel M, Miller MT, Monson E, Parus S, Shi Z-Y, Song A, Thorsrud B, Kopelman R, Ade A, Meixner W, Athey B, Hoyer M, Hill D, Lightle R, Philbert MA (1998) Subcellular optochemical nanobiosensors: probes encapsulated by biologically localised embedding (PEBBLEs). Sens Actuators B 51:12–16
47. Collman JP, Brauman JI, Doxsee KM, Halbert TR, Hayes SE, Suslick KS (1978) Oxygen binding to cobalt porphyrins. J Am Chem Soc 100(9):2761–2766
48. Cook MJ, Lewis AP, McAuliffe GSG, Skarda V, Thomson AJ, Glasper JL, Robbins DJ (1984) Luminescent metal complexes. Part 1. Tris-chelate of substituted 2,2′-bipyriydyls

with ruthenium(II) as dyes for luminescent solar collectors. J Chem Soc Perkin Trans II 1293–1301
49. Cook PLM, Wenzhöfer F, Glud RN, Janssen F, Huettel M (2007) Benthic solute exchange and carbon mineralization on two shallow subtidal sandy sediments: effect of advective pore-water exchange. Limnol Oceanogr 5(52):1943–1963
50. Costa-Fernandez JM, Diaz-Garcia ME, Sanz-Medel A (1998) Sol-gel immobilized room-temperature phosphorescent metal-chelate as luminescent oxygen sensing material. Anal Chem Acta 360:17–26
51. Coyle LM, Gouterman M (1999) Correcting lifetime measurements for temperature. Sens Actuators B 61:92–99
52. Currie MJ, Mapel JK, Heidel TD, Goffri S, Baldo MA (2008) High-efficiency organic solar concentrators for photovoltaics. Science 321(5886):226–228
53. Dawson WR, Kropp JL (1969) Radiationless deactivation and anomalous fluorescence of singlet 1,12-benzperylene. J Phys Chem 73(no. 6):1752–1758
54. Del Bianco A, Baldini F, Bacci M, Klimant I, Wolfbeis OS (1993) A new kind of oxygen-sensitive transducer based on an immobilized metallo-organic compound. Sens Actuators B 11:347–350
55. DeRosa MC, Hodgson DJ, Enright GD, Dawson B, Evans CEB, Crutchley RJ (2004) Iridium luminophore complexes for unimolecular oxygen sensors. J Am Chem Soc 126(24): 7619–7626
56. Djurovich PI, Murphy D, Thompson ME, Hernandez B, Gao R, Hunt PL, Selke M (2007) Cyclometalated iridium and platinum complexes as singlet oxygen photosenitizers: quantum yields, queching rates and correlation with electronic strucures. Dalton Trans 34:3763–3770
57. Dmitriev RI, Ropiak HM, Ponomarev GV, Yashunsky DV, Papkovsky DB (2011) Cell-penetrating conjugates of coproporphyrins with oligoarginine peptides: rational design and application for sensing intracellular O2. Bioconjugate Chem 22(12):2507–2518
58. Dmitriev RI, Zhdanov AV, Ponomarev GV, Yashunski DV, Papkovsky DB (2010) Intracellular oxygen-sensitive phosphorescent probes based on cell-penetrating peptides. Anal Biochem 398(1):24–33
59. Donckt EV, Camerman B, Vandeloise (1996) Fibre-optic oxygen sensor based on luminescence quenching of a Pt(II) complex embedded in polymer matrices. Sens Actuators B 32:121–127
60. Douglas P, Eaton K (2002) Response characteristics of thin film oxygen sensors, Pt and Pd octaethylporphyrins in polymer films. Sens Actuators B 82(2–3):200–208
61. Draxler S, Lippitsch ME, Klimant I, Kraus H, Wolfbeis OS (1995) Effects of polumer matrices on the time-resolved luminescence of a ruthenium complex quenched by oxygen. J Phys Chem 99:3162–3167
62. Dremel B, Li S-Y, Schmid R (1992) On-line determination of glucose and lactate concentrations in animal cell culture based on fibre optic detection of oxygen in flow-injection analysis. Biosens Bioelecron 7(2):133–139
63. Dunphy I, Vinogradov SA, Wilson D (2002) Oxyphor R2 and G2: phosphors for measuring oxygen by oxygen-dependent quenching of phosphorescence. Anal Biochem 310(2):191–198
64. Eastwood D, Gouterman M (1970) Porphyrins: XVIII. Luminescence of (Co), (Ni), Pd, Pt complexes. J Mol Spectrosc 35(3):359–375
65. Erskine RW, Field BO (1976) Reversible oxygenation. Struc Bond 28:1–50
66. Esipova TV, Karagodov A, Miller J, Wilson DF, Busch TM, Vinogradov SA (2011) Two New "protected" oxyphors for biological oximetry: properties and application in tumor imaging. Anal Chem 83(22):8756–8765
67. Fabricius-Dyg J, Mistlberger G, Staal M, Borisov SM, Klimant I, Kühl M (2012) Imaging of surface O2 dynamics in corals with magnetic micro optode particles. Mar Biol 159(7): 1621–1631
68. Feng N, Xie J, Zhang D (2010) Synthesis, characterization, photophysical and oxygen-sensing properties of a novel europium(III) complex. Spectrochim Acta A 77(1):292–296

69. Fercher A, Borisov SM, Zhdanov AV, Klimant I, Papkovsky DB (2011) Intracellular O2 sensing probe based on cell-penetrating phosphorescent nanoparticles. ACS Nano 5(7): 5499–5508
70. Filatov MA, Cheprakov AV (2011) The synthesis of new tetrabenzo- and tetranaphtho-porphyrins via the addition reactions of 4,7-dihydroisoindole. Tetrahedron 67(19):3559–3566
71. Finikova OS, Aleshchenkov SE, Brñas RP, Cheprakov AV, Carroll PJ, Vinogradov SA (2005) Synthesis of symmetrical tetraaryltetranaphtho[2,3]porphyrins. J Org Chem 70(12): 4617–4628
72. Finikova OS, Cheprakov AV, Carroll PJ, Vinogradov SA (2003) Novel route to functionalized tetraaryltetra[2,3]naphthaloporphyrins via oxidative aromatization. J Org Chem 68:7517–7520
73. Finikova OS, Cheprakov AV, Vinogradov SA (2005) Synthesis and luminescence of soluble meso-unsunbstituted tetrabenzo- and tetranaphtho[2,3]porphyrins. J Org Chem 70: 9562–9572
74. Finikova OS, Lebedev AY, Aprelev A, Troxler T, Gao F, Garnacho C, Muro S, Hochstrasser RM, Vinogradov SA (2008) Oxygen microscopy by two-photon-excited phosphorescence. ChemPhysChem 9(12):1673–1679
75. Fischer JPWF (2010) A novel planar optode setup for concurrent oxygen and light field imaging: application to a benthic phototrophic community. Limnol Oceanogr Meth 8:254–268
76. Fischer LH, Borisov SM, Schaeferling M, Klimant I, Wolfbeis OS (2010) Dual sensing of pO2 and temperature using a water-based and sprayable fluorescent paint. Analyst 135: 1224–1229
77. Fischer LH, Stich MIJ, Wolfbeis OS, Tian N, Holder E, Schäferling M (2009) Red- and green-emitting iridium(III) complexes for a Dua barometric and temperature-sensitive paint. Chem Eur J 15:10857–10863
78. Fujiwara Y, Amao Y (2004) Novel optical oxygen sensing material: 1-pyrenedecanoic acid and perfuorodecanoic acid chemisorbed onto anodic oxidized aluminium plate. Sens Actuators B 99:130–133
79. Ge X, Hanson M, Shen H, Kostov Y, Brorson KA, Frey DD, Moreira AR, Rao G (2006) Validation of an optical sensor-based high-throughput bioreactor system for mammalian cell culture. J Biotechnol 122(3):293–306
80. Gernot TJ, Klimant I, Wittmann C, Heinzle E (2003) Integrated optical sensing of dissolved oxygen in microtiter plates: a novel tool for microbial cultivation. Biotechnol Bioeng 81(7):829–836
81. Ghosh RN, Askeland PA, Kramer S, Loloee R (2011) Optical dissolved oxygen sensor utilizing molybdenum chloride cluster phosphorescence. Appl Phys Lett 98:221103–3
82. Ghosh RN, Baker GL, Ruud C, Nocera D (1999) Fiber-optic oxygen sensor using molybdenum chloride cluster luminescence. Appl Phys Lett 75(19):2885–2887
83. Gillanders RN, Tedford MC, Crilly PJ, Bailey RT (2005) A composite thin film optical sensor for dissolved oxygen in contaminated aqueous environments. Anal Chem Acta 545:189–194
84. Glud RN, Kühl MRN (1999) Heterogeneity of oxygen production and consumption in a photosynthetic microbial mat as studied by planar optodes. J Phycol 35:270–279
85. Glud RN, Ramsing NB, Gundersen JK, Klimant I (1996) Planar optrodes: a new tool for fine scale measurements of two dimensional O2 distribution in bethic communities. Mar Ecol Prog Ser 140:217–226
86. Glud RN, Tengberg A, Kühl M, Hall POJ, Klimant I (2001) An in situ instrument for planar O2 optode measurements at benthic interfaces. Limnol Ocenogr 46(8):2073–2080
87. Guo L, Ni Q, Li J, Zhang L, Lin X, Xie Z, Chen G (2008) A novel sensor based on the porous plastic probe for determitation of dissolved oxygen in seawater. Talanta 74:1032–1037
88. Haitao J, Huilin Y, Fan L, Yang L (2012) Fabrication and performances of an optical sensor system constructed by a novel Cu(I) complex embedded on silica matrix. J Lumin 132:198–204

89. Hanson MA, Ge X, Kostov Y, Brorson KA, Moreira AR, Rao G (2007) Comparisons of optical pH and dissolved oxygen sensors with traditional electrochemical probes during mammalian cell culture. Biotechnol Bioeng 97(4):833–841
90. Hanson K, Tamayo A, Diev VV, Whited MT, Djurovich PI, Thompson ME (2010) Efficient dipyrrin-centered phosphorescence at room temperature from *bis*-cyclometalated iridium(III) dipyrrinato complexes. Inorg Chem 49(13):6077–6084
91. Hartmann P, Leiner MJP, Lippitsch ME (1995) Luminescence quenching behavior of an oxygen sensor based on a Ru(II) complex dissolved in polystyrene. Anal Chem 67(1):88–93
92. Hartmann P, Ziegler W, Holst G, Lübbers DW (1997) Oxygen flux fluorescence lifetime imaging. Sens Actuators B 38:110–115
93. He H, Fraatz RJ, Leiner MJP, Rehn MM, Tusa JK (1995) Selection of silicone polymer matrix for optical gas sensing. Sens Actuators B 29:246–250
94. Higgins C, Wencel D, Burke CS, MacCraith BD, McDonagh C (2007) Novel hybrid optical sensor materials for in-breath O2 analysis. Analyst 133:241–247
95. Holst G, Grundwald B (2001) Luminescence lifetime imaging with transparent oxygen optodes. Sens Actuators B 74:78–90
96. Holst G, Kohls O, Klimant I, König B, Kühl M, Richter T (1998) A modular luminescence lifetime imaging system for mapping oxygen distribution in biological samples. Sens Actuators B 51:163–170
97. Imasaka T, Ishibashi K, Ishibashi N (1982) Time-resolved fluorimetry with a sub-nanosecond dye laser source for the determination of polynuclear aromatic hydrocarbons after separation by high-performance liquid chromatography. Anal Chim Acta 142:1–12
98. Jensen ST, Kühl M, Glud RN, Jørgensen BB, Prieme A (2005) Oxic microzones and radial oxygen loss from roots of *Zostera marina*. Mar Ecol Prog Ser 293:49–58
99. Jones PF (1968) On the use of phosphorescence quenching for determining permeabilities of polymeric films to gases. J Polym Sci B Polym Lett 6(7):487–491
100. Kautsky H (1939) Quenching of luminescence by oxygen. Trans Faraday Soc 35:216–219
101. Kellner K, Liebsch G, Klimant I, Wolfbeis OS, Blunk T, Schulz MB, Göpferich A (2002) Determination of oxygen gradients in engineered tissue using a fluorescent sensor. Biotechnol Bioeng 80(1):73–83
102. Khalil G, Gouterman M, Ching S, Costin C, Coyle L, Gouin S, Green E, Sadilek M, Wan R, Yearyean J, Zelelow B (2002) Synthesis and spectroscopic characterization of Ni, Zn, Pd and Pt tetra(pentafuorophenyl)porpholactone with comparison to Mg, Zn, Y, Pd and Pt metal complexes of tetra(pentafuorophenyl)porphine. J Porphyrins Phthalocynines 6:135–145
103. Klimant I, Belser P, Wolfbeis OS (1994) Novel metal-organic ruthenium(II) diimin complexes for use as longwave excitable luminescent oxygen probes. Talanta 41(6):985–991
104. Klimant I, Kühl M, Glud R, Holst G (1997) Optical measurement of oxygen and temperature in microscale: strategies and biological applications. Sens Actuators B 38(1–3):29–37
105. Klimant I, Meyer V, Kühl M (1995) Fiberoptic oxygen microsensors, a new tool in aquatic biology. Limnol Oceanogr 40:1159–1165
106. Klimant I, Ruckruh F, Liebsch G, Stangelmayer A, Wolfbeis OS (1999) Fast response oxygen micro-optodes based on novel soluble ormosil glasses. Mikrochim Acta 131(1):35–46
107. Klimant I, Wolfbeis OS (1995) Oxygen-sensitive luminescent materials based on silicone-soluble ruthenium diimine complexes. Anal Chem 67:3160–3166
108. Knopp JA, Longmuir IS (1972) Intracellular measurement of oxygen by quenching of fluorescence of pyrenebutyric acid. Biochim Biophys Acta 279:393–397
109. Kober EM, Caspar JV, Lumpkin RS, Meyer TJ (1986) Application of the energy gap law to excited-state decay of osmium(II)-polypyridine complexes: calculation of relative nonradiative decay rates from emission spectral profiles. J Phys Chem 90(16):3722–3734
110. Kocincova AS, Nagl S, Arain S, Krause C, Borisov SM, Arnold M, Wolfbeis OS (2008) Multiplex bacterial growth monitoring in 24-well microplates using a dual optical sensor for dissolved oxygen and pH. Biotechnol Bioeng 100(no. 3):430–438

111. Kolle C, Gruber W, Trettnak WBK, Dolezal C, Reininger F (1997) Fast optochemical sensor for continuous monitoring of oxygen in breath-gas analysis. Sens Actuators B 38–39: 141–149
112. König B, Kohls O, Holst G, Glud RN, Kühl M (2005) Fabrication and test of sol–gel based planar oxygen optodes for use in aquatic sediments. Mar Chem 97:262–276
113. Koo Y-EL, Cao Y, Kopelman R, Koo SM, Brasuel M, Philbert MA (2004) Real-time measurements of dissolved oxygen inside live cells by organically modified silicate fluorescent nanosensors. Anal Chem 76(9):2498–2505
114. Koren K, Borisov SMKI (2012) Stable optical oxygen sensing materials based on click-coupling of fluorinated platinum(II) and palladium (II) porphyrins—a convenient way to eliminate dye migration and leaching. Sens Actuators B 169:173–181
115. Koren K, Borisov SM, Saf R, Klimant I (2011) Strongly phosphorescent iridium(III)-porphyrins—new oxygen indicators with tuneable photophysical properties and functionalities. Eur J Inorg Chem 2011(no. 10):1531–1534
116. Koren K, Dmitriev RI, Borisov SM, Papkovsky DB, Klimant I (2012) Complexes of IrIII-octaethylporphyrin with peptides as probes for sensing cellular O2. ChemBioChem 13(8):1184–1190
117. Köse ME, Crutcheley RJ, DeRosa MC, Ananthakrishnan N, Reynolds JR, Schanze KS (2005) Morphology and oxygen sensor response of luminescent Ir-labeled poly(dimethylsiloxane)/polystyrene polymer blend films. Langmuir 21:8255–8262
118. Kostov Y, Harms P, Pilato RS, Rao G (2000) Ratiometric oxygen sensing: detection of dual-emission ratio through a single emission filter. Analyst 125(6):1175–1178
119. Kuhl Y, Cohen T, Dalsgaard B, Jorgensen B, Reversbech NP (1995) Microenvironment and photosynthesis of zooxanthellea in scleractinian corals studied with microsensors for O2, pH and light. Mar Ecol Prog Ser 117:159–172
120. Kühl G, Larkum AWD, Ralph P (2008) Imaging of oxygen dynamics within the endolithic algal community of the massive coral porites lobata. J Phycol 44:541–550
121. Kühl M, Polerecky L (2008) Functional and structural imaging of phototrophic microbial communities and symbioses. Aquat Microb Ecol 53:99–118
122. Kunkely H, Vogler A (1990) Photoluminescence of platinum complex [PtII(4,7-diphenyl-1,10-phenanthroline)(CN)2] in solution. J Am Chem Soc 112(14):5625–5627
123. Lai S-W, Hou Y-J, Che C-M, Pang H-L, Wong K-Y, Chang CK, Zhu N (2004) Electronic spectroscopy, photophysical properties, and emission quenching studies of an oxydatively robust perfuorinated platinum porphyrin. Inorg Chem 43:3724–3732
124. Lakowicz JR (2006) Principle of fluorescence spectroscopy. Springer, Baltimore
125. Lakowicz JR, Berndt K (1991) Lifetime-selective fluorescence imaging using a RF phase sensitive camera. Rev Sci Instrum 62:1727–1734
126. Lamansky S, Djurovich P, Murphy D, Abdel-Razzaq F, Lee H-E, Adachi C, Burrows PE, Forrest SR, Thompson ME (2001) Highly phosphorescent *bis*-cyclometalated iridium complexes: synthesis, photophysical characterization, and use in organic light emitting diodes. J Am Chem Soc 123(18):4304–4312
127. Larkum A, Koch E, Kühl M (2003) Diffusive boundary layers and photosynthesis of teh epilithic algal community of coral reefs. Mar Biol 142:1073–1082
128. Larsen M, Borisov SM, Grundwald B, Klimant I, Glud RN (2011) A simle and inexpensive high resolution color ratiometric planar optode imaging approach: application to oxygen and pH sensing. Limnol Oceanogr Meth 9:348–360
129. Law G-L, Pal R, Palsson LO, Parker D, Wong K-L (2009) Responsive and reactive terbium complexes with an azaxanthone sensitiser and one naphthyl group: applications in ratiometric oxygen sensing in vitro and in regioselective cell killing. Chem Commun 47:7321–7323
130. Lebedev AY, Cheprakov AV, Sakadzic S, Boas DA, Wilson DF, Vinogradov SA (2009) Dendritic phosphorescent probes for oxygen imaging in biological systems. ACS Appl Mater Interfaces 1(6):1292–1304
131. Lecoq J, Parpaleix A, Roussakis E, Ducros M, Houssen YG, Vinogradov SA, Charpak S (2011) Simultaneous two-photon imaging of oxygen and blood flow in deep cerebral vessels. Nat Med 17(7):893–898

132. Lee S-K, Okura I (1997) Optical sensor for oxygen using a porphyrin-doped sol–gel glass. Analyst 122:81–84
133. Lee S-K, Okura I (1997) Porphyrin-doped sol–gel glass as a probe for oxygen sensing. Anal Chem Acta 342:181–188
134. Lee S-K, Okura I (1997) Photostable optical oxygen sening material: platinum tetrakis (pentafluorophenyl)porphyrin immobilized in polystyrene. Anal Comm 34:185–188
135. Lee Y-EK, Ulbrich EE, Kim G, Hah H, Strollo C, Fan W, Gurjar R, Koo S, Kopelman R (2010) Near infrared luminescent oxygen nanosensors with nanoparticle matrix tailored sensitivity. Anal Chem 82(20):8446–8455
136. Li X, Rosenzweig Z (1997) A fiber optic sensor for rapid analysis of bilirubin in serum. Anal Chim Acta 353:263–273
137. Li L, Walt DR (1995) Dual-analyte fiber-optic sensor for the simultaneous and continuous measurement of glucose and oxygen. Anal Chem 67(20):3746–3752
138. Li S, Zhao X (2011) Oxygen sensing nanofibers doped with red-emitting Eu(III) complex: synthesis, characterization, machanism, and sensing performance. Synth Met 161:737–742
139. Liebsch G, Klimant I, Frank B, Holst G, Wolfbeis OS (2000) Luminescence lifetime imaging of oxygen, pH, and carbon dioxide distribution using optical sensors. Appl Spectrosc 54(4):548–559
140. Liebsch G, Klimant I, Wolfbeis OS (1999) Luminescence lifetime temperature sensing based on sol–gels and poly(acrylonitrile)s dyed with ruthenium metal–ligand complexes. Adv Mater 11(15):1296–1299
141. Lin C-T, Böttcher M, Creutz C, Sutin N (1976) Mechanism of the quenching of the emission of substituted polypyridineruthenium(II) complexes by Iron(III), chromium(III) and europium(III) ions. J Am Chem Soc 98:6536–6544
142. Lippitsch ME, Pusterhofer J, Leiner MJP, Wolfbeis OS (1988) Fibre-optic oxygen sensor with the fluorescence decay time as the infomation carrier. Anal Chim Acta 205:1–6
143. Liu Y, Guo H, Zhao J (2011) Ratiometric luminescent molecular oxygen sensors based on uni-luminophores of C[caret]N Pt(II)(acac) complexes that show intense visible-light absorption and balanced fluorescence/phosphorescence dual emission. Chem Comm 47(41):11471–11473
144. Liu Y-M, Pereoro-Garcia R, Valencia-Gonzalez MJ, Diaz-Gracia ME, Sanz-Medel A (1994) Evaluation of some immobilized room-temperature phosphorescent metal chelates as sensing materials for oxygen. Anal Chem 66:836–840
145. Liu X, Sun W, Zou L, Xie Z, Li X, Lu C, Wang L, Cheng Y (2012) Neutral cuprous complexes as ratiometric oxygen gas sensors. Dalton Trans 41(4):1312–1319
146. Lo L-W, Koch CJ, Wilson DF (1996) Calibration of oxygen-dependent quenching of the phosphorescence of Pd-meso-tetra(4-carboxyphenyl)porphine: a phosphor with general application for measuring oxygen concentration in biological systems. Anal Biochem 236: 153–160
147. MacCraith BD, Mc Donagh CM, O'Keffe G, Keyes ET, Vos JG, O'Kelly B, McGilp JF (1993) Fibre optic oxygen sensor based on fluorescence quenching of evanescent-wave excited ruthenium complexes in sol–gel derived porous coatings. Analyst 118:385–388
148. Mack J, Asano Y, Kobayashi N, Stillman MJ (2005) Application of MCD spectroscopy and TD-DFT to a highly non-planar porphyrinoid ring system. New insights on red-shifted porphyrinoid spectral bands. J Am Chem Soc 127(50):17697–17711
149. Mak CSK, Pentlehner D, Stich M, Wolfbeis OS, Chan WK, Yersin H (2009) Exceptional oxygen sensing capabilities and triplet state properties of Ir(ppy-NPh2)3. Chem Mater 21(11):2173–2175
150. Marazuela MD, Moreno-Bondi MC (1998) Determination of choline-containing phospholipids in serum with a fiber-optic biosensor. Anal Chim Acta 374(1):19–29
151. Mayr T, Borisov SM, Abel T, Enko BWK, Mistlberger G, Klimant I (2009) Light harvesting as a simple and versatile way to enhance brightness of luminescent sensors. Anal Chem 81:6541–6545

152. McDonagh C, Bowe P, Mongey KMBD (2002) Characterization of porosity and sensor response times of sol–gel-derived thin films for oxygen sensor application. J Non-Cryst Solids 306:138–148
153. McDonagh C, Burke CS, MacCraith BD (2008) Optical chemical sensors. Chem Rev 108(2):400–422
154. Mcevoy AK, McDonagh C, MacCraith BD (1997) Optimization of sol–gel-derived silica films for optical oxygen sensing. J Sol-Gel Sci Technol 8:1121–1125
155. McLaurin EJ, Greytak AB, Bawendi MG, Nocera DG (2009) Two-photon absorbing nanocrystal sensors for ratiometric detection of oxygen. J Am Chem Soc 131:12994–13001
156. McLean TM, Moody JL, Waterland MR, Telfer SG (2012) Luminescent rhenium(I)-dipyrrinato complexes. Inorg Chem 51:446–455
157. Medina-Castillo AL, Fernandez-Sanchez JF, Klein C, Nazeeruddin MK, Segura-Carretero A, Fernandez-Gutierrez A, Graetzel M, Spichiger-Keller UE (2007) Engineering of efficient phosphorescent iridium cationic complex for developing oxygen-sensitive polymeric and nanostructured films. Analyst 132(9):929–936
158. Meier RJ, Schreml S, Wang X-d, Landthaler M, Babilas P, Wolfbeis OS (2011) Simultaneous photographing of oxygen and pH in vivo using sensor films. Angew Chem Int Ed 50(no. 46):10893–10896
159. Meier B, Werner T, Klimant I, Wolfbeis OS (1995) Novel oxygen sensor material based on a ruthenium bipyridyl complex encapsulated in zeolite Y: dramatic differences in the efficiency of luminescence quenching by oxygen on going from surface-adsorbed to zeolite-encapsulated fluorophores. Sen Actuators B 29:240–245
160. Millikan GA (1942) The oximeter, an instrument for measuring continuously the oxygen saturation of arterial blood in man. Rev Sci Instr 13(10):434–444
161. Mills A (1999) Response characteristics of optical sensors for oxygen: a model based on a distribution in [small tau]oand kq. Analyst 124(9):1309–1314
162. Mills A, Lawrie K, Bardin J, Apedalie A, Skinner GA, O'Rouke C (2012) An O2 smart plastic film for packaging. Analyst 137:106–112
163. Mills A, Lepre A, Theobald BRC, Slade E, Murrer BA (1997) Use of luminescent gold compounds in the design of thin-film oxygen sensors. Anal Chem 69:2842–2847
164. Mills A, Thomas M (1997) Fluorescence-based thin plastic film ion-pair sensors for oxygen. Analyst 122:63–68
165. Mills A, Tommons C, Bailey RT, Crilly P, Tedford MC (2011) Thin-film oxygen sensors using a luminescent polynuclear gold(I) complex. Anal Chem Acta 702:269–273
166. Mingoarranz FJ, Moreno-Bondi MC, Garcia-Fresnadillo D, de Dios C, Orellana G (1995) Oxygen-sensitive layers for optical fibre devices. Mikrochim Acta 121:107–118
167. Mitsubayashi K, Kon T, Hashimoto Y (2003) Optical bio-sniffer for ethanol vapor using an oxygen-sensitive optical fiber. Biosens Bioelectron 19(3):193–198
168. Morin AM, Xu W, Demas JN, DeGraff BA (2000) Oxygen sensors based on quenching of *tris*-(4,7-diphenyl-1.10-phenanthroline)ruthenium(II) in fluorinated polymers. J Fluoresc 10: 7–12
169. Nagl S, Baleizao C, Borisov SM, Schäferling M, Barberan MN, Wolfbeis OS (2007) Optical sensing and imaging of trace oxygen with record response. Angew Chem Int Ed 46: 2317–2319
170. Napp J, Behnke T, Fischer L, Würth C, Wottawa M, Katschinski DM, Alves F, Resch-Genger U, Schäferling M (2011) Targeted luminescent near-infrared polymer-nanoprobes for in vivo imaging of tumor hypoxia. Anal Chem 83:9039–9046
171. Neugebauer U, Pellegrin Y, Devocelle M, Forster RJ, Signac W, Moran N, Keyes TE (2008) Ruthenium polypyridyl peptide conjugates: membrane permeable probes for cellular imaging. Chem Commun 42(42):5307–5309
172. Niedermair F, Borisov SM, Zenkl G, Hofmann OT, Weber H, Saf R, Klimant I (2010) Tunable phosphorescent NIR oxygen indicators based on mixed benzo- and naphthoporphyrin complexes. Inorg Chem 49(no. 20):9333–9342

173. Nock V, Blaikie RJ, David T (2008) Patterning, integration and characterization of polymer optical oxygen sensors for microfluidics devices. Lab Chip 8:1300–1307
174. O'Riordan TC, Zhdanov AV, Ponomarev GV, Papkovsky DB (2007) Analysis of intracellular oxygen and metabolic responses of mammalian cells by time-resolved fluorometry. Anal Chem 79(24):9414–9419
175. Okazaki T, Imasaka T, Ishibashi N (1988) Optical-fiber sensor based on the second-harmonic emission of a near-infrared semiconductor laser as light source. Anal Chim Acta 209: 327–331
176. Opitz N, Graf H-J, Lübbers DW (1988) Oxygen sensor for the temperature range 300 to 500 K based on fluorescence quenching of indicator-treated silicone rubber membranes. Sens Actuators 13(2):159–163
177. Papkovsky DB (1995) New oxygen sensors and their application to biosensing. Sens Actuators B 29(1–3):213–218
178. Papkovsky DB, Olah J, Troyanovsky IV, Sadovsky NA, Rumyantseva VD, Mironov AF, Yaropolov AI, Savitsky AP (1992) Phosphorescent polymer films for optical oxygen sensors. Biosens Bioelectron 7(3):199–206
179. Papkovsky DB, Ponomarev GV, Trettnak W, O'Leary P (1995) Phosphorescent complexes of phorphyrin ketones: optical properties and application to oxygen sensing. Anal Chem 67:4112–4117
180. Park EJ, Reid KR, Tang W, Kennedy RT, Kopelman R (2005) Ratiometric fiber optic sensors for the detection of inter- and intra-cellular dissolved oxygen. J Mater Chem 15(27–28): 2913–2919
181. Pasic A, Koehler H, Klimant I, Schaupp L (2007) Miniaturized fiber-optic hybrid sensor for continuous glucose monitoring in subcutaneous tissue. Sens Actuators B 122:60–68
182. Pasic A, Koehler H, Schaupp L, Pieber T, Klimant I (2006) Fiber-optic flow-through sensor for online monitoring of glucose. Anal Bioanal Chem 386(5):1293–1302
183. Peterson JI, Fitzgerald RV, Buckhold DK (1984) Fiber-optic probe for in vivo measurement of oxygen partial pressure. Anal Chem 56(1):62–67
184. Polerecky L, Lott C, Weber M (2008) In situ measurement of gross photosynthesis using a microsensor-based light-shade shift method. Limnol Oceanogr Meth 6:373–383
185. Pollack M, Pringsheim P, Terwoord D (1944) A method for determining small quantities of oxygen. J Chem Phys 12(7):295–299
186. Puklin E, Carlson B, Gouin S, Costin C, Green E, Ponomarev S, Tanji H, Gouterman M (2000) Ideality of pressure-sensitive paint. I. Platinum tetra(pentafluorophenyl)porphine in fluoroacrylic polymer. J Appl Polym Sci 77:2795–2804
187. Roberts L, Lines R, Reddy S, Hay J (2011) Investigation of polyviologens as oxygen indicators in food packaging. Sens Actuators B 152:63–67
188. Rogers JE, Nguyen KA, Hufnagle DC, McLean DG, Su W, Gossett KM, Burke AR, Vinogradov SA, Pachter R, Fleitz PA (2003) Observation and interpretation of annulated porphyrins: studies on the photophysical properties of meso-tetraphenylmetalloporphyrins. J Phys Chem A 107(51):11331–11339
189. Röösli S, Pretsch E, Morf WE, Tsuchida E, Nishide H (1997) Selective optical response to oxygen of membranes based on immobilized cobalt(II) porphyrins. Anal Chim Acta 338: 119–125
190. Rosenow TC, Walzer K, Leo K (2008) Near-infrared organic light emitting diodes based on heavy metal phthalocyanines. J Appl Phys 103(no. 4):043105
191. Rozhkov VV, Khajehpour M, Vinogradov SA (2003) Luminescent Zn and Pd tetranaphthaloporphyrins. Inorg Chem 42(14):4253–4255
192. Rumsey WL, Vanderkooi JM, Wilson DF (1988) Imaging of phosphorescence: a novel method for measuring oxygen distribution in perfused tissue. Science 241(4873):1649–1651
193. Sacksteder L, Demas JN, DeGraff BA (1993) Design of oxygen sensors based on quenching of luminescent metal complexes: effect of ligand size on heterogeneity. Anal Chem 65(23):3480–3483

194. Sacksteder L, Lee M, Demas JN, DeGraff BA (1993) Long-lived, highly luminescent rhenium(I) complexes as molecular probes: intra- and intermolecular excited-state interactions. J Am Chem Soc 115(18):8230–8238
195. Sakadzic S, Roussakis E, Yaseen MA, Mandeville ET, Srinivasan VJ, Arai K, Ruvinskaya S, Devor A, Lo EH, Vinogradov SA, Boas DA (2010) Two-photon high-resolution measurement of partial pressure of oxygen in cerebral vasculature and tissue. Nat Meth 7(9):755–759
196. Schäferling M (2012) The art of fluorescence imaging with chemical sensors. Angew Chem Int Ed Engl 51(15):3532–3554
197. Schaffar BPH, Wolfbeif OS (1990) A fast responding fibre optic glucose biosensor based on an oxygen optrode. Biosens Bioelectron 5(2):137–148
198. Schmälzlin E, van Dongen JT, Klimant I, Marmodee B, Steup M, Fisahn J, Geigenberger P, Löhmannsröben H-G (2005) An optical multifrequency phase-modulation method using microbeads for measuring intracellular oxygen concentration in plants. Biophys J 89: 1339–1345
199. Schneider K, Schütz V, John G, Heinzle E (2010) Optical device for parallel online measurement of dissolved oxygen and pH in shake flask cultures. Bioprocess Biosyst Eng 33(5): 541–547
200. Schreml S, Meier RJ, Wolfbeis OS, Maisch T, Szeimies RM, Landthaler M, Regensburger J, Santarelli F, Klimant I, Babilas P (2011) 2D luminescence imaging of physiological wound oxygenation. Exp Dermatol 20(7):550–554
201. Schrenkhammer P, Wolfbeis OS (2008) Fully reversible optical biosensors for uric acid using oxygen transduction. Biosens Bioelectron 24:994–999
202. Schröder CR, Polerecky L, Klimant I (2007) Time-resolved pH/pO2 mapping with luminescent hybrid sensors. Anal Chem 79(1):60–70
203. Severinghaus JW, Honda Y (1987) History of blood gas analysis. VII. Pulse oximetry. J Clin Monit 3:135–138
204. Shaw G (1967) Quenching by oxygen diffusion of phosphorescence emission of aromatic molecules in polymethyl methacrylate. Trans Faraday Soc 63:2181–2189
205. Smith CS, Branham CW, Marquardt BJ, Mann KR (2010) Oxygen gas sensing by luminescence quenching in crystals of Cu(xantphos)(phen) + complexes. J Am Chem Soc 132: 14079–14085
206. Smith CS, Mann KR (2012) Exceptionally long-lived luminescence from [Cu(I)(isocyanide) 2(phen)] + complexes in nanoporous crystals enables remarkable oxygen gas sensing. J Am Chem Soc 134(21):8786–8789
207. Sommer JR, Farley RT, Graham KR, Yang Y, Reynolds JR, Xue J, Schanze KS (2009) Efficient near-infrared polymer and organic light-emitting diodes based on electrophosphorescence from (tetraphenyltetranaphtho[2,3]porphyrin)platinum(II). ACS Appl Mater Interfaces 1(2):274–278
208. Songzhu L, Xiangting D, Jinxian W, Guixia L, Wenshen Y, Roukun J (2010) Fabrication of Eu(III) complex doped nanofibrous membrane and their oxygen-sensitive properties. Spectrochim Acta A 77:885–889
209. Spellane PJ, Gouterman M, Kim AAS, Liu YC (1980) Porphyrins 40. Electronic spectra and four-orbital energies of free-base, zinc, copper, and palladium tertrakis(perfluorophenyl) porphyrins. Inorg Chem 19:386–391
210. Steiner MS, Duerkop A, Wolfbeis OS (2011) Optical methods for sensing glucose. Chem Soc Rev 40(9):4805–4839
211. Steunenberg P, Ruggi A, van den Berg NS, Buckle T, Kuil J, Fijs WB, Velders AH (2012) Phosphorescence imaging of living cells with amino acid-functionalized *tris*(2-phenylpyridine) iridium(III) complexes. Inorg Chem 51(no. 4):2105–2114
212. Stich MI, Borisov SM, Henne U, Schäferling M (2009) Read-out of multiple optical chemical sensors by means of digital color cameras. Sens Actuators B 139(1):204–207

213. Stubenrauch K, Sandholzer M, Niedermair F, Waich K, Mayr T, Klimant I, Trimmel G, Slugovc C (2008) Poly(norbornene)s as matrix materials for platinum tetrakis(pentafuorophenyl) porphyrin based optica oxygen sensors. Eur Polym J 44:2558–2566
214. Thévenot DR, Toth K, Durst RA, Wilson GS (2001) Electrochemical biosensors: recommended definitions and classification. Biosens Bioelectron 16:121–131
215. Thomas P, Halter M, Tona A, Raghavan SR, Plant AL, Forry S (2009) A noninvasive thin film sensor for monitoring oxygen tension during in vitro cell culture. Anal Chem 81(22): 9239–9246
216. Tian Y, Shumway BR, Meldrum DR (2010) A New cross-linkable oxygen sensor covalently bonded into poly(2-hydroxyethyl methacrylate)-co-polyacrylamide thin film for dissolved oxygen sensing. Chem Mater 22(6):2069–2078
217. Trettnak W, Kolle C, Reininger F, Dolezal C, O'Leary P (1996) Miniaturized luminescence lifetime-based oxygen sensor instrumentation utilizing a phase modulation technique. Sens Actuators B 35–36:506–512
218. Trettnak W, Leiner MJP, Wolfbeis OS (1988) Optical sensors. Part 34. Fibre optic glucose biosensor with an oxygen optrode as the transducer. Analyst 113(10):1519–1523
219. Tusa JK, He H (2005) Critical care analyzer with fluorescent optical chemosensors for blood analytes. J Mater Chem 15(27–28):2640–2647
220. Van Houten KA, Walters KA, Schanze KS, Pilato RS (2000) Study of the heterocyclic-substituted platinum-1,2-enedithiolate 3ILCT excited states by transient absorption spectroscopy. J Fluoresc 10(1):35–40
221. Vasil'ev VV, Borisov SM (2002) Optical oxygen sensors based on phosphorescent water-soluble platinum metals porphyrins immobilized in perfluorinated ion-exchange membrane. Sensors Actuators B 82(no. 2-3):272–276
222. Vasil'ev VV, Borisov SM, Chubarova YO, Rumyantseva VD (2003) Dimerization, aggregation, and luminescent properties of palladium(II) and platinum(II) complexes with meso-tetrakis(4-carboxyphenyl)porphyrin. Russ J Inorg Chem 48(no. 3):385–390
223. Vogel A, Venugopalan V (2003) Mechanisms of pulsed laser ablation of biological tissues. Chem Rev 103(2):577–644
224. Voraberger HS, Kreimaier H, Biebernik K, Kern W (2001) Novel oxygen optrode withstanding autoclavation: technical solutions and performance. Sens Actuators B 74:179–185
225. Wang X, Chen H, Zhou T, Lin Z, Zeng J, Xie Z, Chen X, Wong K, Chen G, Wang X (2009) Optical colorimetric sensor strip for direct readout glucose measurement. Biosens Bioelectron 24(12):3702–3705
226. Wang Y, Li B, Zhang L, Zuo Q, Li P, Zhang J, Su Z (2011) High-performance oxygen sensors based on EuIII complex/polystyrene composite nanofibrous memabranes prepared by electrospinning. Chem Phys Chem 12:349–355
227. Wang Z, McWilliams AR, Evans CEB, Lu X, Chung S, Winnik MA, Manners I (2002) Covalent attachment of RuII phenanthroline complexes to polythionylphosphazenes: the development and evaluation of single-component polymeric oxygen sensors. Adv Funct Mater 12(6–7):415–419
228. Wang X, Meier RJ, Link M, Wolfbeis OS (2010) Photographing oxygen distribution. Angew Chem Int Edit 49(29):4907–4909
229. Wang XF, Uchida T, Coleman DM, Minami S (1991) A two dimensional fluorescence lifetime imaging system using a gated image intesifier. Appl Spectrosc 45:360–366
230. Wang X, Zhou T, Chen X, Wong K, Wang X (2008) An optical biosensor for the rapid determination of glucose in human serum. Sens Actuators B 129(2):866–873
231. Wenzhöfer F, Glud RN (2004) small-scale spatial and temporal variability in coastal benthic O2 dynamics: effects of fauna activity. Limnol Oceanogr 49(5):1471–1481
232. Werner T, Klimant I, Huber C, Krause C, Wolfbeis OS (1999) Fiber optic ion-microsensors based on luminescence lifetime. Mikrochim Acta 131(1):25–28
233. Wilhem S, Wolfbeis O (2011) Irreversible sensing of oxygen ingress. Biosens Actuators B 153:199–204

234. Wolfbeis OS (2006) Fiber-optic chemical sensors and biosensors. Anal Chem 78(12): 3859–3874
235. Wolfbeis OS, Leiner PMJ, Posch HE (1986) A new sensing material for optical oxygen measurement, with the indicator embedded in an aqueous phase. Mikrochim Acta 90(5): 359–366
236. Wolfbeis OS, Oehme I, Papkovskaya N, Klimant I (2000) Sol-gel based glucose biosensors employing optical oxygen transducers, and a method for compensating for variable oxygen background. Biosens Bioelectron 15:69–76
237. Wolfbeis OS, Posch HE, Kroneis HW (1985) Fiber optical fluorosensor for determination of halothane and/or oxygen. Anal Chem 57:2556–2561
238. Woods RJ, Scypinski S, Cline LJ (1984) Transient digitizer for the determination of microsecond luminescence lifetimes. Anal Chem 56(8):1395–1400
239. Wu XJ, Choi MMF (2003) Hydrogel network entrapping cholesterol oxidase and octadecylsilica for optical biosensing in hydrophobic organic or aqueous micelle solvents. Anal Chem 75:4019–4027
240. Wu XJ, Choi MMF (2004) An optical glucose biosensor based on entrapped-glucose oxidase in silicate xerogel hybridised with hydroxyethyl carboxymethyl cellulose. Anal Chim Acta 514(2):219–226
241. Wu XJ, Choi MMF (2004) Spongiform immobilization architecture of ionotropy polymer hydrogel coentrapping alcohol oxidase and horseradish peroxidase with octadecylsilica for optical biosensing alcohol in organic solvent. Anal Chem 76(15):4279–4285
242. Wu XJ, Choi MMF, Wu XM (2004) An organic-phase optical phenol biosensor coupling enzymatic oxidation with chemical reduction. Analyst 129(11):1143–1149
243. Wu X, Choi MMF, Xiao D (2000) A glucose biosensor with enzyme-entrapped sol–gel and an oxygen-sensitive optode membrane. Analyst 125(no. 1):157–162
244. Wu W, Wu W, Ji S, Guo H, Song P, Han K, Chi L, Shao J, Zhao J (2010) Tuning the emission properties of cyclometalated platinum(II) complexes by intramolecular electron-sink/arylethynylated ligands and its application for enhanced luminescent oxygen sensing. J Mater Chem 20 (43):9775–9786
245. Xavier MP, Garcia-Fresnadillo D, Moreno-Bondi MC, Orellana G (1998) Oxygen sensing in nonaqueous media using porous glass with covalently bound luminescence Ru(II) complexes. Anal Chem 70:5184–5189
246. Xiang H, Zhou L, Feng Y, Cheng J, Wu D, Zhou X (2012) Tunable fluorescent/phosphorescent platinum(II) porphyrin-fluorene copolymers for ratiometric dual emissive oxygen sensing. Inorg Chem 51(9):5208–5212
247. Xiao D, Choi MMF (2002) Aspartame optical biosensor with bienzyme-immobilized eggshell membrane and oxygen-sensitive optode membrane. Anal Chem 74(4):863–870
248. Xie K, Zhang X-W, Huang L, Wang Y-T, Lei Y, Rong J, Qian C-W, Xie Q-L, Wang Y-F, Hong A, Xiong S (2011) On-line monitoring of oxygen in TubeSpin, a novel, small-scale disposable bioreactor. Cytotechnology 63(4):345–350
249. Xu H, Aylott JW, Kopelman R, Miller TJ, Philbert MA (2001) A real-time ratiometric method for the determination of molecular oxygen inside living cells using sol–gel-based spherical optical nanosensors with applications to Rat C6 glioma. Anal Chem 73(17): 4124–4133
250. Xu W, Kneas KA, Demas JN, DeGraff BA (1996) Oxygen sensors based on luminescence quenching of metal complexes: osmium complexes suitable for laser diode excitation. Anal Chem 68(15):2605–2609
251. Xu W, McDonough RC, Langsdorf B, Demas JN, DeGraff BA (1994) Oxygen sensor based on luminescence quenching: Interactions of metal complexes with the polymer supports. Anal Chem 66:4133–4141
252. Xu W, Schmidt R, Whaley M, Demas JN, DeGraff BA, Karikari EK, Farmer BL (1995) Oxygen sensors based on luminescence quenching: interations of pyrene with the polumer supports. Anal Chem 67:3172–3180

253. Yingkui L (2011) High performance oxygen sensing nanofibrous membranes of Eu(III) complex/polystyrene prepared by electrospinning. Spectrochim Acta A 79:356–360
254. Yoshihara T, Yamaguchi Y, Hosaka M, Takeuchi T, Tobita S (2012) Ratiometric molecular sensor for monitoring oxygen levels in living cells. Angew Chem Int Ed 51:4148–4151
255. Zanzotto A, Szita N, Boccazzi P, Lessard P, Sinskey AJ, Jensen KF (2004) Membrane-aerated microbioreactor for high-throughput bioprocessing. Biotechnol Bioeng 87(2): 243–254
256. Zhang G, Chen J, Payne SJ, Kooi SE, Demas JN, Fraser CL (2007) Multi-emissive difluoroboron dibenzoylmethane polylactide exhibiting intense fluorescence and oxygen-sensitive room-temperature phosphorescence. J Am Chem Soc 129:8942–8943
257. Zhang S, Hosaka M, Yoshihara T, Negishi K, Iida Y, Tobita S, Takeuchi T (2010) Phosphorescent light-emitting iridium complexes serve as a hypoxia-sensing probe for tumor imaging in living animals. Cancer Res 70(11):4490–4498
258. Zhang G, Palmer GM, Dewhirst MW, Fraser CL (2009) A dual-emissive-materials design concept enables tumour hypoxia imaging. Nat Mater 8:747–751
259. Zhujun Z, Seitz WR (1986) Optical sensor for oxygen based on immobilized hemoglobin. Anal Chem 58(1):220–222
260. Zuo Q, Li B, Zhang L, Wang Y, Liu Y, Zhang J, Chen Y, Guo L (2010) Synthesis, photophysical and oxygen-sensing properties of a novel Eu3+ complex incorporated in mesoporous MCM-41. J Solid State Chem 183:1715–1720

BIOREV (2014) 1: 71–130
DOI: 10.1007/11663_2013_2

Published online: 13 October 2013

Electron transfer mechanisms between microorganisms and electrodes in bioelectrochemical systems

Sunil A. Patil, Cecilia Hägerhäll, and Lo Gorton

Abstract Microbes have been shown to naturally form veritable electric grids in which different species acting as electron donors and others acting as electron acceptors cooperate. The uptake of electrons from cells adjacent to them is a mechanism used by microorganisms to gain energy for cell growth and maintenance. The external discharge of electrons in lieu of a terminal electron acceptor, and the reduction of external substrates to uphold certain metabolic processes, also plays a significant role in a variety of microbial environments. These vital microbial respiration events, viz. extracellular electron transfer to and from microorganisms, have attracted widespread attention in recent decades and have led to the development of fascinating research concerning microbial electrochemical sensors and bioelectrochemical systems for environmental and bioproduction applications involving different fuels and chemicals. In such systems, microorganisms use mainly either (1) indirect routes involving use of small redox-active organic molecules referred to as redox mediators, secreted by cells or added exogenously, (2) primary metabolites or other intermediates, or (3) direct modes involving

Originally published as an article in the journal "Bioanalytical Reviews" (Patil SA, Hägerhäll C, Gorton L (2013) Electron transfer mechanisms between microorganisms and electrodes in bioelectrochemical systems. Bioanal Rev. 4(2), 159–192. doi:10.1007/s12566-012-0033-x).

S.A. Patil (✉)
Department of Biochemistry and Structural Biology, Center for Molecular Protein Science, Lund University, P.O. Box 124, 22100 Lund, Sweden

Presently at Laboratory of Microbial Ecology and Technology (LabMET), Ghent University, Coupure Links 653, B-9000 Gent, Belgium
e-mail: sunilmicro12@gmail.com

C. Hägerhäll, and L. Gorton
Department of Biochemistry and Structural Biology, Center for Molecular Protein Science, Lund University, P.O. Box 124, 22100 Lund, Sweden
e-mail: Cecilia.Hagerhall@biochemistry.lu.se; Lo.Gorton@biochemistry.lu.se

physical contact in which naturally occurring outer-membrane *c*-type cytochromes shuttle electrons for the reduction or oxidation of electrodes. Electron transfer mechanisms play a role in maximizing the performance of microbe–electrode interaction-based systems and help very much in providing an understanding of how such systems operate. This review summarizes the mechanisms of electron transfer between bacteria and electrodes, at both the anode and the cathode, in bioelectrochemical systems. The use over the years of various electrochemical approaches and techniques, cyclic voltammetry in particular, for obtaining a better understanding of the microbial electrocatalysis and the electron transfer mechanisms involved is also described and exemplified.

Keywords Microbial extracellular electron transfer · Microbe–electrode interactions · Bioelectrochemical systems · *c*-type cytochromes · Redox mediators · Nanowires · Cyclic voltammetry

Contents

Abbreviations

BESs	Bioelectrochemical systems
CA	Chronoamperometry
CV	Cyclic voltammetry
DET	Direct electron transfer
ET	Electron transfer
EET	Extracellular electron transfer
EABs	Electroactive biofilms
EIS	Electrochemical impedance spectroscopy
ITO	Tin-doped indium oxide
MFCs	Microbial fuel cells
MET	Mediated electron transfer
ORR	Oxygen reduction reaction

OMCs	Outer-membrane cytochromes
PQQ	Pyrroloquinoline quinone
SCE	Standard calomel electrode
ST	Substrate turnover
SNT	Substrate non-turnover
SHE	Standard hydrogen electrode
SEIRAS	Surface-enhanced infrared absorption spectroscopy
SERRS	Surface-enhanced resonance Raman spectroscopy
UV–Vis	Ultraviolet–Visible

1 Introduction

Long-range electron transfers (ET) are essential elements in the metabolism of various microbial forms of life. Microorganisms regulate their ET pathways in a manner enabling electrons from an electron donor to be transferred to an available electron acceptor and, to the extent they are able, to maximize their energy gain by selecting the electron acceptor with the highest potential available [1, 2]. When there is a scarcity of the soluble electron acceptors present in various natural environments, microorganisms either turn to fermentation, in a manner depending upon the substrate and environment available or make use of non-soluble solid electron acceptors. In the latter case, microbes transport electrons out of the cell, so as to achieve the reduction needed, this being referred to as extracellular electron transfer (EET). Soluble electron donors, like electron acceptors too, are depleted in some environments. In such cases, the microorganisms can oxidize insoluble electron donors through EET. Thus, EET can pertain to electron transport both in and out of the microbial cells. The linking of microbial respiration to an electrode through EET has resulted in the development of microbial bioelectrochemical systems (BESs) in which electrical current can be generated or consumed for the generation of a given product or for carrying out a particular process [3, 4]. In addition, there are cooperative behaviors in the form of interspecies ET that have been described as involving the diffusion of redox chemicals and direct contact in cell aggregates or, as reported recently, involving the passage of electric currents through naturally conductive minerals [5].

The breakthroughs in understanding of natural EET abilities of mineral-respiring bacteria [6, 7], the strong interest in producing value-added products from wastes and the demand for new sustainable energy sources for reducing dependency upon fossil-based fuels have provided a strong basis for the initiation, development, and expansion of BES research. In recent decades, EET has been exploited considerably for the development of microbial electrochemical biosensors for environmental, food, and medical applications [8–12]. The possibility of using microbes as the biological recognition elements in biosensors has attracted considerable interest

over the years due to their advantages over other bio-recognition elements, such as enzymes and cell organelles. Of the various sensing techniques reviewed recently by Su et al. [13], electrochemical techniques along with optical techniques, are the techniques most widely used for the development of microbial biosensors. In amperometric biosensors, the current signal which is generated through microbial reduction or through the oxidation of a substrate, a metabolic product or an intermediate on the electrode is recorded, and is correlated with the concentration of the analyte [12]. The EET mechanisms to be discussed in the sections that follow can also be relevant to an understanding of microbial electrochemical sensors, although the emphasis in this review is primarily on the electron exchange or transfer between microorganisms and electrodes in BESs. The light-driven microbial BESs that are receiving increasing attention nowadays are not dealt with here, however.

2 Microbe–electrode interaction-based systems

Although research on the exploitation of microbe–electrode interactions in BESs has expanded appreciably within the last decade, both in terms of number of publications and range of applications [14, 15], the ability of microorganisms to produce low-level currents was reported by Potter more than 100 years ago, in 1911 [16]. The reports on work within this area between the 1930s and the 1960s, despite their being only intermittent and sometimes rare, kept research regarding it afloat [17–20]. Efforts by various researchers in the area during the 1980s and 1990s [21–28] brought this appealing technology to the notice of a larger research community. Since then, interest in the microbe–electrode interaction-based systems has grown tremendously, due to the highly improved understanding of the fundamentals, advancements in research, as well as microbial and engineering breakthroughs [15, 29–31]. The prime examples of systems based on microbe–electrode interactions are (a) microbial fuel cells (MFCs), viewed as a potential bioelectrochemical means of producing energy in the form of electricity while treating wastewater [32], and (b) microbial electrochemical sensors for the biosensing of environmental pollutants, biological oxygen demands, toxins, fermentation products, and the like [13]. In principle, the electrons released in MFCs after microbial oxidation of a substrate are captured at the anode, then flowing through an external circuit to produce electricity, and reacting finally with protons and oxygen at the cathode (in the case of an oxygen reduction reaction), producing water as the final and clean product.

It has also been known for several years that it is possible to donate electrons to microorganisms by using electron shuttles or other indirect approaches so as to stimulate microbial metabolism or to facilitate the reduction of organic compounds to obtain useful products or to carry out certain processes [33–36]. Researchers have tried using electricity to stimulate microbial respiratory processes from fermentations to anaerobic reduction of toxic compounds ([33] and references therein). Initial reports on the use of microbial cathodes in BESs involved use of

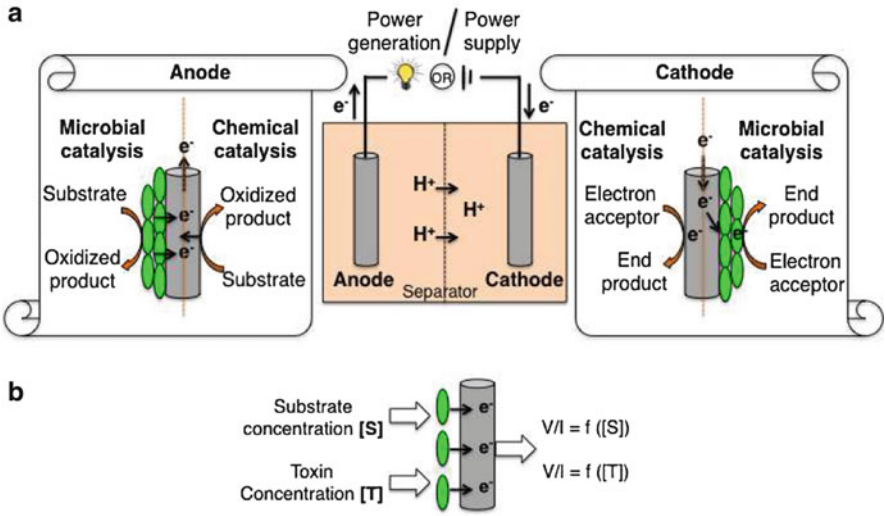

Fig. 1 Microbe–electrode interaction-based microbial bioelectrochemical systems (**a**) showing several alternative anodic and cathodic reactions (adapted from [57]) and simplified microbial electrochemical sensors (**b**)

an Mn(IV) and an Fe(III) reduction approach [37, 38]. He and Angenent reviewed in detail in 2006 the importance of biocathodes in MFCs [39]. Overcoming the limitations of abiotic cathodes and making MFC technology entirely microbial-driven have been major motives behind the idea of employing microorganisms at cathodes for catalyzing oxygen reduction reaction (ORR) [40–42]. Improvements in ORR at the cathodes achieved through use of either pure microbial cultures or enriched mixed microbial cultures have been reported consistently during the last few years [43–49]. A comprehensive review of the use of microbes for ORR at cathodes has been published recently [42]. Lovley and coworkers confirmed for the first time the direct transfer of electrons from the cathode to *Geobacter metallireducens* and to *Geobacter sulfurreducens* to achieve reduction reactions [50]. Also, use of mixed microbial inoculum sources such as sewage and wastewater, at cathodes in particular, for catalyzing denitrification reactions has been tried out [51, 52]. The discovery that hydrogen can be produced at the cathode by adding external power to the MFC [53, 54] triggered renewed interest in cathodic catalysis, the type of system involved being referred to as a microbial electrolysis cell [55]. Recent research has also shown that the anode of an MFC can be used to offset the voltage needed for chemical production at the cathode driven by electric current, a process referred to as microbial electrosynthesis, one that has created a wide range of processes for and applications of microbe–electrode interaction-based systems [56–58]. Although most of the initial studies of employing microbes at the cathode were concerned primarily with the ORR, the novel concept of microbial electrosynthesis, which is still in its infancy, has broadened the horizon of BES research and gained momentum in recent years [59–67]. All systems of this sort

exploiting microbial ET at the electrodes are classified as BESs (Fig. 1a). An overview of the concepts and processes based on microbe–electrode interactions is presented in Fig. 1. Figure 1a shows BESs with the possibility of exploiting microbe–electrode interactions at both the anode and the cathode, thus resulting in a highly versatile technology. Figure 1b, in turn, depicts microbial electrochemical biosensors for biological oxygen demand and for toxicity. In this case, the detectable current or voltage response is a function of the concentration of the analyte.

The possibility of controlling oxidation and reduction reactions at electrodes (as shown in Fig. 1) has created a vast range of applications for BESs. These include their use for generating electricity [3] as well as for denitrification [51, 52, 59], bioremediation [68, 69], desalination [70–73], metal recovery [74], and the production of reduced products such as multicarbon compounds [56, 60], hydrogen [75–78], hydrogen peroxide [63, 64, 79] and methane [80–82]. An integrated BES has also been reported to be able to simultaneously desalinate salt water, produce hydrogen gas and, potentially, treat wastewater [73, 83]. In addition, MFCs have often been proposed for use as biosensors for the monitoring of microbial activity and the measurement of both biological oxygen demand and toxicity of wastewaters [84–92]. The cathodic reaction involved depends on the energy or product output or process that determines the BES configuration [93]. In BESs, potential electrochemical losses (categorized either as operational or as catalyst-based losses) during ET occur at different levels, in particular those of bacterial metabolism, of ET at the anode, of system resistance (including that produced by the electrolyte and by the separator) and of ET at the cathode [93, 94]. Regardless of the bioelectrochemical device, the efficiency of the ET from microbes to the electrodes or vice-versa is the most important factor defining the overall performance of such systems.

3 Microorganisms exploited in bioelectrochemical systems

Irrespective of their habitat and respiration pathways, ETs are natural to microorganisms for energy generation and for survival. Microbial attachment to mineral surfaces is an activity of central importance in many biogeochemical processes [95–98]. In natural environments, the final electron acceptors can be soluble molecules such as oxygen, carbon dioxide, nitrate, sulfate, dimethyl sulfoxide and formate or insoluble compounds such as the Fe(III) and Mn(IV) oxides [99]. In the case of dissimilatory metal-reducing microbes that use minerals as terminal electron acceptors, EET leads to the reduction of minerals containing primarily iron and manganese oxides [100–102]. There has been reported to be a highly diverse group of microorganisms involved in mineral respiration [101, 103, 104]. The most thoroughly studied bacteria in this respect include several *Geobacter* sp. that are Gram-negative, as well as strict anaerobes that have been found to dominate the iron-reducing populations in a variety of subsurface environments [103, 105]. Recent genome-scale metabolic modeling of *Geobacter* spp. has provided an in-depth

understanding of their metabolism [106] and revealed the broad spectrum of putative applications available. Another commonly used group of bacteria is that of *Shewanella* sp. [102, 107]. These are Gram-negative as well as iron-reducing facultative anaerobes that thrive at redox interfaces. Several species and strains of *Shewanella* have been tried out in BES studies (see the supplementary information regarding this in [108, 109]). Of the different prominent metal reducers, *G. sulfurreducens* and *Shewanella oneidensis* MR-1 have been the choice of many researchers for use as model exoelectrogens in studying BES applications and parameters [3]. Exoelectrogens are microbes that possess the ability to transfer electrons (out of the cell) to electrodes. Numerous other microbial systems that include both Gram-positive and Gram-negative bacteria, such as *Proteus vulgaris* [110, 111], *Pseudomonas* sp. [112–114], *Escherichia coli* [115, 116], *Klebsiella pneumoniae* [117–119], *Bacillus subtilis* [120], and *Corynebacterium* sp. [121], have also been exploited to check their applicability in MFCs. Various other pure culture microorganisms are taken up in the section "Electron transfer from microorganisms to the electrodes (anodic)". Quite a different approach is to use bacteria that are genetically and metabolically well characterized, and to enhance their ability to communicate effectively with electrodes. Alferov et al., for example, used cytochrome-enriched *E. coli* to facilitate ET [122], whereas Coman et al. used engineered *B. subtilis* cells overproducing both the substrate-oxidizing enzyme and a connected transmembrane diheme containing cytochrome to enhance the overall electrochemical performance [123]. The use of several other types of pure microbial cultures [124, 125] and of natural sources of inoculum such as wastewater, sludge and soil have been explored regarding their applicability for the generation of electricity in MFCs [3]. Members of various bacterial phyla such as *alpha-*, *beta-*, *gamma-*, and *deltaproteobacteria*, *firmicutes*, *acidobacteria*, *sphingobacteria*, *bacteroides* enriched from different natural sources of inoculum fed in the anode chamber with either pure substrates or complex ones such as wastewaters of different types have been reported on thus far [126–132]. Also, the ability of such yeasts as *Saccharomyces cerevisiae* [133–135], *Arxula adeninivorans* [136], and *Hansenula polymorpha* [137] to serve as anode catalysts has been demonstrated [138, 139]. Exploration of the use of microorganisms for catalyzing anodic reactions has not been limited to the natural exoelectrogens but also includes various non-exoelectrogens in BESs [125].

It is interesting to note that the mineral reduction ability of various microbes does not necessarily predict their ability to transfer electrons to the anode in MFCs [140], whereas other microbes not found to play any significant role in natural mineral respiration have been used successfully in microbe–electrode based systems. In addition, it is now evident and well established that several microbes could use electrodes (of a type referred to as biocathodes) as a source of energy in the form of electrons, for catalyzing reduction reactions at the cathode [33, 40]. Interestingly, the applicability as biocathode catalysts of *G. sulfurreducens* [50, 141] and *S. oneidensis* MR-1 [142], which are prominent anode catalysts, has also been demonstrated. The suitability of many other *Shewanella* species as biocathode catalysts for BES applications has been investigated recently [143, 144]. Such microbes as *P. aeruginosa* [46] and several others [145] have been used to catalyze ORR for

MFC applications. Similarly, anodophilic microbial communities have been reported to be useful for catalyzing ORR at the cathode [146]. The use of natural sources of inoculum for enriching microbes that are effective for catalyzing ORR [44, 49, 147] or various other reactions such as hydrogen production [76, 148] and denitrification [52, 59] have also been investigated. The use of such natural sources of inoculum as wastewater, seawater, sludge, and soil for catalyzing ORR, and the enrichment of mixed-culture populations composed largely of *alpha-*, *beta-*, *gamma-*, and *deltaproteobacteria*, *bacteroidetes*, and *firmicutes*, which display a broad microbial diversity, have been discussed by Erable et al. ([42] and references therein). Microbes that are able to catalyze certain reactions by accepting electrons from electrodes are of particular interest in biocathode-based BESs. Other microbes used at cathodes are taken up in the section "Electron transfer from electrodes to microorganisms (cathodic)". It should be noted that the engineered environment of BESs results in the enrichment and selective growth of microbes from mixed-culture inocula, depending upon the processes involved. In addition, the ability of microorganisms both to accept electrons from the cathode and to transfer electrons to the anode is ubiquitous. The key mechanisms that are recognized as supporting microbial EET both to and from electrodes, or are proposed as doing so, are discussed in later sections.

4 Extracellular electron transfer in microbial bioelectrochemical systems

The microbial electron exchange in natural environments, such as with minerals and other extracellular electron acceptors and donors, has been suggested over the years to represent an evolutionary development of EET capabilities [149]. In such BESs as MFCs, the ability of microorganisms to transfer electrons out of the cells, such as to minerals, has been exploited by replacing such natural acceptors by the anode, which functions as an insoluble solid terminal electron acceptor [126]. The molecular mechanisms of mineral respiration in the case of the metal reducers differ, depending upon their environment or habitat and the minerals involved [150–152]. The ET to minerals has been well studied as far as metal reducers are concerned [151, 153, 154]. The role of outer-membrane cytochromes (OMCs) and conductive pili or cell appendages (referred to as nanowires) in facilitating direct electron transfer (DET) to minerals in both *Geobacter* and *Shewanella* spp. has been explored and reported on extensively [155–163]. In addition, other redox proteins, such as multi-copper proteins (OmpB and OmpC), have been shown to be important in EET during Fe(III) reduction [164]. The role of OMCs in reducing extracellular soluble redox compounds such as anthraquinone-2,6-disulfonate, humic acid [165] and riboflavins [166, 167] has also been confirmed. In addition to DET, another major pathway involved in mineral respiration is the mediated electron transfer (MET) in which redox mediators are involved in the shuttling

of electrons between cells and minerals [167–170]. In addition, the involvement of more than one pathway, or overlapping pathways, in mineral respiration has been suggested, for instance in the case of *Shewanella* sp. [102, 171]. A wide variety of microorganisms can donate electrons to electrodes without the involvement of exogenous mediators. However, the DET to electrodes has been investigated mainly for *G. sulfurreducens* and *S. oneidensis* MR-1.

In a similar fashion, the involvement of *c*-type cytochromes in microbial electron uptake from electron donors is a common process in natural environments [98, 172, 173]. For example, the OMC Cyc2 of *Acidithiobacillus ferrooxidans* has been reported to accept electrons from the iron (II) oxidation reaction [174, 175]. In *Leptospirillum ferriphilum*, a chemolithoautotrophic iron oxidizer, the periplasmic cytochrome cyt579 has been proposed to be a primary iron oxidoreductase [176]. The mechanisms involved in direct microbial electron uptake processes have still not been well established. Although these EET mechanisms can be applicable in BESs, as discussed in the sections that follow, they may or may not involve molecules or components of the types described above.

4.1 Electron transfer from microorganisms to the electrodes (anodic)

The ability of living microorganisms to transfer electrons liberated during oxidative substrate degradation has been exploited at the anode in different BESs. The anode chamber of BESs can support the growth of both biofilm-forming and planktonic microorganisms that may or may not transfer electrons outside of the cells. The key mechanisms involved in microbial ET to the electrodes that have been identified thus far are shown in Fig. 2. The electrons produced during microbial metabolism can be transferred to the electrodes via (a) membrane-spanning cytochromes [177–179] and/or electrically conductive pili or nanowires [155, 156, 180], or (b) through the involvement of self-excreted or exogenous redox mediators [113, 166, 181–184], and (c) via the oxidation of reduced primary metabolites [185–187], all depending on the microbial catalysts used and their ability to achieve EET. Electron transport via periplasmic and membrane-bound cytochromes and conductive nanowires represents DET (Fig. 2A), the most evident mechanism in case of a few exoelectrogens such as *G. sulfurreducens* [188–191] and *S. oneidensis* MR-1 [155, 192, 193]. It involves close physical contact of the bacterial cell, or any organelle-like cell appendages, with the electrode and does not necessarily require the participation of soluble redox mediators. The involvement of terminal reductases such as *c*-type OMCs in EET to the electrodes has been reported predominantly for *S. oneidensis* MR-1 [178, 192, 193] and *G. sulferreducens* [188, 194], which are notable iron reducers in their natural environments. Numerous electrochemical studies of *G. sulfurreducens* have shown *c*-type cytochromes to establish electrochemical communication with the anodes [179, 195–203]. It is

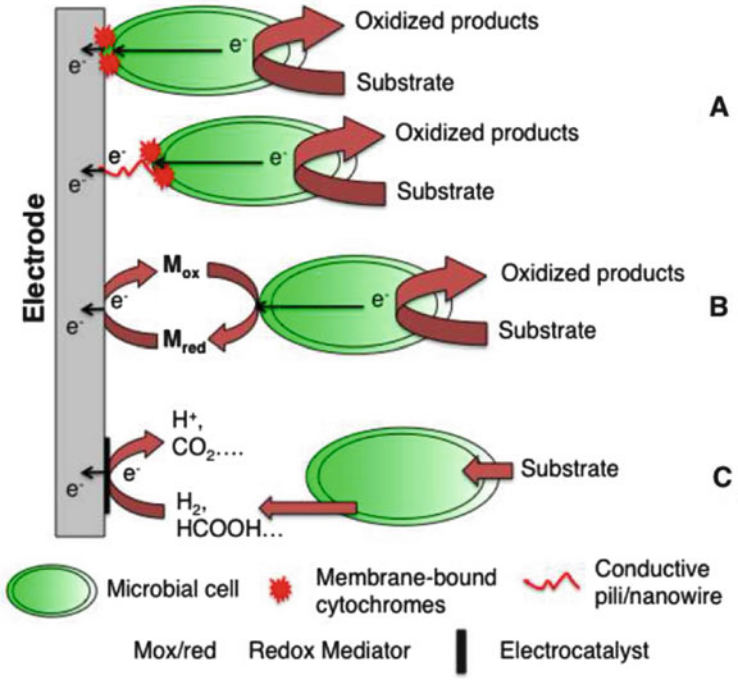

Fig. 2 Simplified representations of ET mechanisms from microorganisms to the electrodes in bioelectrochemical systems. It occurs via **A** cell-membrane-bound cytochromes and/or electrically conductive pili (nanowires), **B** self-secreted (by microbes) or exogenous redox mediators, and **C** via oxidation of reduced primary metabolites

postulated that the electron flow starts from the inner membrane protein MacA and continues to the periplasmic protein PpcA, which then transfers electrons to the OMCs at the cell surface. Studies at the genetic level have shown several outer-membrane *c*-type cytochromes such as OmcS, OmcB, and OmcZ to be involved in the current-producing biofilms of *G. sulfurreducens* [204, 205]. Analysis at the molecular level of the genes encoding OMCs has indicated the abundance and the functional redundancy of the OmcZ molecules, above all, to be responsible for the DET to the electrodes [188, 194, 204–206]. The prominent role of OmcZ in ET to the anodes has also been demonstrated in electrochemical studies [200]. OmcZ has eight hemes that display a broad range of redox potentials, from −0.420 V to −0.060 V, with a midpoint potential of −0.220 V (vs. the standard hydrogen electrode [SHE], [188]). Thus, several studies suggest that OmcZ is the main *c*-type cytochrome establishing an electrochemical communication between *G. sulferreducens* and the anode. It has also been confirmed that some of the OMCs involved in ET to metal oxides are not required for ET to electrodes [200, 204]. Also, the OMCs are reported to act as capacitors for storing electrons in the absence of EET [157, 197, 207]. Lovley and coworkers reported biofilm conductivity to be a decisive variable in high current-producing *G. sulfurreducens*

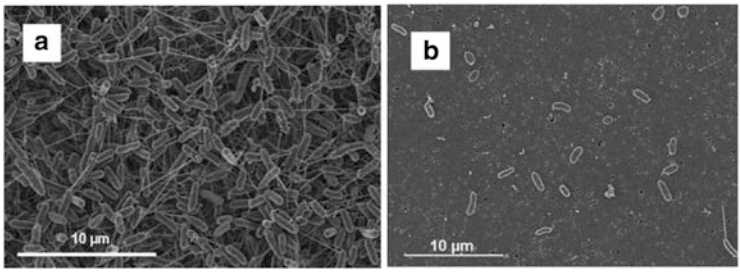

Fig. 3 Scanning electron microscopy images of *S. oneidensis* MR-1 from (**a**) electron-acceptor-limited chemostat showing nanowires and (**b**) chemostat operating with the excess of electron acceptor (20 % dissolved O_2). Reproduced from [155]. Copyright (2006) National Academy of Sciences, USA

based MFCs recently [208]. They proposed, on the basis of the electronic properties of electroactive biofilms (EABs) due to the presence of conductive cytochrome networks, their probable function as supercapacitors [209]. In addition, putative multi-copper proteins may have a role in EET to electrodes [58, 164], a matter in need of further investigation.

A direct involvement of the Mtr respiratory pathway, which consists of an inner membrane-associated quinol oxidase (CymA), periplasmic, and outer-membrane MtrCAB-OmcA complexes in EET to electrodes occurring either directly or via flavins, has been established in the case of the *S. oneidensis* MR-1 strain [193, 210–215]. In these complexes, MtrA and MtrC are multi-heme *c*-type cytochromes, and MtrB is an outer-membrane ß-barrel non-heme protein that connects the two cytochromes [211]. The three proteins in the MtrCAB complex are physically linked and are functionally dependent upon each other. The electrons from the quinone pool are passed to the inner membrane CymA, then to MtrA, and finally exit at MtrC and OmcA. A homologous complex of MtrCAB, one denoted as MtrFDE, has also been reported in *S. oneidensis* MR-1 [216]. OmcA is an outer-membrane decaheme *c*-type cytochrome, considered to be a homologue of MtrC and MtrF, that can receive electrons from MtrCAB or MtrFDE complexes [217]. It has been shown that MtrC plays a more prominent role than OmcA does in the *S. oneidensis* MR-1 EET process [213, 214]. Several electrochemical investigations have also confirmed the involvement of these cytochromes in ET to electrodes [178, 212, 213, 218]. The ET to electrodes via *c*-type cytochromes has also been reported for other *Shewanella* strains, such as *Shewanella loihica* [219, 220] and *Shewanella putrefaciens* [108]. A terminal reductase, Shew2525, has been suggested to be the OMC involved in ET in *S. loihica* PV-4 [220, 221], but further evidence is needed to confirm this.

The role of nanowires in ET to the anode has mainly been shown for *G. sulfurreducens* [190, 222]. The production of nanowires in direct response to a limited availability of electron acceptors (e.g., see Fig. 3) has also been reported for *S. oneidensis* MR-1 and for the cyanobacteria *Synechocystis* [155, 180]. The "nanowires" are pili or pilus-like extracellular appendages of bacteria that

are electronically conductive [180, 191, 222]. Whereas *Shewanella* nanowires are filamentous, *Geobacter* nanowires are divergent pili having conductor-like properties. The concept of conductive biofilms and of the ET occurring across thick EABs is rather new and not well explored [191]. Conductivity across thick biofilms is essential for achieving high current densities, since it allows microbial cells to facilitate ET to distant electrodes and contributes to current generation [153, 208]. For mixed species, a high level of conductivity in current-producing biofilms composed mainly of *Geobacteraceae* and various other microorganisms enriched with wastewater sludge has been reported recently [223]. It is speculated that the nanowires (pili networks) and the conductive proteins in the extracellular polymeric matrix play a key role both in conferring and in maintaining conductivity in thick EABs [99, 224–226]. Nevin et al. showed that the deletion of the PilA gene in *G. sulferreducens* reduces the level of nanowire production and adversely affects the current generation in thick biofilms [205]. The *c*-type cytochrome OmcS has been found by use of transmission electron microscopy to be aligned along the nanowires of *G. sulfurreducens* [227], although their being at a considerable distance from each other (>2 nm) has been reported to be a prohibitive or limiting factor for the hopping of electrons along the nanowires. Recent direct ex situ conductivity measurement studies of *G. sulferreducens* pili conducted by Malvankar et al. have highlighted the role of nanowires in long-range DET via a metallic-like conductivity [222]. According to Lovley et al. [228], the metallic-like conductivity properties of the *G. sulferreducens* pili rule out the involvement of pili associated-cytochromes in ET via electron hopping or tunneling. They have provided several pieces of experimental evidence for there being a lack of cytochrome involvement in long-range ET across biofilms and nanowires (see [229]). Scanning tunneling microcopy studies with cell-associated pili also suggest that cytochromes are unlikely to confer conductivity to nanowires [230]. However, more evidence is needed to confirm the role of the metallic-like conductivity of nanowires in ET across intact, actively respiring anodic biofilms. At the same time, an alternative model designated as superexchange ET, based on the predominant involvement of *c*-type cytochromes in EET, involving electron hopping or tunneling via a network of extracellular cytochromes associated with outer cell membranes, occurring both within extracellular polymeric substances and along pili for the electron conduction across EABs, has been proposed [231, 232]. The necessity of an extracellular polysaccharide network for cytochrome anchoring and for *G. sulferreducens* biofilm formation on metal oxides and electrodes has been reported [233]. Direct structural evidence for the association of cytochromes along the nanowires and for their proposed role in long-range ET across biofilms is required in order to establish the validity of superexchange ET model. These two models, that of the metallic-like conductivity of nanowires and the superexchange via ET within a network of cytochromes to support conductivity in *G. sulferreducens* biofilms has led recently to a marked debate concerning ET across thick biofilms [191, 224, 234, 235]. The current conception of these models can only be confirmed by accurate and reliable measurements of conductivity in actively respiring biofilms at the anode. Obtaining such measurements necessitates

researchers' to develop combined approaches for investigating EABs and collecting further and more adequate evidence for the occurrence of the ET across biofilms at anodes. Investigations of cell-to-cell ET at electrodes in EABs, which hitherto has not been well understood, could also contribute to establishing the ET across thick biofilms.

In the case of *S. oneidensis* MR-1, the necessity of *c*-type OMCs in conferring conductivity to nanowires was suggested earlier on the basis of gene deletion experiments [155]. Electron hopping via a succession of closely arranged redox molecules was suggested recently, on the basis of physical modeling, to apply to the ET that takes place along the nanowires of *S. oneidensis* MR-1 [236]. Conductance along the length of the *S. oneidensis* MR-1 filaments has also been reported [180], although there is no substantial proof of the association of cytochromes along the filaments [191]. In addition, the absolute role of the filaments in long-range ET is still unclear and questionable [193, 237], since flavins contribute mainly to ET in the case of *S. oneidensis* MR-1 biofilms. Recently, Okamoto et al. demonstrated the sequential redox cycling of OMCs to be responsible for long-range electron conduction in the multilayer biofilms of *S. oneidensis* MR-1 [178]. Based on electrochemical measurements carried out, they suggested that cell-membrane-bound *c*-type cytochromes play a predominant role in long-range electron conduction in *S. oneidensis* MR-1 biofilms. Overcoming the impedance in ET caused by polysaccharides through their biosynthesis being disrupted has been reported to improve ET across the biofilms in this organism [238], quite in contrast to what has been found for *G. sulferreducens* biofilms. The generation of current by *S. oneidensis* MR-1 [221, 239] and by *Shewanella japonica* [240] has been reported to be dominated by planktonic cells, whereas the generation of current by S. *loihica* PV-4 [219, 221], *Shewanella decolorationis* [241, 242], and *S. putrefaciens* [108] has been suggested to be biofilm-dominated, indicating there to be diverse ET mechanisms in different *Shewanella* species. In all these strains, ET has been attributed mainly to the *c*-type OMCs. Overall, the microorganisms involved in DET lead to the formation of EABs at the electrodes and can transfer electrons directly from the cell-membrane-bound OMCs to the electrodes/or across the biofilm via the conductive biofilm matrix, due to the presence of nanowires, cytochromes or endogenous mediators (e.g., flavins in *S. oneidensis* MR-1) [243]. In terms of the current level of understanding, and as explained with the EABs of *G. sulfurreducens* (Fig. 4), the combination of long-range ET through thick biofilms via nanowires and a network of extracellular cytochromes and short-range ET (between the conductive biofilm and the electrode) via *c*-type cytochromes contributes to the DET to the electrodes [228, 231].

DET to the electrodes has also been reported or been proposed for various other microbes, such as *Desulfobulbus propionicus* [244], *Thermincola ferriacetica* [245], *K. pneumoniae* [119], *Hansenula anomala* [138], and *Enterobacter aerogenes* [246], although more evidence and further studies will be needed to adequately probe the type and the role of the biomolecules involved in ET and to thus determine the DET process involved. Recently, for example, the DET via *c*-type cytochromes for

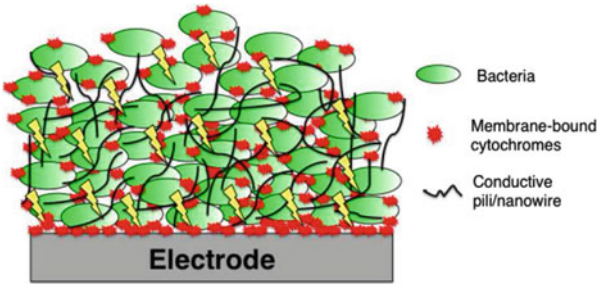

Fig. 4 Overall ET across a thick *G. sulferreducens* biofilm matrix potentially via electrically conductive pili/nanowires and membrane-bound cytochromes (adapted from [228]). In case of *S. oneidensis* MR-1, membrane-bound cytochromes [178] and self-secreted mediators such as flavins most probably play an important role in ET through a biofilm at the anode [193]

Thermincola potens as based on physiological, genetic and electrochemical measurements was reported [247, 248].

Figure 2B shows MET, another prominent ET mechanism, which is facilitated by redox mediators. Microbes that either are not capable of using a DET route or are not in physical contact with the anode (planktonic cells) utilize an indirect ET mechanism that is mediated by electron shuttles. Such mediators can gain electrons from the electron carrier within the cell or from the outer cell membrane, leaving the cell in a reduced state, and eventually transfer the electrons to the anode. In order to deliver metabolically produced electrons to the electrodes, mediators should ideally (a) possess good electrochemical reversibility, (b) have a redox potential sufficiently positive to facilitate ET from the cell and (c) not interfere with the cellular metabolism. The redox mediators can be artificial (added exogenously) or can be metabolites produced by the microorganisms (endogenous) [94]. Evidence for the role of endogenous redox mediators such as flavins (e.g., riboflavins and flavins mononucleotide) [166, 249, 250], phenazines [113, 170, 181, 251], and quinones [220, 252, 253] in ET to electrodes has been reported on extensively. ET via flavins has been found to be the predominant route to anodes associated with *S. oneidensis* MR-1, the results being confirmed rather well in electrochemical studies [166, 213, 239]. The role of flavins in ET in the case of *S. loihica* PV-4, studied by means of electrochemical and spectroscopic measurements, has also been described recently [220]. A diverse group of both Gram-positive and Gram-negative bacteria has been shown to have the ability to secrete endogenous mediators so as to promote ET to the anodes [120, 127, 254]. In mixed-culture populations, redox mediators produced by one type of microorganism have been reported to be useful for enabling another microorganism to achieve ET to the electrode [113, 249], mutualism of this sort being reported to enhance current generation in MFCs [255]. During the initial years of MFC research, use of exogenous mediators was very common [24, 35, 256, 257]. Although their use has since declined, exogenous mediators are nevertheless still being used to improve MFC performance [258–260]. The artificial mediators used most frequently to facilitate

microbe–electrode interactions in BESs include neutral red [182], thionin [257], and quinone derivatives [183, 184]. These are often used as well for the exploration of microbes that are unable to transfer electrons from their central metabolism or outer cell surfaces to the outside of the cell. Their use for large-scale BES applications has certain inherent limitations, which include the requirement of continuous addition to the system, unstable nature and drawbacks of up-scaling [261]. Since one of the most important concerns regarding their application is that of toxicity at higher concentrations, mediators are employed at low concentrations, which can restrict the overall BES performance. Nevertheless, redox mediators are extensively used in microbial electrochemical biosensors [10–13, 262]. The primary motive in using such mediators in amperometric biosensors is the possibility they provide of conducting measurements at lower overpotentials, which minimizes the occurrence of interfering reactions that could contribute to the response signal, thus increasing the selectivity. The microorganisms used as the sensing element in most amperometric microbial biosensors are either immobilized at the electrode or suspended in a medium, additional electron mediators being employed for the shuttling of electrons to the electrode. Readers are directed to the following review articles [13, 262, 263] for further details concerning direct and mediated bioelectrocatalysis in such biosensors. ET to the anode as well in BESs has been described in detail in various reviews during the last decade [261, 264, 265]. The use of polymeric redox mediators in BESs has also been surfacing due to their successful application in enzymatic biosensors and biofuel cells. The application of osmium-based redox systems and polymers for facilitating electrochemical communication between microbes and electrodes has gained momentum lately [122, 123, 137, 266, 267], a matter we have reviewed recently [268].

Another indirect ET mechanism is that obtained through the interaction at the anode of such reduced microbial metabolic products as H_2 (Fig. 2C) [127]. This mechanism is mainly applicable in MFCs that employ fermentative microorganisms and yeasts [269–271]. Although it enables the versatile microbial catalysts and substrates to be explored, systems of this sort possess low coulombic efficiencies and are less efficient for the generation of electricity, due to many of the fermentation products, organic acids included, reacting very slowly with the electrodes. Although it is possible to modify the anode surfaces with use of additional catalysts to increase their reactivity with some of the metabolic products [185], these electrodes tend to foul in the presence of oxidation products. The need of electrocatalytically very active anodes in facilitating the oxidation of such reduced metabolites limits the use of this mechanism in large-scale BES applications.

In a broader sense, the microorganisms able to use DET tend to form EABs at the anode. DET-based systems are considered to have various technological advantages over their mediated counterparts, such as the possibility they provide of working with continuous-flow systems and with large-scale BES applications. A large number of diverse and complex mixed microbial communities in the anode chamber of BESs have been identified, their having natural inoculum sources and complex substrates such as wastewaters or fermentable substrates such as glucose [125–127, 130, 272, 273]. Thus, anodic ET is considered to be ubiquitous amongst

the diverse groups of microorganisms involved. It is also not limited to the metal reducers, although enrichment of *G. sulfurreducens* from natural inocula (in particular with acetate as a substrate) has been widely reported [274, 275]. In a mixed-culture anode chamber, both electrochemically active and inactive microbes can grow and enrich depending upon the available substrates. Mutual and symbiotic associations in the MFCs have been proposed to be involved when such is the case [128, 243]. Microbes such as *S. oneidensis* MR-1 can make use of both DET and MET mechanisms (the latter via flavins) for facilitating ET to the electrodes [214, 218] and together with *G. sulfurreducens* (that use DET) are widely recognized as model exoelectrogens. Considerable electrochemical evidence for the involvement of both DET and MET mechanisms in the *S. loihica* PV-4 biofilms formed at graphite electrodes has also been provided recently [220]. Researchers have consistently used both of these ET approaches in exploring microbe–electrode interactions. The combining of both the mediated and the inherent DET abilities of exoelectrogens to enhance electrocatalysis at electrodes [276] can be considered to be one of important strategies for enhancing ET rates. Attempts to better understand the ET across thick EABs is another important task, since it can help in engineering the EABs as well as in designing electrode materials for enhancing the performance of BESs.

4.2 Electron transfer from electrodes to microorganisms (cathodic)

Microorganisms have also been used for reducing various electron acceptors at electrodes, mainly within the context of bioremediation [33]. ET from cathodes to microorganisms has either focused at ORR for maximizing the generation of electricity or for facilitating reduction reactions for bioproduction (of H_2, CH_4 or multicarbon compounds), bioremediation or denitrification processes. Although research on biocathode-based BESs has gained considerable attention recently, very little is known concerning the molecular mechanisms of microbial electron uptake from the cathode [40, 41]. The microbial ET mechanisms for the uptake of electrons from the cathode that have been proposed or identified thus far are shown in Fig. 5. They can occur either (a) directly from the electrode surface or (b) indirectly via soluble redox mediators, or (c) through the oxidation of hydrogen in various ways, all depending upon the microbial inoculum, the operational conditions that apply, and the reactions of the target. These mechanisms appear to be similar to those of anodic ET, but the components involved may differ slightly and function primarily at different potentials. As Rosenbaum et al. have indicated, the cathodic electron uptake, unlike anodic ET, is essentially not energy conserving for the microorganisms involved [40]. The fact that the formation of thin biofilms by electron-consuming *G. sulferreducens* also suggests that the energy conservation in cathodic biofilms functions less well than in their anodic counterparts [149].

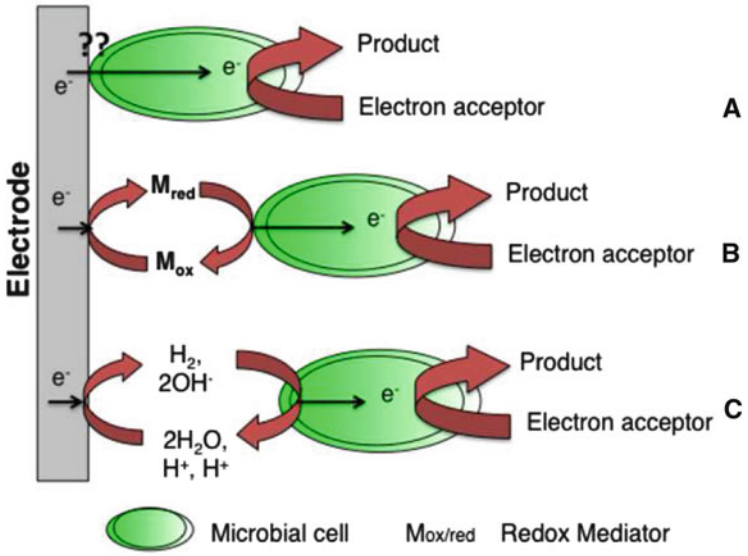

Fig. 5 ET mechanisms from electrodes to microorganisms. It occurs **A** by a proposed direct route, **B** mediated by electron shuttles, and **C** indirectly by oxidation of hydrogen by microorganisms

While many investigations have been aimed at achieving a better understanding of the DET to the anode, thus far not much is known regarding the molecular mechanisms involved in DET from the cathode to the microbes in BESs (Fig. 5A). *G. sulfurreducens*, a well-known exoelectrogen, has also been tested and confirmed as an effective cathode catalyst for reduction processes [50, 77, 141, 277]. The discovery that *G. sulferreducens* is able to accept electrons from the electrode directly [50] has been considered to be one of the major achievements thus far in the development of microbial electrosynthesis [57]. The mechanisms of direct electrode oxidation are not well recognized, although the direct electrode reduction by *G. sulfurreducens* has been attributed to the involvement of OMCs and of nanowires (see "Electron transfer from microorganisms to the electrodes (anodic)"). On the basis of experiments in which they analyzed gene expression patterns and the impact of gene deletion, Strycharz et al. noted recently that ET mechanisms from the cathode to *G. sulfurreducens* that reduce fumarate differ significantly from anodic ET mechanisms [278]. Notably, in the case of current-consuming *G. sulfurreducens*, a lesser expression of genes for pili and OmcZ (both of them required for ET to the anode) has been observed. Instead, another mono-heme *c*-type cytochrome (predicted to be located in the periplasmic space) has been proposed as playing a role in electron uptake by *Geobacter* cells [278]. Dumas and coworkers have also reported the possibility of a different mechanism being involved in the process of electron uptake by *G. sulfurreducens* [141]. In addition, different *Shewanella* strains have been exploited for catalyzing ORR [143], and for the reduction of chromate [144] and of fumarate [142]. The same Mtr pathway

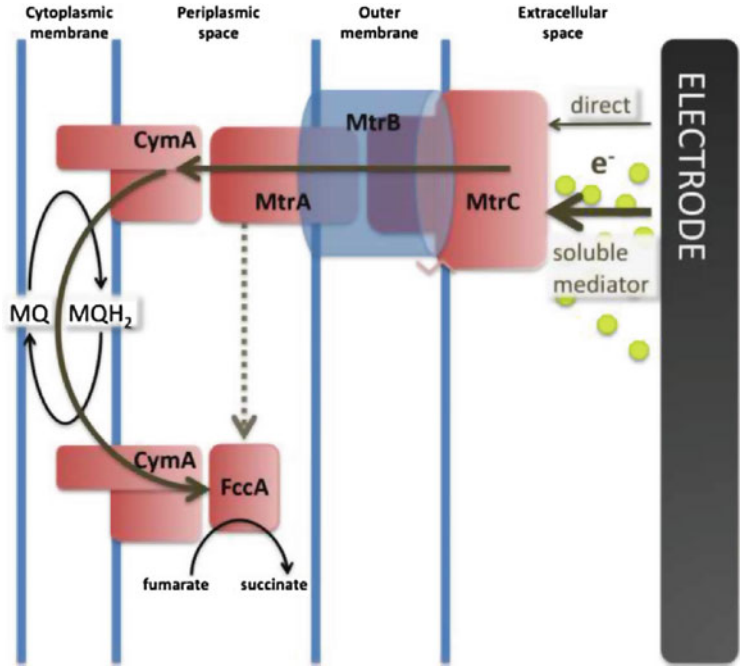

Fig. 6 Proposed model for reversible electron transfer via the Mtr respiratory pathway from electrode to *S. oneidensis* MR-1 involved in fumarate reduction [142]. It shows direct/mediated electron flow from the electrode to MtrC, then to MtrA through MtrB and subsequently to the CymA complex. From this point, electrons are passed to another CymA through the menaquinone pool and finally to FccA (periplasmic fumarate reductase) that reduces fumarate to succinate. Electrons can also divert directly from MtrA to FccA, which is proposed to be a less dominant mechanism. Reproduced from [142]

(responsible for EET to anodes) in *S. oneidensis* MR-1 (as shown in Fig. 6) has been reported recently to be able to catalyze fumarate reduction by accepting electrons from the cathode, as based on genetic, electrochemical, and thermodynamic evidence [142]. It is important, however, to obtain further evidence for reverse ET via the Mtr pathway and regarding the mechanisms involved in such processes. These results reflect differences in complexity and in the mechanisms involved, between the electron uptake processes of the *Geobacter* and *Shewanella* strains.

G. metallireducens [50], *Geobacter lovleyi* [279], *Anaeromyxobacter dehalogenanas* [62], and *Methanobacterium palustre* [82] are other microbes that have been reported to perform anaerobic respiration at cathodes. Recently, several acetogenic bacteria, such as *Sporomusa ovata* [56], *Sporomusa sphaeroides*, *Sporomusa silvacetica*, *Clostridium aceticum*, *Clostridium ljungdahlii*, and *Moorella thermoacetica* [60], were reported to accept electrons from the electrode for the reduction of CO_2 to organic compounds. In these proof-of-concept microbial electrosynthesis studies, the possible involvement of H_2 as an intermediary carrier of electrons from the cathode to the cells was excluded, indicating a DET

mechanism to be involved. Aulenta and coworkers provided electrochemical insight recently into the ability of *Desulfovibrio paquesii* to consume electrons directly from the polarized cathode and to catalyze H_2 production [78]. The use of enriched anodic biofilms that possess the ability not only to donate electrons to the electrode but also to consume electrons, pointing to the occurrence of DET to the microbes, has been recognized [146, 280]. Different microbial communities enriched at the cathode, enabling denitrification [52, 59], H_2 production [148] and other reduction reactions to take place [61, 65, 66], have also been described. In addition, both the existence of several pure microbial cultures [46, 145, 281] and the colonization and enrichment of mixed microbial communities [44, 49, 147, 282, 283] at the cathode, catalyzing ORR, have been well documented [42], although both the direct and indirect role of these communities in catalyzing the cathode reactions in question is unclear. The molecular mechanisms of direct electron uptake by several pure microbial cultures have not been established. The possible DET from cathodes to microorganisms has been reviewed in detail recently by Lovley [149]. It has been predicted that *c*-type cytochromes, along with hydrogenases, play a crucial role in microbial electron uptake from the cathode [40]. As an example, Freguia et al. reported that *c*-type cytochromes of a *S. putrefaciens* strain catalyze the cathodic ORR [284]. Further research is required to elucidate and identify the components involved in DET mechanism, since the use of microbes at the cathode has demonstrated efficient ORR and its feasibility for several microbial electrosynthesis processes.

An indirect ET mechanism that does not require physical contact between the microbial cells and the cathode takes place through redox mediators that can be either self-secreted or added exogenously (as shown in Fig. 5B). Microorganisms can use several mediators to facilitate electron uptake from the cathode. Electron shuttles frequently used to mediate the ET from cathodes to microbes include 2,4-anthraquinone disulfonate, neutral red, methyl viologen, and cobalt sepulchrate [33, 285–293]. Exploitation of self-secreted mediators such as pyrroloquinoline quinone (PQQ) by *Acinetobacter calcoaceticus* [284] and of unidentified mediators by enriched hydrogenophilic dechlorinating culture [294, 295] has been reported in connection with ET from the cathode to microbes. The role of self-secreted flavins along with that of *c*-type cytochromes in ORR in the case of *S. loihica* PV-4 has also been reported on recently [143]. Despite the excellent electron shuttling capabilities of artificial electron mediators, as well as other advantages they possess, their use for catalyzing cathodic reduction processes has certain limitations, such as the limited stability they show, their toxicity to microbes, difficulties in the product recovery achieved through microbial electrosynthesis, the questionability of large-scale and sustainable use of them, and environmental implications. Thus, their use in various electricity-driven bioproduction applications has been of limited scope. Nevertheless, the use of such mediators could help in providing a better understanding of certain fundamental aspects of the microbial electron uptake process.

Another indirect mechanism of microbial electron uptake from the cathode is through molecular hydrogen. Figure 5C shows the electrolysis of water and the electrochemical reduction of protons at the cathode leading to the production of H_2,

which is then oxidized by microbes coupled to the reduction of a final electron acceptor that can be nitrate, sulfate or CO_2. Hydrogen can be utilized as an electron donor by a variety of different microorganisms, such as chemolithotrophs and acetogens (for details, see [33]). The ET to microbes via H_2 has been explored mainly for denitrification reactions in wastewater treatment [296–299]. Recently Villano et al. reported on the bioelectrochemical reduction of CO_2 to CH_4 via both direct and indirect ET (involving abiotically produced hydrogen gas in the latter case) by a hydrogenophilic methanogenic culture, thus pointing out the possibility of two mechanisms being involved in ET from the cathode to microbes [81]. Although ET taking place through microbial oxidation of H_2 seems appealing, various concerns, such as the low solubility of H_2, its explosive nature and the need of using expensive metallic electrocatalysts to facilitate proton reduction associated with its use as a driver of microbial metabolism (described in [33, 57]) could restrict its future use in bioproduction.

A variety of pure microbial cultures from diverse phylogenetic lineages have been found to catalyze cathodic reduction reactions by using either one of the ET mechanisms referred above or a combination of them [33, 40]. In addition to the *c*-type cytochromes and hydrogenases, it is mainly oxidoreductases such as laccases that are proposed as being major components for accepting electrons from the cathode for catalyzing reduction reactions (for details, see [40]). Different ET mechanisms involved in ORR by microorganisms in corrosion processes that have been discussed recently [42] can be considered for use in studying the microbial electron uptake process involved in ORR in MFCs. Although direct bioelectrocatalysis has certain disadvantages, such as limitations to the diffusion in biofilms that can occur [300], several advantages [149] associated with it makes the use of DET to microorganisms approach both attractive and feasible for various emerging BES-based bioproduction processes. The applicability and viability of all these approaches depends on the target product, the operational mode, and the microorganisms used [300]. Overall, the ET mechanisms responsible for catalyzing ORR and other reduction reactions for facilitating bioproduction or other processes at electrodes are relatively unexplored, their thus being in need of extensive research.

5 Electrochemical techniques that provide a better understanding of microbial electrocatalysis at the electrodes

A three-electrode configuration controlled by a potentiostat has been the choice of many researchers for investigating the fundamentals of BESs and the influence of various operational as well as electrochemical parameters on either the anode or the cathode side [3]. Figure 7 shows such a three-electrode configuration and a list of frequently employed electrochemical techniques for the investigation of different processes at the microbial-electrode interfaces [301]. Although these devices are used mainly for fundamental research, they are also useful for boosting current

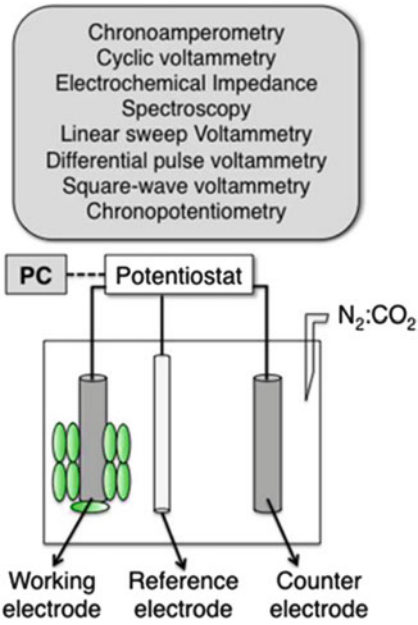

Fig. 7 A three-electrode configuration controlled by the potentiostat commonly employed to investigate various parameters of microbial EABs enriched at the electrodes in BESs by different techniques (upper gray box)

generation in MFCs as well as for biocathode-based applications. In these systems, the working electrode is provided with a constant potential (vs. the reference electrode), depending upon both the target output and the process involved, under favorable electrochemical conditions. While the chronoamperometry (CA) technique has tended to be preferred for extracting quantitative information concerning microbial electrocatalysis, it is primarily cyclic voltammetry (CV) [196] and electrochemical impedance spectroscopy (EIS) [302] that have been used to obtain qualitative information concerning the electrochemical behavior or the ET thermodynamics of the active microbes at the electrodes and of the systems involved. Linear sweep voltammetry has mostly been used to estimate the power production of MFCs [303, 304].

It is now routine practice to grow or to enrich the electrocatalytically active bacteria and to speed up the EAB formation by means of an electrochemical enrichment technique making use of a poised electrode as the electron acceptor, as well as to investigate different parameters involved in EAB formation and the bioelectrocatalytic performance of BESs using the CA technique [108, 274, 305–311]. Various studies have addressed effects of the potential employed on the bacterial activity at anodes [309, 312–315]. As reviewed by Logan et al. [316], positive anode potentials have generally been shown to favor ET from the bacterial cells to the electrode. These authors have also reviewed studies of microorganisms favoring ET at potentials that are more negative and have suggested that the potential of the terminal respiratory proteins used by the exoelectrogens rather than the anode potential applied determines the optimal growth conditions. It has been shown recently that applying polarization to an established EAB formed under

open circuit conditions may be a promising approach for improving the performance of microbial anodes [317]. Here, we will consider certain reports in which such electrochemical techniques as CV have been employed for obtaining a better understanding of the ET mechanisms involved in BESs. All the redox-potential data and the figures (with legends) referred to here are that presented in the original research articles so as to provide clear insight into the studies cited here.

Although for several decades now, CV has been regarded as a powerful, time-honored electrochemical technique used extensively for studying charge transfers occurring at electrodes in electrochemical systems, its use for gaining insight into the electrochemistry of microorganisms at electrodes has only gained momentum very recently. Harnisch and Freguia provided an excellent basic tutorial recently on the application (under appropriate conditions) of a non-destructive CV technique for the investigation of microbial EABs in BESs [318]. In microbe–electrode interface based systems, it has been used mainly for investigating the mechanisms of ET from microbes to the surface of the electrode by changing the driving force through varying the electrode potential (E). The rate of change of E (termed as voltammetric scan rate, v) while monitoring the current (i) as a function of E yields i–E–v dependencies, which can provide a great deal of information concerning the ET mechanism. In the case of microbial EABs, using the term "formal potential" rather than "(biological) standard potential" is thought to be more accurate, since the standard biological conditions are generally not fulfilled [318]. CV experiments conducted under substrate turnover (ST) and substrate non-turnover (SNT) conditions can provide information regarding in particular the formal potentials of the redox species involved in ET, the reversibility of the redox species and their dependency on the scan rate, the bioelectrocatalytically active sites and mediated or direct ET [318]. The formal potentials (the arithmetic mean of the anodic and the cathodic peak potentials) of the active sites of the redox moieties involved in ET to the electrodes are generally derived from CV curves obtained under SNT conditions. In addition, CV under SNT conditions can provide insight into reasonably complex mass transfers that occur at the EAB–electrode interface. Furthermore, the peak-shaped CV curves that can be obtained at high scan rates under ST conditions, due to the delayed mass-transfer effects involved, can provide information on the reaction kinetics at the biofilm–electrode interface [318, 319]. Comparative CV analyses carried out under ST conditions with respect to the current density at a given potential can enable a comparison of different catalysts, electrode materials, operational conditions, variables, biofilm formation and the like, under similar sets of experimental conditions. Lower scan rates usually permit the resolution of closely related redox waves, which could be difficult to resolve at higher scan rates. Therefore, when EABs are present on the electrode, lower scan rates are often employed in performing CV experiments. Comparisons of CV curves obtained during SNT conditions with use of substrate-depleted medium containing cells and of a cell-free medium can likewise be carried out to clarify the role of planktonic cells or of mediators secreted by microbes in ET mechanisms. In the sections that follow, we will discuss a variety of reports on applications of the CV technique and advancements in its use over the years in

providing a better understanding of microbial ET mechanisms both from and to the electrodes in BESs.

5.1 Cyclic voltammetry to provide a better understanding of anodic bioelectrocatalysis

The use of CV under ST and SNT conditions to identify redox centers involved in ET to the anode in BESs has been exploited to a considerable degree during the last few years [3]. Initial reports on employing CV concerned primarily the characterization of the bioelectrocatalysis at the microbe–anode interface [138, 320–326]. Liu et al. employed CV for investigating oxidation-reduction reactions at electrodes enriched with a mixed-culture biofilm [327]. In that study, the CV curves that were obtained at high scan rates suggested DET to the electrodes rather than MET to be the major mechanism for the transport of electrons from the microbes to the electrodes. Earlier, CV observations by Kim et al. [322] showed that the electrochemical activity of the metal-reducing *S. putrefaciens* could be attributed to DET from such electron carriers as OMCs located on the cell surfaces to the electrodes. The involvement of either membrane-bound or excreted redox mediators by the enriched microbial community in ET to the anodes was also reported [328]. Bond and coworkers, carrying out a series of CV experiments at lower scan rates (10 mV/s), showed that *G. sulfurreducens* biofilms (immobilized in pectin) at the anode exhibit electrochemical behavior consistent with catalytic protein film voltammetry [198]. Making use of in situ CV measurements, they provided the first report thus far of the correlation between the potential of the species involved in the ET from *Geobacter* biofilms to the electrodes and the midpoint potentials of the multi-heme cytochromes. Marsili et al. from the same group later employed CV (at 1 mV/s) for probing electrochemically the intact biofilms of two *Shewanella sp.* grown by using a poised electrode as an electron acceptor. They found, on the basis of CV results they obtained (shown in Fig. 8), that *S. oneidensis* MR-1 and *Shewanella sp.* MR-4 cells secreted flavins (mainly riboflavin), which acted as soluble mediators in EET from individual cells present in intact biofilms to the anodes [166]. In continuation of their work, this group, making use of active *G. sulfurreducens* biofilms, found the use of CV under ST conditions at low scan rates (1 mV/s) to be a promising tool for studying the main redox-active moieties in ET to the electrodes [199].

In vivo voltammetric analysis of *G. sulfurreducens* by Busalmen et al. provided considerable electrochemical insight into the mechanism of ET to the anode and the adaptation of EABs needed for an optimal EET [195]. A comparison of the expression of a new redox protein at an applied potential of 0.6 V with acclimation at 0.1–0.4 V (vs. Ag|AgCl) was reported on in this study, suggesting adaptation and self-regulation of the ET pathways at the electrode potential set to lead to an optimization of the energy generation in the organism in question. That same year, the suitability of the CV technique for investigating EAB-based anodic ET

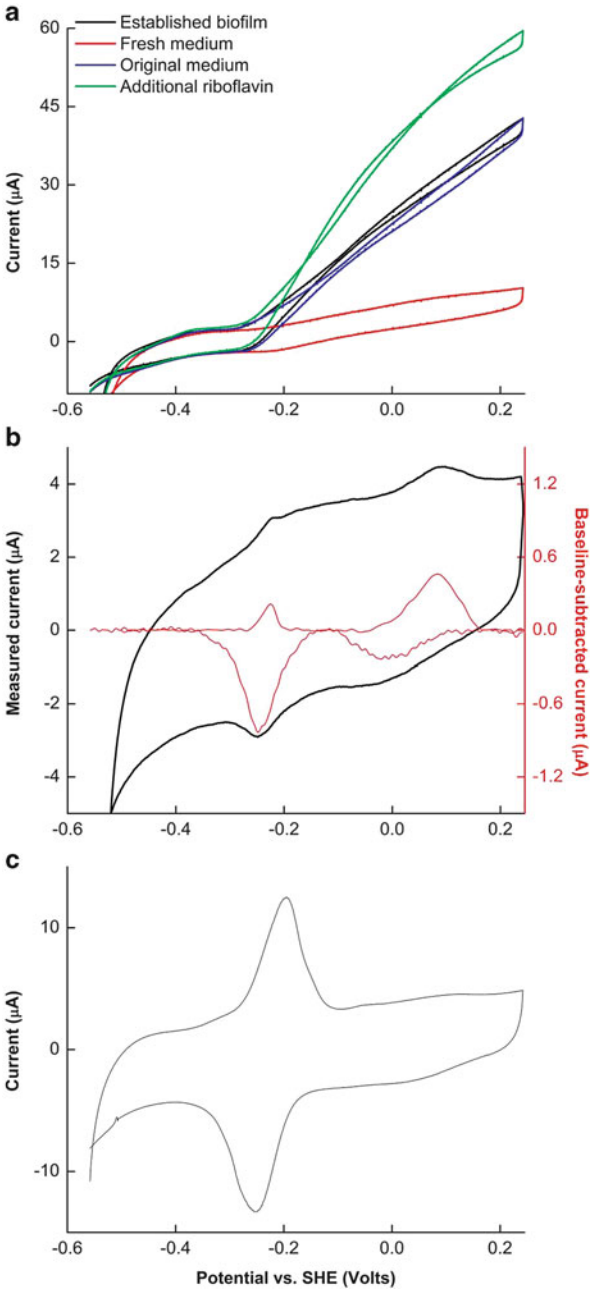

Fig. 8 Evidence for flavins to support electron transfer to electrodes. (**a**) CV curve of *Shewanella* MR-4 in the presence of electron donor (lactate), showing current–voltage relationships for established biofilms (*black trace*), the same biofilms washed in medium free of redox mediators (*red trace*), and reimmersed in the original medium (*blue trace*). The *green trace* shows the effect

processes carried out with use of *G. sulfurreducens* was effectively demonstrated by Schröder and team [196]. In that study, the large amount of information one can obtain by performing CV measurements at different stages of EAB formation and activity was demonstrated. In addition, the advantages of employing lower scan rates in obtaining information regarding the redox centers involved in the ET process were highlighted. They also correlated potentials of the redox systems derived from CV curves (obtained under ST and SNT conditions) with OMCs so as to study their role in the DET to the anodes. They likewise employed CV for analyzing mixed-culture EABs enriched from wastewater that were fed with acetate. On the basis of comparisons they made of the voltammetric characteristics of biofilms, it appeared to them that *G. sulfurreducens* (or closely related genus) represents the major electrochemically active bacterial species in these EABs [308]. An excellent study published later by Richter et al. proposed a new model for ET between the *G. sulfurreducens* biofilm and the MFC anode, based on the electrochemical behavior of these biofilms, investigated by use of the CV technique [200]. They interpreted CV data they obtained for the wild-type and the mutant strains of *G. sulfurreducens* that they investigated as indicating there to be a conductive network of bound ET mediators (cytochromes) consisting of OmcZ in the case of homogenous ET through the biofilm, and of OmcB in the case of a heterogeneous ET across the biofilm–electrode interface. They also found that the type IV pili present are important in both of the ET processes involved, and that other OMCs, such as OmcS and OmcT, play only a secondary role in ET to the anode. They also reported that the OmcE is not involved in EET to the anode. The CV data indicated protons to have a role in homogenous ET. Overall, their results provided convincing electrochemical evidence for DET in *G. sulfurreducens* biofilms, as well as for the distinct roles of several OMCs in EET to the anode, and complemented to a certain extent findings obtained with use of molecular biology approaches.

The first mechanistic insight into how EET can occur in Gram-positive bacteria without the addition of soluble electron shuttling mediators was provided by Marshall et al., using a *T. ferriacetica* biofilm [245]. The CV data obtained (see Fig. 9) suggested that the *T. ferriacetica* biofilm follows the DET mode in transferring electrons to the anode. The midpoint potential of the catalytic site for bioelectrocatalysis was −0.28 V vs Ag|AgCl, a result that can easily be visualized by use of a plot of the first derivative (Fig. 9 inset). After establishing the role of flavins in EET by *S. oneidensis* MR-1, Bond et al. expanded use of the CV technique, employing it to describe the significance and the complementary nature of cytochrome and flavin-mediated EET to the anode at different potentials with use of this microbial strain [213]. They showed two different redox-active centers of the

Fig. 8 (continued) of adding 250 nM riboflavin (approximately double the concentration). (**b**) Non-turnover CV, showing a peak centered at −0.21 V. Raw data are shown in *black*, baseline-subtracted data are in *red*. (**c**) CV of riboflavin at identical sterile carbon electrodes. Figure reproduced with permission from [166]; Copyright (2006) National Academy of Sciences, USA

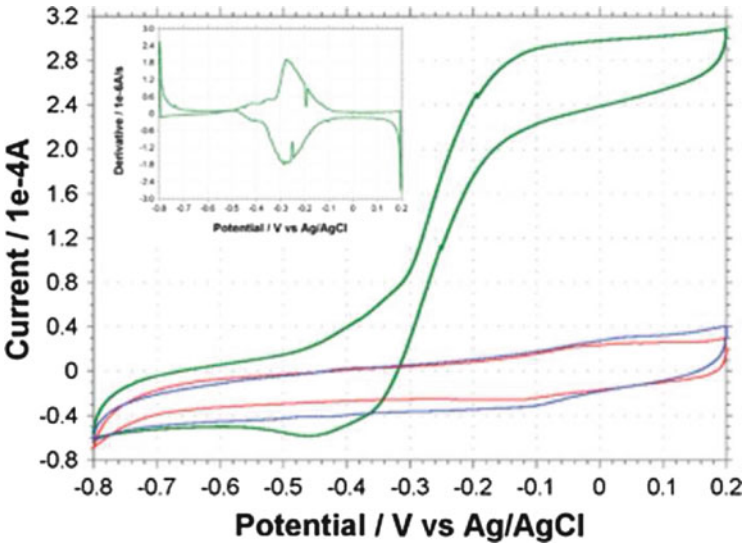

Fig. 9 Cyclic voltammograms of *Thermincola ferriacetica* biofilms (*green line*), sterile medium (*red line*) and spent medium from MFC (*blue line*). *Inset figure* shows the first derivative of the biofilm-associated catalytic wave represented by the *green line*. Scan rates were 1 mV s^{-1}. Reproduced from [245]—by permission of The Royal Society of Chemistry

adsorbed cells to be responsible for DET and MET there. Later, they reported on the physiology of EET in *G. sulfurreducens* at different stages of EAB growth, and in response to changes in the electron acceptor potential, making use of slow scan rates in their experiments [197]. The CV analysis they carried out at different stages of growth showed there to be a similar and well-defined sigmoidal catalytic wave at each stage, indicating a consistent and identical model of ET to the electrode to be present. In addition, results for CV under SNT conditions confirmed the involvement of multiple redox species of the EAB attached to the electrode in an EET. In two independent studies involving use of *G. sulferreducens* grown at different anode potentials, the authors were able to demonstrate on the basis of potentials of the oxidation peaks determined in separate CVs that the range of the anode potentials employed (from −0.36 V to 0.4 V vs. Ag|AgCl) did not affect the ET components in this organism [312, 329]. The voltammetric behavior of mixed-culture EABs enriched with acetate at different growth temperatures (as shown in Fig. 10) led Schröder and coworkers to confirm the electrochemical ET characteristics being identical and thus the composition of all the biofilms being similar (irrespective of differences in growth temperature and the markedly different maximum bioelectrocatalytic performances shown) [307]. The enriched EABs were later identified, through flow cytometry and terminal restriction fragment length polymorphism analysis, as being composed mainly of *G. sulfurreducens* [274]. CV analysis was also used by the same group to demonstrate the dependence of the ET thermodynamics of EABs on the growth medium pH value [305].

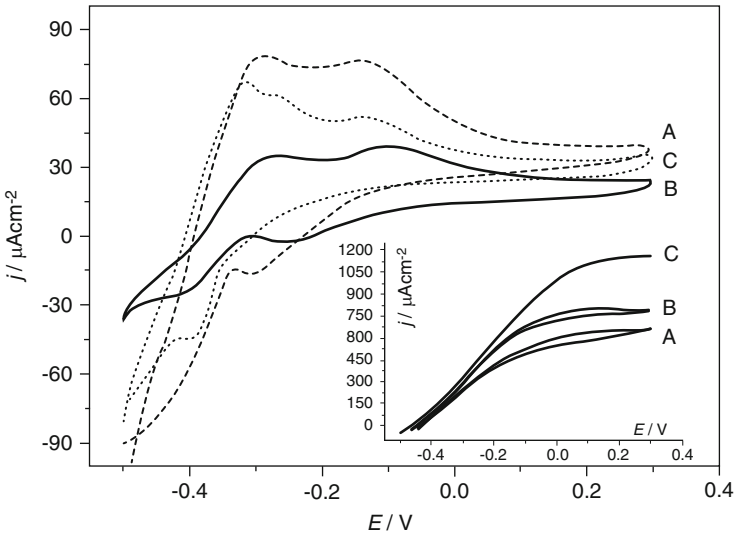

Fig. 10 CVs of microbial biofilms grown at three different temperatures **A** 22 °C, **B** 27 °C and **C** 35 °C, and recorded under non-turnover conditions. *Inset* CV curves of the same biofilms recorded under turnover conditions at the respective growth temperature. Scan rate: 1 mV s^{-1}. (E/V provided is vs. AglAgCl). Figure reprinted from [307], Copyright (2010) with permission from Elsevier

Recently, Strycharz et al. reported on an excellent model for predicting, through qualitative analysis of the CV obtained by use of biofilm-modified anodes coupled with computational methods, possible rate-limiting steps in the generation of current by the *G. sulfurreducens* strains DL1 and KN400 [202]. They suggested, on the basis of comparative voltammetric analysis carried out at different growth stages, that the major hindrances to catalytic current generation were the limited EET through the biofilm and the ET across the biofilm–electrode interface, as well as the probable proton transport out of the biofilm, though not the mass transport or turnover of the substrate. Continuing then with use of the CV technique to investigate the mechanism of the catalytic activity of the *G. sulfurreducens* strain DL1 at different stages of biofilm growth at the anodes, they suggested the catalytic current density during growth to be limited by ET from within the cells to the EET cofactors [201]. Marsili and coworkers have reported on the CVs obtained for *G. sulfurreducens* grown at tin-doped indium oxide (ITO) electrodes and on the use of a spectroelectrochemical approach in characterizing the EABs [330]. The CVs obtained under both ST and SNT conditions (see Fig. 11) and thus the information on the ET reported by them was in close agreement with the results reported by Fricke et al. [196] and by Richter et al. [200] in earlier electrochemical studies.

Schröder and team employed an advanced data processing procedure recently making use of the open-source software SOAS for in-depth analysis of CV data obtained in investigating ET mechanisms of the wild-type as well as nanofilament and several cytochrome knock-out mutant strains of *S. oneidensis* MR-1 with

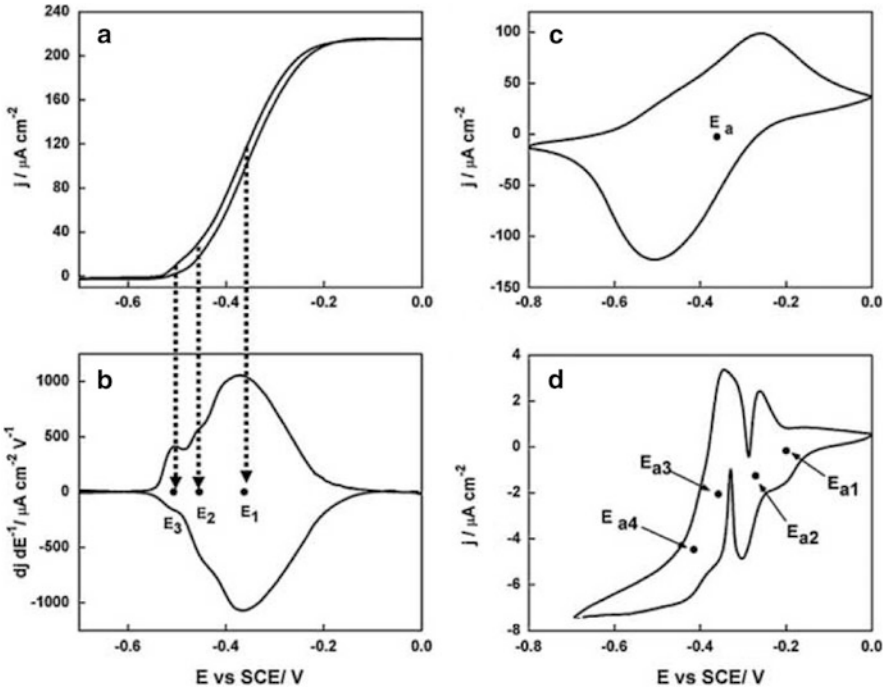

Fig. 11 CV curve (**a**) and first derivative of CV (**b**) of the *G. sulfurreducens* biofilm grown in medium containing acetate (turnover conditions), CV under non-turnover conditions, at high scan rate 50 mV/s (**c**) and slow scan rate 1 mV/s (**d**). Note that the redox couple at −0.361 V (E_1) vs. SCE actually contributes to the catalytic electron transfer at the anode, whereas E_2 and E_3 appear electrocatalytically inactive. Figure reprinted from [330], Copyright (2011) with permission from Elsevier

limited electrocatalysis [218]. The results they obtained (Fig. 12) indicated that the ET-relevant mutant strains of *S. oneidensis* MR-1 could bypass hindered DET through alternative redox proteins and self-mediated pathways. They extended this approach in studying EET by *S. putrefaciens* strain grown at different applied potentials, and showed DET rather than MET by the planktonic cells to be the major ET mechanism applying to the anode [108]. Direct electrochemical characterization of the interaction between a single *Shewanella* cell and a microelectrode through use of an optical tweezers technique under controlled conditions, providing a platform for understanding the microbe–electrode interaction occurring at the single cell level, has been reported [331]. Direct evidence for the formation of a conductive bacterial network by the *S. loihica* PV-4 strain [219], as well as the first electrochemical identification of *c*-type cytochromes in living cells through marking hemes chemically by use of nitric monoxide, were provided by Hashimoto et al. [332]. In the quest for elucidating EET mechanisms by use of CV, they later reported in vivo identification of the role of outer-membrane OmcA–MtrCAB complexes (with a midpoint potential of +50 mV vs. SHE) of *S. oneidensis* MR-1

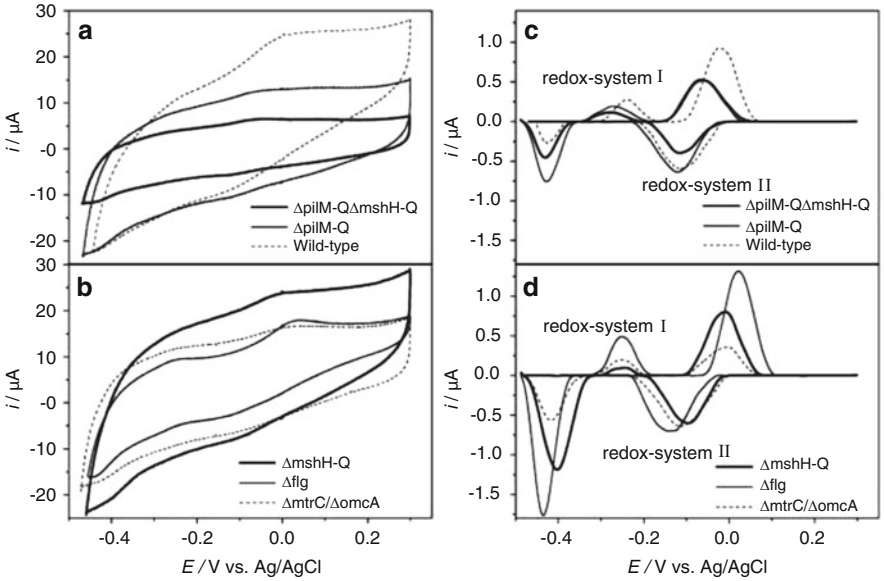

Fig. 12 CV curves (in **a** and **b**) obtained during non-turnover conditions for *S. oneidensis* MR-1 wild-type and mutant strains using a scan rate of 1 mV s^{-1}; **c** and **d** provide the respective baseline corrected curves. Figure reprinted from [218], Copyright (2011) with permission from Elsevier

and provided the first direct electrochemical evidence in DET to the electrodes [212]. The CV measurements of several *S. oneidensis* MR-1 mutant strains (including cytochrome, pilin, menaquinone biosynthesis, as well as capsular polysaccharide deficient strains) led to these findings, which were also confirmed by use of a chemical marking technique. They found as well the inner membrane-bound CymA protein, as well as menaquinone, to play no apparent role in DET, and the ET feature of the OmcA–MtrCAB complex to not be appreciably affected by the extracellular polysaccharide. They also reported recently the involvement of OMCs in long-range electron conduction across the *S. oneidensis* MR-1 biofilms and the relevance of electron conductivity to current generation [178]. They quantified by use of whole-cell voltammetry the abundance of OMCs in monolayer (approx. 0.5 µm thick) and multilayer (16 µm thick) biofilms that were wired electrically with the surface of the electrodes (see Fig. 13). The role of these OMCs in current generation was confirmed by slow-scan voltammetry. On the basis of experiments with several OMC and polysaccharide deficient mutants, they also suggested that the cell-surface-bound OMCs located on pili play a predominant role in long-range electron conduction across the thick *S. oneidensis* MR-1 biofilm. Very recently, low-scan CV has been used to characterize and confirm biofilm (enriched with soil) associated current generation on platinum wire microelectrodes of differing diameter [310]. In addition, the concentrations of the redox molecules in biofilms were derived from SNT CV data. The authors speculated, in comparing

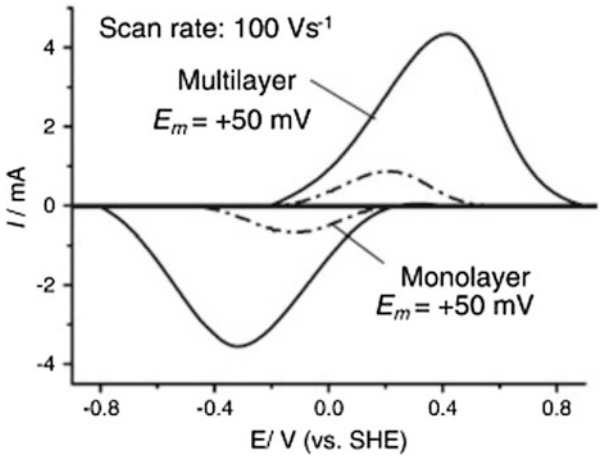

Fig. 13 Baseline-subtracted cyclic voltammograms of multilayer (*solid line*) and monolayer (*dotted line*) biofilms of wild-type *S. oneidensis* MR-1. It indicates an eight-fold larger coulombic area in the redox-wave with a multilayer than that of a monolayer biofilm. The scan rate was 100 Vs^{-1}. E_m is the midpoint potential. The raw data for these voltammograms are shown in the supporting information in [178]. Reprinted with permission from Elsevier, Copyright (2011)

their CV data with published reports on pure cultures, there to be an enrichment of the *G. sulfurreducens* community in EABs.

Both DET and MET mechanisms, via membrane cytochromes and self-secreted mediators, respectively, were demonstrated recently, on the basis of CV and differential pulse voltammetry along with fluorescence spectroscopy, to be involved in ET in *S. loihica* PV-4 biofilms [220]. A gradual switch from DET to MET in these biofilms, as shown by voltammetric data (Fig. 14) obtained at different stages of biofilm formation, was also reported. The authors attributed this to the accumulation over time of various mediators, such as flavins, at the biofilm–graphite electrode interface, this also being confirmed by fluorescence spectroscopy [220]. Logan and team have reported recently, using CV, the presence of up to seven redox peaks in *G. sulfurreducens* biofilms grown at different set potentials over relatively long periods of time (>20 days), (see Fig. 15), indicating there to be possible additional respiratory components in this microbe [203]. Thus, they provided electrochemical evidence for the expression of additional EET components through the expansion of the electrode potential range originally set, as well as for longer acclimation periods, suggesting an adjustment of this exoelectrogen to have taken place in accordance with the terminal electron acceptor. Regarding CV measurements obtained under ST conditions, Leech and coworkers have reported there to be heterogeneous ET, one electron at a time, from *G. sulfurreducens* biofilms (grown at 0 V vs. Ag|AgCl) to a graphite electrode, through a dominant redox species centered at −0.41 V, attributed to the octa-heme OmcZ cytochrome [333]. They also extended the use of voltammograms recorded

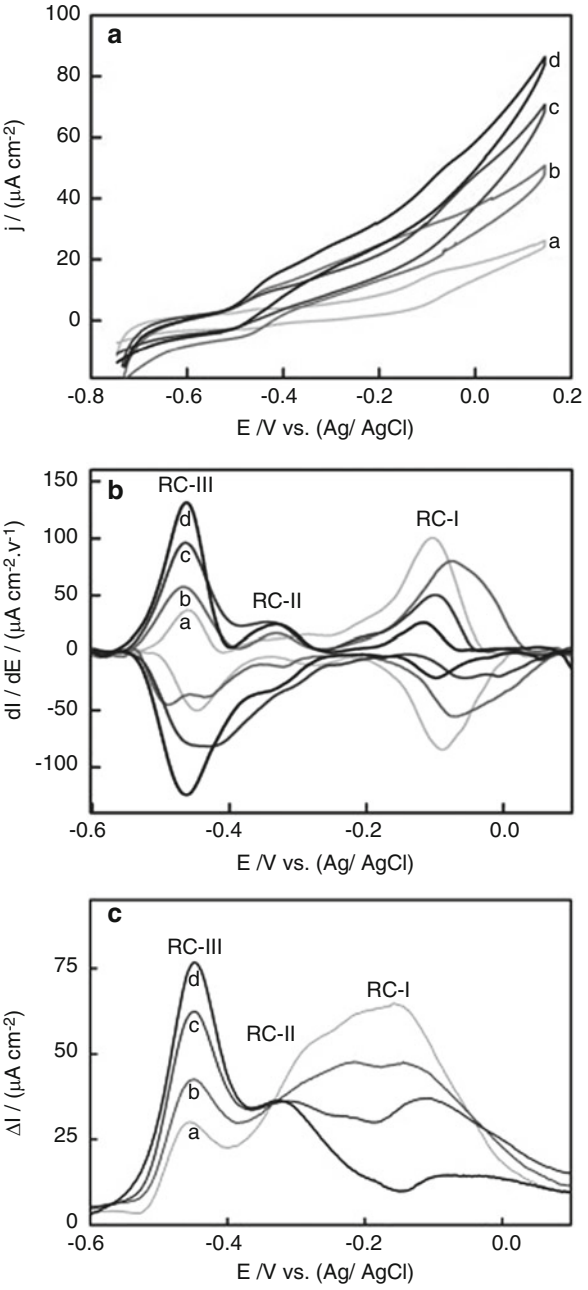

Fig. 14 (**a**) Cyclic voltammograms at scan rate of 1 mV s^{-1} obtained at (*a*) 24 h, (*b*) 48 h, (*c*) 72 h and (*d*) 96 h after medium change, and (**b**) first-order derivatives of corresponding CVs of *S. loihica* PV-4 biofilms formed at graphite electrode. The major redox centers in first-order derivatives of CVs (**b**) were identified as RC-I = −0.07 V, RC-II = −0.35 V, and RC-III = −0.44 V vs. Ag|AgCl that are attributed to outer-membrane c-type cytochrome, quinone derivative and riboflavin, respectively. (**c**) Differential pulse voltammetry of these biofilms associated with graphite electrode collected at regular time intervals shows these major redox centers that confirms the CV information and gradual shift from the DET to MET mechanism. Figure reprinted from [220], Copyright (2012) with permission from Elsevier

under SNT conditions to obtain an estimate of the redox species surface coverage, its concentration, and the charge-transport diffusion coefficients.

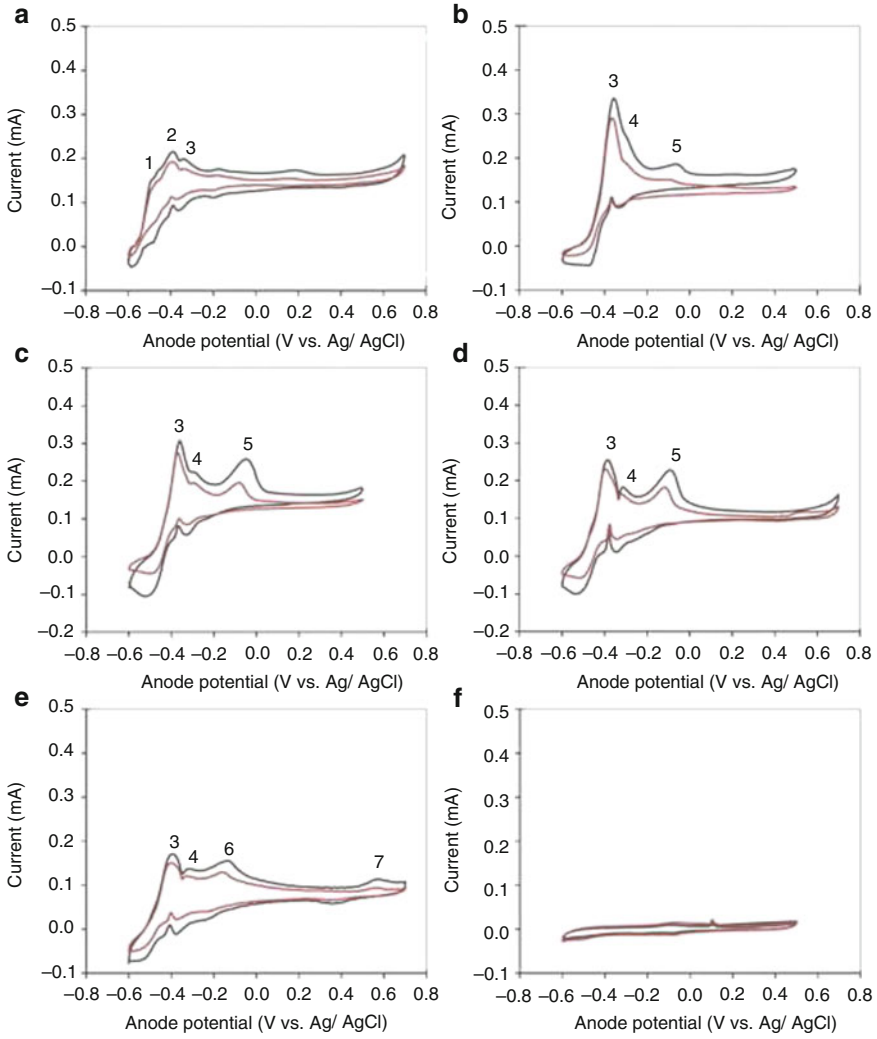

Fig. 15 Cyclic voltammograms of *G. sulfurreducens* grown at different anode potentials of (**a**) −0.46 V, (**b**) −0.30 V, (**c**) 0 V, (**d**) 0.3 V, (**e**) 0.60 V, and (**f**) blank in sodium acetate depleted growth media at different scan rates (*black lines* 1 mV/s; *red lines* 0.5 mV/s). The peaks *p1* and *p6* have not been previously observed, expanding the range of known electron transfer components in *G. sulfurreducens*. Figure reprinted from [203], Copyright (2012) with permission from Elsevier

The CV data on anode-bound *S. oneidensis* MR-1 and *G. sulfurreducens* (that have emerged as model exoelectrogens) differs very considerably (as evident in the literature), reflecting the fundamental differences in the EET properties involved. For electrodes having either thin biofilms or EABs low in bioelectrocatalysis, use of alternative electroanalytical techniques, such as square-wave voltammetry, which amplifies the Faradic current response, has been proposed [318]. CV has also been

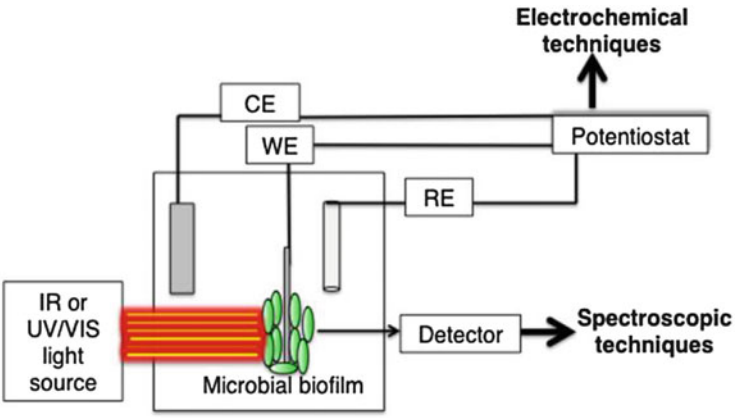

Fig. 16 Scheme showing the three-electrode set-up (*CE* counter electrode, *WE* working electrode, *RE* reference electrode) for possible simultaneous investigation on EABs by applying both electrochemical and spectroscopic techniques

employed for investigating ET pathways in several other microorganisms. Wu et al., for example, provided electrochemical evidence to support occurrence of the DET mechanism in the sulfate-reducing bacterium *Desulfovibrio desulfuricans* via periplasmic cytochromes and hydrogenases, as well as the role of palladium nanoparticles in EET [334]. Wrighton and coworkers employed electrochemical analysis to support DET by the Gram-positive bacterium *Thermincola potens* strain JR [247] isolated from the anode surface of the MFC [129].

5.1.1 Combining electrochemical and spectroscopic techniques

Spectroelectrochemical techniques can provide information on the types of chemical bonds, and thus relevant structural information regarding the electroactive species at the cell surfaces. A combined approach (shown in Fig. 16) involving use of surface-enhanced infrared absorption spectroscopy (SEIRAS) [179, 207], surface-enhanced resonance Raman spectroscopy (SERRS) [335] and ultraviolet–visible (UV–Vis) spectroscopy [336], together with CV, has been reported on and has gained broad acceptance as a means of studying the redox processes and moieties involved in ET at the microbe–electrode interface. Approaches of this type have been explored for use both with pure cultures of exoelectrogens, such as *G. sulfurreducens*, and with EABs enriched from natural sources of inoculum, such as, wastewater. Use of spectroscopic techniques provides a clear opportunity to obtain detailed information concerning the microbe–electrode interface. Busalmen et al. exploited this combined approach for the first time to obtain insight into the identity of molecules involved in ET from *G. sulfurreducens* to the electrode [179]. Recognizing the power of attenuated total reflection-SEIRAS in selective and specific resolution of bacterial cell surface molecules that are in direct contact with the electrode when studying the

Pseudomonas fluorescens strain [337], they later applied this technique for investigating the interface between *G. sulfurreducens* and a polarized thin-film gold electrode. They described, on the basis of attenuated total reflection-SEIRAS data and subtractively normalized interfacial Fourier transform infrared spectroscopy data concerned with the amide bands (as spectral indicators) and its correlation with CV data, the role of OMCs in DET to the electrodes during current generation, obtaining an in vivo understanding of the molecular mechanisms of ET in whole-cell systems. They extended this work then for analyzing the electrochemical features of *G. sulfurreducens* adsorbed at a gold electrode, reporting the occurrence of at least two different redox pairs of OMCs on the cell surface in response to the polarization potential used, their results suggesting the existence of alternative pathways for ET [207]. The first application of UV–Vis spectroscopy to the measurement of absorption spectra and determination of the spectroelectrochemical properties of cell-membrane-associated multi-heme *c*-type cytochromes in intact cells was reported by Hashimoto and coworkers, making use of *S. loihica* PV-4 [338]. They revealed, through use of UV–Vis evanescent wave spectroscopy, there being large differences in the redox properties of various purified proteins and protein complexes in viable bacteria adsorbed at ITO electrodes, indicating the importance of in vivo studies of membrane proteins. Through chemically marking hemes with nitric monoxide, they later were able to demonstrate the first electrochemical identification of *c*-type cytochromes in living cells, their also reporting on the in vivo ET kinetics evident in the same *Shewanella* species [332], although these studies were conducted on bacterial cells adsorbed to the electrodes rather than on fully grown and viable EABs. With regard to the need of investigating redox proteins in viable EABs, Marsili et al. reported the feasibility of using UV–Vis spectroscopy for studying the *c*-type cytochromes behavior in a thin and viable *G. sulfurreducens* biofilm grown at ITO electrodes [330]. They reported too on the in vivo characterization of reversible redox conversion of cyt c_{552} in a viable biofilm.

The first in situ spectroscopic characterization of OMCs by use of SERRS in microbial EABs grown at a silver electrode was reported by Millo et al. [335]. Through complementing SERRS data with CV information, they were able to reveal the presence of two different *c*-type cytochromes in EABs enriched with wastewater and acetate. In addition, the possibility of two parallel ET pathways, one from each of the cytochromes to the electrode, or two electron exits interconnected via an electron relay, was suggested. Recently, Bond and coworkers succeeded through use of simultaneous CV and UV–Vis spectroscopy analysis, in revealing the redox status of cytochromes, their confirming *c*-type cytochromes being the primary electron reservoirs within active EABs of *G. sulfurreducens* [336]. They also predicted the involvement of the periplasmic cytochrome PpcA in serving as a gate for the electron flow to the OMCs in *G. sulfurreducens* biofilms. They extended the use of spectroscopy in analyzing EABs through continuous monitoring of their cytochrome redox status at different stages of growth in both the presence and absence of the electron donor (acetate) [339]. In monitoring the redox status of *c*-type cytochromes, they observed an accumulation of electrons within cytochromes in an EAB after multiple layer formation at the electrode. They

also suggested that ET to and from the cytochromes within the biofilm represents the rate-limiting step in the overall electron exchange process.

All of these reports strongly support the understanding of DET to the electrodes as occurring mainly via *c*-type cytochromes in model exoelectrogens, while addressing other aspects of ET at the EAB–anode interface as well. The review of the literature reported here also highlights the advancements through the use of sophisticated CV techniques that have occurred over the years in gaining a better understanding of microbe–electrode interactions. The combined spectroscopic and electrochemical approach described here is capable of providing, with further exploitation of it, structural and functional information on OMCs in intact EABs or electron exchange processes at the microbe–electrode interface with use of well-characterized electrode materials such as gold, platinum, and silver. In addition, the combined approach of using both topographic characterization and spectroscopic techniques [340] can provide help in understanding the ET dynamics and the molecular interactions occurring on such engineered interfaces.

5.2 *Cyclic voltammetry to provide a better understanding of cathodic bioelectrocatalysis*

In comparison with the remarkably rapid advances that have been made in anodic bioelectrocatalysis, the progress achieved in the use of microorganisms at the cathode for catalyzing reduction reactions has been rather slow, but has gained renewed attention. Despite the demonstration quite a few years ago of the ability of *G. sulfurreducens* and *G. metallireducens* to use the electrode directly as an electron source [50], this area has remained a bit obscure over the years during the development of BESs. As noted earlier, microbial electron uptake from the cathode has not been understood particularly well. Studies on the involvement of cytochromes of microbes grown on the cathodes that act as electron donors are rare. Initial attempts of using microbes at the cathode were directed mainly at ORR, aimed at making MFCs completely microbially driven and thus cost-effective. The recent revival of electrically driven microbial bioproduction has triggered an increasing interest in exploiting microbes at the cathode, as well as in understanding the molecular mechanisms of ET from the cathode to microbes. Although CV has been utilized extensively for elucidating anodic ET mechanisms, it has not been exploited much for identifying microbial electron uptake from the cathode. Thus far, it has been used primarily to confirm biofilm-associated direct electrode oxidation. For example, the voltammetric evidence for reversible electroactivity of *Clostridium isatidis* on the graphite electrode for the bacterial-driven reduction of indigo dye has been reported [341]. Researchers have used it mainly to confirm the results of microbial electrocatalysis at cathodes [141] and to investigate the electrochemical reduction of oxygen [43, 46, 64, 145, 281, 342]. Bergel and coworkers, for example, implemented the use of CV for studying electrochemical

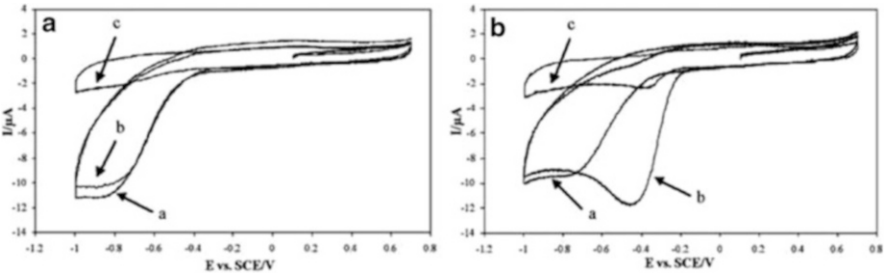

Fig. 17 Cyclic voltammograms of (**a**) phosphate buffer alone and (**b**) *P. aeruginosa* PA01 in phosphate buffer (*line a*), after 1 h of gentle stirring (*line b*) and after 20 min of nitrogen bubbling (*line c*). Reprinted from [46], Copyright (2010) with permission from Elsevier

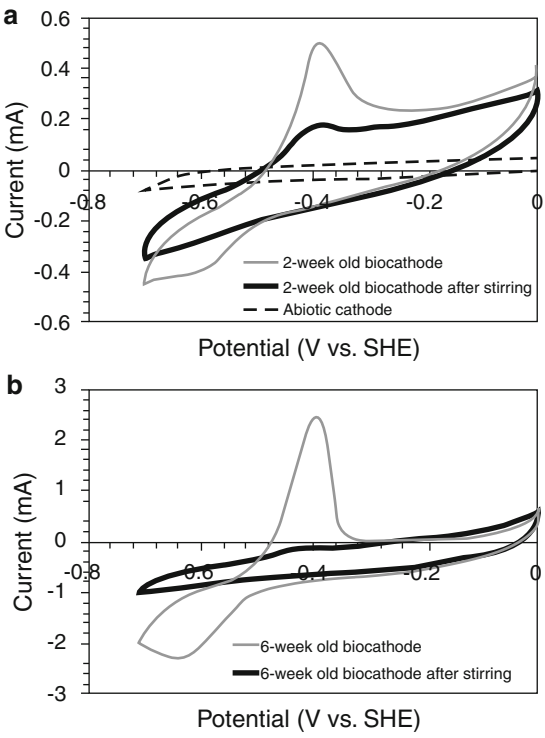

Fig. 18 CV curves (scan rate: 50 mV/s) carried out on the 2-week-old (**a**) and 6-week-old (**b**) biocathode before and after stirring (1 min at 150 rpm) of the liquid phase. Reprinted from [294], Copyright (2010) with permission from Elsevier

O_2 reduction by a wide range of aerobic and facultative bacteria [145]. The direct transfer of electrons from electrodes to microbes was confirmed on the basis of CV data they obtained, their suggesting that electroactive bacteria are widespread in different groups. Further studies in the form of long-term MFC experiments are needed, however, to determine their role in efficient ORR. The authors just referred to have also reported the ability of several isolates of *Pseudomonas aeruginosa* (that can catalyze oxidation reactions at an anode) to catalyze the electrochemical

reduction of O_2 (see Fig. 17) without the involvement of such mediators as phenazines [46]. Recently, they reported, on the basis of CV tests, of several bacterial isolates from EABs being formed in seawater for electrochemical O_2 reduction [281]. Similarly, Heijne et al. used it to confirm catalytic O_2 reduction, in comparing the performance of biocathodes grown at different potentials [43].

Aulenta et al. have employed CV for revealing the presence of redox-active components in electroactive biocathodes proposed as being involved in the EET process in the bioelectrochemical dechlorination of trichloroethene to form ethene [294]. CV data obtained here revealed for the first time a direct electrochemical dechlorination reaction without the use of mediators being required (Fig. 18). It also revealed the detachment of redox-active components possibly involved in the EET process after vigorous magnetic stirring. The direct role of attached microorganisms at the cathode in the reductive dechlorination of trichloroethene was further confirmed by microscopic, molecular and electrochemical (such as EIS) techniques. They also used CV to show that the capacity of the hydrogenophilic methanogenic culture for EET with the electrodes was a constitutive feature during bioelectrochemical reduction of CO_2 to CH_4 [81]. The extensive use of CV to elucidate ET pathways in the case of *A. calcoaceticus*- and *S. putrefaciens*-based biocathodes has been reported by Freguia et al. [284]. On the basis of the results obtained, they suggested the use of mediated ET via self-secreted redox compounds (close to PQQ) by *A. calcoaceticus* and the involvement of outer-membrane-bound redox compounds in ET in the case of *S. putrefaciens.*

CV has also been used for studying the bioelectrochemical behavior of cathodic biofilms during their long-term operation [45]. Recently, Bond and coworkers employed voltammetric techniques for demonstrating the fumarate reduction reaction in *S. oneidensis* MR-1 in which electrons from the cathode were consumed [142]. Through comparing several mutants, they obtained evidence for the involvement of Mtr pathway proteins in the cathodic electron uptake process. Liu et al. reported on the potential role of flavins secreted by *S. loihica* PV-4 in cathodic ORR, making use of CV measurements in their study [143]. Aulenta et al. have recently applied it to investigate the electron consumption mechanism by *D. paquesii* producing H_2 [78]. However, except for these few reports, none of the studies considered here addressed in a systematic way by use of the CV technique the uptake of electrons by microbes from the cathode. Detailed investigations are clearly needed to determine and adequately understand the ET mechanisms from cathodes to microorganisms. Use of a molecular or genetic approach along with the exploitation of electrochemical and spectroelectrochemical techniques is called for here.

5.3 Use of electrochemical impedance spectroscopy in microbial bioelectrochemical systems

EIS is a well-known non-destructive electrochemical technique for measuring the impedance of a system at different frequencies, one that is conducted by use of a potentiostat with EIS functions. Although its use in BES research can result in a number of important developments, it has been mainly employed for measuring system resistance ([343] and references therein). Several years ago, Strik et al. came up with a number of recommendations and associated criteria regarding the feasibility of using EIS for investigating MFCs [344]. He and Mansfeld also discussed the use of EIS for investigating various parameters in BESs [302]. They suggested its use, for example, in characterizing electrode materials, measuring capacitance, analyzing biofilm enrichment and development, and examining different experimental conditions and bacterial interactions with the electrodes in BESs [302]. Initially, it was used mainly for determining the internal resistance or the impedance of individual electrodes in MFCs [304, 345, 346]. EIS data analyses of *G. sulfurreducens* biofilms immobilized at the anode could be used to indicate, for example, on the basis of a possible decrease in the charge transfer resistance together with an increase in the capacitance, which ET processes were active [198, 199]. It has also been employed to investigate biofilm growth on the basis of electrochemical activity, through determining the resistance of the anode charge transfer, which is inversely proportional to the rate of ET [347]. The linking of EAB growth with changes in the capacitance of the anode brought about by a double layer of electrodes being formed on the biofilm has also been reported recently [348]. In addition, EIS has been found to be useful for investigating such process parameters as flow rate, ionic strength and pH in connection with proton transfer and MFC performance [349, 350]. Dominguez-Benetton and coworkers have critically reviewed recently the use, analysis, and interpretation of EIS data [343], and have also provided examples of the correct and improved interpretation of EIS data for providing an understanding of BESs and for optimizing their use.

Although the application of EIS for investigating biocathodes has not been developed thus far, its use for characterizing the ET performance of a dechlorinating biocathode has been reported [294]. There, EIS was used to obtain experimental evidence regarding the role of attached microorganisms on a polarized carbon paper electrode in an EET process. Heijne et al. used it to identify the charge and mass-transfer resistances of an O_2-reducing biocathode [351]. Lovley and coworkers also demonstrated recently, on the basis of EIS measurements, that the highly conductive EABs show a reduced resistance during electron flow through the biofilm and a low activation energy barrier for ET from the biofilm to the anode [208]. They have also exploited EIS, CV and galvanostatic charge–discharge cycling to demonstrate the pseudocapacitive properties of EABs based on the *c*-type cytochromes that are embedded in the conductive matrix of *G. sulfurreducens* biofilms [209]. EIS has also been employed recently for determining the rate-limiting factors in H_2 production at a cathode produced by use of

D. paquesii [78]. The increasing use of the EIS technique for investigating various parameters that determine or limit the performance of the bioanode or the biocathode, or both, can be expected to pave the way for their broader application in BES research.

The effectiveness of these electrochemical techniques in providing a better understanding of fundamental ET mechanisms (redox centers and moieties), as well as of process parameters, and of other electrochemical activities occurring at the microbe–electrode interface has been demonstrated. The ET models and the information regarding other parameters that have been obtained by various researchers on the basis of the CV and EIS data they have gathered have increased very much the basic understanding of BESs, which will be of considerable help in designing future strategies aimed at advancing application of them. Their ability to provide extremely useful qualitative and quantitative information concerning many matters of interest, along with the simple operational protocols they offer, point to their extensive use for investigating the microbiology-electrochemistry interface in BESs of different types. These techniques also have prospects of being developed into diagnostic tools for large-scale, on-line BES assessment. Although they have certain limitations, with accurate analysis they can be expected, when employed either independently or in combination with various other techniques, to provide highly useful information regarding ET thermodynamics at microbe–electrode interfaces.

6 Conclusions and future prospects

Alongside the rather thoroughly studied application of BESs for generating electricity, there is an increasing interest in electricity-driven, microbially catalyzed reactions at the cathode that are of industrial or environmental relevance. These call for a better understanding of the molecular mechanisms involved in microbial electron donation and uptake, to and from the electrodes. In the review presented here, the ET mechanisms that microorganisms employ for using the electrodes as electron acceptors or donors were discussed. The literature on exploiting bioanalytical techniques such as CV for elucidating such ET mechanisms was also reviewed. Notably, in such microbes as *S. oneidensis* MR-1 and *G. sulfurreducens* that have been studied in detail, the ET mechanisms are strikingly different. Various applications of the microbe–electrode interactions can be expected to emerge with advances in the understanding of microbial EET mechanisms and the introduction of new and possibly novel microbial catalysts. The main component of BESs is the microbe–electrode interface, a better understanding of which could provide new and important insights into the fundamentals of microbial responses in such engineered systems. The investigations of such matters as long-range ET across EABs, ET kinetics and charge accumulation appear to be highly promising aspects of BES research as it can be envisioned. The combined approach of using bioanalytical techniques (such as CV) together

with mathematical modeling (involving additional software) and spectroscopic, microscopic and molecular biological methods can enhance current knowledge in the area considerably and clarify the microbial ET mechanisms of relevance within biofilms and at both the anodic and the cathodic interfaces.

Although the basic electrochemistry of the microbial anodes has been studied extensively, the ET mechanisms are still far from clear. For DET to the electrodes, it is well documented that OMCs participate in the electron transport, yet further authentication of the proteins from various other microorganisms is needed in considering large-scale applications of BESs. Since the conduction of electrons through the thick EABs to the distant electrodes is of utmost importance in the designing and manufacturing of high performance anodes in MFCs [319], it is highly important to learn more of the molecular mechanisms of ET across such EABs. It is also important to investigate other microorganisms that possess conductive filaments or pili, including their functioning and their mechanisms of electron conduction, so as to be able to determine the role of such filaments in EET. As suggested by Lovely in a recent review on "Electromicrobiology", investigations of natural analogs of electrodes, such as graphite deposits, could enhance our understanding of the microbe–electrode interactions [228]. In addition, in-depth investigations of other organisms and mixed-culture microbial biofilms capable of DET to electrodes are needed. At the same time, there is much yet to be aimed at regarding the understanding of microbial electron uptake from cathodes, since research in this area is still being at an early stage. Researchers from various disciplines are likely to become involved in tracing these mechanisms. Biocathode-based BESs can be regarded as possessing tremendous potential for future bioproduction. In particular, DET at biocathodes represents a promising area for future research, since initial results (e.g., for *G. sulferreducens*) indicate that the mechanisms of microbes receiving electrons from electrodes are distinctly different from those of the donation of electrons to electrodes [278]. Collaborative efforts in molecular and spectroelectrochemical methods, along with microscopic approaches, could enable ways of explaining ET from the cathode to the microbes to advance at a faster pace. For self-mediated ET, the identification of the extracellular redox compounds involved is not an easy task, since the processes required for isolating these tiny molecules from a mixture containing several different metabolites are very tedious. Combining various techniques such as those of proteomics, downstreaming, chromatography, and electrochemistry can help scientists to better identify self-secreted electron shuttles involved in the EET of microbes. Although large-scale applications of mediator-based BESs are uncertain, their use for investigating ET events at the molecular level could be beneficial in BES research.

In addition to electrochemical techniques, a real-time monitoring of EABs by use of imaging techniques could contribute to an understanding of the structure of such biofilms and thus of the microbial interactions with electrodes that are involved. A non-invasive, non-destructive method based on use of confocal Raman microscopy for the in vivo morphological characterization of living EABs, using *c*-type cytochromes as metabolic indicators, has been reported recently [352]. Measuring in this way the spectroscopic properties (through

resonance Raman fingerprinting of the cytochromes) has revealed real-time morphological characteristics of EAB at different stages of growth. In addition, the dependence of the spectral response of *c*-type cytochromes on the redox state of the heme protein in EABs has been studied, pointing to the possible use of this technique for investigating the redox electrochemistry of such biofilms. The combining of protein film voltammetry with anaerobic affinity chromatography has been shown in the case of *S. oneidensis* to be useful in monitoring the direction and the stoichiometry of ET between the redox partners involved [353]. The genomes of the model exoelectrogens *S. oneidensis* MR-1 and *G. sulfurreducens* have been revealed, enabling researchers to utilize genetic approaches in investigating EET mechanisms. Frank et al., for example, have used non-destructive real-time spatial gene expression analysis recently for investigating the physiology of current-producing *G. sulfurreducens* biofilms [354]. The genomes for various other *Shewanella* and *Geobacter* spp. are also available (www.genomesonline.org), this providing a powerful database for comparative EET analysis. Although several techniques have been reported to be useful for analyzing EABs, standardization of these techniques, as taken up recently by Harnisch and Rabaey, is important for providing comparability while at the same time avoiding conflicting information, so as to further advance the field of BES research [355].

Achieving a better understanding of microbe–electrode interactions at the molecular level, together with the identification and screening of new and versatile microbial catalysts, can help researchers to employ genetic engineering approaches in a way that can result in superior microbial strains having high ET rates, which can enhance the performance of BESs in a variety of practical applications. The structural recognition of specific molecular events and molecules (e.g. cytochrome MtrF in *Shewanella* sp. [356]) can advance the understanding of ET mechanisms at the molecular level. Also, the natural ability of microorganisms to form electrical associations for interspecies ET [357–359] as well as such developments as that of the recently discovered long-range ET over centimeter distances by filamentous bacteria [360] can be expected to advance both the use of BES technologies as well as the research in the electromicrobiology domain. With the expansion of knowledge regarding biocathode-based systems, electrically driven microbial metabolism can be expected to generate promising outcomes and a wide range of applications. Irrespective of the nature of a system (direct or mediated) and its areas of application, future studies should take account of the overall efficiency of EET rates at microbe–electrode interfaces.

Acknowledgments The authors gratefully acknowledge the financial support provided by the Research Executive Agency (REA) of the European Union under Grant Agreement number PITN-GA-2010-264772 (ITN CHEBANA), the Swedish Research Council (2010-5031), and the nmC@LU.

References

1. Hernandez ME, Newman DK (2001) Extracellular electron transfer. Cell Mol Life Sci 58:1562–1571
2. Heijnen JJ (1999) Bioenergetics of microbial growth. In: Flickinger MC, Drew SW (eds) Encyclopedia of bioprocess technology: fermentation, biocatalysis, bioseparation. Wiley, New York, pp 267–291
3. Rabaey K, Angenent L, Schröder U, Keller J (eds) (2010) Bioelectrochemical systems: from extracellular electron transfer to biotechnological application. IWA, London
4. Logan BE, Hamelers B, Rozendal R, Schröder U, Keller J, Freguia S, Aelterman P, Verstraete W, Rabaey K (2006) Microbial fuel cells: methodology and technology. Environ Sci Technol 40:5181–5192
5. Kato S, Hashimoto K, Watanabe K (2012) Microbial interspecies electron transfer via electric currents through conductive minerals. Proc Natl Acad Sci USA 109:10042–10046. doi:10.1073/pnas.1117592109
6. Lovley DR, Phillips EJP (1988) Novel mode of microbial energy metabolism: organic carbon oxidation coupled to dissimilatory reduction of iron or manganese. Appl Environ Microbiol 54:1472–1480
7. Myers CR, Nealson KH (1988) Bacterial manganese reduction and growth with manganese oxide as the sole electron acceptor. Science 240:1319–1321
8. Bentley A, Atkinson A, Jezek J, Rawson DM (2001) Whole cell biosensors—electrochemical and optical approaches to ecotoxicity testing. Toxicol in Vitro 15:469–475
9. Pasco N, Weld R, Hay J, Gooneratne R (2011) Development and applications of whole cell biosensors for ecotoxicity testing. Anal Bioanal Chem 400:931–945
10. Shimomura-Shimizu M, Karube I (2010) Applications of microbial cell sensors. In: Belkin S, Gu MB (eds) Whole cell sensing system II, vol 118. Springer, Berlin, pp 1–30
11. Nakamura H, Shimomura-Shimizu M, Karube I (2008) Development of microbial sensors and their application. In: Renneberg R, Lisdat F (eds) Biosensing for the 21st century, vol 109. Springer, Berlin, pp 351–394
12. Ding L, Du D, Zhang X, Ju H (2008) Trends in cell-based electrochemical biosensors. Curr Med Chem 15:3160–3170
13. Su L, Jia W, Hou C, Lei Y (2011) Microbial biosensors: a review. Biosens Bioelectron 26:1788–1799
14. Arends JBA, Verstraete W (2012) 100 years of microbial electricity production: three concepts for the future. Microb Biotechnol 5:333–346
15. Schröder U (2011) Discover the possibilities: microbial bioelectrochemical systems and the revival of a 100-year-old discovery. J Solid State Electr 15:1481–1486
16. Potter MC (1912) Electrical effects accompanying the decomposition of organic compounds. Proc Roy Soc London (B) 84:260–276
17. Cohen B (1931) The bacterial culture as an electrical half-cell. J Bacteriol 21:18–19
18. Lewis K (1966) Biochemical fuel cells. Bacteriol Rev 30:101–113
19. Canfield JH, Goldner BH, Lutwack R (1963) Utilization of human wastes as electrochemical fuels. In: NASA Technical Report, Magna Corporation, Anaheim CA. p 63
20. Davis JB, Yarbrough HF (1962) Preliminary experiments on a microbial fuel cell. Science 137:615–616
21. Ardeleanu I, Mărgineanu D-G, Vais H (1983) Electrochemical conversion in biofuel cells using *Clostridium butyricum* or *Staphylococcus aureus* Oxford. Bioelectrochem Bioenerg 11:273–277
22. Karube I, Matsunga T, Tsuru S, Suzuki S (1977) Biochemical fuel cell utilizing immobilized cells of *Clostridium butyricum*. Biotechnol Bioeng 21:1727–1733
23. Bennetto HP, Stirling JL, Tanaka K, Vega CA (1983) Anodic reactions in microbial fuel cells. Biotechnol Bioeng 25:559–568

24. Akiba T, Bennetto HP, Stirling JL, Tanaka K (1987) Electricity production from alkalophilic organisms. Biotechnol Lett 9:611–616
25. Tanaka K, Tamamushi R, Ogawa T (1985) Bioelectrochemical fuel-cells operated by the cyanobacterium, *Anabaena variabilis*. J Chem Technol Biot 35:191–197
26. Allen RM, Bennetto HP (1993) Microbial fuel cells: electricity production from carbohydrates. Appl Biochem Biotech 39(40):27–40
27. Zhang X-C, Halme A (1985) Modelling of a microbial fuel cell process. Biotechnol Lett 17:809–814
28. Kim BH, Ikeda T, Park HS, Kim HJ, Hyun MS, Kano K, Takagi K, Tatsumi H (1999) Electrochemical activity of an Fe(III)-reducing bacterium, *Shewanella putrefaciens* IR-1, in the presence of alternative electron acceptors. Biotechnol Tech 13:475–478
29. Yang Y, Sun G, Xu M (2011) Microbial fuel cells come of age. J Chem Technol Biot 86:625–632
30. Oh ST, Kim JR, Premier GC, Lee TH, Kim C, Sloan WT (2011) Sustainable wastewater treatment: how might microbial fuel cells contribute. Biotechnol Adv 28:871–881
31. Logan BE (2010) Scaling up microbial fuel cells and other bioelectrochemical systems. Appl Microbiol Biot 85:1665–1671
32. Logan BE (2008) Microbial fuel cells. Wiley, New York
33. Thrash JC, Coates JD (2008) Review: direct and indirect electrical stimulation of microbial metabolism. Environ Sci Technol 42:3921–3931
34. Park DH, Zeikus JG (1999) Utilization of electrically reduced neutral red by *Actinobacillus succinogenes*: physiological function of neutral red in membrane-driven fumarate reduction and energy conservation. J Bacteriol 181:2403–2410
35. Park DH, Laivenieks M, Guettler MV, Jain MK, Zeikus JG (1999) Microbial utilization of electrically reduced neutral red as the sole electron donor for growth and metabolite production. Appl Environ Microbiol 65:2912–2917
36. Ro D-K, Paradise EM, Ouellet M, Fisher KJ, Newman KL, Ndungu JM, Ho KA, Eachus RA, Ham TS, Kirby J, Chang MCY, Withers ST, Shiba Y, Sarpong R, Keasling JD (2006) Production of the antimalarial drug precursor artemisinic acid in engineered yeast. Nature 440:940–943
37. ter Heijne A, Hamelers HVM, de Wilde V, Rozendal RA, Buisman CJN (2006) A bipolar membrane combined with ferric iron reduction as an efficient cathode system in microbial fuel cells. Environ Sci Technol 40:5200–5205
38. Rhoads A, Beyenal H, Lewandowski Z (2005) Microbial fuel cell using anaerobic respiration as an anodic reaction and biomineralized manganese as a cathodic reactant. Environ Sci Technol 39:4666–4671
39. He Z, Angenent LT (2006) Application of bacterial biocathodes in microbial fuel cells. Electroanal 18:2009–2015
40. Rosenbaum M, Aulenta F, Villano M, Angenent LT (2011) Cathodes as electron donors for microbial metabolism: which extracellular electron transfer mechanisms are involved? Bioresource Technol 102:324–333
41. Huang L, Regan JM, Quan X (2011) Electron transfer mechanisms, new applications, and performance of biocathode microbial fuel cells. Bioresource Technol 102:316–323
42. Erable B, Féron D, Bergel A (2012) Microbial catalysis of the oxygen reduction reaction for microbial fuel cells: a review. ChemSusChem 5:975–987
43. ter Heijne A, Strik DPBTB, Hamelers HVM, Buisman CJN (2010) Cathode potential and mass transfer determine performance of oxygen reducing biocathodes in microbial fuel cells. Environ Sci Technol 44:7151–7156
44. Rabaey K, Read ST, Clauwaert P, Freguia S, Bond PL, Blackall LL, Keller J (2008) Cathodic oxygen reduction catalyzed by bacteria in microbial fuel cells. ISME J 2:519–527
45. Chung K, Fujiki I, Okabe S (2011) Effect of formation of biofilms and chemical scale on the cathode electrode on the performance of a continuous two-chamber microbial fuel cell. Bioresource Technol 102:355–360

46. Cournet A, Bergé M, Roques C, Bergel A, Délia M-L (2010) Electrochemical reduction of oxygen catalyzed by *Pseudomonas aeruginosa*. Electrochim Acta 55:4902–4908
47. Clauwaert P, van der Ha D, Boon N, Verbeken K, Verhaege M, Rabaey K, Verstraete W (2007) Open air biocathode enables effective electricity generation with microbial fuel cells. Environ Sci Technol 41:7564–7569
48. Prasad D, Sivaram TK, Berchmans S, Yegnaraman V (2006) Microbial fuel cell constructed with a micro-organism isolated from sugar industry effluent. J Power Sources 160:991–996
49. Bergel A, Féron D, Mollica A (2005) Catalysis of oxygen reduction in PEM fuel cell by seawater biofilm. Electrochem Commun 7:900–904
50. Gregory KB, Bond DR, Lovley DR (2004) Graphite electrodes as electron donors for anaerobic respiration. Environ Microbiol 6:596–604
51. Lefebvre O, Al-Mamun A, Ng HY (2008) A microbial fuel cell equipped with a biocathode for organic removal and denitrification. Water Sci Technol 58:881–885
52. Clauwaert P, Rabaey K, Aelterman P, De Schamphelaire L, Pham TH, Boeckx P, Boon N, Verstraete W (2007) Biological denitrification in microbial fuel cells. Environ Sci Technol 41:3354–3360
53. Rozendal RA, Hamelers HVM, Euverink GJW, Metz SJ, Buisman CJN (2006) Principle and perspectives of hydrogen production through biocatalyzed electrolysis. Int J Hydrogen Energ 31:1632–1640
54. Cheng S, Logan BE (2007) Sustainable and efficient biohydrogen production via electrohydrogenesis. Proc Natl Acad Sci USA 104:18871–18873
55. Rinaldi A, Mecheri B, Garavaglia V, Licoccia S, Di Nardo P, Traversa E (2008) Engineering materials and biology to boost performance of microbial fuel cells: a critical review. Energ Environ Sci 1:417–429
56. Nevin KP, Woodard TL, Franks AE, Summers ZM, Lovley DR (2010) Microbial electrosynthesis: feeding microbes electricity to convert carbon dioxide and water to multicarbon extracellular organic compounds. mBio 1:e00103–e00110
57. Rabaey K, Rozendal RA (2010) Microbial electrosynthesis—revisiting the electrical route for microbial production. Nat Rev Microbiol 8:706–716
58. Lovley DR, Nevin KP (2011) A shift in the current: new applications and concepts for microbe-electrode electron exchange. Curr Opin Biotech 22:441–448
59. Virdis B, Read ST, Rabaey K, Rozendal RA, Yuan Z, Keller J (2011) Biofilm stratification during simultaneous nitrification and denitrification (SND) at a biocathode. Bioresource Technol 102:334–341
60. Nevin KP, Hensley SA, Franks AE, Summers ZM, Ou J, Woodard TL, Snoeyenbos-West OL, Lovley DR (2011) Electrosynthesis of organic compounds from carbon dioxide is catalyzed by a diversity of acetogenic microorganisms. Appl Environ Microb 77:2882–2886
61. Wrighton KC, Virdis B, Clauwaert P, Read ST, Daly RA, Boon N, Piceno Y, Andersen GL, Coates JD, Rabaey K (2010) Bacterial community structure corresponds to performance during cathodic nitrate reduction. ISME J 4:1443–1455
62. Strycharz SM, Gannon SM, Boles AR, Franks AE, Nevin KP, Lovley DR (2010) Reductive dechlorination of 2-chlorophenol by *Anaeromyxobacter dehalogenans* with an electrode serving as the electron donor. Environ Microbiol Reports 2:289–294
63. Rozendal RA, Leone E, Keller J, Rabaey K (2009) Efficient hydrogen peroxide generation from organic matter in a bioelectrochemical system. Electrochem Commun 11:1752–1755
64. Fu L, You S-J, Yang F-L, Gao M-M, Fang X-H, Zhang G-Q (2010) Synthesis of hydrogen peroxide in microbial fuel cell. J Chem Technol Biot 85:715–719
65. Butler CS, Clauwaert P, Green SJ, Verstraete W, Nerenberg R (2010) Bioelectrochemical perchlorate reduction in a microbial fuel cell. Environ Sci Technol 44:4685–4691
66. Tandukar M, Huber SJ, Onodera T, Pavlostathis SG (2009) Biological chromium(VI) reduction in the cathode of a microbial fuel cell. Environ Sci Technol 43:8159–8165
67. Mu Y, Rozendal RA, Rabaey K, Keller J (2009) Nitrobenzene removal in bioelectrochemical systems. Environ Sci Technol 43:8690–8695

68. Zhang T, Gannon SM, Nevin KP, Franks AE, Lovley DR (2010) Stimulating the anaerobic degradation of aromatic hydrocarbons in contaminated sediments by providing an electrode as the electron acceptor. Environ Microbiol 12:1011–1020
69. Mu Y, Rabaey K, Rozendal RA, Yuan Z, Keller J (2009) Decolorization of azo dyes in bioelectrochemical systems. Environ Sci Technol 43:5137–5143
70. Jacobson KS, Drew DM, He Z (2011) Efficient salt removal in a continuously operated upflow microbial desalination cell with an air cathode. Bioresource Technol 102:376–380
71. Cao X, Huang X, Liang P, Xiao K, Zhou Y, Zhang X, Logan BE (2009) A new method for water desalination using microbial desalination cells. Environ Sci Technol 43:7148–7152
72. Kim Y, Logan BE (2013) Microbial desalination cells for energy production and desalination. Desalination 308:122–130
73. Mehanna M, Basséguy R, Délia M-L, Bergel A (2010) *Geobacter sulfurreducens* can protect 304 L stainless steel against pitting in conditions of low electron acceptor concentrations. Electrochem Commun 12:724–728
74. ter Heijne A, Liu F, Weijden RVD, Weijma J, Buisman CJN, Hamelers HVM (2010) Copper recovery combined with electricity production in a microbial fuel cell. Environ Sci Technol 44:4376–4381
75. Villano M, De Bonis L, Rossetti S, Aulenta F, Majone M (2011) Bioelectrochemical hydrogen production with hydrogenophilic dechlorinating bacteria as electrocatalytic agents. Bioresource Technol 102:3193–3199
76. Jeremiasse AW, Hamelers HVM, Buisman CJN (2010) Microbial electrolysis cell with a microbial biocathode. Bioelectrochemistry 78:39–43
77. Geelhoed JS, Stams AJM (2010) Electricity-assisted biological hydrogen production from acetate by *Geobacter sulfurreducens*. Environ Sci Technol 45:815–820
78. Aulenta F, Catapano L, Snip L, Villano M, Majone M (2012) Linking bacterial metabolism to graphite cathodes: electrochemical insights into the H_2-producing capability of *Desulfovibrio* sp. ChemSusChem 5:1080–1085
79. Modin O, Fukushi K (2012) Development and testing of bioelectrochemical reactors converting wastewater organics into hydrogen peroxide. Water Sci Technol 66:831–836
80. van Eerten-Jansen MCAA, ter Heijne A, Buisman CJN, Hamelers HVM (2012) Microbial electrolysis cells for production of methane from CO_2: long-term performance and perspectives. Int J Energ Res 36:809–819
81. Villano M, Aulenta F, Ciucci C, Ferri T, Giuliano A, Majone M (2010) Bioelectrochemical reduction of CO_2 to CH_4 via direct and indirect extracellular electron transfer by a hydrogenophilic methanogenic culture. Bioresource Technol 101:3085–3090
82. Cheng S, Xing D, Call DF, Logan BE (2009) Direct biological conversion of electrical current into methane by electromethanogenesis. Environ Sci Technol 43:3953–3958
83. Luo H, Jenkins PE, Ren Z (2010) Concurrent desalination and hydrogen generation using microbial electrolysis and desalination cells. Environ Sci Technol 45:340–344
84. Di Lorenzo M, Curtis TP, Head IM, Scott K (2009) A single-chamber microbial fuel cell as a biosensor for wastewaters. Water Res 43:3145–3154
85. Stein NE, Keesman KJ, Hamelers HVM, van Straten G (2011) Kinetic models for detection of toxicity in a microbial fuel cell based biosensor. Biosens Bioelectron 26:3115–3120
86. Peixoto L, Min B, Martins G, Brito AG, Kroff P, Parpot P, Angelidaki I, Nogueira R (2011) In situ microbial fuel cell-based biosensor for organic carbon. Bioelectrochemistry 81:99–103
87. Dávila D, Esquivel JP, Sabaté N, Mas J (2011) Silicon-based microfabricated microbial fuel cell toxicity sensor. Biosens Bioelectron 26:2426–2430
88. Di Lorenzo M, Curtis TP, Head IM, Velasquez-Orta SB, Scott K (2009) A single chamber packed bed microbial fuel cell biosensor for measuring organic content of wastewater. Water Sci Technol 60:2879–2887
89. Tront JM, Fortner JD, Plötze M, Hughes JB, Puzrin AM (2008) Microbial fuel cell biosensor for in situ assessment of microbial activity. Biosens Bioelectron 24:586–590

90. Kumlanghan A, Liu J, Thavarungkul P, Kanatharana P, Mattiasson B (2007) Microbial fuel cell-based biosensor for fast analysis of biodegradable organic matter. Biosens Bioelectron 22:2939–2944
91. Kim BH, Chang IS, Gil GC, Park HS, Kim HJ (2003) Novel BOD (biological oxygen demand) sensor using mediator-less microbial fuel cell. Biotechnol Lett 25:541–545
92. Patil S, Harnisch F, Schröder U (2010) Toxicity response of electroactive microbial biofilms—a decisive feature for potential biosensor and power source applications. Chemphyschem 11:2834–2837
93. Harnisch F, Schröder U (2010) From MFC to MXC: chemical and biological cathodes and their potential for microbial bioelectrochemical systems. Chem Soc Rev 39:4433–4448
94. Rabaey K, Verstraete W (2005) Microbial fuel cells: novel biotechnology for energy generation. Trends Biotechnol 23:291–298
95. Hochella MF, Lower SK, Maurice PA, Penn RL, Sahai N, Sparks DL, Twining BS (2008) Nanominerals, mineral nanoparticles, and earth systems. Science 319:1631–1635
96. Nealson K, Belz A, McKee B (2002) Breathing metals as a way of life: geobiology in action. A Van Leeuw 81:215–222
97. Lovley DR (1991) Dissimilatory Fe(III) and Mn(IV) reduction. Microbiol Rev 55:259–287
98. Weber KA, Achenbach LA, Coates JD (2006) Microorganisms pumping iron: anaerobic microbial iron oxidation and reduction. Nat Rev Microbiol 4:752–764
99. Nealson KH, Finkel SE (2011) Electron flow and biofilms. MRS Bull 36:380–384
100. Lovley DR (1993) Dissimilatory metal reduction. Annu Rev Microbiol 47:263–290
101. Nealson KH, Saffarini D (1994) Iron and manganese in anaerobic respiration: environmental significance, physiology, and regulation. Annu Rev Microbiol 48:311–343
102. Fredrickson JK, Romine MF, Beliaev AS, Auchtung JM, Driscoll ME, Gardner TS, Nealson KH, Osterman AL, Pinchuk G, Reed JL, Rodionov DA, Rodrigues JLM, Saffarini DA, Serres MH, Spormann AM, Zhulin IB, Tiedje JM (2008) Towards environmental systems biology of *Shewanella*. Nat Rev Microbiol 6:592–603
103. Lonergan DJ, Jenter HL, Coates JD, Phillips EJ, Schmidt TM, Lovley DR (1996) Phylogenetic analysis of dissimilatory Fe(III)-reducing bacteria. J Bacteriol 178:2402–2408
104. Lovley DR (1995) Microbial reduction of iron, manganese, and other metals. In: Donald LS (ed) Advances in agronomy, vol 54. Academic, New York, pp 175–231
105. Lovley DR, Ueki T, Zhang T, Malvankar NS, Shrestha PM, Flanagan KA, Aklujkar M, Butler JE, Giloteaux L, Rotaru A-E Holmes DE, Franks AE, Orellana R, Risso C, Nevin KP (2011) *Geobacter*: the microbe electric's physiology, ecology, and practical applications. Adv Microb Physiol 59:1–100
106. Mahadevan R, Palsson BØ, Lovley DR (2011) In situ to in silico and back: elucidating the physiology and ecology of *Geobacter* spp. using genome-scale modelling. Nat Rev Microbiol 9:39–50
107. Nealson K, Scott J (2006) Ecophysiology of the genus *Shewanella*. In: Dworkin M, Falkow S, Rosenberg E, Schleifer K-H, Stackebrandt E (eds) The prokaryotes. Springer, New York, pp 1133–1151
108. Carmona-Martinez AA, Harnisch F, Kuhlicke U, Neu TR, Schröder U (2013) Electron transfer and biofilm formation of *Shewanella putrefaciens* as function of anode potential. Bioelectrochemistry 93:23–29
109. Yang Y, Xu M, Guo J, Sun G (2012) Bacterial extracellular electron transfer in bioelectrochemical systems. Process Biochem 47:1707–1714. http://dx.doi.org/10.1016/j.procbio.2012.07.032
110. Yuan Y, Ahmed J, Zhou L, Zhao B, Kim S (2011) Carbon nanoparticles-assisted mediator-less microbial fuel cells using *Proteus vulgaris*. Biosens Bioelectron 27:106–112
111. Kim N, Choi Y, Jung S, Kim S (2000) Effect of initial carbon sources on the performance of microbial fuel cells containing *Proteus vulgaris*. Biotechnol Bioeng 70:109–114
112. Venkataraman A, Rosenbaum M, Arends JBA, Halitschke R, Angenent LT (2010) Quorum sensing regulates electric current generation of *Pseudomonas aeruginosa* PA14 in bioelectrochemical systems. Electrochem Commun 12:459–462
113. Pham T, Boon N, Aelterman P, Clauwaert P, De Schamphelaire L, Vanhaecke L, De Maeyer K, Höfte M, Verstraete W, Rabaey K (2008) Metabolites produced by *Pseudomonas*

sp. enable gram positive bacterium to achieve extracellular electron transfer. Appl Microbiol Biot 77:1119–1129
114. Timur S, Haghighi B, Tkac J, Pazarlioglu N, Telefoncu A, Gorton L (2007) Electrical wiring of *Pseudomonas putida* and *Pseudomonas fluorescens* with osmium redox polymers. Bioelectrochemistry 71:38–45
115. Weld RJ, Glithero N, Pasco N (2011) *Escherichia coli* knock-out mutants with altered electron transfer activity in the Micredox® assay and in microbial fuel cells. Int J Environ Anal Chem 91:138–149
116. Veer Raghavulu S, Sarma PN, Venkata Mohan S (2011) Comparative bioelectrochemical analysis of *Pseudomonas aeruginosa* and *Escherichia coli* with anaerobic consortia as anodic biocatalyst for biofuel cell application. J Appl Microbiol 110:666–674
117. Xia X, Cao X-X, Liang P, Huang X, Yang S-P, Zhao G-G (2010) Electricity generation from glucose by a *Klebsiella* sp. in microbial fuel cells. Appl Microbiol Biot 87(1):383–390
118. Deng L, Li F, Zhou S, Huang D, Ni J (2010) A study of electron-shuttle mechanism in *Klebsiella pneumoniae* based-microbial fuel cells. Chinese Sci Bull 55:99–104
119. Zhang L, Zhou S, Zhuang L, Li W, Zhang J, Lu N, Deng L (2008) Microbial fuel cell based on *Klebsiella pneumoniae* biofilm. Electrochem Commun 10:1641–1643
120. Nimje VR, Chen C-Y, Chen C-C, Jean J-S, Reddy AS, Fan C-W, Pan K-Y, Liu H-T, Chen J-L (2009) Stable and high energy generation by a strain of *Bacillus subtilis* in a microbial fuel cell. J Power Sources 190(2):258–263
121. Liu M, Yuan Y, Zhang L-X, Zhuang L, Zhou S-G, Ni J-R (2010) Bioelectricity generation by a Gram-positive *Corynebacterium* sp. strain MFC03 under alkaline condition in microbial fuel cells. Bioresource Technol 101:1807–1811
122. Alferov S, Coman V, Gustavsson T, Reshetilov A, von Wachenfeldt C, Hägerhäll C, Gorton L (2009) Electrical communication of cytochrome enriched *Escherichia coli* JM109 cells with graphite electrodes. Electrochim Acta 54:4979–4984
123. Coman V, Gustavsson T, Finkelsteinas A, von Wachenfeldt C, Hägerhäll C, Gorton L (2009) Electrical wiring of live, metabolically enhanced *Bacillus subtilis* cells with flexible osmium-redox polymers. J Am Chem Soc 131:16171–16176
124. Schaetzle O, Barriere F, Baronian K (2008) Bacteria and yeasts as catalysts in microbial fuel cells: electron transfer from microorganisms to electrodes for green electricity. Energ Environ Sci 1:607–620
125. Sharma V, Kundu PP (2010) Biocatalysts in microbial fuel cells. Enzyme Microb Tech 47 (5):179–188
126. Logan BE (2009) Exoelectrogenic bacteria that power microbial fuel cells. Nat Rev Microbiol 7:375–381
127. Rabaey K, Rodriguez J, Blackall LL, Keller J, Gross P, Batstone D, Verstraete W, Nealson KH (2007) Microbial ecology meets electrochemistry: electricity-driven and driving communities. ISME J 1:9–18
128. Kiely PD, Regan JM, Logan BE (2011) The electric picnic: synergistic requirements for exoelectrogenic microbial communities. Curr Opin Biotech 22:378–385
129. Wrighton KC, Agbo P, Warnecke F, Weber KA, Brodie EL, DeSantis TZ, Hugenholtz P, Andersen GL, Coates JD (2008) A novel ecological role of the Firmicutes identified in thermophilic microbial fuel cells. ISME J 2:1146–1156
130. Patil SA, Surakasi VP, Koul S, Ijmulwar S, Vivek A, Shouche YS, Kapadnis BP (2009) Electricity generation using chocolate industry wastewater and its treatment in activated sludge based microbial fuel cell and analysis of developed microbial community in the anode chamber. Bioresource Technol 100:5132–5139
131. Jung S, Regan J (2007) Comparison of anode bacterial communities and performance in microbial fuel cells with different electron donors. Appl Microbiol Biot 77:393–402
132. Chae K-J, Choi M-J, Lee J-W, Kim K-Y, Kim IS (2009) Effect of different substrates on the performance, bacterial diversity, and bacterial viability in microbial fuel cells. Bioresource Technol 100:3518–3525

133. Raghavulu SV, Goud RK, Sarma PN, Mohan SV (2011) *Saccharomyces cerevisiae* as anodic biocatalyst for power generation in biofuel cell: Influence of redox condition and substrate load. Bioresource Technol 102:2751–2757
134. Ducommun R, Favre M-F, Carrard D, Fischer F (2010) Outward electron transfer by *Saccharomyces cerevisiae* monitored with a bi-cathodic microbial fuel cell-type activity sensor. Yeast 27:139–148
135. Walker AL, Walker CW Jr (2006) Biological fuel cell and an application as a reserve power source. J Power Sources 160:123–129
136. Haslett ND, Rawson FJ, Barrië re F, Kunze G, Pasco N, Gooneratne R, Baronian KHR (2011) Characterisation of yeast microbial fuel cell with the yeast *Arxula adeninivorans* as the biocatalyst. Biosens Bioelectron 26:3742–3747
137. Shkil H, Schulte A, Guschin DA, Schuhmann W (2011) Electron transfer between genetically modified *Hansenula polymorpha* yeast cells and electrode surfaces via Os-complex modified redox polymers. Chemphyschem 12:806–813
138. Prasad D, Arun S, Murugesan M, Padmanaban S, Satyanarayanan RS, Berchmans S, Yegnaraman V (2007) Direct electron transfer with yeast cells and construction of a mediatorless microbial fuel cell. Biosens Bioelectron 22:2604–2610
139. Babanova S, Hubenova Y, Mitov M (2011) Influence of artificial mediators on yeast-based fuel cell performance. J Biosci Bioeng 112:379–387
140. Richter H, Lanthier M, Nevin KP, Lovley DR (2007) Lack of electricity production by *Pelobacter carbinolicus* indicates that the capacity for Fe(III) oxide reduction does not necessarily confer electron transfer ability to fuel cell anodes. Appl Environ Microbiol 73:5347–5353
141. Dumas C, Basseguy R, Bergel A (2008) Microbial electrocatalysis with *Geobacter sulfurreducens* biofilm on stainless steel cathodes. Electrochim Acta 53:2494–2500
142. Ross DE, Flynn JM, Baron DB, Gralnick JA, Bond DR (2011) Towards electrosynthesis in *Shewanella*: energetics of reversing the Mtr pathway for reductive metabolism. PLoS One 6: e16649
143. Liu H, Matsuda S, Hashimoto K, Nakanishi S (2012) Flavins secreted by bacterial cells of *Shewanella* catalyze cathodic oxygen reduction. Chem Sus Chem 5:1054–1058
144. Hsu L, Masuda SA, Nealson KH, Pirbazari M (2012) Evaluation of microbial fuel cell *Shewanella* biocathodes for treatment of chromate contamination. RSC Adv 2:5844–5855
145. Cournet A, Délia M-L, Bergel A, Roques C, Bergé M (2010) Electrochemical reduction of oxygen catalyzed by a wide range of bacteria including Gram-positive. Electrochem Commun 12:505–508
146. Cheng KY, Ho G, Cord-Ruwisch R (2009) Anodophilic biofilm catalyzes cathodic oxygen reduction. Environ Sci Technol 44:518–525
147. Erable B, Vandecandelaere I, Faimali M, Délia M-L, Etcheverry L, Vandamme P, Bergel A (2010) Marine aerobic biofilm as biocathode catalyst. Bioelectrochemistry 78:51–56
148. Rozendal RA, Jeremiasse AW, Hamelers HVM, Buisman CJN (2007) Hydrogen production with a microbial biocathode. Environ Sci Technol 42:629–634
149. Lovley DR (2011) Powering microbes with electricity: direct electron transfer from electrodes to microbes. Environ Microbiol Reports 3:27–35
150. Lovley DR, Holmes DE, Nevin KP (2004) Dissimilatory Fe(III) and Mn(IV) reduction. Adv Microb Physiol 49:219–286
151. Fredrickson JK, Zachara JM (2008) Electron transfer at the microbe–mineral interface: a grand challenge in biogeochemistry. Geobiology 6:245–253
152. Shi L, Squier TC, Zachara JM, Fredrickson JK (2007) Respiration of metal (hydr)oxides by *Shewanella* and *Geobacter*: a key role for multihaem *c*-type cytochromes. Mol Microbiol 65:12–20
153. Lovley DR (2011) Live wires: direct extracellular electron exchange for bioenergy and the bioremediation of energy-related contamination. Energ Environ Sci 4:4896–4906

154. Richardson DJ, Butt JN, Fredrickson JK, Zachara JM, Shi L, Edwards MJ, White G, Baiden N, Gates AJ, Marritt SJ, Clarke TA (2012) The 'porin–cytochrome' model for microbe-to-mineral electron transfer. Mol Microbiol 85:201–212
155. Gorby YA, Yanina S, McLean JS, Rosso KM, Moyles D, Dohnalkova A, Beveridge TJ, Chang IS, Kim BH, Kim KS, Culley DE, Reed SB, Romine MF, Saffarini DA, Hill EA, Shi L, Elias DA, Kennedy DW, Pinchuk G, Watanabe K, Ishii S, Logan B, Nealson KH, Fredrickson JK (2006) Electrically conductive bacterial nanowires produced by *Shewanella oneidensis* strain MR-1 and other microorganisms. Proc Natl Acad Sci USA 103:11358–11363
156. Reguera G, McCarthy KD, Mehta T, Nicoll JS, Tuominen MT, Lovley DR (2005) Extracellular electron transfer via microbial nanowires. Nature 435:1098–1101
157. Esteve-Núñez A, Sosnik J, Visconti P, Lovley DR (2008) Fluorescent properties of c-type cytochromes reveal their potential role as an extracytoplasmic electron sink in *Geobacter sulfurreducens*. Environ Microbiol 10:497–505
158. Peng L, You S-J, Wang J-Y (2010) Electrode potential regulates cytochrome accumulation on *Shewanella oneidensis* cell surface and the consequence to bioelectrocatalytic current generation. Biosens Bioelectron 25:2530–2533
159. Lovley DR (2008) Extracellular electron transfer: wires, capacitors, iron lungs, and more. Geobiology 6:225–231
160. Qian X, Mester T, Morgado L, Arakawa T, Sharma ML, Inoue K, Joseph C, Salgueiro CA, Maroney MJ, Lovley DR (2011) Biochemical characterization of purified OmcS, a c-type cytochrome required for insoluble Fe(III) reduction in *Geobacter sulfurreducens*. BBA Bioenergetics 1807:404–412
161. Tremblay P-L, Summers ZM, Glaven RH, Nevin KP, Zengler K, Barrett CL, Qiu Y, Palsson BO, Lovley DR (2011) A c-type cytochrome and a transcriptional regulator responsible for enhanced extracellular electron transfer in *Geobacter sulfurreducens* revealed by adaptive evolution. Environ Microbiol 13:13–23
162. Shi L, Richardson DJ, Wang Z, Kerisit SN, Rosso KM, Zachara JM, Fredrickson JK (2009) The roles of outer membrane cytochromes of *Shewanella* and *Geobacter* in extracellular electron transfer. Environ Microbiol Reports 1:220–227
163. Richter K, Schicklberger M, Gescher J (2012) Dissimilatory reduction of extracellular electron acceptors in anaerobic respiration. Appl Environ Microbiol 78:913–921
164. Holmes DE, Mester T, O'Neil RA, Perpetua LA, Larrahondo MJ, Glaven R, Sharma ML, Ward JE, Nevin KP, Lovley DR (2008) Genes for two multicopper proteins required for Fe (III) oxide reduction in *Geobacter sulfurreducens* have different expression patterns both in the subsurface and on energy-harvesting electrodes. Microbiology 154:1422–1435
165. Voordeckers JW, Kim B-C, Izallalen M, Lovley DR (2010) Role of *Geobacter sulfurreducens* outer surface c-type cytochromes in reduction of soil humic acid and anthraquinone-2,6-disulfonate. Appl Environ Microbiol 76:2371–2375
166. Marsili E, Baron DB, Shikhare ID, Coursolle D, Gralnick JA, Bond DR (2008) *Shewanella* secretes flavins that mediate extracellular electron transfer. Proc Natl Acad Sci USA 105:3968–3973
167. von Canstein H, Ogawa J, Shimizu S, Lloyd JR (2008) Secretion of flavins by *Shewanella* species and their role in extracellular electron transfer. Appl Environ Microbiol 74:615–623
168. Lovley DR, Fraga JL, Blunt-Harris EL, Hayes LA, Phillips EJP, Coates JD (1998) Humic substances as a mediator for microbially catalyzed metal reduction. Acta Hydroch Hydrob 26:152–157
169. Newman DK, Kolter R (2000) A role for excreted quinones in extracellular electron transfer. Nature 405:94–97
170. Pierson L, Pierson E (2010) Metabolism and function of phenazines in bacteria: impacts on the behavior of bacteria in the environment and biotechnological processes. Appl Microbiol Biot 86:1659–1670
171. Lies DP, Hernandez ME, Kappler A, Mielke RE, Gralnick JA, Newman DK (2005) *Shewanella oneidensis* MR-1 uses overlapping pathways for iron reduction at a distance

and by direct contact under conditions relevant for biofilms. Appl Environ Microbiol 71:4414–4426
172. Jeans C, Singer SW, Chan CS, VerBerkmoes NC, Shah M, Hettich RL, Banfield JF, Thelen MP (2008) Cytochrome 572 is a conspicuous membrane protein with iron oxidation activity purified directly from a natural acidophilic microbial community. ISME J 2:542–550
173. Emerson D, Fleming EJ, McBeth JM (2010) Iron-oxidizing bacteria: an environmental and genomic perspective. Annu Rev Microbiol 64:561–583
174. Castelle C, Guiral M, Malarte G, Ledgham F, Leroy G, Brugna M, Giudici-Orticoni M-T (2008) A new iron-oxidizing/O_2-reducing supercomplex spanning both inner and outer membranes, isolated from the extreme acidophile *Acidithiobacillus ferrooxidans*. J Biol Chem 283:25803–25811
175. Yarzábal A, Brasseur G, Ratouchniak J, Lund K, Lemesle-Meunier D, DeMoss JA, Bonnefoy V (2002) The high-molecular-weight cytochrome c Cyc2 of *Acidithiobacillus ferrooxidans* is an outer membrane protein. J Bacteriol 184:313–317
176. Singer SW, Chan CS, Zemla A, VerBerkmoes NC, Hwang M, Hettich RL, Banfield JF, Thelen MP (2008) Characterization of cytochrome 579, an unusual cytochrome isolated from an iron-oxidizing microbial community. Appl Environ Microbiol 74:4454–4462
177. Bond DR, Lovley DR (2003) Electricity production by *Geobacter sulfurreducens* attached to electrodes. Appl Environ Microbiol 69:1548–1555
178. Okamoto A, Hashimoto K, Nakamura R (2012) Long-range electron conduction of *Shewanella* biofilms mediated by outer membrane c-type cytochromes. Bioelectrochemistry 85:61–65
179. Busalmen JP, Esteve-Núñez A, Berná A, Feliu JM (2008) C-type cytochromes wire electricity-producing bacteria to electrodes. Angew Chem Int Edit 47:4874–4877
180. El-Naggar MY, Wanger G, Leung KM, Yuzvinsky TD, Southam G, Yang J, Lau WM, Nealson KH, Gorby YA (2010) Electrical transport along bacterial nanowires from *Shewanella oneidensis* MR-1. Proc Natl Acad Sci USA 107:18127–18131
181. Rabaey K, Boon N, Höfte M, Verstraete W (2005) Microbial phenazine production enhances electron transfer in biofuel cells. Environ Sci Technol 39:3401–3408
182. Park DH, Zeikus JG (2000) Electricity generation in microbial fuel cells using neutral red as an electronophore. Appl Environ Microbiol 66:1292–1297
183. Tang X, Du Z, Li H (2010) Anodic electron shuttle mechanism based on 1-hydroxy-4-aminoanthraquinone in microbial fuel cells. Electrochem Commun 12:1140–1143
184. Feng C, Ma L, Li F, Mai H, Lang X, Fan S (2010) A polypyrrole/anthraquinone-2,6-disulphonic disodium salt (PPy/AQDS)-modified anode to improve performance of microbial fuel cells. Biosens Bioelectron 25:1516–1520
185. Rosenbaum M, Zhao F, Schröder U, Scholz F (2006) Interfacing electrocatalysis and biocatalysis with tungsten carbide: a high-performance, noble-metal-free microbial fuel cell. Angew Chem Int Edit 45:6658–6661
186. Niessen J, Schröder U, Rosenbaum M, Scholz F (2004) Fluorinated polyanilines as superior materials for electrocatalytic anodes in bacterial fuel cells. Electrochem Commun 6:571–575
187. Schröder U, Nießen J, Scholz F (2003) A generation of microbial fuel cells with current outputs boosted by more than one order of magnitude. Angew Chem Int Edit 42:2880–2883
188. Inoue K, Qian X, Morgado L, Kim B-C, Mester T, Izallalen M, Salgueiro CA, Lovley DR (2010) Purification and characterization of OmcZ, an outer-Surface, octaheme c-type cytochrome essential for optimal current production by *Geobacter sulfurreducens*. Appl Environ Microbiol 76:3999–4007
189. Yi H, Nevin KP, Kim B-C, Franks AE, Klimes A, Tender LM, Lovley DR (2009) Selection of a variant of *Geobacter sulfurreducens* with enhanced capacity for current production in microbial fuel cells. Biosens Bioelectron 24:3498–3503
190. Reguera G, Nevin KP, Nicoll JS, Covalla SF, Woodard TL, Lovley DR (2006) Biofilm and nanowire production leads to increased current in *Geobacter sulfurreducens* fuel cells. Appl Environ Microbiol 72:7345–7348
191. Malvankar NS, Lovley DR (2012) Microbial nanowires, a new paradigm for biological electron transfer and bioelectronics. ChemSusChem 5:1039–1046

192. Meitl LA, Eggleston CM, Colberg PJS, Khare N, Reardon CL, Shi L (2009) Electrochemical interaction of *Shewanella oneidensis* MR-1 and its outer membrane cytochromes OmcA and MtrC with hematite electrodes. Geochim Cosmochim Ac 73:5292–5307
193. Bouhenni RA, Vora GJ, Biffinger JC, Shirodkar S, Brockman K, Ray R, Wu P, Johnson BJ, Biddle EM, Marshall MJ, Fitzgerald LA, Little BJ, Fredrickson JK, Beliaev AS, Ringeisen BR, Saffarini DA (2010) The role of *Shewanella oneidensis* MR-1 outer surface structures in extracellular electron transfer. Electroanal 22:856–864
194. Inoue K, Leang C, Franks AE, Woodard TL, Nevin KP, Lovley DR (2011) Specific localization of the c-type cytochrome OmcZ at the anode surface in current-producing biofilms of *Geobacter sulfurreducens*. Environ Microbiol Reports 3:211–217
195. Busalmen JP, Esteve-Núñez A, Feliu JM (2008) Whole cell electrochemistry of electricity-producing microorganisms evidence an adaptation for optimal exocellular electron transport. Environ Sci Technol 42:2445–2450
196. Fricke K, Harnisch F, Schröder U (2008) On the use of cyclic voltammetry for the study of anodic electron transfer in microbial fuel cells. Energ Environ Sci 1:144–147
197. Marsili E, Sun J, Bond DR (2010) Voltammetry and growth physiology of *Geobacter sulfurreducens* biofilms as a function of growth stage and imposed electrode potential. Electroanal 22:865–874
198. Srikanth S, Marsili E, Flickinger MC, Bond DR (2008) Electrochemical characterization of *Geobacter sulfurreducens* cells immobilized on graphite paper electrodes. Biotechnol Bioeng 99:1065–1073
199. Marsili E, Rollefson JB, Baron DB, Hozalski RM, Bond DR (2008) Microbial biofilm voltammetry: direct electrochemical characterization of catalytic electrode-attached biofilms. Appl Environ Microbiol 74:7329–7337
200. Richter H, Nevin KP, Jia H, Lowy DA, Lovley DR, Tender LM (2009) Cyclic voltammetry of biofilms of wild type and mutant *Geobacter sulfurreducens* on fuel cell anodes indicates possible roles of OmcB, OmcZ, type IV pili, and protons in extracellular electron transfer. Energ Environ Sci 2:506–516
201. Strycharz-Glaven SM, Tender LM (2012) Study of the mechanism of catalytic activity of *G. sulfurreducens* biofilm anodes during biofilm growth. ChemSusChem 5:1106–1118
202. Strycharz SM, Malanoski AP, Snider RM, Yi H, Lovley DR, Tender LM (2011) Application of cyclic voltammetry to investigate enhanced catalytic current generation by biofilm-modified anodes of *Geobacter sulfurreducens* strain DL1 vs. variant strain KN400. Energ Environ Sci 4:896–913
203. Zhu X, Yates MD, Logan BE (2012) Set potential regulation reveals additional oxidation peaks of *Geobacter sulfurreducens* anodic biofilms. Electrochem Commun 22:116–119
204. Holmes DE, Chaudhuri SK, Nevin KP, Mehta T, Methé BA, Liu A, Ward JE, Woodard TL, Webster J, Lovley DR (2006) Microarray and genetic analysis of electron transfer to electrodes in *Geobacter sulfurreducens*. Environ Microbiol 8:1805–1815
205. Nevin KP, Kim B-C, Glaven RH, Johnson JP, Woodard TL, Methé BA, DiDonato RJ, Covalla SF, Franks AE, Liu A, Lovley DR (2009) Anode biofilm transcriptomics reveals outer surface components essential for high density current production in *Geobacter sulfurreducens* fuel cells. PLoS One 4:e5628
206. Kim B-C, Postier BL, DiDonato RJ, Chaudhuri SK, Nevin KP, Lovley DR (2008) Insights into genes involved in electricity generation in *Geobacter sulfurreducens* via whole genome microarray analysis of the OmcF-deficient mutant. Bioelectrochemistry 73:70–75
207. Busalmen JP, Esteve-Nuñez A, Berná A, Feliu JM (2010) ATR-SEIRAs characterization of surface redox processes in *G. sulfurreducens*. Bioelectrochemistry 78:25–29
208. Malvankar NS, Tuominen MT, Lovley DR (2012) Biofilm conductivity is a decisive variable for high-current-density *Geobacter sulfurreducens* microbial fuel cells. Energ Environ Sci 5:5790–5797

209. Malvankar NS, Mester T, Tuominen MT, Lovley DR (2012) Supercapacitors based on c-type cytochromes using conductive nanostructured networks of living bacteria. Chemphyschem 13:463–468
210. Bretschger O, Obraztsova A, Sturm CA, Chang IS, Gorby YA, Reed SB, Culley DE, Reardon CL, Barua S, Romine MF, Zhou J, Beliaev AS, Bouhenni R, Saffarini D, Mansfeld F, Kim B-H, Fredrickson JK, Nealson KH (2007) Current production and metal oxide reduction by *Shewanella oneidensis* MR-1 wild type and mutants. Appl Environ Microbiol 73:7003–7012
211. Hartshorne RS, Reardon CL, Ross D, Nuester J, Clarke TA, Gates AJ, Mills PC, Fredrickson JK, Zachara JM, Shi L, Beliaev AS, Marshall MJ, Tien M, Brantley S, Butt JN, Richardson DJ (2009) Characterization of an electron conduit between bacteria and the extracellular environment. Proc Natl Acad Sci USA 106:22169–22174
212. Okamoto A, Nakamura R, Hashimoto K (2011) In-vivo identification of direct electron transfer from *Shewanella oneidensis* MR-1 to electrodes via outer-membrane OmcA-MtrCAB protein complexes. Electrochim Acta 56:5526–5531
213. Baron D, LaBelle E, Coursolle D, Gralnick JA, Bond DR (2009) Electrochemical measurement of electron transfer kinetics by *Shewanella oneidensis* MR-1. J Biol Chem 284:28865–28873
214. Coursolle D, Baron DB, Bond DR, Gralnick JA (2010) The Mtr respiratory pathway is essential for reducing flavins and electrodes in *Shewanella oneidensis*. J Bacteriol 192:467–474
215. Marritt SJ, Lowe TG, Bye J, McMillan DGG, Shi L, Fredrickson J, Zachara J, Richardson DJ, Cheesman MR, Jeuken LJC, Butt JN (2012) A functional description of CymA, an electron-transfer hub supporting anaerobic respiratory flexibility in *Shewanella*. Biochem J 444:465–474
216. Coursolle D, Gralnick JA (2010) Modularity of the Mtr respiratory pathway of *Shewanella oneidensis* strain MR-1. Mol Microbiol 77:995–1008
217. Shi L, Chen B, Wang Z, Elias DA, Mayer MU, Gorby YA, Ni S, Lower BH, Kennedy DW, Wunschel DS, Mottaz HM, Marshall MJ, Hill EA, Beliaev AS, Zachara JM, Fredrickson JK, Squier T (2006) Isolation of a high-affinity functional protein complex between OmcA and MtrC: two outer membrane decaheme c-type cytochromes of *Shewanella oneidensis* MR-1. J Bacteriol 188:4705–4714
218. Carmona-Martinez AA, Harnisch F, Fitzgerald LA, Biffinger JC, Ringeisen BR, Schröder U (2011) Cyclic voltammetric analysis of the electron transfer of *Shewanella oneidensis* MR-1 and nanofilament and cytochrome knock-out mutants. Bioelectrochemistry 81:74–80
219. Nakamura R, Kai F, Okamoto A, Newton GJ, Hashimoto K (2009) Self-constructed electrically conductive bacterial networks. Angew Chem Int Edit 48:508–511
220. Jain A, Zhang X, Pastorella G, Connolly JO, Barry N, Woolley R, Krishnamurthy S, Marsili E (2012) Electron transfer mechanism in *Shewanella loihica* PV-4 biofilms formed at graphite electrode. Bioelectrochemistry 87:28–32
221. Newton GJ, Mori S, Nakamura R, Hashimoto K, Watanabe K (2009) Analyses of current-generation mechanisms of *Shewanella loihica* PV-4 in microbial fuel cells in comparison with *Shewanella oneidensis* MR-1. Appl Environ Microbiol 75:7674–7681
222. Malvankar NS, Vargas M, Nevin KP, Franks AE, Leang C, Kim B-C, Inoue K, Mester T, Covalla SF, Johnson JP, Rotello VM, Tuominen MT, Lovley DR (2011) Tunable metallic-like conductivity in microbial nanowire networks. Nat Nano 6:573–579
223. Malvankar NS, Lau J, Nevin KP, Franks AE, Tuominen MT, Lovley DR (2012) Electrical conductivity in a mixed-species biofilm. Appl Environ Microbiol 78:5967–5971. doi:10.1128/AEM.01803-12
224. Strycharz-Glaven SM, Snider RM, Guiseppi-Elie A, Tender LM (2011) On the electrical conductivity of microbial nanowires and biofilms. Energ Environ Sci 4:4366–4379
225. Magnuson TS (2011) How the xap locus put electrical "Zap" in *Geobacter sulfurreducens* biofilms. J Bacteriol 193(5):1021–1022
226. Cao B, Shi L, Brown RN, Xiong Y, Fredrickson JK, Romine MF, Marshall MJ, Lipton MS, Beyenal H (2011) Extracellular polymeric substances from *Shewanella* sp. HRCR-1 biofilms: characterization by infrared spectroscopy and proteomics. Environ Microbiol 13:1018–1031

227. Leang C, Qian X, Mester TN, Lovley DR (2010) Alignment of the c-type cytochrome OmcS along pili of *Geobacter sulfurreducens*. Appl Environ Microbiol 76:4080–4084
228. Lovley DR (2012) Electromicrobiology. Annu Rev Microbiol 66:391–409
229. Malvankar NS, Tuominen MT, Lovley DR (2012) Lack of cytochrome involvement in long-range electron transport through conductive biofilms and nanowires of *Geobacter sulfurreducens*. Energ Environ Sci 5:8651–8659
230. Veazey JP, Reguera G, Tessmer SH (2011) Electronic properties of conductive pili of the metal-reducing bacterium *Geobacter sulfurreducens* probed by scanning tunneling microscopy. Phys Rev E 84:060901
231. Bond DR, Strycharz-Glaven SM, Tender LM, Torres CI (2012) On electron transport through *Geobacter* biofilms. ChemSusChem 5:1099–1105
232. Schrott GD, Bonanni PS, Robuschi L, Esteve-Núñez A, Busalmen JP (2011) Electrochemical insight into the mechanism of electron transport in biofilms of *Geobacter sulfurreducens*. Electrochim Acta 56:10791–10795
233. Rollefson JB, Stephen CS, Tien M, Bond DR (2011) Identification of an extracellular polysaccharide network essential for cytochrome anchoring and biofilm formation in *Geobacter sulfurreducens*. J Bacteriol 193:1023–1033
234. Malvankar NS, Tuominen MT, Lovley DR (2012) Comment on "On electrical conductivity of microbial nanowires and biofilms" by Strycharz-Glaven SM, Snider RM, Guiseppi-Elie A, Tender LM (2011) Energ Environ Sci 4:4366". Energ Environ Sci 5:6247–6249
235. Strycharz-Glaven SM, Tender LM (2012) Reply to the 'Comment on "On electrical conductivity of microbial nanowires and biofilms" by Malvankar NS, Tuominen MT, Lovley DR (2012) Energ Environ Sci 5:6247–6249'. Energ Environ Sci 5:6250–6255
236. Polizzi NF, Skourtis SS, Beratan DN (2012) Physical constraints on charge transport through bacterial nanowires. Faraday Discuss 155:43–61
237. Fitzgerald LA, Petersen ER, Ray RI, Little BJ, Cooper CJ, Howard EC, Ringeisen BR, Biffinger JC (2012) *Shewanella oneidensis* MR-1 Msh pilin proteins are involved in extracellular electron transfer in microbial fuel cells. Process Biochem 47:170–174
238. Kouzuma A, Meng X-Y, Kimura N, Hashimoto K, Watanabe K (2010) Disruption of the putative cell surface polysaccharide biosynthesis gene SO3177 in *Shewanella oneidensis* MR-1 enhances adhesion to electrodes and current generation in microbial fuel cells. Appl Environ Microbiol 76:4151–4157
239. Jiang X, Hu J, Fitzgerald LA, Biffinger JC, Xie P, Ringeisen BR, Lieber CM (2010) Probing electron transfer mechanisms in *Shewanella oneidensis* MR-1 using a nanoelectrode platform and single-cell imaging. Proc Natl Acad Sci USA 107:16806–16810
240. Biffinger JC, Fitzgerald LA, Ray R, Little BJ, Lizewski SE, Petersen ER, Ringeisen BR, Sanders WC, Sheehan PE, Pietron JJ, Baldwin JW, Nadeau LJ, Johnson GR, Ribbens M, Finkel SE, Nealson KH (2011) The utility of *Shewanella japonica* for microbial fuel cells. Bioresource Technol 102:290–297
241. Yang Y, Sun G, Guo J, Xu M (2011) Differential biofilms characteristics of *Shewanella decolorationis* microbial fuel cells under open and closed circuit conditions. Bioresource Technol 102:7093–7098
242. Li S-L, Freguia S, Liu S-M, Cheng S-S, Tsujimura S, Shirai O, Kano K (2010) Effects of oxygen on *Shewanella decolorationis* NTOU1 electron transfer to carbon-felt electrodes. Biosens Bioelectron 25:2651–2656
243. Borole AP, Reguera G, Ringeisen B, Wang Z-W, Feng Y, Kim BH (2011) Electroactive biofilms: current status and future research needs. Energ Environ Sci 4:4813–4834
244. Holmes DE, Bond DR, Lovley DR (2004) Electron transfer by *Desulfobulbus propionicus* to Fe(III) and graphite electrodes. Appl Environ Microbiol 70:1234–1237
245. Marshall CW, May HD (2009) Electrochemical evidence of direct electrode reduction by a thermophilic Gram-positive bacterium, *Thermincola ferriacetica*. Energ Environ Sci 2:699–705
246. Zhuang L, Zhou S, Yuan Y, Liu T, Wu Z, Cheng J (2011) Development of *Enterobacter aerogenes* fuel cells: from in situ biohydrogen oxidization to direct electroactive biofilm. Bioresource Technol 102:284–289

247. Wrighton KC, Thrash JC, Melnyk RA, Bigi JP, Byrne-Bailey KG, Remis JP, Schichnes D, Auer M, Chang CJ, Coates JD (2011) Evidence for direct electron transfer by a Gram-positive bacterium isolated from a microbial fuel cell. Appl Environ Microbiol 77:7633–7639
248. Carlson HK, Iavarone AT, Gorur A, Yeo BS, Tran R, Melnyk RA, Mathies RA, Auer M, Coates JD (2012) Surface multiheme c-type cytochromes from *Thermincola potens* and implications for respiratory metal reduction by Gram-positive bacteria. Proc Natl Acad Sci USA 109:1702–1707
249. Masuda M, Freguia S, Wang Y-F, Tsujimura S, Kano K (2010) Flavins contained in yeast extract are exploited for anodic electron transfer by *Lactococcus lactis*. Bioelectrochemistry 78:173–175
250. Velasquez-Orta S, Head I, Curtis T, Scott K, Lloyd J, von Canstein H (2010) The effect of flavin electron shuttles in microbial fuel cells current production. Appl Microbiol Biot 85:1373–1381
251. Zhang T, Zhang L, Su W, Gao P, Li D, He X, Zhang Y (2011) The direct electrocatalysis of phenazine-1-carboxylic acid excreted by *Pseudomonas alcaliphila* under alkaline condition in microbial fuel cells. Bioresource Technol 102(14):7099–7102
252. Freguia S, Masuda M, Tsujimura S, Kano K (2009) *Lactococcus lactis* catalyses electricity generation at microbial fuel cell anodes via excretion of a soluble quinone. Bioelectrochemistry 76:14–18
253. Qiao Y, Li CM, Bao SJ, Lu ZS, Hong YH (2008) Direct electrochemistry and electrocatalytic mechanism of evolved *Escherichia coli* cells in microbial fuel cells. Chem Commun 11:1290–1292
254. Bond DR, Lovley DR (2005) Evidence for involvement of an electron shuttle in electricity generation by *Geothrix fermentans*. Appl Environ Microbiol 71:2186–2189
255. Venkataraman A, Rosenbaum MA, Perkins SD, Werner JJ, Angenent LT (2011) Metabolite-based mutualism between *Pseudomonas aeruginosa* PA14 and *Enterobacter aerogenes* enhances current generation in bioelectrochemical systems. Energ Environ Sci 4:4550–4559
256. Kim N, Choi Y, Jung S, Kim S (2000) Development of microbial fuel cells using *Proteus vulgaris*. B Korean Chem Soc 21:44–48
257. Thurston CF, Bennetto HP, Delaney GM, Mason JR, Roller SD, Stirling JL (1985) Glucose metabolism in a microbial fuel cell: stoichiometry of product formation in a thionine-mediated *Proteus vulgaris* fuel cell and its relation to coulombic yields. J Gen Microbiol 131:1393–1401
258. Wen Q, Kong F, Ma F, Ren Y, Pan Z (2011) Improved performance of air-cathode microbial fuel cell through additional Tween 80. J Power Sources 196:899–904
259. Ho PI, Kumar GG, Kim AR, Kim P, Nahm KS (2011) Microbial electricity generation of diversified carbonaceous electrodes under variable mediators. Bioelectrochemistry 80:99–104
260. Wen Q, Kong F, Ren Y, Cao D, Wang G, Zheng H (2010) Improved performance of microbial fuel cell through addition of rhamnolipid. Electrochem Commun 12:1710–1713
261. Schröder U (2007) Anodic electron transfer mechanisms in microbial fuel cells and their energy efficiency. Phys Chem Chem Phys 9:2619–2629
262. Kimmel DW, LeBlanc G, Meschievitz ME, Cliffel DE (2011) Electrochemical sensors and biosensors. Anal Chem 84:685–707
263. Eltzov E, Marks R (2011) Whole-cell aquatic biosensors. Anal Bioanal Chem 400:895–913
264. Xu F, Duan J, Hou B (2010) Electron transfer process from marine biofilms to graphite electrodes in seawater. Bioelectrochemistry 78:92–95
265. Qiao Y, Bao S-J, Li CM (2010) Electrocatalysis in microbial fuel cells-from electrode material to direct electrochemistry. Energ Environ Sci 3(5):544–553
266. Hasan K, Patil SA, Górecki K, Leech D, Hägerhäll C, Gorton L (2013) Electrochemical communication between heterotrophically grown *Rhodobacter capsulatus* with electrodes mediated by an osmium redox polymer. Bioelectrochemistry 93:30–36

267. Rawson FJ, Garrett DJ, Leech D, Downard AJ, Baronian KHR (2011) Electron transfer from *Proteus vulgaris* to a covalently assembled, single walled carbon nanotube electrode functionalised with osmium bipyridine complex: application to a whole cell biosensor. Biosens Bioelectron 26:2383–2389
268. Hasan K, Patil SA, Leech D, Hägerhäll C, Gorton L (2012) Electrochemical communication between microbial cells and electrodes via osmium redox systems. Biochem Soc T 40 (6):1330–1335
269. Niessen J, Schröder U, Harnisch F, Scholz F (2005) Gaining electricity from in situ oxidation of hydrogen produced by fermentative cellulose degradation. Lett Appl Microbiol 41:286–290
270. Niessen J, Schröder U, Scholz F (2004) Exploiting complex carbohydrates for microbial electricity generation: a bacterial fuel cell operating on starch. Electrochem Commun 6:955–958
271. Karube I, Matsunaga T, Tsuru S, Suzuki S (1977) Biochemical fuel cell utilizing immobilized cells of *Clostridium butyricum*. Biotechnol Bioeng 19:1727–1733
272. Velasquez-Orta SB, Head IM, Curtis TP, Scott K (2011) Factors affecting current production in microbial fuel cells using different industrial wastewaters. Bioresource Technol 102:5105–5112
273. Ren Z, Yan H, Wang W, Mench MM, Regan JM (2011) Characterization of microbial fuel cells at microbially and electrochemically meaningful time scales. Environ Sci Technol 45:2435–2441
274. Harnisch F, Koch C, Patil SA, Hübschmann T, Müller S, Schröder U (2011) Revealing the electrochemically driven selection in natural community derived microbial biofilms using flow-cytometry. Energ Environ Sci 4:1265–1267
275. Bond DR, Holmes DE, Tender LM, Lovley DR (2002) Electrode-reducing microorganisms that harvest energy from marine sediments. Science 295:483–485
276. Patil SA, Hasan K, Leech D, Hägerhäll C, Gorton L (2012) Improved microbial electrocatalysis with osmium polymer modified electrodes. Chem Commun 48:10183–10185
277. Gregory KB, Lovley DR (2005) Remediation and recovery of uranium from contaminated subsurface environments with electrodes. Environ Sci Technol 39:8943–8947
278. Strycharz SM, Glaven RH, Coppi MV, Gannon SM, Perpetua LA, Liu A, Nevin KP, Lovley DR (2011) Gene expression and deletion analysis of mechanisms for electron transfer from electrodes to *Geobacter sulfurreducens*. Bioelectrochemistry 80:142–150
279. Strycharz SM, Woodard TL, Johnson JP, Nevin KP, Sanford RA, Löffler FE, Lovley DR (2008) Graphite electrode as a sole electron donor for reductive dechlorination of tetrachlorethene by *Geobacter lovleyi*. Appl Environ Microbiol 74:5943–5947
280. Strik DPBTB, Hamelers HVM, Buisman CJN (2009) Solar energy powered microbial fuel cell with a reversible bioelectrode. Environ Sci Technol 44:532–537
281. Parot S, Vandecandelaere I, Cournet A, Délia M-L, Vandamme P, Bergé M, Roques C, Bergel A (2011) Catalysis of the electrochemical reduction of oxygen by bacteria isolated from electro-active biofilms formed in seawater. Bioresource Technol 102:304–311
282. You SJ, Ren NQ, Zhao QL, Wang JY, Yang FL (2009) Power generation and electrochemical analysis of biocathode microbial fuel cell using graphite fibre brush as cathode material. Fuel Cells 9:588–596
283. Vandecandelaere I, Nercessian O, Faimali M, Segaert E, Mollica A, Achouak W, De Vos P, Vandamme P (2010) Bacterial diversity of the cultivable fraction of a marine electroactive biofilm. Bioelectrochemistry 78:62–66
284. Freguia S, Tsujimura S, Kano K (2010) Electron transfer pathways in microbial oxygen biocathodes. Electrochim Acta 55:813–818
285. Aulenta F, Catervi A, Majone M, Panero S, Reale P, Rossetti S (2007) Electron transfer from a solid-state electrode assisted by methyl viologen sustains efficient microbial reductive dechlorination of TCE. Environ Sci Technol 41:2554–2559

286. Park DH, Zeikus JG (1999) Utilization of electrically reduced neutral red by *Actinobacillus succinogenes*: physiological function of neutral red in membrane-driven fumarate reduction and energy conservation. J Bacteriol 181:2403–2410
287. Emde R, Schink B (1990) Enhanced propionate formation by *Propionibacterium freudenreichii* subsp. *freudenreichii* in a three-electrode amperometric culture system. Appl Environ Microbiol 56:2771–2776
288. Shin HS, Jain MJ, Chartrain MC, Zeikus JZ (2001) Evaluation of an electrochemical bioreactor system in the biotransformation of 6-bromo-2-tetralone to 6-bromo-2-tetralol. Appl Microbiol Biot 57(4):506–510
289. Hongo M, Iwahara M (1979) Determination of electro-energizing conditions for L-glutamic acid fermentation. Agric Biol Chem 43:2083–2086
290. Steinbusch KJJ, Hamelers HVM, Schaap JD, Kampman C, Buisman CJN (2009) Bioelectrochemical ethanol production through mediated acetate reduction by mixed cultures. Environ Sci Technol 44:513–517
291. Aulenta F, Canosa A, Majone M, Panero S, Reale P, Rossetti S (2008) Trichloroethene dechlorination and H_2 evolution are alternative biological pathways of electric charge utilization by a dechlorinating culture in a bioelectrochemical system. Environ Sci Technol 42:6185–6190
292. Thrash JC, Van Trump JI, Weber KA, Miller E, Achenbach LA, Coates JD (2007) Electrochemical stimulation of microbial perchlorate reduction. Environ Sci Technol 41:1740–1746
293. Lojou E, Durand MC, Dolla A, Bianco P (2002) Hydrogenase activity control at *Desulfovibrio vulgaris* cell-coated carbon electrodes: biochemical and chemical factors influencing the mediated bioelectrocatalysis. Electroanal 14:913–922
294. Aulenta F, Reale P, Canosa A, Rossetti S, Panero S, Majone M (2010) Characterization of an electro-active biocathode capable of dechlorinating trichloroethene and cis-dichloroethene to ethene. Biosens Bioelectron 25:1796–1802
295. Aulenta F, Canosa A, Reale P, Rossetti S, Panero S, Majone M (2009) Microbial reductive dechlorination of trichloroethene to ethene with electrodes serving as electron donors without the external addition of redox mediators. Biotechnol Bioeng 103:85–91
296. Sakakibara Y, Kuroda M (1993) Electric prompting and control of denitrification. Biotechnol Bioeng 42:535–537
297. Park HI, Dk K, Choi Y-J, Pak D (2005) Nitrate reduction using an electrode as direct electron donor in a biofilm-electrode reactor. Process Biochem 40:3383–3388
298. Feleke Z, Araki K, Sakakibara Y, Watanabe T, Kuroda M (1998) Selective reduction of nitrate to nitrogen gas in a biofilm-electrode reactor. Water Res 32:2728–2734
299. Cast KL, Flora JRV (1998) An evaluation of two cathode materials and the impact of copper on bioelectrochemical denitrification. Water Res 32:63–70
300. Rabaey K, Girguis P, Nielsen LK (2011) Metabolic and practical considerations on microbial electrosynthesis. Curr Opin Biotech 22:371–377
301. Zhao F, Slade RCT, Varcoe JR (2009) Techniques for the study and development of microbial fuel cells: an electrochemical perspective. Chem Soc Rev 38(7):1926–1939
302. He Z, Mansfeld F (2009) Exploring the use of electrochemical impedance spectroscopy (EIS) in microbial fuel cell studies. Energ Environ Sci 2:215–219
303. Watson VJ, Logan BE (2011) Analysis of polarization methods for elimination of power overshoot in microbial fuel cells. Electrochem Commun 13:54–56
304. Manohar AK, Bretschger O, Nealson KH, Mansfeld F (2008) The polarization behavior of the anode in a microbial fuel cell. Electrochim Acta 53:3508–3513
305. Patil SA, Harnisch F, Koch C, Hübschmann T, Fetzer I, Carmona-Martinez AA, Müller S, Schröder U (2011) Electroactive mixed culture derived biofilms in microbial bioelectrochemical systems: the role of pH on biofilm formation, performance and composition. Bioresource Technol 102:9683–9690
306. Chen S, Hou H, Harnisch F, Patil SA, Carmona-Martinez AA, Agarwal S, Zhang Y, Sinha-Ray S, Yarin AL, Greiner A, Schröder U (2011) Electrospun and solution blown three-

dimensional carbon fiber nonwovens for application as electrodes in microbial fuel cells. Energ Environ Sci 4:1417–1421
307. Patil SA, Harnisch F, Kapadnis B, Schröder U (2010) Electroactive mixed culture biofilms in microbial bioelectrochemical systems: the role of temperature for biofilm formation and performance. Biosens Bioelectron 26:803–808
308. Liu Y, Harnisch F, Fricke K, Sietmann R, Schröder U (2008) Improvement of the anodic bioelectrocatalytic activity of mixed culture biofilms by a simple consecutive electrochemical selection procedure. Biosens Bioelectron 24:1006–1011
309. Torres CI, Krajmalnik-Brown R, Parameswaran P, Marcus AK, Wanger G, Gorby YA, Rittmann BE (2009) Selecting anode-respiring bacteria based on anode potential: phylogenetic, electrochemical, and microscopic characterization. Environ Sci Technol 43:9519–9524
310. Pocaznoi D, Erable B, Delia M-L, Bergel A (2012) Ultra microelectrodes increase the current density provided by electroactive biofilms by improving their electron transport ability. Energ Environ Sci 5:5287–5296
311. Parot S, Délia M-L, Bergel A (2008) Forming electrochemically active biofilms from garden compost under chronoamperometry. Bioresource Technol 99:4809–4816
312. Wei J, Liang P, Cao X, Huang X (2010) A new insight into potential regulation on growth and power generation of *Geobacter sulfurreducens* in microbial fuel cells based on energy viewpoint. Environ Sci Technol 44:3187–3191
313. Aelterman P, Freguia S, Keller J, Verstraete W, Rabaey K (2008) The anode potential regulates bacterial activity in microbial fuel cells. Appl Microbiol Biot 78:409–418
314. Finkelstein DA, Tender LM, Zeikus JG (2006) Effect of electrode potential on electrode-reducing microbiota. Environ Sci Technol 40:6990–6995
315. Cheng KY, Ho G, Cord-Ruwisch R (2008) Affinity of microbial fuel cell biofilm for the anodic potential. Environ Sci Technol 42:3828–3834
316. Wagner RC, Call DF, Logan BE (2010) Optimal set anode potentials vary in bioelectrochemical systems. Environ Sci Technol 44:6036–6041
317. Pocaznoi D, Erable B, Etcheverry L, Delia M-L, Bergel A (2012) Forming microbial anodes under delayed polarisation modifies the electron transfer network and decreases the polarisation time required. Bioresource Technol 114:334–341
318. Harnisch F, Freguia S (2012) A basic tutorial on cyclic voltammetry for the investigation of electroactive microbial biofilms. Chem Asian J 7:466–475
319. Torres CI, Marcus AK, Lee H-S, Parameswaran P, Krajmalnik-Brown R, Rittmann BE (2010) A kinetic perspective on extracellular electron transfer by anode-respiring bacteria. FEMS Microbiol Rev 34:3–17
320. Park HS, Kim BH, Kim HS, Kim HJ, Kim GT, Kim M, Chang IS, Park YK, Chang HI (2001) A novel electrochemically active and Fe(III)-reducing bacterium phylogenetically related to *Clostridium butyricum* isolated from a microbial fuel cell. Anaerobe 7:297–306
321. Zhang T, Cui C, Chen S, Ai X, Yang H, Shen P, Peng Z (2006) A novel mediatorless microbial fuel cell based on direct biocatalysis of *Escherichia coli*. Chem Commun 21:2257–2259
322. Kim HJ, Park HS, Hyun MS, Chang IS, Kim M, Kim BH (2002) A mediator-less microbial fuel cell using a metal reducing bacterium, *Shewanella putrefaciens*. Enzyme Microb Tech 30:145–152
323. Rabaey K, Ossieur W, Verhaege M, Verstraete W (2005) Continuous microbial fuel cells convert carbohydrates to electricity. Water Sci Technol 52:515–523
324. Yoon SM, Choi CH, Kim M, Hyun MS, Shin SH, Yi D, Kim HJ (2007) Enrichment of electrochemically active bacteria using a three-electrode electrochemical cell. J Microbiol Biotechnol 17:110–115
325. He Z, Minteer SD, Angenent LT (2005) Electricity generation from artificial wastewater using an upflow microbial fuel cell. Environ Sci Technol 39:5262–5267

326. Pham CA, Jung SJ, Phung NT, Lee J, Chang IS, Kim BH, Yi H, Chun J (2003) A novel electrochemically active and Fe(III)-reducing bacterium phylogenetically related to *Aeromonas hydrophila*, isolated from a microbial fuel cell. FEMS Microbiol Lett 223:129–134
327. Liu H, Cheng S, Logan BE (2004) Production of electricity from acetate or butyrate using a single-chamber microbial fuel cell. Environ Sci Technol 39:658–662
328. Rabaey K, Boon N, Siciliano SD, Verhaege M, Verstraete W (2004) Biofuel cells select for microbial consortia that self-mediate electron transfer. Appl Environ Microbiol 70:5373–5382
329. Katuri KP, Kavanagh P, Rengaraj S, Leech D (2010) *Geobacter sulfurreducens* biofilms developed under different growth conditions on glassy carbon electrodes: insights using cyclic voltammetry. Chem Commun 46:4758–4760
330. Jain A, Gazzola G, Panzera A, Zanoni M, Marsili E (2011) Visible spectroelectrochemical characterization of *Geobacter sulfurreducens* biofilms on optically transparent indium tin oxide electrode. Electrochim Acta 56:10776–10785
331. Liu H, Newton GJ, Nakamura R, Hashimoto K, Nakanishi S (2010) Electrochemical characterization of a single electricity-producing bacterial cell of *Shewanella* by using optical tweezers. Angew Chem Int Edit 49:6596–6599
332. Okamoto A, Nakamura R, Ishii K, Hashimoto K (2009) In vivo electrochemistry of C-type cytochrome-mediated electron-transfer with chemical marking. Chembiochem 10:2329–2332
333. Katuri KP, Rengaraj S, Kavanagh P, O'Flaherty V, Leech D (2012) Charge transport through *Geobacter sulfurreducens* biofilms grown on graphite rods. Langmuir 28:7904–7913
334. Wu X, Zhao F, Rahunen N, Varcoe JR, Avignone-Rossa C, Thumser AE, Slade RCT (2011) A role for microbial palladium nanoparticles in extracellular electron transfer. Angew Chem Int Edit 50:427–430
335. Millo D, Harnisch F, Patil SA, Ly HK, Schröder U, Hildebrandt P (2011) In situ spectroelectrochemical investigation of electrocatalytic microbial biofilms by surface-enhanced resonance Raman spectroscopy. Angew Chem Int Edit 50:2625–2627
336. Liu Y, Kim H, Franklin RR, Bond DR (2011) Linking spectral and electrochemical analysis to monitor c-type cytochrome redox status in living *Geobacter sulfurreducens* biofilms. Chemphyschem 12:2235–2241
337. Busalmen JP, Berná A, Feliu JM (2007) Spectroelectrochemical examination of the interaction between bacterial cells and gold electrodes. Langmuir 23:6459–6466
338. Nakamura R, Ishii K, Hashimoto K (2009) Electronic absorption spectra and redox properties of c type cytochromes in living microbes. Angew Chem Int Edit 48:1606–1608
339. Liu Y, Bond DR (2012) Long-distance electron transfer by *G. sulfurreducens* biofilms results in accumulation of reduced c-type cytochromes. ChemSusChem 5:1047–1053
340. Biju V, Pan D, Gorby YA, Fredrickson J, McLean J, Saffarini D, Lu HP (2006) Combined spectroscopic and topographic characterization of nanoscale domains and their distributions of a redox protein on bacterial cell surfaces. Langmuir 23:1333–1338
341. Compton RG, Perkin SJ, Gamblin DP, Davis J, Marken F, Padden AN, John P (2000) *Clostridium isatidis* colonised carbon electrodes: voltammetric evidence for direct solid state redox processes. New J Chem 24:179–181
342. Parot S, Nercessian O, Délia ML, Achouak W, Bergel A (2009) Electrochemical checking of aerobic isolates from electrochemically active biofilms formed in compost. J Appl Microbiol 106:1350–1359
343. Dominguez-Benetton X, Sevda S, Vanbroekhoven K, Pant D (2012) The accurate use of impedance analysis for the study of microbial electrochemical systems. Chem Soc Rev 41:7228–7246
344. Strik DP, Ter Heijne A, Hamelers HVM, Saakes M, Buisman C (2008) Feasibility study on electrochemical impedance spectroscopy for microbial fuel cells: measurement modes & data validation. ECS Trans 13:27–41

345. He Z, Wagner N, Minteer SD, Angenent LT (2006) An upflow microbial fuel cell with an interior cathode: assessment of the internal resistance by impedance spectroscopy. Environ Sci Technol 40:5212–5217
346. Ouitrakul S, Sriyudthsak M, Charojrochkul S, Kakizono T (2007) Impedance analysis of bio-fuel cell electrodes. Biosens Bioelectron 23:721–727
347. Ramasamy RP, Ren Z, Mench MM, Regan JM (2008) Impact of initial biofilm growth on the anode impedance of microbial fuel cells. Biotechnol Bioeng 101:101–108
348. Borole AP, Aaron D, Hamilton CY, Tsouris C (2010) Understanding long-term changes in microbial fuel cell performance using electrochemical impedance spectroscopy. Environ Sci Technol 44:2740–2745
349. Aaron D, Tsouris C, Hamilton CY, Borole AP (2010) Assessment of the effects of flow rate and ionic strength on the performance of an air-cathode microbial fuel cell using electrochemical impedance spectroscopy. Energies 3:592–606
350. He Z, Huang Y, Manohar AK, Mansfeld F (2008) Effect of electrolyte pH on the rate of the anodic and cathodic reactions in an air-cathode microbial fuel cell. Bioelectrochemistry 74:78–82
351. ter Heijne A, Schaetzle O, Gimenez S, Fabregat-Santiago F, Bisquert J, Strik DPBTB, Barriere F, Buisman CJN, Hamelers HVM (2011) Identifying charge and mass transfer resistances of an oxygen reducing biocathode. Energ Environ Sci 4:5035–5043
352. Virdis B, Harnisch F, Batstone DJ, Rabaey K, Donose BC (2012) Non-invasive characterization of electrochemically active microbial biofilms using confocal Raman microscopy. Energ Environ Sci 5:7017–7024
353. Firer-Sherwood MA, Bewley KD, Mock J-Y, Elliott SJ (2011) Tools for resolving complexity in the electron transfer networks of multiheme cytochromes c. Metallomics 3:344–348
354. Franks AE, Glaven RH, Lovley DR (2012) Real-time spatial gene expression analysis within current-producing biofilms. ChemSusChem 5:1092–1098
355. Harnisch F, Rabaey K (2012) The diversity of techniques to study electrochemically active biofilms highlights the need for standardization. ChemSusChem 5:1027–1038
356. Clarke TA, Edwards MJ, Gates AJ, Hall A, White GF, Bradley J, Reardon CL, Shi L, Beliaev AS, Marshall MJ, Wang Z, Watmough NJ, Fredrickson JK, Zachara JM, Butt JN, Richardson DJ (2011) Structure of a bacterial cell surface decaheme electron conduit. Proc Natl Acad Sci USA 108:9384–9389
357. Summers ZM, Fogarty HE, Leang C, Franks AE, Malvankar NS, Lovley DR (2010) Direct exchange of electrons within aggregates of an evolved syntrophic coculture of anaerobic bacteria. Science 330:1413–1415
358. Morita M, Malvankar NS, Franks AE, Summers ZM, Giloteaux L, Rotaru AE, Rotaru C, Lovley DR (2011) Potential for direct interspecies electron transfer in methanogenic wastewater digester aggregates. mBio 2(4):e00159–11
359. Rotaru A-E, Shrestha PM, Liu F, Ueki T, Nevin K, Summers ZM, Lovley DR (2012) Interspecies electron transfer via H_2 and formate rather than direct electrical connections in co-cultures of *Pelobacter carbinolicus* and *Geobacter sulfurreducens*. Appl Environ Microbiol 78(21):7645–7651
360. Pfeffer C, Larsen S, Song J, Dong M, Besenbacher F, Meyer RL, Kjeldsen KU, Schreiber L, Gorby YA, El-Naggar MY, Leung KM, Schramm A, Risgaard-Petersen N, Nielsen LP (2012) Filamentous bacteria transport electrons over centimetre distances. Nature 491:218–221

BIOREV (2014) 1: 131–154
DOI: 10.1007/11663_2013_4

Published online: 4 October 2013

Synthesis of Monodisperse Polymeric Nano- and Microparticles and Their Application in Bioanalysis

Isabel M. Perez de Vargas-Sansalvador, Francesco Canfarotta, and Sergey A. Piletsky

Abstract The production of highly monodisperse polymer particles is very important in different fields, such as research and industry. This interest is due to their wide potential applications, ranging from drug/gene delivery to large scale separation, sensor fabrication and diagnostic applications, due to their special characteristics of uniformity in size, shape and structure. Different methods for the synthesis of monodisperse particles have been reported, but there is a necessity to find new approaches for the synthesis of *functionalized* monodisperse particles, in order to satisfy growing needs of industry in products with specific characteristics.

This review describes several approaches for fabrication of monodisperse polymer particles with size varying from 1 nm to 1,000 μm, highlighting problems associated with their synthesis and furnishes analysis of present and prospective areas for their applications.

Keywords Bioanalytical applications · Diagnostic applications · Monodisperse particles · Polymeric particles

Contents

I.M. Perez de Vargas-Sansalvador (✉), F. Canfarotta and S.A. Piletsky
Cranfield Health, Cranfield University, Cranfield, Bedfordshire MK43 0AL, UK
e-mail: isabelpdv@hotmail.com

1 Introduction

Monodisperse particles (MP) are defined as particles with uniform size, shape and mass. MP typically possess a narrow distribution function (less than 10 % in mean size) [1]. Monodisperse *polymer* particles have been used in research and industrial fields due to their wide variety of applications such as column packing materials for chromatography [2] paint and coatings, photonic crystals [3, 4], chemical and biological sensors [5], drug/gene delivery [6], tools for instrument calibration [7], immunological analysis and medical research [8]. Since the properties of particles depend decisively on their characteristics such as size, shape, surface chemistry and structure, the particular significance of monodisperse particles may be ascribed to their uniformity in these characteristics [9] making them ideal models for fundamental studies, but also offering a broad range of applications as ideal particulate materials [1].

Several techniques have been used for the synthesis of monodisperse polymeric microspheres such as the successive seeding method [10], the activated swelling method [11], the dynamic swelling method [12] and the Shirasu Porous Glass emulsification technique [13]. However, these approaches are tedious and typically required several preparation steps [14]. The most conventional methods for the synthesis of monodisperse polymer particles are emulsion or dispersion polymerization and a large number of various polymer particles have been prepared by these techniques [15]. These latter together with other techniques for the fabrication of monodisperse organic particles in the micrometre and nanometre range will be discussed in the first part of this review. Furthermore, their applications in the diagnostic field will be analysed, focusing on the importance of the monodispersity for their use.

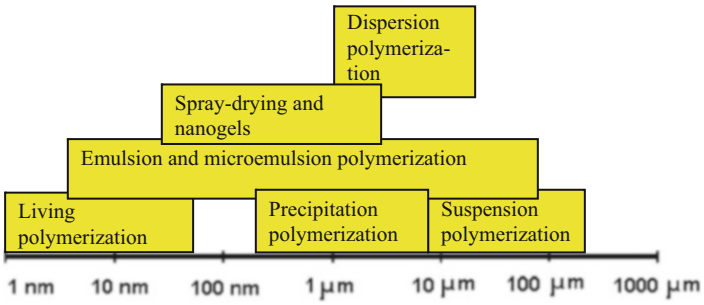

Fig. 1 Polymerization approaches used for manufacturing monodisperse particles

2 Fabrication of Monodisperse Nano- and Microparticles

2.1 General Aspects

Traditionally, micrometre and sub-micrometre polymer particles are produced by heterogeneous polymerization including precipitation polymerization and various forms of suspension, emulsion and dispersion polymerizations. Different methods could be applied for synthesis of particles with size varying from 1 nm to practically 1 mm (Fig. 1). Each of these methods has different application, advantages and disadvantages discussed below.

2.2 Suspension Polymerization

Suspension polymerization is a well-established approach for producing commercial quantities of polystyrene and polyvinyl chloride polymers beads. In suspension polymerization the reaction proceeds in heterogeneous conditions with monomer, initiator and surface-active agent being dispersed in the solvent. During polymerization the monomer droplets, formed by agitation, convert into suspension of solid polymer particles with size 10–500 µm. The surface-active agents such as polyvinyl acetate or polyvinyl alcohol adsorb at the monomer/solvent interface ensuring stability of drops against coalescence. The yield of product is reasonably high, typically 50–70 %. The control of particle size in suspension polymerization reactors is achieved by careful optimization of agitation and polymerization conditions [16]. Furthermore, It is possible to perform polymerization by dispersing monomer mixture either in aqueous or in immiscible organic phases [17, 18]. However, the synthesized particles would often contain entrapped surfactant which could affect their performance in drug delivery and diagnostics.

2.3 Precipitation Polymerization

Precipitation polymerization starts as homogeneous process with radical initiator (e.g. AIBN) and monomers dissolved in appropriate solvent. No surfactant is added for stabilizing particles. As the polymerization proceeds, polymer particles precipitate from the solution forming beads with size 0.3–10 μm, depending on the conditions [19]. The stabilization factor in forming stable suspension of polymer particles is the cross-linked nature of the synthesized polymers. Spherical particles could be formed only if the ratio between cross-linker and monomer exceeds 1:2. The synthesized microparticles usually do not swell and have stabilizer-free surface [20]. The precipitation polymerization however is arguably the most difficult process to control for producing particles with predictable size range.

2.4 Dispersion Polymerization

Dispersion polymerization is an attractive and advantageous method to prepare monodisperse polymeric particles in a single step. Therefore, the preparation of monodisperse homopolymer particles by dispersion polymerization have been extensively studied, especially polystyrene [21] and poly(methyl methacrylate) [14] based particles.

Dispersion polymerization is very similar to precipitation polymerization since it also starts in a homogeneous reaction mixture. In contrast to the last one, it employs a suspension agent or steric stabilizer such as hydroxypropyl cellulose or poly (*N*-vinylpyrrolidone). Upon initiation (either by heat or UV irradiation), free radicals grow in the continuous phase, forming polymer nanoparticles as soon as the chain length has reached its solubility limit. Sufficiently large polymer particles precipitate and adsorb both non-reacted monomer and stabilizer from the continuous phase. The formation of new nuclei stops after the short initiation and the nucleation period. From now on polymerization mainly takes place within the monomer-swollen particles until most of the monomer is consumed. Depending on the polymerization conditions, such as type and concentration of monomers, initiator and stabilizer, stirring speed, and temperature, monodisperse particles with sizes between 1 and 20 μm can be obtained. The mechanisms of forming monodisperse microparticles by dispersion polymerization are presented in Fig. 2 [22].

Dispersion polymerization has been successfully performed in supercritical carbon dioxide, using a commercially available carboxylic acid end-capped perfluoropolyether oil (Krytox 157FSL) as stabilizer [23]. The benefit of this approach lies in the possibility of easy removal of the polymerization solvent from the synthesized beads.

Similar to suspension polymerization, the synthesized particles would contain traces of suspension agent.

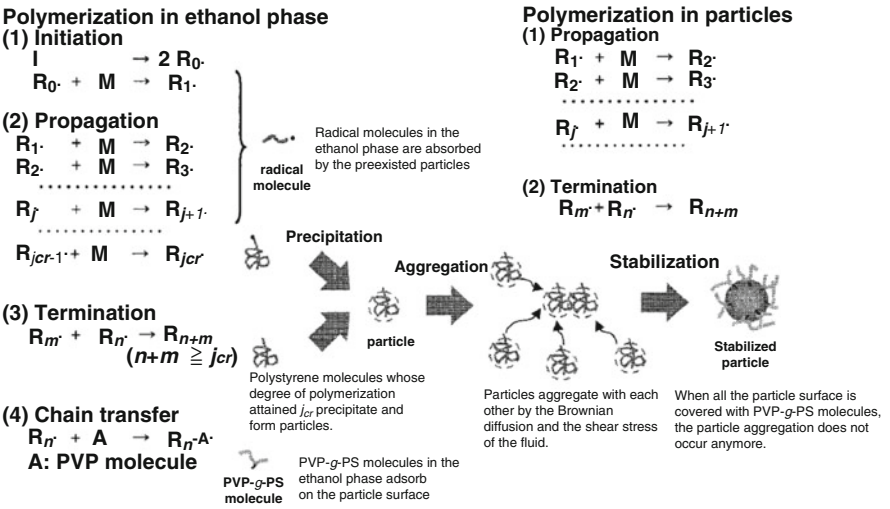

Fig. 2 Schematic illustration of particle formation stage in dispersion polymerization. Reprinted with permission from [22]. Copyright 2001 American Chemical Society

2.5 Emulsion Polymerization

Emulsion polymerization is probably the most popular approach used for fabricating monodisperse polymer particles [24], since its first description in 1932. Emulsion polymerization is carried out in heterogeneous systems, can be applied for water-soluble monomers (e.g. acrylic acid or acrylamide) in water-in-oil (w/o) emulsions and for hydrophobic monomers (e.g. styrene or methyl methacrylate) in oil-in-water (o/w). In a typical reaction, the desired amount of monomer(s) is added to an aqueous solution of surfactant (pentan-1-ol, cetyltrimethylammonium bromide or sodium dodecyl sulphate) and the mixture is stirred until a milky emulsion is formed. In emulsions the droplet size is determined by the amount of monomer and water, the monomer solubility and the amount of surfactant. Initiation can be performed either with water-soluble initiators such as H_2O_2/ascorbic acid or ammonium persulphate/tetramethyldiaminomethane, or with oil soluble, such as 2,2-dimethoxy-2-phenylacetophenone. The particles can be isolated by washing with organic solvent or water depending on polymer solubility [25]. The emulsion polymerization allows producing stable suspensions of polymer particles with different size, typically 1–100 μm. The variation of this technique called microemulsion polymerization could be used for producing even smaller particles in the nanosize range (5–50 nm) [26]. The process differentiates from emulsion polymerization by the high concentration of added surfactant/cosurfactant (pentanol, HEA, HBA or HPMA) (Fig. 3).

The emulsions can be used also for producing polymer particles with size 1–100 μm from prefabricated polymers. Thus in emulsification solvent evaporation

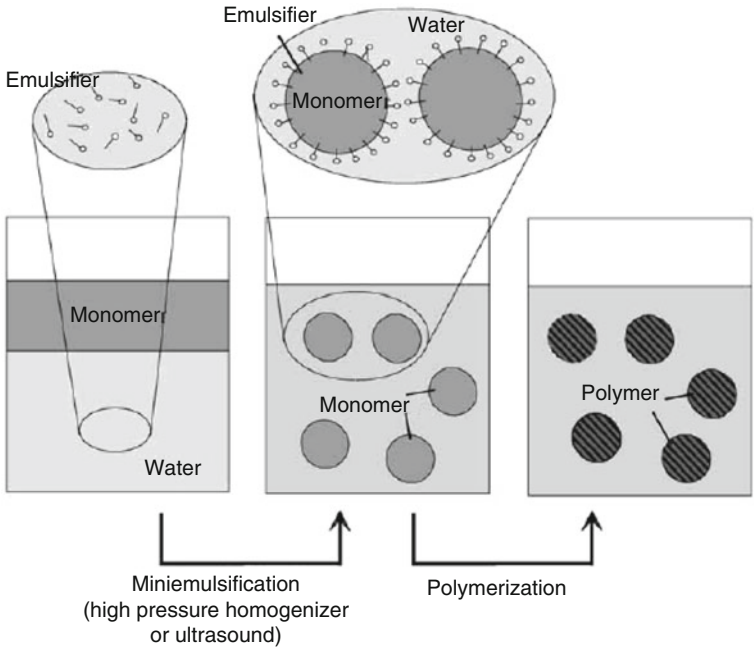

Fig. 3 The principle of miniemulsion polymerization. Reprinted from [115] with permission from Elsevier

technique (ESE) a polymer solution is broken up in microdroplets by the shear stress produced by homogenizer in the presence of a surface-active agent. This process is followed by particle hardening through solvent evaporation and/or extraction methods. Figure 4 illustrates the process of formation of polymer particles by ESE. Depending on the solubility of polymer simple or multiple emulsion techniques, e.g. oil-in-water (O/W) and water-in-oil-in-water (W/O/W) methods, are used. In the first case, the polymer is dissolved in an organic solvent, which is dispersed into an aqueous phase. Upon contact, the organic solvent diffuses into the water and evaporates at its surface precipitating the polymer. In the second case aqueous solution of water-soluble components is emulsified into an organic solvent containing the dissolved polymer. This primary W/O emulsion is dispersed into water. Upon solvent diffusion/evaporation, the polymer precipitates entrapping the water-soluble components. This process is used for drug formulation as encapsulation process [29].

The emulsification can be achieved with the help of glass membranes with defined size of pores. These membranes produce monodisperse oil droplets by pumping oil phase through the pores to an aqueous solution containing stabilizers. Subsequent suspension polymerization of the monomer droplets or evaporation of solvent from the polymer solution yields uniform polymer particles. Particle size distributions of emulsions correspond to pore-size distributions of the membrane used [30].

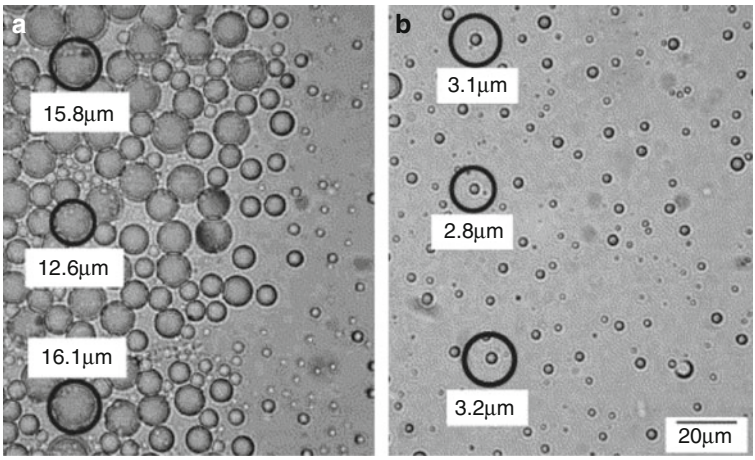

Fig. 4 The first (**a**) and last (**b**) image of the emulsion microdroplets transformation into the final microparticles. Reprinted from [28] with permission from Elsevier

Advantages of this method are high polymerization rate, final particles with high molecular weight, possibility to tune the final polymer by the addition of transfer agents. Particles synthesized by emulsion polymerization contain traces of suspension agent and surfactants which are difficult to remove, excluding their use for applications where high purity is required. An additional drawback in using this method is the excessive use of solvent [31].

2.6 Synthesis of Nano- and Microparticles from Prefabricated Polymers: Spray-Drying and Nanogels

Another technique for producing polymer nano- and microparticles (70 nm to 5 μm) from prefabricated polymer is the spray-drying process which involves three distinctive steps: (a) atomization or jetting of the feed into a spray and bringing it into contact with air, (b) drying of the spray and (c) separation of the dried product from the drying gas [32, 33].

In the pharmaceutical industry spray-drying is used to manufacture particles that form the basis for dry dosage forms. A study of evaporation and particle formation processes have been carried out to improve knowledge about the formation of particles to enable prediction of the morphology of multi-component particles [34].

Nanoparticles could also be formed from soluble polymers in the form of nanogels. Thus by heating atactic chloromethylpolystyrene of $M_w = 330{,}000$ Da and $M_w/M_n = 1.04$ with $SnCl_4$ in a very dilute solution in ethylene dichloride, the polymeric coils were converted into intramolecularly hypercross-linked macromolecules of molecular weight of about 370,000 Da and a diameter of

about 17 nm. The particles could assemble into clusters consisting of 13 spherical subunits with 5.0×10^6 Da as molecular weight and 45 nm as average diameter [35]. The serious disadvantage in using this approach lies in restricted availability of pre-formed polymer with homogeneous size distribution.

2.7 Synthesis of Nanoparticles by Living Polymerization

Living radical polymerization provides an excellent control over key elements of macromolecular structure such as molecular weight, polydispersity and composition, and it has been successfully used for the preparation of nanoparticles with size 5–50 nm [36]. Several different forms of living polymerization exist including anionic, cationic, coordination, ring-opening and living radical polymerizations. All of these methods are based on establishing a rapid dynamic equilibrium between a minute amount of growing free radicals and a large majority of the dormant species. The dormant chains may be alkyl halides, as in atom transfer radical polymerization (ATRP) or degenerative transfer (DT), thioesters, as in reversible addition fragmentation chain transfer processes (RAFT), alkoxyamines, as in nitroxide mediated polymerization (NMP) or stable free radical polymerization (SFRP), and potentially even organometallic species [37]. Free radicals may be generated by the spontaneous thermal process (NMP, SFRP) via a catalysed reaction (ATRP) or reversibly via the degenerative exchange process with dormant species (DT, RAFT). The living radical polymerization allows a major variation in the composition of the polymerization mixture, and it could be better suited for producing functionalized nanoparticles. This approach however cannot be used for producing monodisperse microparticles.

The effects of various polymerization parameters on the characteristics of the PS particles synthesis by the living free-radical dispersion polymerization with a RAFT agent have been studied. Regarding RAFT concentration, insufficient or excessive amount of stabilizer leads to the coagulation or broad polydispersity value. When increasing concentrations of monomer and initiator, larger PS particles are obtained. Thus, in the RAFT-mediated dispersion polymerization of styrene, the RAFT agent alters the inverse behaviour between the molecular weight and the particle size shown in the conventional dispersion polymerization [38]. Furthermore, living radical polymerization allows the use of iniferters (initiator transfer-agent terminator) which can bear dithiocarbamyl groups (for photo-polymerization) or carbon–carbon or azo groups (for thermal polymerization). The most employed iniferters yield two different kinds of radicals: the highly reactive carbon radical which initiates the polymerization, and the less reactive dithiocarbamyl radical which can terminate the polymerization. However, product formed after termination can further generate a new propagating radical upon application of the stimulus triggering the polymerization [39]. In this way, sequential polymerizations with other monomers can be re-initiated, in order to tailor properties or functionalities of the synthesized particles [40]. Moreover, another advantage of

living polymerization in contrast to conventional radical polymerization is that the latter can undergo autoacceleration process, whereas the former proceeds at low rate, allowing a better control over some parameters such as the polymer chain length and the particle size.

3 Functionalized Micro- and Nanoparticles Including MIPs

Most of the existing protocols for fabrication of nano- and microparticles cannot be used without modification for producing functionalized materials capable of performing several functions, such as recognition and catalysis. Typically monodisperse particles consist of only one monomer, usually cross-linker. The problem lies in the delicate balance required for fabricating particles by emulsion or dispersion polymerization. Thus, even small changes in composition, temperature or pressure would change size and properties of the synthesized particles. Due to this fact, it might be difficult to introduce a new functionality by adding a new polymer to the polymerization mixture. The most reliable approach for introducing functional groups is by grafting a second monomer to the surface of prefabricated particles [41]. Several functional groups such as boronate or aldehyde derivatives could be grafted to the particles surface and used for detection or binding of analytes [42, 43].

Some modifications of classic methods have been developed to synthesize monodisperse functionalized particles such as the delayed addition method, which consists in an emulsion polymerization where the addition of the cross-linking agent is delayed by varying time. Furthermore, the longer the delayed time of cross-linking agent addition, the better the monodispersity of particles. Highly cross-linked PS composite particles with functional hydrophilic group on its surface have been obtained by this method [44]. Through distillation copolymerization, monodisperse hydrophilic polymer microspheres bearing carboxylic acid groups have been prepared by means of copolymerizations of (meth)acrylic acid with either ethyleneglycol dimethacrylate or divinylbenzene as cross-linker. The polymer microspheres are formed and precipitated out from the reaction medium during the distillation of the solvent from the reaction system [45]; another method that has been used is the two-stage precipitation polymerization, which allowed to obtain narrow-disperse and monodisperse cross-linked core–shell polymer particles containing different functional groups, such as esters, hydroxyls, chloromethyls, carboxylic acids, amides, cyanos and glycidyls, in the shell layers. Micrometre size range particles can be obtained by this method without using any stabilizer. The copolymerization of the functional comonomers is carried out during a second stage of the precipitation polymerization [46]; copolymerization is also a way to functionalize particles. In this strategy, a well-controlled emulsion polymerization is carried out, at first, to produce monodispersed polymer nanospheres with high density of surface functionalities. These latter are able to react with small organic molecules to produce the final desirable surfaces. Several authors have employed

this method to produce monodisperse microspheres. Using acrylonitrile as comonomer, the nitrile group can be derived by amidoximizing with hydroxylamine [47]. Another approach employs thiol-epoxy coupling reaction to functionalize the surfaces of the polymer nanospheres with amine, carboxyl or hydroxyl groups [48]. Song and Winnik employed a new method called two-stage dispersion polymerization which is a modification of the conventional dispersion polymerization method. The aforementioned method consists in delaying the addition of the cross-linking agent until after the end of the nucleation stage of the reaction. This method avoids the broadening of the particle size distribution that leads to irregular particles, or coagulation. [49]. The use of polymerizable dyes in two-stage dispersion polymerization offers a possible way to prepare monodisperse micron-sized dye-labelled PS particles. Furthermore, the authors demonstrated by GPC that dyes were covalently incorporated into the polystyrene particles [50]. In light of the potentialities offered by the functionalization of polymeric particles, novel synthetic approaches are envisaged to be developed for different applications.

Other kind of polymeric particles are based on molecular imprinted polymers (MIPs). MIPs are synthetic materials prepared by means of polymers able to form a tridimensional matrix with specific recognition cavities for the imprinted molecule; such recognition cavities are complementary to the template molecule, in terms of size, shape and functionality. Theoretically the polymer will be able to rebind only the template or its structural analogues. The molecular recognition properties of these polymers are similar as observed between antigen and antibody, and between ligand and receptor, thus showing high affinity and specificity. Compared with antibodies, the synthesis of MIPs is simpler and cheaper. In addition, MIPs show high resistance to heat and to extreme pH and pressure conditions, and they can be used in both organic and aqueous medium [51, 52]. Several synthetic procedures have been developed for the preparation of monodisperse MIPs microparticles such as suspension polymerization, seed polymerization, dispersion/precipitation polymerization, grafting imprinting and hierarchical imprinting. We will not discuss these methods since they have been recently discussed in a review [53]. To the best of our knowledge just few examples about synthesis of monodisperse MIP NPs have been reported so far [54, 55], so their applications are not yet widespread.

4 Problems Associated with the Fabrication of Monodisperse Particles

All techniques presented above have some limitations that include difficulties in controlling particle size, excessive use of solvent and surfactant, and general lack of system tolerance towards change in polymer composition or polymerization conditions. The latter can be demonstrated by comparing the size of the particles prepared in varying experimental conditions (Fig. 5) [27]. The synthesis of particles in multiphase system suffers from the heterogenic nature of the process.

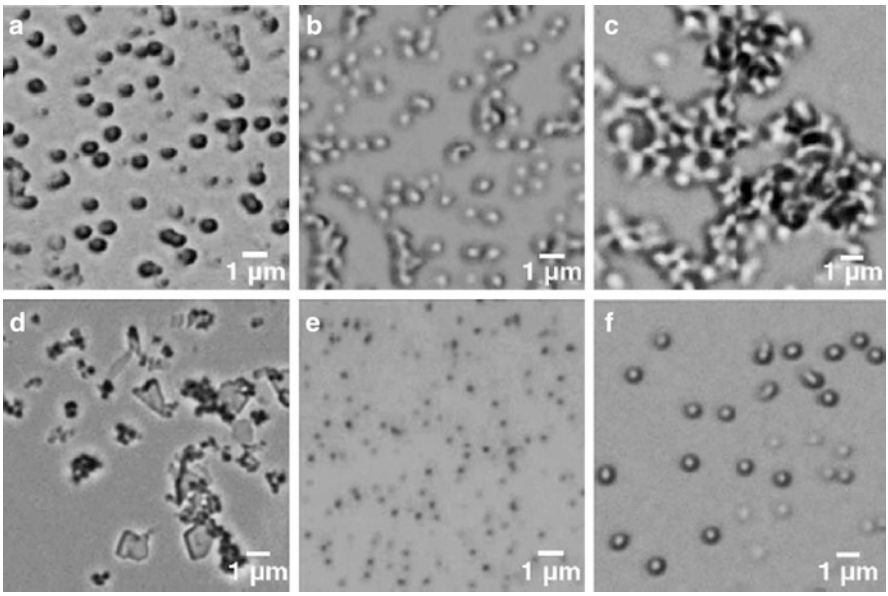

Fig. 5 Optical micrographs of poly (MAA-co-EGDMA) beads prepared with different monomer ratios (MAA:EGDMA in (**a**) 8:6; (**b**) 8:10; (**c**) 8:14; (**d**) 8:16) and poly (MAA-co-TRIM) beads prepared at different temperatures ((**e**) 60 °C; (**f**) 70 °C) synthesized by precipitation polymerization. Reprinted from [27] with permission from Elsevier

The synthesized polymer particles are the product of a kinetically controlled growth and are built from the centre to the surface, where all the monomer has to be transported by diffusion through immiscible solvent. Thus, the composition of the particle inner core might be different from its outer part. In most approaches the serious disadvantages, such as the lack of homogeneity of synthesized particles and the restrictions in the convenient composition range, cannot be avoided. The different distribution of monomers between different phases is also an issue which can compromise the consistency in polymer compositions. In conclusion, neither of the described protocols can be used as a generic tool for producing really monodisperse polymer particles. Hence, researchers and engineers should be ready to spend generous time and resources for optimizing manufacturing process.

5 Polymer Coating

An advantage of polymeric nanoparticles is the possibility to tailor some of their properties. Even for inorganic nanomaterials such as magnetic NPs or quantum dots, their surface modification with specific polymers allows them to be stabilized against agglomeration, to enhance their solubility in different solvents, to provide functional groups for further derivatization, to improve their mechanical and

chemical stability or to reduce their potential toxicity. For instance in QD-based nanosystems, the cytotoxicity may arise from the potential release of heavy metals. To reduce such release, many authors have used polymeric coatings, especially with water-soluble polymers [56].

Especially for in vivo applications, several authors employed neutral hydrophilic polymers, able to reduce the NP cellular internalization and then their cytotoxicity [57]. PEG is the most often employed hydrophilic polymer for increasing the blood circulation time, due to its capacity to reduce the adsorption of opsonins onto the NPs [58]. The minimum molecular weight of PEG able to achieve such property is 2,000 Da, because shorter chains lose the flexibility needed to repulse sterically the absorption of opsonins. However thickness, surface density, charge and functional groups of the polymeric layer affect NPs biodistribution, since they influence the interactions with opsonins [59]. It is worth mentioning that NPs blood circulation time is also affected by their size, shape and surface properties [60]. Some authors investigated the role of the polymer coating on the circulation lifetime. In particular, they injected PEG-coated QDs into the mouse blood stream, which showed to stay in the blood circulation for long period of time (half-life around 3 h), whereas the clearance of organic dyes is within few minutes from their injection [61]. Such features are due to the hydrophilic polymer layer which reduces the NP opsonization, allowing their use for lymph node imaging [62]. Furthermore, the size of these NPs was enough to avoid renal clearance, underlining the importance of NP size in the circulation lifetime. Dextran is another typical neutral polymer used especially in MNPs clinically approved [63]. Even charged polymers such as poly(acrylic acid) or polyethyleneimine (synthetic polymers), and hyaluronic acid or chitosan (natural polymers) have been employed for in vivo applications to improve the NPs biocompatibility. Interestingly, some authors successfully used both PEG and chitosan coating to further increase the blood circulation time [64].

6 Applications

MP can find applications in a wide range of fields as discussed above. The application of monodisperse polymer particles depends on their size and composition (Fig. 6).

6.1 Drug Delivery

One of the new fast-growing area for application of nanoparticles with size 1–100 nm is delivery systems for drugs, DNA and cells. Monodisperse particles are important in drug delivery applications for decreasing side effects of drugs, for improving their bioavailability and biocompatibility. This is linked to the fact that the distribution profile of particles in tissue depends on the particle size. Larger

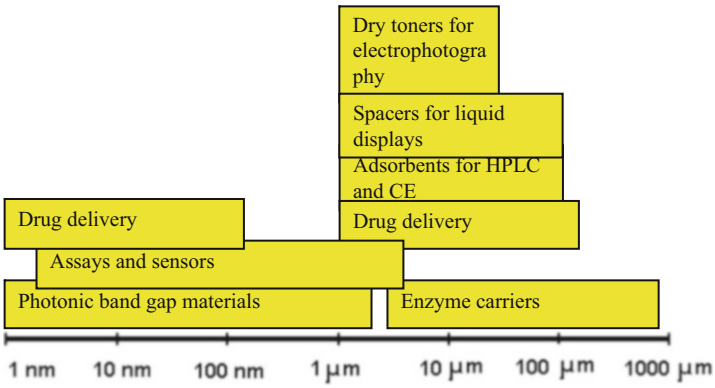

Fig. 6 Application of monodisperse polymer particles depending on their size

particles with size 1–5 µm are used in pulmonary delivery and 5–300 µm particles in oral application. The basic requirement for such application is biocompatibility (preferable choice is biodegradable materials, such as polylactic polyglycolic acid). Monodisperse MIP microparticles have been also used as controlled drug delivery systems, as we will point out in the next section.

6.2 Miscellaneous Applications

The unusual but fast-growing market for particles with size 2 nm to 2 µm is as photonic band gap materials. Furthermore, the particles with size 1–100 µm are used as packing materials for column chromatography, capillary electrochromatography, dry toners for electrophotography and particle-assisted soft lithography, spacers for liquid crystal displays and particles for biomedical analyses [65]. Highly stable nano- and microparticles with specific affinities for new diagnostic targets and cell phenotypes are required to aid developments in genomics, proteomics and metabolomics. Specific applications for these affinity particles are in clinical and research assays, lateral flow and other home diagnostics, lab-on-a-chip analytical systems. Broad variety of monosized particles with different sizes are needed as instrument calibration standards [7]. Different sensors have been developed using MP, such as optical sensors for gas analysis [66, 67], Cu^{2+} sensor [68], glucose sensors [5] and glucose biosensors where silica particles were used as enzyme carriers [69].

The use of monodisperse molecularly imprinted polymer microparticles has attracted great interest for separation purposes due to their high affinity for target molecules. They have found applications mainly in chromatographic techniques where the monodispersity of packing materials is crucial for getting high resolution in separations. Some examples are given by their application in affinity chromatography, for the separation of cholesterol [70], cinchonidine [71], creatinine [72] and

theophylline [73]. Similarly, Zhou et al. synthesized monodisperse MIP microparticles for the resolution of cinchona alkaloids [74]. By means of a chiral monomer and the consequent chiral cavity generated, the authors successfully achieved chiral recognition properties. Due to their unique recognition capabilities and their excellent stability properties both in organics and in water, these MIP microparticles have been employed as extraction agents in a biphasic solvent system [75].

Monodisperse MIP microparticles have been also used as controlled drug delivery. The release of drug (5-aminosalicylic acid) from the imprinted particles was slower than the one observed in non-imprinted particles, due to the interactions between the drug molecules and the recognition cavities [76]. Unfortunately, such a slow release was obtained only within the first 5 h. However, this work shows the potentialities of MIP particles as delayed drug delivery system. Applications of monodisperse MIP particles have been poorly developed in other areas, especially nanoparticles which to the best of our knowledge have not found applications so far, which is an interesting field for research in order to achieve new applications in different fields.

MP applications have been briefly discussed above. Now we will focus on the applications of monodispersed micro- and nanoparticles in diagnosis and monitoring of biological systems (bioapplications).

6.3 *Diagnostic Applications of Monodisperse Microparticles and Nanoparticles*

Monodisperse polymeric particles are widely applied in the biomedical world as support materials in diagnostic test kits (e.g. latex agglutination tests for pregnancy and rheumatoid fever), as carriers in bioaffinity chromatographic separation, for immobilization of bioactive agents (i.e. enzymes, cells, etc.) and in many other related applications such as imaging, as bioseparation tools and within immunoassays [77].

The use of monodisperse particles in immunoassays started to be considered in 1983 [78, 79]. Particle-based flow cytometry assays use microspheres as solid supports for different assays such as immunoassays and affinity assays which are analysed in a flow cytometer. Several assays have been carried out by this method since the first one in 1977 for antigen detection, through the use of antibody-coated MP [80]. Simultaneous analysis has been carried out by flow cytometry for cucumber mosaic virus, potato virus and tomato mosaic virus. The possibility to enable simultaneous analysis distinguishes this technique from ELISA, which is an important characteristic [81]. Mycotoxins have also been analysed by this technique. An indirect competitive fluoroimmunoassay was first developed to quantify two mycotoxins, Fumonisin B1 and Ochratoxin [82] and then modified to achieve the detection up to six different human health hazard mycotoxins: Ochratoxin A,

Fig. 7 Commercial AT. The Pastorex™ Meningitis kit. Bio-Rad Laboratories

Aflatoxin B1, Fumonisin B1, T-2 toxin, Deoxynivalenol and Zearalenone, which can be found in grain products [83]. When this new assay is compared to commercial ELISA, it showed improved sensitivity.

Furthermore, monodisperse particles have been used for separation purposes, like magnetic poly(2-hydroxyethyl methacrylate-co-glycidyl methacrylate) microparticles functionalized with streptavidin for DNA isolation [84].

One of the most extended applications of monodisperse particles is their use in agglutination tests (AT). It was first reported in 1956 by Singer and Plotz for diagnosis of rheumatoid arthritis [85], and it is still popular [86, 87]. Among AT advantages are easy preparation that make them suitable for clinical and field applications, fast results and low cost. For latex agglutination tests, latex particles have to be coated with a specific antibody or antigen. When these coated latex particles are mixed with a sample containing the specific antigen or antibody, a visible agglutination can be observed by naked eye. Nowadays, several companies commercialize AT for detection of diseases, infections, drugs and hormones with examples such as Pastorex™ Meningitis kit (Fig. 7) and Pastorex™ Rotavirus kit commercialized by Bio-Rad Laboratories. Direct or indirect agglutination tests have been developed for their use in different applications (Table 1).

Other examples include commercial AT [FDPL® Test (FDP-L) and FDP Plasma "RD" (FDP-P)] for discrimination between blood and menstrual blood which is important in police field to investigate sexual assaults to women [86]. A new AT has been developed for the evaluation of neosporosis that is associated with the parasite *Neospora caninum* and causes abortion in bovine animals [87]. A fast AT have been developed for Aflatoxin B1 using carboxylated polystyrene latex particles The comparison of this new test with the ELISA showed similar sensitivity and shorter time of analysis for AT [91]. Yet another example involves AT test for the detection of antibodies against avian influenza virus which is faster than agar gel precipitation test and allows the detection of antibodies for longer time after infection [93].

As mentioned before, the monodispersity is important because size affects some of the properties of particles. For instance, nanosystems such as quantum dots possess size-dependent optical properties. In this case even small size variations can change their emission wavelength. Moreover, NPs size can affect their interactions with proteins and ligands immobilized on solid surfaces, influencing

Table 1 Examples of AT tests developed

Samples	Ref	Subject	Ref	Diagnosis	Ref
Urine	[88]	Human	[89]	Leishmaniasis	[90]
Blood	[86]	Grain agricultural products	[91]	Brucellosis	[92]
Sera	[87]	Animals	[92–94]	Tuberculosis	[95]
Faecal	[96]			Aftatoxin B1	[91]

the NP affinity to potential biological receptors [97]. Even NPs shape can influence their optical features, like for upconverting nanosystems and metal-based system (e.g. gold nanorods) [98]. Furthermore, from a physiological point of view, both biocompatibility and biodistribution of NPs are influenced by their size [59, 99]. Thus, it is very important to develop monodisperse NPs which possess homogeneous optical and biological properties, suitable for diagnostic purposes. The synthesis of monodisperse particles has advanced through years, incorporating in polymer material luminescent, magnetic and isotopic compounds [100].

Phosphorescent monodisperse nanoparticles have been used in different assays, such as lateral flow assay and detection of C-reactive protein, providing high sensitivity [101]. A fluoroimmunoassay for detecting trace level of hepatitis B surface antigen has been developed using fluorescent hybrid silica particles in sandwich-model immunoassay. The sensitivity achieved (0.1 ng/ml) was better than the one obtained with the immunoassay that used directly the fluorophore labelling [102]. One promising therapeutic application for monodisperse NPs has been cancer therapy, based on magnetic fluid hyperthermia (MFH) [103, 104]. This approach is based on the generation of localized heating of the tumour area, by means of the relaxation losses of iron oxide magnetic NPs within an alternating magnetic field. Khandhar et al. synthesized 16 nm polymeric MNPs with uniform shape and monodispersity, and excellent hyperthermia efficiency in Jurkat cells [103]. Usually, conventional cancer treatments have side effects and can lead to severe systemic toxicity and produce drug resistant cells [105]. In order to achieve active targeting in tumour therapy, Simnick et al. successfully produced monodisperse polymeric micelles able to target receptors mainly upregulated in the tumour vasculature [106]. Other authors employed polymeric nanosystems for tumour ablation. O'Neal et al. used near infrared-absorbing polyethylene-coated gold nanoshells of 130 nm for photothermal ablation of tumour in mice, enhancing their survival up to 90 days [107]. A potential new technique for the treatment of ovarian cancer peritoneal metastasis has been studied. Folate-targeted nanoparticles were synthesized encapsulating chemotherapy and/or radiotherapy. This study opens a new way to fight this kind of cancer [8]. As shown in Fig. 8 treatment with folate-targeted particles containing chemotherapy and/or radiotherapy increase the time of survival.

Moreover, nanosystems for in vivo detection and imaging of analytes such as hydrogen peroxide have been developed. Since its overproduction is involved in the progress of many diseases, nanosystems able to visualize hydrogen peroxide in vivo have great interest. Murthy et al. synthesized polymeric NPs containing peroxalate

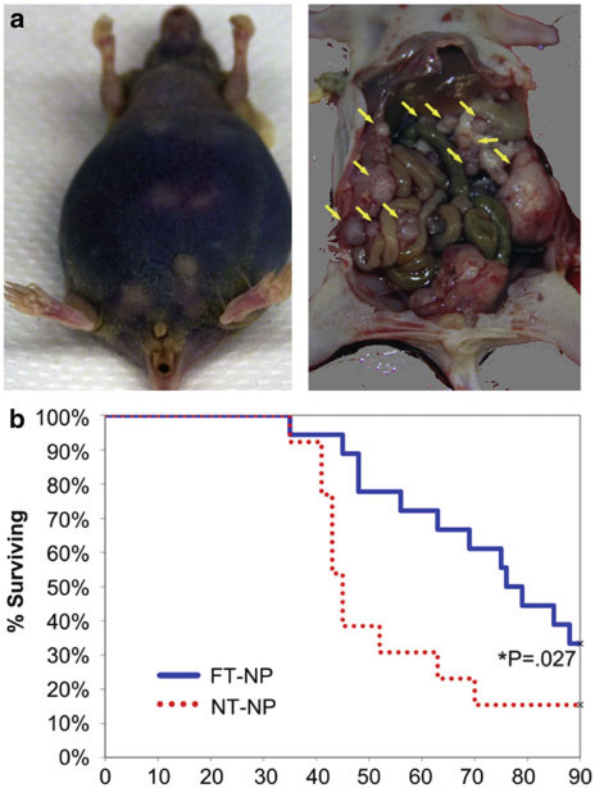

Fig. 8 In vivo efficacy of folate-targeted NPs. (**a**) Mouse having murine ovarian intraperitoneal metastasis. (**b**) Survival analysis comparing folate-targeted NP (FT-NP) treatment arms to combined NT-NP (NPs non-targeted) arms. Adapted from [8] with permission from Elsevier

ester groups, which generate a specific intermediate (dioxetanedione) in the presence of H_2O_2, able to excite fluorescent dyes through a chemiluminescent mechanism, thus allowing hydrogen peroxide to be imaged in mice (Fig. 9). With this system the authors achieved good specificity for hydrogen peroxide over other reactive oxygen species, with nanomolar LOD [108]. Afterwards, the same authors added a PEG corona to these NPs in order to evade the macrophage phagocytosis, and reduced the NP size down to 33 nm to enhance the extravasation into tissues [111].

Other monodisperse nanosystems have found applications in theranostics, which allows simultaneously diagnosis and treatment of diseases. The most widespread NPs for theranostics are used for cancer detection and treatment [63, 112]. An emerging theranostic field is related to nanosystems able to achieve controlled release of drugs and contrast agents upon enzymatic/temperature control, since specific enzymatic activity can be related to cancer and atherosclerotic disease. Yu et al. developed enzymatic- and temperature-sensitive polymeric NPs, in which the NP clusters due to conjugated complementary single-stranded DNA, lead to changes in magnetic relaxation. Then because of enzymatic cleavage events undergone by the DNA, "declustering" of the NPs was achieved [113]. Since

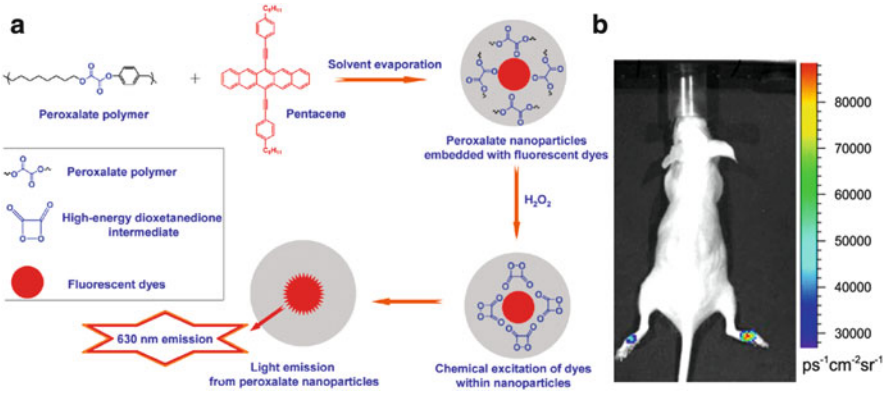

Fig. 9 (**a**) Peroxalate nanoparticles embedded with pentacene as fluorescent dyes, employed for H_2O_2 in vivo imaging through a chemiluminescent process. Adapted with permission from [108, 109]. Copyright 2010 American Chemical Society. (**b**) In vivo H_2O_2 imaging in lipopolysaccharide-induced inflammatory responses in mouse [110]

these NPs are coated by poly(propylene sulphide)-bl-poly(ethylene glycol) copolymers which are known to have excellent properties for smart delivery of drugs, they might find future applications as both smart drug delivery system and imaging agent.

As stated above, multifunctional nanosystems have found applications in several fields, due to their potential multimodal detection. For instance, Ye et al. developed silica-coated magnetic NPs with an outmost layer of thermosensitive poly (*N*-isopropylacrylamide-co-acrylamide) [114]. These 85 nm monodisperse NPs are potentially useful for simultaneous temperature-controlled drug release and magnetic resonance imaging, and for temperature-programmed magnetic separation.

7 Conclusion

Several different methods for the preparation of monodisperse particles have been described, ranging from dispersion polymerization to living polymerization. Despite of general progress in this field there is still need for a generic low cost method for MP synthesis. Monodisperse particles are used in immunoassays, in vivo applications, drug release, etc. Encouraging results have been found using MP as treatment for cancer and biomedical imaging. Even more exciting applications are foreseen for functionalized particles which could perform several functions such as recognition and signalling, recognition and catalytic or selective release response. Nevertheless the preparation of highly functionalized monodisperse nano- and microparticles remains a poorly developed area of research and technology. There is an urgent need for inexpensive and safe mass manufacture

of nano- and microparticles with a variety of properties to address the current and future market need.

Acknowledgement This research was supported by the Research Executive Agency (REA) of the European Union under Grant Agreement number PITN-GA-2010-264772 (ITN CHEBANA).

References

1. Sugimoto T (2001) Monodispersed particles, 1st edn. Elsevier Science, Amsterdam
2. Gong B, Ren L, Yan C (2007) Preparation of normal-phase HPLC stationary phase based on monodisperse hydrophilic polymeric beads and their application. J Appl Polym Sci 106:2730–2735
3. McGrath JG, Bock RD, Cathcart JM, Lyon LA (2007) Self-assembly of "paint-on" colloidal crystals using poly(styrene-co-n-isopropylacrylamide) spheres. Chem Mater 19:1584–1591
4. Zhenyu Luo CZ, Syed S, Syarbaini LA, Chen G (2012) Highly monodisperse chemically reactive sub-micrometer particles: polymer colloidal photonic crystals. Colloid Polym Sci 290:141–150
5. Honda M, Kataoka K, Seki T, Takeoka Y (2009) Confined stimuli-responsive polymer gel in inverse opal polymer membrane for colorimetric glucose sensor. Langmuir 25:8349–8356
6. Roy I, Stachowiak MK, Bergey EJ (2008) Nonviral gene transfection nanoparticles: function and applications in the brain. Nanomedicine 4:89–97
7. Chen S-L, Yuan G, Hu C-T (2011) Preparation and size determination of monodisperse silica microspheres for particle size certified reference materials. Powder Technol 207:232–237
8. Werner ME, Karve S, Sukumar R, Cummings ND, Copp JA, Chen RC, Zhang T, Wang AZ (2011) Folate-targeted nanoparticle delivery of chemo- and radiotherapeutics for the treatment of ovarian cancer peritoneal metastasis. Biomaterials 32:8548–8554
9. Sugimoto T (2003) Formation of monodispersed nano- and micro-particles controlled in size, shape, and internal structure. Chem Eng Technol 26:313–321
10. Vanderhoff JW, El-Aasser MS, Micale FJ, Sudol ED, Tseng CM, Silwanowicz A, Kornfeld DM, Vicente FA (1984) Preparation of large-particle-size monodisperse latexes in space: polymerization kinetics and process development. J Dispers Sci Technol 5:231–246
11. Ugelstad J, Mórk PC, Kaggerud KH, Ellingsen T, Berge A (1980) Swelling of oligomer-polymer particles. New methods of preparation. Adv Colloid Interface Sci 13:101–140
12. Okubo M, Shiozaki M, Tsujihiro M, Tsukuda Y (1991) Preparation of micron-size monodisperse polymer particles by seeded polymerization utilizing the dynamic monomer swelling method. Colloid Polym Sci 269:222–226
13. Omi S, Ki K, Yamamoto A, Iso M (1994) Synthesis of polymeric microspheres employing SPG emulsification technique. J Appl Polym Sci 51:1–11
14. Chen C-W, Chen C-Y, Lin C-L (2011) Preparation of monodisperse poly(methyl methacrylate) microspheres: effect of reaction parameters on particle formation, and optical performances of its diffusive agent application. J Polym Res 18:587–594
15. Esen C, Schweiger G (1996) Preparation of monodisperse polymer particles by photopolymerization. J Colloid Interface Sci 179:276–280
16. Kotoulas C, Kiparissides C (2006) A generalized population balance model for the prediction of particle size distribution in suspension polymerization reactors. Chem Eng Sci 61:332–346
17. Nilsson H, Mosbach R, Mosbach K (1972) The use of bead polymerization of acrylic monomers for immobilization of enzymes. Biochim Biophys Acta 268:253–256
18. Mayes AG, Mosbach K (1996) Molecularly imprinted polymer beads: suspension polymerization using a liquid perfluorocarbon as the dispersing phase. Anal Chem 68:3769–3774
19. Li K, Stöver HDH (1993) Synthesis of monodisperse poly(divinylbenzene) microspheres. J Polym Sci A Polym Chem 31:3257–3263

20. Hoshino M, Arishima K (1995) Survey of preparation techniques of monodispersed microspheres of glycidyl methacrylate and its derivatives. J Appl Polym Sci 57:921–930
21. Lok KP, Ober CK (1985) Particle size control in dispersion polymerization of polystyrene. Can J Chem 63:209–216
22. Yasuda M, Seki H, Yokoyama H, Ogino H, Ishimi K, Ishikawa H (2001) Simulation of a particle formation stage in the dispersion polymerization of styrene. Macromolecules 34:3261–3270
23. Casimiro T, Banet-Osuna AM, Ramos AM, da Ponte MN, Aguiar-Ricardo A (2005) Synthesis of highly cross-linked poly(diethylene glycol dimethacrylate) microparticles in supercritical carbon dioxide. Eur Polym J 41:1947–1953
24. Brouwer WM (1989) The preparation of small polystyrene latex particles. J Appl Polym Sci 38:1335–1346
25. Lowe PJ, Temple CS (1994) Calcitonin and insulin in isobutylcyanoacrylate nanocapsules: protection against proteases and effect on intestinal absorption in rats. J Pharm Pharmacol 46:547–552
26. Larpent C, Bernard E, Richard J, Vaslin S (1997) Polymerization in microemulsions with polymerizable cosurfactants: a route to highly functionalized nanoparticles. Macromolecules 30:354–362
27. Wei S, Molinelli A, Mizaikoff B (2006) Molecularly imprinted micro and nanospheres for the selective recognition of 17β-estradiol. Biosens Bioelectron 21:1943–1951
28. Rosca ID, Watari F, Uo M (2004) Microparticle formation and its mechanism in single and double emulsion solvent evaporation. J Control Release 99:271–280
29. Blanco D, MaJ A (1998) Protein encapsulation and release from poly(lactide-co-glycolide) microspheres: effect of the protein and polymer properties and of the co-encapsulation of surfactants. Eur J Pharm Biopharm 45:285–294
30. Omi S, Ma G-H, Nagai M (2000) Membrane emulsification a versatile tool for the synthesis of polymeric microspheres. Macromol Symp 151:319–330
31. Qun W, Shoukuan F, Tongyin Y (1994) Emulsion polymerization. Prog Polym Sci 19:703–753
32. Raula J, Eerikäinen H, Kauppinen EI (2004) Influence of the solvent composition on the aerosol synthesis of pharmaceutical polymer nanoparticles. Int J Pharm 284:13–21
33. Jarmer DJ, Lengsfeld CS, Randolph TW (2003) Manipulation of particle size distribution of poly(l-lactic acid) nanoparticles with a jet-swirl nozzle during precipitation with a compressed antisolvent. J Supercrit Fluids 27:317–336
34. Vehring R, Foss WR, Lechuga-Ballesteros D (2007) Particle formation in spray drying. J Aerosol Sci 38:728–746
35. Davankov VA, Ilyin MM, Timofeeva GI, Tsyurupa MP, Yaminsky IV (1999) Atomic force microscopy imaging of novel macromolecular species, nanosponges, and their clusters. J Polym Sci A Polym Chem 37:1451–1455
36. Koh K, Ohno K, Tsujii Y, Fukuda T (2004) Synthesis of well-defined polymers with protected silanol groups by atom transfer radical polymerization and their use for the fabrication of polymeric nanoparticles. Eur Polym J 40:2665–2670
37. Matyjaszewski K, Xia J (2001) Atom transfer radical polymerization. Chem Rev 101:2921–2990
38. Saikia PJ, Lee JM, Lee K, Choe S (2008) Reaction parameters in the raft mediated dispersion polymerization of styrene. J Polym Sci A Polym Chem 46:872–885
39. Shim SE, Shin Y, Jun JW, Lee K, Jung H, Choe S (2003) Living-free-radical emulsion photopolymerization of methyl methacrylate by a surface active iniferter (suriniferter). Macromolecules 36:7994–8000
40. Guerreiro AR, Chianella I, Piletska E, Whitcombe MJ, Piletsky SA (2009) Selection of imprinted nanoparticles by affinity chromatography. Biosens Bioelectron 24:2740–2743

41. Aydınlı B, Tinççer T (2001) Radiation grafting of various water-soluble monomers on ultra-high molecular weight polyethylene powder. Part II: Thermal, FTIR and morphological characterisation. Radiat Phys Chem 62:337–343
42. Cannizzo C, Amigoni-Gerbier S, Larpent C (2005) Boronic acid-functionalized nanoparticles: synthesis by microemulsion polymerization and application as a re-usable optical nanosensor for carbohydrates. Polymer 46:1269–1276
43. Amigoni-Gerbier S, Larpent C (1999) Synthesis and properties of selective metal-complexing nanoparticles. Macromolecules 32:9071–9073
44. Gong T, Wang C (2008) Preparation of highly cross-linked monodispersed functional polystyrene particles by utilizing the delayed addition method. J Mater Sci 43:1926–1932
45. Bai F, Yang X, Li R, Huang B, Huang W (2006) Monodisperse hydrophilic polymer microspheres having carboxylic acid groups prepared by distillation precipitation polymerization. Polymer 47:5775–5784
46. Bai F, Yang X, Huang W (2006) Narrow-disperse or monodisperse crosslinked and functional core–shell polymer particles prepared by two-stage precipitation polymerization. J Appl Polym Sci 100:1776–1784
47. Chen C-W, Chen C-Y, Cioul Z-H (2010) Preparation of monodisperse functional poly (styrene-co-acrylamidoxime) microsphere with chelating amidoxime group. Colloid Polym Sci 288:665–672
48. Song X-J, Hu J, Wang C-C (2011) Synthesis of highly surface functionalized monodispersed poly(st/dvb/gma) nanospheres with soap-free emulsion polymerization followed by facile "click chemistry" with functionalized alkylthiols. Colloids Surf A Physicochem Eng Asp 380:250–256
49. Song J-S, Winnik MA (2005) Cross-linked, monodisperse, micron-sized polystyrene particles by two-stage dispersion polymerization. Macromolecules 38:8300–8307
50. Song J-S, Tronc F, Winnik MA (2006) Monodisperse, controlled micron-size dye-labeled polystyrene particles by two-stage dispersion polymerization. Polymer 47:817–825
51. Poma A, Turner APF, Piletsky SA (2010) Advances in the manufacture of mip nanoparticles. Trends Biotechnol 28:629–637
52. Piletsky SA, Turner NW, Laitenberger P (2006) Molecularly imprinted polymers in clinical diagnostics—future potential and existing problems. Med Eng Phys 28:971–977
53. Haginaka J (2008) Monodispersed, molecularly imprinted polymers as affinity-based chromatography media. J Chromatogr B 866:3–13
54. Yoshimatsu K, Reimhult K, Krozer A, Mosbach K, Sode K, Ye L (2007) Uniform molecularly imprinted microspheres and nanoparticles prepared by precipitation polymerization: the control of particle size suitable for different analytical applications. Anal Chim Acta 584:112–121
55. Dvorakova G, Haschick R, Chiad K, Klapper M, Müllen K, Biffis A (2010) Molecularly imprinted nanospheres by nonaqueous emulsion polymerization. Macromol Rapid Commun 31:2035–2040
56. Lewinski N, Colvin V, Drezek R (2008) Cytotoxicity of nanoparticles. Small 4:26–49
57. Riehemann K, Schneider SW, Luger TA, Godin B, Ferrari M, Fuchs H (2009) Nanomedicine – challenge and perspectives. Angew Chem Int Ed 48:872–897
58. Yang Z, Zheng S, Harrison WJ, Harder J, Wen X, Gelovani JG, Qiao A, Li C (2007) Long-circulating near-infrared fluorescence core-cross-linked polymeric micelles: synthesis, characterization, and dual nuclear/optical imaging. Biomacromolecules 8:3422–3428
59. Owens DE 3rd, Peppas NA (2006) Opsonization, biodistribution, and pharmacokinetics of polymeric nanoparticles. Int J Pharm 307:93–102
60. Stark WJ (2011) Nanoparticles in biological systems. Angew Chem Int Ed 50:1242–1258
61. Ballou B, Lagerholm BC, Ernst LA, Bruchez MP, Waggoner AS (2004) Noninvasive imaging of quantum dots in mice. Bioconjug Chem 15:79–86

62. Ballou B, Ernst LA, Andreko S, Harper T, Fitzpatrick JAJ, Waggoner AS, Bruchez MP (2007) Sentinel lymph node imaging using quantum dots in mouse tumor models. Bioconjug Chem 18:389–396
63. Brigger I, Dubernet C, Couvreur P (2002) Nanoparticles in cancer therapy and diagnosis. Adv Drug Deliv Rev 54:631–651
64. Sheng Y, Liu C, Yuan Y, Tao X, Yang F, Shan X, Zhou H, Xu F (2009) Long-circulating polymeric nanoparticles bearing a combinatorial coating of peg and water-soluble chitosan. Biomaterials 30:2340–2348
65. Liang Z, Susha AS, Caruso F (2002) Metallodielectric opals of layer-by-layer processed coated colloids. Adv Mater 14:1160–1164
66. Perez de Vargas-Sansalvador IM, Carvajal MA, Roldan-Munoz OM, Banqueri J, Fernandez-Ramos MD, Capitan-Vallvey LF (2009) Phosphorescent sensing of carbon dioxide based on secondary inner-filter quenching. Anal Chim Acta 655:66–74
67. Chu C-S, Lo Y-L (2009) Highly sensitive and linear optical fiber carbon dioxide sensor based on sol–gel matrix doped with silica particles and HPTS. Sens Actuators B Chem 143:205–210
68. Sung T-W, Lo Y-L (2012) Highly sensitive and selective sensor based on silica-coated CdSe/ZnS nanoparticles for Cu^{2+} ion detection. Sens Actuators B Chem 165:119–125
69. Yang H, Zhu Y (2006) Size dependence of SiO_2 particles enhanced glucose biosensor. Talanta 68:569–574
70. Kitahara K-I, Yoshihama I, Hanada T, Kokuba H, Arai S (2010) Synthesis of monodispersed molecularly imprinted polymer particles for high-performance liquid chromatographic separation of cholesterol using templating polymerization in porous silica gel bound with cholesterol molecules on its surface. J Chromatogr A 1217:7249–7254
71. Liu Y, Hoshina K, Haginaka J (2010) Monodispersed, molecularly imprinted polymers for cinchonidine by precipitation polymerization. Talanta 80:1713–1718
72. Haginaka J, Miura C, Funaya N, Matsunaga H (2012) Monodispersed molecularly imprinted polymer for creatinine by modified precipitation polymerization. Anal Sci 28:315–315
73. Wang J, Cormack PAG, Sherrington DC, Khoshdel E (2003) Monodisperse, molecularly imprinted polymer microspheres prepared by precipitation polymerization for affinity separation applications. Angew Chem Int Ed 42:5336–5338
74. Zhou Q, He J, Tang Y, Xu Z, Li H, Kang C, Jiang J (2012) A novel hydroquinidine imprinted microsphere using a chirality-matching n-acryloyl-l-phenylalanine monomer for recognition of cinchona alkaloids. J Chromatogr A 1238:60–67
75. Castell OK, Allender CJ, Barrow DA (2006) Novel biphasic separations utilising highly selective molecularly imprinted polymers as biorecognition solvent extraction agents. Biosens Bioelectron 22:526–533
76. Ulubayram K, Tunc Y, Baykara E (2007) Molecularly imprinted acrylic-based microspheres for colonic delivery of 5-aminosalicylic acid. J Optoelectron Adv Mater 9:3479–3483
77. Pişkin E, Tuncel SA, Ercan MT, Caner BE (1991) Micron-size monodisperse PSPA beads by phase inversion polymerization for biomedical applications: preparation and a case study. Clin Mater 8:159–164
78. Stanski DR (1983) Radioimmunoassay and related procedures in medicine–1982. Proceedings series; international atomic energy agency. 1983. 823 pp. 15 × 24 cm. J Pharm Sci 72:1234
79. Nustad KJL, Ugelstad J, Ellingsen T, Berge A (1984) Hydrophilic monodisperse particles as solid-phase material in immunoassays: comparison of shell-and-core particles with compact particles. Eur Surg Res 16:80–87
80. Horan PK, Wheeless LL Jr (1977) Quantitative single cell analysis and sorting. Science 198 (4313):149–157
81. Iannelli D, D'Apice L, Cottone C, Viscardi M, Scala F, Zoina A, Del Sorbo G, Spigno P, Capparelli R (1997) Simultaneous detection of cucumber mosaic virus, tomato mosaic virus and potato virus y by flow cytometry. J Virol Methods 69:137–145

82. Anderson GP, Kowtha VA, Taitt CR (2010) Detection of fumonisin B1 and ochratoxin A in grain products using microsphere-based fluid array immunoassays. Toxins 2:297–309
83. Czeh A, Mandy F, Feher-Toth S, Torok L, Mike Z, Koszegi B, Lustyik G (2012) A flow cytometry based competitive fluorescent microsphere immunoassay (CFIA) system for detecting up to six mycotoxins. J Immunol Methods 384(1–2):71–80. doi:10.1016/j.jim.2012.07.010
84. Horák D, Španová A, Tvrdíková J, Rittich B (2011) Streptavidin-modified magnetic poly (2-hydroxyethyl methacrylate-co-glycidyl methacrylate) microspheres for selective isolation of bacterial DNA. Eur Polym J 47:1090–1096
85. Plotz CM, Singer JM (1956) The latex fixation test. I. Application to the serologic diagnosis of rheumatoid arthritis. Am J Med 21:888–892
86. Akutsu T, Watanabe K, Motani H, Iwase H, Sakurada K (2012) Evaluation of latex agglutination tests for fibrin–fibrinogen degradation products in the forensic identification of menstrual blood. Leg Med 14:51–54
87. Moraveji M, Hosseini A, Moghaddar N, Namavari MM, Eskandari MH (2012) Development of latex agglutination test with recombinant NcSAG1 for the rapid detection of antibodies to Neospora caninum in cattle. Vet Parasitol 189(2–4):211–217. doi:10.1016/j.vetpar.2012.04.010
88. Aoki K, Shikama Y, Yoshida T, Kuroiwa Y (1996) Enzyme-linked immunosorbent assay and latex agglutination inhibition reaction test for cocaine and benzoylecgonine in urine. Forensic Sci Int 77:151–157
89. de Assis TS, Braga AS, Pedras MJ, Oliveira E, Barral A, de Siqueira IC, Costa CH, Costa DL, Holanda TA, Soares VY, Biá M, Caldas Ade J, Romero GA, Rabello A (2011) Multi-centric prospective evaluation of rk39 rapid test and direct agglutination test for the diagnosis of visceral leishmaniasis in Brazil. Trans R Soc Trop Med Hyg 105:81–85
90. Sundar S, Singh RK, Maurya R, Kumar B, Chhabra A, Singh V, Rai M (2006) Serological diagnosis of Indian visceral leishmaniasis: direct agglutination test versus rk39 strip test. Trans R Soc Trop Med Hyg 100:533–537
91. Ye Y, Wang P, Zhou Y, Chen F, Wang X (2011) Evaluation of latex agglutination inhibition reaction test for rapid detection of aflatoxin b1. Food Control 22:1072–1077
92. Keid LB, Soares RM, Vasconcellos SA, Megid J, Salgado VR, Richtzenhain LJ (2009) Comparison of agar gel immunodiffusion test, rapid slide agglutination test, microbiological culture and pcr for the diagnosis of canine brucellosis. Res Vet Sci 86:22–26
93. Horie M, Ogawa H, Yamada K, Hara A, Bui VN, Awad SS, Yoshikawa R, Mase M, Tsukamoto K, Yamaguchi S, Nakamura K, Imai K (2009) A latex agglutination test using a recombinant nucleoprotein for detection of antibodies against avian influenza virus. J Virol Methods 161:259–264
94. Jiang T, Gong D, L-a M, Nie H, Zhou Y, Yao B, Zhao J (2008) Evaluation of a recombinant MIC3 based latex agglutination test for the rapid serodiagnosis of toxoplasma gondii infection in swines. Vet Parasitol 158:51–56
95. Bhaskar S, Banavaliker JN, Hanif M (2003) Large-scale validation of a latex agglutination test for diagnosis of tuberculosis. FEMS Immunol Med Microbiol 39:235–239
96. Nonaka N, Oka M, Kamiya M, Oku Y (2008) A latex agglutination test for the detection of Echinococcus multilocularis coproantigen in the definitive hosts. Vet Parasitol 152:278–283
97. Piletska EV, Piletsky SA (2010) Size matters: influence of the size of nanoparticles on their interactions with ligands immobilized on the solid surface. Langmuir 26:3783–3785
98. Grassian VH (2008) When size really matters: size-dependent properties and surface chemistry of metal and metal oxide nanoparticles in gas and liquid phase environments. J Phys Chem C 112:18303–18313
99. Yang Z, Leon J, Martin M, Harder JW, Zhang R, Liang D, Lu W, Tian M, Gelovani JG, Qiao A, Li C (2009) Pharmacokinetics and biodistribution of near-infrared fluorescence polymeric nanoparticles. Nanotechnology 20(16):165101
100. Gallach D, Recio Sánchez G, Muñoz Noval A, Manso Silván M, Ceccone G, Martín Palma RJ, Torres Costa V, Martínez Duart JM (2010) Functionality of porous silicon particles: surface modification for biomedical applications. Mater Sci Eng B 169:123–127

101. Song X, Huang L, Wu B (2008) Bright and monodispersed phosphorescent particles and their applications for biological assays. Anal Chem 80:5501–5507
102. Yang W, Zhang CG, Qu HY, Yang HH, Xu JG (2004) Novel fluorescent silica nanoparticle probe for ultrasensitive immunoassays. Anal Chim Acta 503:163–169
103. Khandhar AP, Ferguson RM, Simon JA, Krishnan KM (2012) Tailored magnetic nanoparticles for optimizing magnetic fluid hyperthermia. J Biomed Mater Res A 100(3): 728–737
104. Wolinsky JB, Grinstaff MW (2008) Therapeutic and diagnostic applications of dendrimers for cancer treatment. Adv Drug Deliv Rev 60:1037–1055
105. Gwinn MR, Vallyathan V (2006) Nanoparticles: health effects – pros and cons. Environ Health Perspect 114:1818–1825
106. Simnick AJ, Amiram M, Liu W, Hanna G, Dewhirst MW, Kontos CD, Chilkoti A (2011) In vivo tumor targeting by a ngr-decorated micelle of a recombinant diblock copolypeptide. J Control Release 155:144–151
107. O'Neal DP, Hirsch LR, Halas NJ, Payne JD, West JL (2004) Photo-thermal tumor ablation in mice using near infrared-absorbing nanoparticles. Cancer Lett 209:171–176
108. Lee D, Khaja S, Velasquez-Castano JC, Dasari M, Sun C, Petros J, Taylor WR, Murthy N (2007) In vivo imaging of hydrogen peroxide with chemiluminescent nanoparticles. Nat Mater 6:765–769
109. Hu J, Liu S (2010) Responsive polymers for detection and sensing applications: current status and future developments. Macromolecules 43:8315–8330
110. Lee I, Hwang O, Yoo D, Khang G, Lee D (2011) Detection of hydrogen peroxide in vitro and in vivo using peroxalate chemiluminescent micelles. Bull Korean Chem Soc 32:2187–2192
111. Lee D, Erigala VR, Dasari M, Yu J, Dickson RM, Murthy N (2008) Detection of hydrogen peroxide with chemiluminescent micelles. Int J Nanomedicine 3:471–476
112. Cole AJ, Yang VC, David AE (2011) Cancer theranostics: the rise of targeted magnetic nanoparticles. Trends Biotechnol 29:323–332
113. Yu SS, Scherer RL, Ortega RA, Bell CS, O'Neil CP, Hubbell JA, Giorgio TD (2011) Enzymatic- and temperature-sensitive controlled release of ultrasmall superparamagnetic iron oxides (USPIOs). J Nanobiotechnology 9:7
114. Ye F, Qin J, Toprak MS, Muhammed M (2011) Multifunctional core-shell nanoparticles: superparamagnetic, mesoporous, and thermosensitive. J Nanopart Res 13:6157–6167
115. Antonietti M, Landfester K (2002) Polyreactions in miniemulsions. Prog Polym Sci 27:689–757

BIOREV (2014) 1: 155–204
DOI: 10.1007/11663_2013_3

Published online: 26 September 2013

Upconverting Phosphor Labels for Bioanalytical Assays

Terhi Riuttamäki (née Rantanen) and Tero Soukka

Abstract Upconverting phosphors (UCPs) are photoluminescent inorganic crystals capable of photon upconversion upon absorption of two or more sequential photons. UCPs produce bright, structured emission at wavelengths shorter than the excitation radiation rendering them highly advanced labels for bioanalytical assays. The exceptional anti-Stokes emission allows total elimination of autofluorescence originating mainly from biomolecules and other sample components. UCPs are excited with near-infrared radiation which provides several advantages over ultraviolet excitation—including optimal penetration of biological material. This chapter summarizes the bioanalytical *in vitro* applications of UCPs and discusses the advantages and challenges of the emerging label technology. In addition, synthesis of the UCP labels and some of the instruments used for UCP detection are shortly reviewed. Bioimaging and therapeutic applications based on UCPs are outside of the scope of this chapter.

Keywords Bioanalytics · Lanthanides · Nanoparticles · Near-infrared excitation · Photon upconversion · Upconverting phosphors

Contents

T. Riuttamäki (née Rantanen) (✉)
Department of Biotechnology, University of Turku, Tykistökatu 6A, 20520 Turku, Finland

Present address: Kaivogen Oy, Tykistökatu 4D, 20520 Turku, Finland
e-mail: terhi.riuttamaki@kaivogen.com

T. Soukka
Department of Biotechnology, University of Turku, Tykistökatu 6A, 20520 Turku, Finland

Abbreviations

APTE	Addition of photons by transfer of energy (upconversion mechanism)
CCD	Charge-coupled device (light detector)
CTAB	Cetyltrimethylammonium bromide (cationic surfactant)
EDTA	Ethylenediaminetetraacetic acid (chelating agent)
ELISA	Enzyme-linked immunosorbent assay
EMU	Energy migration-mediated upconversion (upconversion mechanism)
ESA	Excited state absorption (upconversion mechanism)
ETU	Energy transfer upconversion (upconversion mechanism)
f-PSA	Free prostate-specific antigen (prostate cancer marker)
GSA	Ground-state absorption
LD	Laser diode (excitation source)
LED	Light emitting diode (excitation source)
LF	Lateral flow (assay format)
LOD	Limit of detection
LOQ	Limit of quantification
LRET	Lanthanide resonance energy transfer
NIR	Near-infrared radiation (wavelength 750–1,400 nm)
PA	Photon avalanche (upconversion mechanism)
PD	Photodiode (light detector)
PEI	Polyethyleneimine
PMT	Photomultiplier tube (light detector)
POCT	Point-of-care testing
PVP	Polyvinylpyrrolidone
R_0	Förster radius (the distance at which energy transfer efficiency is 50 %)
RET	Resonance energy transfer (nonradiative energy transfer mechanism)
SEB	Staphylococcal enterotoxin B

SET	Surface energy transfer (energy transfer to a metallic surface)
TEM	Transmission electron microscopy
TOP	Trioctylphosphine
TOPO	Trioctylphosphine oxide
UCP	Upconverting phosphor (photoluminescent inorganic compound)
UC-RET	Upconversion resonance energy transfer
UV	Ultraviolet radiation (wavelength <380 nm)

1 Introduction

Bioanalytical assays are used in medical diagnostics as well as in food safety assurance and environmental monitoring to determine the concentration of analytes, such as biomolecules, toxins, drugs, and pathogens. Although highly sensitive luminescent labels nowadays dominate over other detection technologies (e.g., radiolabels) [1], some problems related to photoluminescence measurement are still resolved only partially or the existing solution is rather complex. The main limitations affecting the assay performance are attributed to the autofluorescence originating from biological material and to the absorption properties of non-transparent sample matrixes. In certain applications, also the stability issues (i.e., photobleaching) may disturb the use of organic fluorophores.

The recent trend in assay development has been toward point-of-care testing (POCT) [2, 3], which will inevitably reshape the conventions of the sample analysis as an option for the high-capacity centralized laboratory testing. The label technology used for analyte quantification in POCT system plays an important role in order to allow sensitive (i.e., low detection limit), simple (i.e., small-sized reader), and low-cost (i.e., inexpensive materials and instrumentation) detection. Uniquely, the near-infrared (NIR) excitable labels capable of photon upconversion provide a comprehensive solution to the above-mentioned limitations and, furthermore, the expectations of the POCT are met.

Photon upconversion is a process generating higher-energy emission from low-energy radiation. The increase in energy is achieved by absorbing multiple (usually two or three) photons per single emitted photon. The transition from the excited electronic state back to the ground state, or to another lower-lying energy level, produces luminescence at wavelengths shorter than the original excitation wavelength. This nonlinear optical process, also called anti-Stokes photoluminescence, involves intermediate excited states, which can be either virtual or real electronic states. Utilization of non-existing *virtual* intermediate states (i.e., multiphoton absorption [4–7] and second-harmonic generation [8, 9]) requires an extremely high excitation power density (10^6–10^9 W/cm^2) because multiple photons need to be absorbed *simultaneously* [6]. To avoid thermal decomposition of the sample under intense radiation, expensive ultrafast pulse lasers are employed as excitation sources, for example in multiphoton microscopy [10]. However, in certain inorganic compounds having *real* metastable intermediate states, an

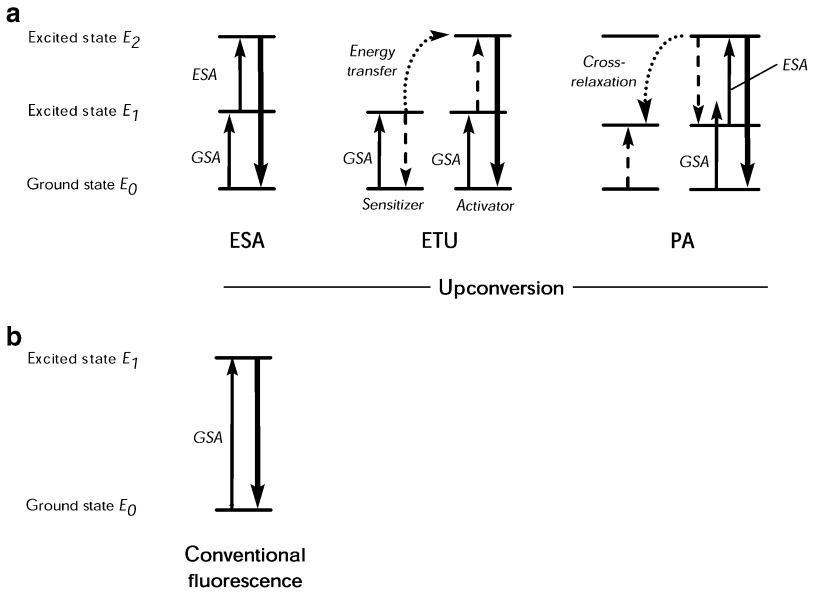

Fig. 1 Simplified energy diagrams of (**a**) the most significant upconversion mechanisms and (**b**) a conventional fluorescence for comparison. *Upward* and *downward solid arrows* represent absorption and emission processes, respectively, while *dashed arrows* symbolize transitions related to energy transfer between the sensitizer and the activator or cross-relaxation between neighboring ions. *GSA* ground-state absorption, *ESA* excited state absorption, *ETU* energy transfer upconversion, *PA* photon avalanche

affordable continuous wave laser diode with ~10^6 times lower output power is sufficient to promote the photon upconversion. In this case, the photons can be absorbed *sequentially* one after the other. Inorganic upconverting phosphors (UCPs) show the most efficient upconversion capabilities [6], rendering them highly promising luminescent labels for ultrasensitive bioanalytical assays [11, 12].

Several upconversion mechanisms have been recognized (Fig. 1) and they may appear alone or in combinations. The most efficient mechanism usually dominates in the case of low excitation power density, but an increase in the pumping power enables emergence of the less-efficient mechanisms, too [13]. Some upconversion mechanisms involve only one type of ion, while the other mechanisms stipulate the contribution of both sensitizer and activator ions [14].

The simplest upconversion process involving only a single ion is *excited state absorption* (*ESA*) [15]. The first pump photon populates the intermediate excited state E_1 (ground-state absorption, GSA), followed by a second absorption (ESA) triggering the upconversion emission from the higher E_2 state. Another upconversion mechanism featuring two different neighboring ions (a sensitizer and an activator) is referred to as an *energy transfer upconversion* (*ETU*) or alternatively as addition of photons by transfer of energy (APTE) [16, 17]. In this mechanism, the GSA is followed by a nonradiative resonant energy transfer from the sensitizer ion to the activator ion, which leads to population of the higher excited state E_2 of the latter. The energy transfer process is most efficient if the sensitizer ion has no

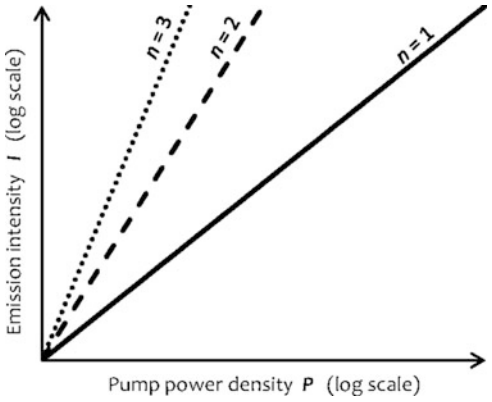

Fig. 2 Relationship between excitation pump power density P (W/cm^2) and emission intensity I in logarithmic scale when n photons are absorbed per one emitted photon. The graph applies when low or moderate P is used (below the saturation level). Conventional fluorescence ($n = 1$) is a linear optical process while upconversion ($n > 1$) is nonlinear

resonant energy states above state E_1 of its own. This mechanism is about 100 times more efficient than the ESA mechanism. *Photon avalanche* (*PA*), involving cross-relaxation energy transfer between neighboring ions, is a more complex mechanism observed when the pump flux exceeds a certain critical threshold [18, 19]. The cross-relaxation step assists in population of the intermediate excited state E_1 because the excitation energy is not resonant with the GSA transition directly but only with the following ESA transition. The GSA step in the beginning is eminently inefficient, but subsequently the ESA step populates the higher excited state E_2 very effectively. The cross-relaxation step results in population of the intermediate state E_1 of both neighboring ions, and the avalanche process is boosted. Even though PA is eventually a highly efficient upconversion mechanism, it is poorly exploitable due to the slow response to the excitation (up to seconds).

The likelihood of populating the higher luminescent energy level E_2 by re-excitation depends on the lifetime of the lower intermediate state E_1 acting as "an energy store" [14]. Excited molecules can relax to the ground state (or another lower-lying electronic state) through either a *radiative* or a *nonradiative* path. The former involves the emission of a photon with energy determined by the energy difference of the two states. Nonradiative relaxations comprise all alternative relaxations (e.g., multiphonon decay) but those leading to luminescence. A third relaxation option is to *transfer the energy* in a nonradiative manner to a suitable energy acceptor in close proximity. All the three above-mentioned depopulation paths of the intermediate state E_1 should be minimized in order to increase the excited state lifetime and, consequently, the upconversion efficiency. The lifetime defines the excitation power density needed for generation of photon upconversion [20].

From the 1960s when research began in this area, it was known that the upconversion luminescence intensity I is proportional to the nth power of the absorbed pump power density P ($I \propto P^n$), where n denotes the number of pump photons absorbed per upconversion photon emitted. In other words, when I versus P is plotted in a double-logarithmic representation, the slope is n (Fig. 2). As more powerful NIR excitation sources became available, saturation of the upconversion-induced luminescence was observed, and it was realized that the power-dependence

of upconversion emission bands changes with excitation power density [21, 22]. In reality, the dependence decreases from P^n down to P^1 with increasing excitation power density and, accordingly, the above-mentioned slope will approach 1 (regardless of the number of photons involved). However, it is crucial to note that the excitation power has a higher impact on the luminescence intensity in the case of photon upconversion ($n > 1$) than in the case of conventional fluorescence ($n = 1$).

2 Upconverting Phosphors

UCPs are composed of a transparent host lattice doped with certain trivalent lanthanide ions (or less frequently transition metals) [14]. Both components have an effect on the photophysical properties (i.e., emission wavelength and intensity) of upconverting materials. The UCP material choices have been comprehensively reviewed by Haase and Schäfer [11].

2.1 Host Material

The host material forms a crystalline lattice that maintains the correct arrangement of the hybrid material. Suitable inorganic compounds comprise trivalent rare earth ions (Y^{3+}, La^{3+}, Gd^{3+}, Sc^{3+}) or other cations [e.g., alkaline earth ions (Ca^{2+}, Sr^{2+}, Ba^{2+}) or certain transition metals (Zr^{4+}, Ti^{4+}, Mn^{2+})] having similar ionic radius with the dopant ions [23]. A low phonon energy lattice is essential in order to reduce the multiphonon relaxation (i.e., to minimize energy losses) and to increase the lifetime of the intermediate states involved in upconversion (i.e., to maximize radiative emission) [24, 25]. The most practical hosts are halides (e.g., $NaYF_4$, YF_3, LaF_3), oxides (e.g., Y_2O_3, ZrO_2), and oxysulfides (e.g., Y_2O_2S, La_2O_2S) [25–27]. The lowest phonon energies are typical for the halide-based lattices (<400 cm^{-1}), but only the lightest halide, fluoride, is practical in actual use due to the hygroscopic nature of the heavier ones [28]. Oxide-based lattices have better chemical stability, but they suffer from relatively high phonon energies (>500 cm^{-1}) [23, 28].

2.2 Dopant Ions

The active dopant ions play a central role by actually absorbing and emitting the photons. They determine, for example, the color of the emitted light. Many trivalent lanthanide ions have metastable intermediate electronic states (“energy stores”) that are suitable for generation of the upconversion emission. The favorable photoluminescent properties of lanthanides are predominated by the well-shielded 4*f* electrons [29, 30]. The long-lived excited states (up to few ms) and appropriately

spaced ladder-like energy levels of Er^{3+}, Tm^{3+}, and Ho^{3+} render these ions suitable dopants in upconverting materials.

To further enhance the upconversion efficiency, above-mentioned activator ions are commonly co-doped with a Yb^{3+} sensitizer ion [25], which has a relatively large absorption cross-section describing the probability of an absorption process (approximately tenfold compared to Er^{3+} ion at 980 nm [31, 32]). In addition, the Yb^{3+} ions have a lesser tendency for concentration-dependent quenching compared to the other lanthanide ions and, therefore, quite high Yb^{3+} concentrations can be used to boost the excitation probability of the activator ions [33]. The Yb^{3+} sensitizer is excited with the 980-nm radiation and the energy is subsequently transferred to the activator ions by the ETU mechanism (Fig. 3). Yb^{3+}–Er^{3+} pair produces the brightest anti-Stokes photoluminescence as the energy levels of Yb^{3+} ($^2F_{5/2}$) and Er^{3+} ($^4I_{11/2}$) are almost perfectly resonant (only a few cm^{-1} energy mismatch), thus enabling highly efficient energy transfer to the Er^{3+} ion without a phonon-mediated step [34].

To expand the selection for the activators over those three frequently used ions, Wang et al. [36] have proposed a special process called *energy migration-mediated upconversion* (*EMU*). Exceptionally, dopant ions *without* long-lived intermediate energy states may be used as activators in a system involving separate core and shell materials (Fig. 4). In the core, the NIR radiation is first upconverted to the ultraviolet (UV) region through a 5-photon process between the Yb^{3+} sensitizer and a Tm^{3+} accumulator. Then the energy is transferred to the shell material doped with an activator ion (e.g., lanthanide ions Tb^{3+}, Eu^{3+}, Dy^{3+}, or Sm^{3+}) having energy states at the UV region from which the energy is further relaxed to the emittive energy states of the activator. The energy transfer between the separate material layers is conducted by migration through Gd^{3+} ions that exist in both layers. Gd^{3+} lacks energy states below UV region minimizing other competitive processes. The EMU process brings more flexibility to the upconverting materials (e.g., more emission colors).

In addition to active dopants described above, optically passive dopant ions have recently been studied to tailor the crystal structure of the nano-sized UCPs. This topic is covered in the Sect. 4.2.

Dopant ions have also been incorporated to UCP materials to tune the optical properties toward pure single-band emission [37, 38]. As the lanthanide-based activator ions have more than one metastable excited state (Fig. 3), they typically produce multiple emission bands. However, certain applications (e.g., bioimaging and homogeneous assays) benefit most from the low-energy emission bands. Addition of Mn^{2+} ions to the UCP material was demonstrated to attenuate the high-energy emissions by transferring the energy to the lower emittive states resulting in pure red or NIR emission depending on the selected activator ion.

2.3 Doping Concentration

To maximize the upconversion efficiency, the amount of sensitizer and activator ions must be optimal in the host lattice. Logically, the emission intensity increases

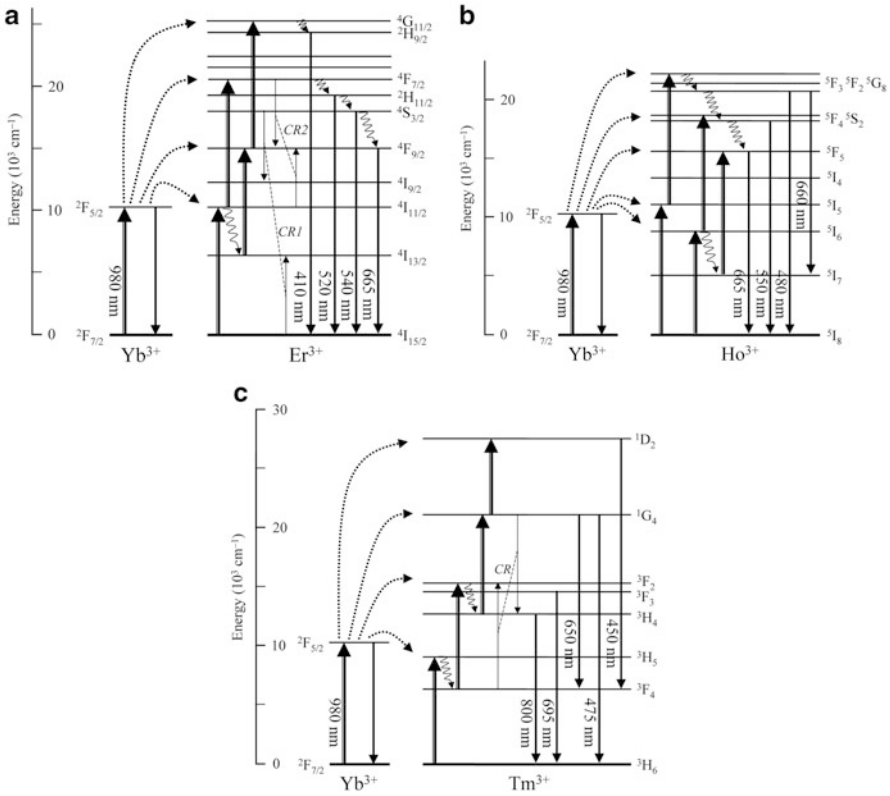

Fig. 3 Energy diagrams of the dopant ions used in the most applicable upconverting phosphor materials. Highly efficient photon upconversion is achieved with the ETU mechanism involving Yb^{3+} as a sensitizer ion and (**a**) Er^{3+}, (**b**) Ho^{3+}, or (**c**) Tm^{3+} as an emitting activator ion. The *bold arrows* indicate absorbed pump photons, the *dotted arrows* symbolize nonradiative energy transfer, *curled arrows* represent nonradiative multiphonon decay, and the *downward arrows* emission. Cross-relaxation (CR) is illustrated with a pair of *reversed arrows*. Only those transitions producing emission at the visible region or $\leq$800 nm are expressed. Modified from Suyver et al. [25], Wang and Liu [23], and Wei et al. [35]

along with the growing concentration of activator ion (e.g., Er^{3+} or Tm^{3+}), but a too-dense population of the activators leads to concentration quenching caused by cross-relaxation processes between the neighboring activator ions [13, 39, 40]. The Yb^{3+} sensitizer is not sensitive to the concentration quenching as mentioned earlier—therefore, the concentration may be multifold compared to the activator ion. In the optimal case, the activator ions should be surrounded by as many Yb^{3+} neighbors as possible to enable an efficient ETU process [32, 41, 42]. However, the dopant ions must be diluted with a sufficient number of "inactive" ions (such as Y^{3+} or La^{3+} in the host material) to limit the energy migration from the activator ions to killer traps, which cause quenching of the desired luminescence [39, 43]. In addition, extremely high Yb^{3+} concentrations promote energy back-transfer from the

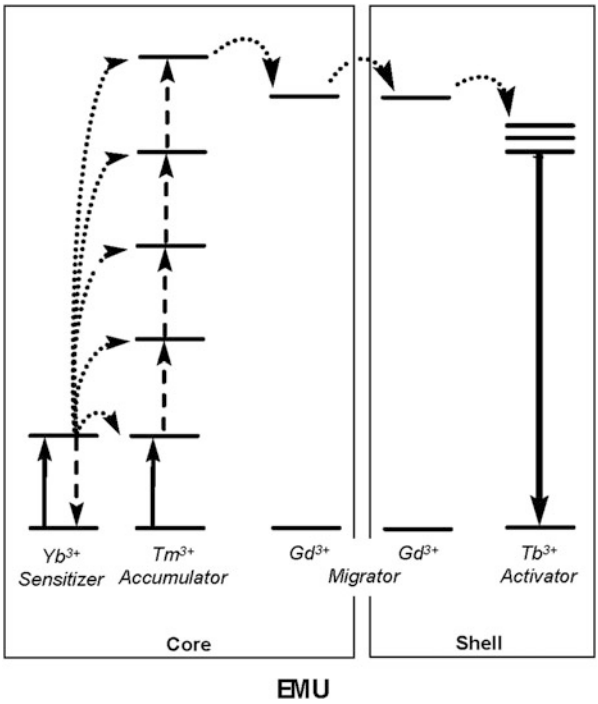

Fig. 4 Simplified energy diagram of the proposed energy migration-mediated upconversion process. *Upward* and *downward solid arrows* represent absorption and emission processes, respectively, while *bent arrows* symbolize energy transfer between the neighboring ions. Modified from Wang et al. [36]

activator ions to the Yb^{3+} resulting in impaired luminescence intensity (concerns especially green- and blue-emitting energy states of the Er^{3+} activator) [44].

To summarize, the molar fraction of rare earth dopants are in the range of 5–30 % for Yb^{3+} (generally 18 % with Er^{3+} or 25 % with other activators) in combination with either 1–3 % Er^{3+} (generally 2 %) or 0.1–0.6 % Tm^{3+} or Ho^{3+} (generally 0.3 %) [26, 45].

3 Upconversion Efficiency

The quantum yield is defined as "number of photons emitted per number of photons absorbed" and may have values from 0 % to 100 %. This rule applies to conventional fluorescence. As the photon upconversion is a nonlinear optical process, the definition of quantum yield becomes more complicated. The maximal quantum yield is not 100 % but 50 % for a two-photon system, 33 % for a three-photon system, and so on—and these different systems may be present simultaneously [25]. Additionally, the comparison of reported quantum yield values for a certain UCP material is not that straightforward as the values are dependent on measurement conditions. In contrast to conventional fluorescent materials, the excitation power density affects the quantum yield of the UCPs as the emission process is

nonlinear according to Fig. 2. Also differences in particle size (bulk material vs. nanocrystal), crystallographic phase (cubic vs. hexagonal), and environment of the surface ions (dry powder vs. colloid) may cause discrepancy in measured values. Furthermore, scattering should be taken into account especially in case of non-colloidal particle suspensions.

The upconversion efficiency for bulk Yb^{3+}–Er^{3+} doped $NaYF_4$ is reported to be maximally 3–6 % [46–48]. For another dopant ion pair, Yb^{3+}–Tm^{3+}, the studies state that approximately 2 % of the absorbed NIR photons were upconverted and emitted at blue wavelengths [47]. The Tm^{3+}-doped material involves a higher order process (3 or 4 absorbed photons) compared to the 2-photon system characteristic to the Er^{3+}-doped material, which explains the lower efficiency. However, the infrared emission of Tm^{3+} at 800 nm (2 absorbed photons) has a greater efficiency [25]. This NIR-to-NIR upconversion might open up additional applications for the Tm^{3+}-doped UCPs in future (e.g., high contrast or deep tissue imaging [49] and diffuse optical tomography [50, 51]). The upconversion efficiency of other activator ions has not been extensively discussed in literature.

Nano-sized UCPs produce upconversion photoluminescence with even lower efficiency than the bulk UCP materials. However, the quantum yield may be improved significantly if the dopant ions of nanocrystalline UCP core are protected with an undoped inorganic shell grown around the particle [46, 51]. Also dye-sensitized upconversion was suggested to enhance the quantum yield of poorly absorptive UCPs [52]. An organic NIR dye on the UCP surface acted as an antenna by collecting efficiently the NIR photons. The energy was further transferred to the UCP core resulting in intensive anti-Stokes emission. Gnach and Bednarkiewicz have recently reviewed the various efforts to improve the upconversion quantum yield of nano-sized UCPs [12].

4 Recent Development Trends in Upconverting Materials

4.1 Phase-Purity of $NaYF_4$-Based UCPs

The most efficient upconverting materials known today are hexagonal (β-phase) $NaYF_4$:Yb^{3+},Er^{3+} and $NaYF_4$:Yb^{3+},Tm^{3+} [33, 43, 45, 53]. The crystallographic phase is absolutely essential as the cubic (α-phase) structure produces approximately an order of magnitude less anti-Stokes photoluminescence than the hexagonal one [43, 54–56]. Lastusaari et al. [57] anticipated that there are at least two reasons causing the differences between the α- and β-phases. The more densely packed β-phase allows more efficient energy transfer between the lanthanide ions, and the close-to-stoichiometric structure of the β-phase contains fewer defects than the α-phase, which needs additional F^- ions to balance the charge of the enriched rare earth ions. Renero-Lecuna et al. [58] explained the high luminescence efficiency of the β-phase by the structural crystal disorder that creates different

environments for the activator ions. Much research has lately been carried out to identify controlled ways to produce phase-pure hexagonal $NaYF_4$:Yb^{3+},Er^{3+}/Tm^{3+}, and constantly diminishing attention has been addressed to the other UCP host materials intended for bioanalytical applications.

Factors affecting the upconversion efficiency and phase-purity of the fluorides include the dopant concentrations, the ratio of sodium to rare earth ions, the impurities, the crystal growth temperature, and time [25, 43, 59, 60]. At low synthesis temperatures the α-phase is formed while higher temperatures favor β-phase formation until certain point where the α-phase begins to predominate again [43, 55, 61, 62]. The exact phase transition temperatures depend on the UCP synthesis method.

The hexagonal phase usually dominates in *micrometer*-sized $NaYF_4$:Yb^{3+},Er^{3+} bulk material [63], which is applicable to areas such as NIR sensors, lasers and displays, but the particle size is too large to form colloidal dispersions required for bioanalytical applications.

4.2 Down to Nano-sized UCP Particles

The trend has been toward *nano*-sized UCPs with a uniform size and shape. As a consequence, other parameters in addition to the crystallographic phase need to be simultaneously controlled. Variables affecting the crystal size during the synthesis step comprise the concentration of the metal precursors, the nature of the coordinative solvent, the reaction time, and the temperature [64, 65]. When the physical dimensions of the UCP particle are reduced to the nano-scale (e.g., $<$50 nm), different kinds of problems causing decreased upconversion efficiency are encountered [23]. First, as the surface area-to-volume ratio increases, a relatively larger proportion of the emitting ions are located close to the surface, exposed to quenchers and surface defects. Second, high surface tension triggers the phase transformation from hexagonal to less efficient, but thermodynamically more stable cubic form [64].

Several shielding options have been proposed to protect the near-surface dopant ions from nonradiative relaxation processes induced by the surrounding high-energy vibrational oscillators such as the OH- and CH-groups of organic ligands and solvents [25, 66]. The quantum yield of nanocrystalline UCPs has been increased multifold by growing an inert, undoped $NaYF_4$ shell (with a thickness of a few nanometers) around an Yb^{3+}–Er^{3+}/Tm^{3+}-doped $NaYF_4$ core [46, 51, 54, 65]. The addition of an inorganic shell also lengthens the decay time constant and affects the green-to-red emission intensity ratio [67]. Dominating red emission from $NaYF_4$:Yb^{3+},Er^{3+} nanocrystals is a clear indication of nearby oscillators as the red-emitting energy level ($^4F_{9/2}$) is not efficiently populated without assistance of high-energy phonons [68]. An inorganic shell provides better protection for the near-surface dopants than organic shells as possible interactions between UCPs and

organic molecules may still cause quenching [54]. However, an organic coating has other advantages (e.g., allowing direct biofunctionalization).

To promote the hexagonal phase in nano-sized UCPs, different strategies have been developed. For example, co-doping with larger, optically passive rare earth ions (e.g., Gd^{3+}, La^{3+}, Ce^{3+}) has been suggested to favor the desired β-phase [64, 69]. Wang et al. [64] found that partial substitution of Y^{3+} ions with Gd^{3+} (molar fraction 30 %) leads to expansion in unit-cell volume, and no traces of α-phase were observed even though a lower synthesis temperature (200 °C instead of 300 °C) was used. Based on the calculations, it was stated that $NaGdF_4$ is energetically more stable than $NaYF_4$ in β-phase. However, the Gd^{3+}-induced reduction in particle size (from 25 nm to 10 nm) cancelled the positive effects of the phase transition leading to an upconversion efficiency similar to the control synthesis without Gd^{3+}. In addition to rare earth ion substitutions, also Na^+ cation sites in the $NaYF_4$ host has been co-doped with other alkali metals (e.g., smaller Li^+ or larger K^+) in order to distort the local symmetry around the activator ions [70, 71]. These diverse intentional impurities in the crystal lattice are under active research to find ways to force the phase transition toward β-phase. Furthermore, Sui et al. [72] reported that the phase transition requires energy for the rearrangement of Na^+ and Y^{3+} cations. They anticipated that oleate ligands adsorbed on the UCP surface during the solution-phase UCP synthesis lower the energy barrier promoting the formation of β-phase structure.

4.3 From Solid-State Synthesis to Solution-Phase Methods

The UCP synthesis (for bioanalytical applications) aims at the following characteristics: monodisperse, water-dispersible, and phase-pure nanocrystals with high upconversion efficiency and a uniform shape and size (e.g., preferably spherical, Ø <50 nm for bioaffinity assays). The nano-sized UCPs have been synthesized using several methods, from which the most commonly used processes are coprecipitation, thermal decomposition, crystallization in high-boiling-point organic solvent, hydrothermal and solvothermal methods (several reviews available [23, 60, 73, 74]). The synthesis always involves high temperature due to the high free-energy barrier for the phase transformation from α-phase to β-phase.

Commercial activities concerning the synthesis of nano-sized UCPs have started only recently. For example, among the first suppliers Intelligent Material Solutions Inc. (Princeton, NJ, USA) provides custom-made nano-sized UCPs as well as UCP products under Sunstone® trademark.

4.3.1 Solid-State Synthesis

The *coprecipitation* method involves a particle growth step in aqueous environment (at room temperature) followed by precipitation of the precursor material and

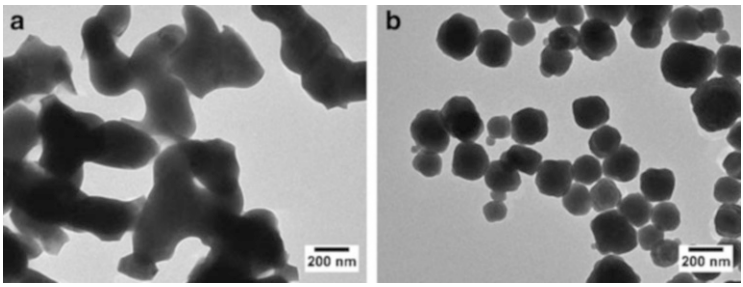

Fig. 5 Effect of the post-annealing temperature upon the size and crystallographic phase of the UCPs in the coprecipitation synthesis. TEM images from $NaYF_4$:Yb^{3+},Er^{3+} annealed for 5 h (**a**) at 450 °C (β-phase) and (**b**) at 300 °C (α-phase)

finally an annealing step in which the lattice structure of the dried UCP material is rearranged under high temperature (typically ~400 °C) to generate brightly luminescent β-phase particles [35, 61]. Unfortunately, transmission electron microscopy (TEM) images suggest that the resulting particles tend to sinter together during the final step at high temperatures (Fig. 5), which is a crucial step for activating the optical properties of the UCP material [35]. Smaller-sized material was pursued by milling and crushing, but fractured crystalline lattice structure results in decreased emission intensity [75]. A synthesis procedure directly leading to non-sintered UCPs was developed and patented by Sanjuro et al. [76]. The fluidized-bed process maintained the particle size and the monodispersity of the precursor material as the particles were kept in constant movement relative to one another by utilizing either inert or reactive gases [77].

4.3.2 Solution-Phase Synthesis

The synthetic routes described below involve a solution-phase crystal growth step at elevated temperatures and, thus, a post-annealing step inducing the particle sintering is unnecessary. Metal trifluoroacetates *thermally decompose* to give the corresponding metal fluorides at relatively low temperatures (~300 °C). The thermal decomposition method in ambient pressure utilizes high-boiling organic solvents (e.g., 1-octadecene, oleylamine) in combination with organic additives (i.e., coordinating solvents) containing polar capping groups and long hydrocarbon chains [e.g., oleic acid, oleylamine, trioctylphosphine oxide (TOPO), trioctylphosphine (TOP)] [63, 78–83]. The fluorinated side products are toxic, and the experimental conditions are very rigorous as they demand a water- and oxygen-free environment protected with an inert gas. However, the quality of the resulting UCP crystals is excellent. To avoid toxic side products, similar reaction conditions have also been exploited to crystallize precursors other than trifluoroacetates (e.g., rare earth chlorides and acetates) in high-boiling organic solvents [59, 64, 66, 84].

Even lower reaction temperatures (<250 °C) are used in *hydrothermal* and *solvothermal* synthesis. Elevated pressure combined with the heat is exploited to

alleviate the crystallization of precursor components (typically containing rare earth chlorides or nitrates) either in aqueous environment (hydrothermal route) [85–87] or in organic solvent (e.g., alcohol; solvothermal route [44, 88]) supplemented with organic additives (e.g., oleic acid, ethylenediaminetetraacetic acid (EDTA), cetyltrimethylammonium bromide (CTAB), or sodium citrate). The reaction conditions are easily controllable, the yields are high, and the costs are lower than those of thermal decomposition method. However, the reaction times are long (up to days) and due to the high pressure, a specialized Teflon-lined reaction vessel (i.e., an autoclave) is required.

Additives in the synthesis reactions are essential to control the morphology and especially the size of the UCPs. The characteristic features of a capping ligand affect the outcome. A chelating agent, EDTA, is known to reduce the particle size but it seems to suppress the phase transition of $NaYF_4$ material from α- to β-phase [35, 61]. In contrast, TOPO was reported to reduce the energy barrier of the phase transition [89]. Stabilization with oleic acid results in hydrophobic UCPs and manipulation of the surface chemistry is required before dispersion to aqueous solutions [60]. Polyethyleneimine (PEI) [44] directly functionalizes the surface with amine groups, and polyvinylpyrrolidone (PVP) [90] is a water-soluble ligand providing hydrophilic properties. The addition of a cationic surfactant, CTAB, promotes formation of rod-shaped UCPs instead of roundish particles [39].

The first *nano*-sized UCPs (*phosphate* host lattice) were prepared by the solvothermal method [91] and published in the year 2003 [92, 93]. Two years later $NaYF_4$ nanocrystals with purely hexagonal crystallographic phase were reported [39, 94]. In future, the development of UCP synthesis will focus on high-quality end products but may also be directed toward low-cost and low-temperature pathways, and methods avoiding toxic organic solvents [60]. Safety concerns are also related to excessive fluoride reagents that may decompose and produce HF gas and fluorinated species at elevated temperatures [95]. The reproducibility and scale-up of UCP nanocrystal synthesis are limited by sensitive kinetics related to solution-phase synthesis methods [96]. Variation in synthesis may be caused due to alteration in heating and cooling rates, side reactions, and the presence of impurities. Automated systems with precisely controlled reaction parameters might be an attractive choice in future. Chan et al. [96] have already taken the first step by introducing an automated platform for inorganic nanoparticle synthesis.

5 Advantages of UCP Labels

5.1 Excitation with Near-Infrared Radiation

NIR excitation provides a basis for several advantageous features that render the UCPs interesting labels for bioanalytical applications. The main merit of the UCP

label technology based on anti-Stokes photoluminescence detection is the absence of autofluorescence, which commonly deteriorates the detection limits of assays involving biological components. The autofluorescence commonly originates from endogenous fluorophores of biological material and is thus observed at wavelengths longer than the excitation radiation—equally to the fluorescence of conventional labels. Under NIR excitation the possible autofluorescence is observed at the NIR region several hundred nanometers away from the visible wavelengths where the emission of UCPs is collected (anti-Stokes' shift up to 500 nm). This advantage enables, at least in theory, more sensitive bioanalytical assays as the background fluorescence can be minimized. Our research group demonstrated a nearly sevenfold improvement in the signal-to-noise ratio when NIR excitation and UCP label were utilized in an enzyme activity assay instead of red-absorbing organic fluorophore [97]. An optional way to eliminate the autofluorescence is to use a pulsed excitation source and time-gated measurement in combination with labels having a long emission lifetime [98, 99]. However, time resolution requires more sophisticated instrumentation than the technology based on photon upconversion, which simply relies on spectral separation of the autofluorescence.

For several different reasons, UV excitation is nonpreferred in bioanalytical assays, but is commonly used for exciting the conventional fluorescent labels (e.g., quantum dots, lanthanide chelates). The penetration depth of the lower-energy NIR excitation in biological tissue is much greater compared to the highly absorptive UV region. The absorption band of Yb^{3+} at 980 nm lies on the wavelength region of 600–1,200 nm, where tissues have the lowest absorption (originating mainly from water, blood, and pigments) [100, 101]. In addition, NIR radiation does not cause damage to the biological specimen. This issue is prominent in applications involving long illumination times (e.g., imaging). Also the label itself—especially organic fluorophores—may be degraded by the high-energy UV radiation causing photobleaching [102, 103]. The NIR-excitable inorganic UCPs show extremely high photochemical stability in repeated excitation cycles [43, 65, 104]. As high excitation intensities may be utilized without photodegradation of the UCPs, high signal levels are expected even from a relatively small number of UCPs. Weak emission can, in turn, be collected and integrated over a longer time period under continuous excitation [26].

The good penetration properties of NIR radiation are beneficial also in homogeneous assay concepts. The sample matrix is present during the fluorescence measurement and lower signal levels are expected if excitation and/or emission wavelengths are absorbed by the sample. Whole blood—one of the most common sample matrixes in health care—cannot be used as such in homogeneous applications. Instead, the red blood cells need to be removed prior to the analysis due to the intensive absorption at wavelengths below 600 nm. Usually, methods other than luminescence-based ones (such as electrochemical detection [105, 106]) must be used for separation-free assays carried out in whole blood. The UCP technology exceptionally enables fluorescence measurements in the presence of whole blood because the NIR excitation and the red emission band are both above

600 nm. We demonstrated that equal calibration curves for the 17β-estradiol were obtained in colorless plasma and in red-colored whole blood (both 20 % v/v) [107]. The use of whole blood matrix was also reported in papers demonstrating an enzyme activity assay [97] and a pH sensor [108] based on UCP technology.

If energy transfer from one fluorophore to another is exploited (e.g., in proximity-based bioanalytical assays), the excitation should be perfectly selective to avoid direct excitation of the acceptor fluorophores. Uniquely, NIR radiation allows exclusive excitation of the UCP donor, and background fluorescence originating from the acceptor is eliminated [109].

5.2 *Photophysical Properties of Lanthanides*

Highly structured emission is characteristic to lanthanides [29], which in practice means that between the sharp emission bands (bandwidths ~20–50 nm) there is no detectable emission at all. Those wavelengths can be exploited to accurately measure the emission of other fluorescent labels without spectral contamination, which is important in applications concerning energy transfer to another fluorophore or in multiplexed assays with several fluorophores involved. In contrast, conventional organic fluorophores have much wider excitation and emission bands, which results in spectral overlap and unselective detection in systems comprising more than one such fluorophore.

UCPs with different compositions each produce different emissions (at blue, green, red, or NIR), enabling detection of at least two targets simultaneously based on discriminating emission colors [110]. One excitation source is compatible with all these labels as the Yb^{3+} ion acts as a sensitizer in all UCP materials favored presently. Similarly, quantum dots producing multiple emission colors depending on their diameter are well known for their wide excitation band at the UV region, which suits perfectly multiplexed assays requiring only one excitation source [111, 112]. However, the UV excitation of quantum dots has certain drawbacks discussed in sect. 5.1.

Lanthanide chelates and cryptates have been utilized in the time-resolved fluorometry exploiting the long excited state lifetimes of lanthanides [113–116]. The UCPs carrying lanthanide dopants share this feature [117, 118], but due to unproven added value, time-gated measurement has not been commonly utilized in UCP-based bioanalytical assays. There is no practical motivation to complicate the collection of the emission by waiting until the short-lived endogenous fluorescence has faded because all autofluorescence is already eliminated due to the photon upconversion. However, in the bioimaging applications the luminescence lifetime is generally more informative than the luminescence intensity as the distribution of the label particles is uncontrollable.

Several emitting centers are incorporated into each UCP particle leading to high specific activity. In combination with all above-mentioned advantageous

characteristics reducing the background fluorescence, this feature results in the high signal-to-background ratios appreciated in ultrasensitive bioanalytical assays.

6 Challenges of UCP Labels

The UCPs are inorganic crystals originally bearing no functional groups at all. Commonly the UCPs are hydrophobic in nature following the non-aqueous synthesis routes. The particles are transformed into a hydrophilic form by surface modification, which also introduces useful functional groups on the surface. Only functionalized UCPs may further be conjugated with biomolecules used for recognizing the analyte with high specificity. Production of a stable, reproducible coating with a desired thickness is quite challenging as such, but also the agglomeration of UCP particles during (or due to) the modification procedure must be avoided. Liu and co-workers have reviewed [23, 119] various solutions for surface functionalization including silica-encapsulation, layer-by-layer assembly, ligand oxidation, ligand attraction, and ligand exchange.

The spectral properties of the UCPs (e.g., the ratio between the emission colors [34, 67]) depend on the excitation power density (W/cm^2). The green emission of $NaYF_4:Yb^{3+},Er^{3+}$ predominates at low power density occasions, while the intensity of the red emission increases more rapidly along with the power density followed by the emergence of a violet emission [34, 47, 120, 121]. Suyver et al. [34] showed that population of the $^4I_{13/2}$ energy state becomes a two-photon process (possibly through a cross-relaxation CR1 in Fig. 3) at high excitation power, while it otherwise is populated through a multiphonon relaxation from the state $^4I_{11/2}$ (one-photon process). Increased population of $^4I_{13/2}$ further enhances the population of the red-emitting state. The excitation power density has seldom been reported in research papers and therefore the findings presented in the literature are not directly comparable. It may be challenging to determine the exact power density of the laser beam traveling through optics and fluid sample matrix before reaching the UCPs. However, quite exact estimation may be drawn if excitation beam is guided through a fiber optics with defined diameter. Still, the results from even the same setup are not completely comparable in all cases. An increase in the sample turbidity may lead to an increased scattering of the excitation radiation. A broadened excitation area results in a lower power density and, thus, may bias the result. For example, the volume of blood cells (i.e., hematocrit) in a sample varies between patients [122], resulting in dissimilar scattering properties and unequal power densities. However, significant problems are not expected due to the scattering as the effects are mostly marginal in only mildly turbid samples typical for the clinical diagnostics.

Heterogeneous composition of the UCPs resulting in nonuniform spectroscopic properties may produce anomalous results in bioanalytical tests. Morgan et al. [20] reported that one particular commercial UCP bulk material contained differing UCP particles, from which part produced a dominantly red emission while the others were mainly emitting at green wavelengths. We confirmed the finding with

help from Leiden University Medical Center (Leiden, the Netherlands). Dr. Paul Corstjens and his research group examined the PTIR550/F material with a confocal fluorescence microscope equipped with a two-photon NIR laser and concluded that red-to-green ratios varied from 0.77 to 2.26 between individual UCP crystals (unpublished data). The differences were independent of the crystal size and the focal plane (i.e., laser focus). Despite the finding, this UCP material has been used in energy transfer-based applications without any alarming behavior. Because all crystals were producing both green and red emission, it is likely that each crystal was able to transfer energy from both energy states to acceptor fluorophores in close proximity, and the assay performance was not greatly compromised due to the heterogeneity.

7 Bioanalytical Applications

The various bioanalytical applications utilizing UCP labels are here divided based on the type of assay concept. The number of publications in this field has grown enormously since the year 2005, expressing the ample interest among the scientists. The critical features of bioanalytical assays include limit of detection (LOD) and limit of quantification (LOQ), selectivity (effects of interferents, such as structurally similar molecules), dynamic range (the range from the lowest to the highest reliably measurable concentration), precision (reproducibility, repeatability), and accuracy (trueness of the measured concentration) [123, 124]. Sometimes also other completely different factors, such as the time required for the final result, overall costs, portability of the analyzer, or ease of use, play an important role. Depending on the analyte, its clinically relevant levels and the intended application, some characteristics of the test are more important than others, influencing the choice of the assay type.

Although the UCPs are an extremely hot topic in the *in vivo* imaging and photodynamic therapy (reviewed in [60, 119, 125–127]), they lie outside of the scope of this review concentrating solely on the diagnostic applications.

7.1 Heterogeneous Bioaffinity Assays

The bound and unbound labeled biomolecules are physically separated in heterogeneous bioaffinity assays before the final measurement step which usually results in greater sensitivity compared to the separation-free homogeneous assays. To enable the washing procedure, the analyte molecules and the labels are collected onto a solid support (e.g., walls of reaction vessel, surface of particles). A few examples of UCP-based heterogeneous bioaffinity assays are listed in Table 1. As the luminescent label in this case is a particle, kinetics and steric hindrance play important roles, and the size of the particle also affects the assay performance.

Table 1 Examples of heterogeneous bioaffinity assays based on the UCP labels

Analyte	Type of assay	Limit of detection	Sample volume	UCP material (coating, diameter)	Reference
In glass capillary					
Staphylococcal enterotoxin B (SEB)	Sandwich immunoassay	35 fmol	– (spiked buffer)	Y_2O_2S:Yb,Er (silica, Ø 400 nm)	[128]
On magnetic beads					
Staphylococcal enterotoxin B (SEB)	Sandwich immunoassay	180 fmol (1.8 nM)	100 µL (spiked buffer)	Y_2O_2S:Yb,Er (silica, Ø 400 nm)	[128]
Target DNA (model assay)	Sandwich hybridization	– (7.8 nM)	– (spiked buffer)	$NaYF_4$:Yb,Er (LbL, Ø 50 nm)	[130]
Streptococcus pneumoniae lytA gene (pathogen)	Sandwich hybridization	Low amol range (<1 ng genomic DNA)	– (isolated genomic DNA)	Y_2O_2S:Yb,Er (silica, Ø 400 nm)	[110]
In microtiter wells					
Biotinylated small molecule (model assay)	Competitive bioaffinity assay	~50 fmol (1 nM)	50 µL (spiked buffer)	$NaYF_4$:Yb,Er[a] (PAA, Ø 280 nm)	[132]
Biotinylated large molecule (model assay)	Sandwich bioaffinity assay	~0.75 fmol (15×10^{-3} nM)	50 µL (spiked buffer)	$NaYF_4$:Yb,Er[a] (PAA, Ø 280 nm)	[132]
		1.5 fmol (30×10^{-3} nM)	50 µL (spiked buffer)	$NaYF_4$:Yb,Er[a] (PAA, Ø 240 nm)	[133]
Anti-cytomegalo-virus IgM and IgG (immune response)	Dual-parameter sandwich immunoassay	10,000-fold dilution of positive serum	– (serum)	Y_2O_2S:Yb,Er and Y_2O_2S:Yb,Tm (silica, Ø 400 nm)	[110]
Free prostate specific antigen (f-PSA) (cancer marker)	Sandwich immunoassay	0.2×10^{-3} fmol (20×10^{-6} nM)	10 µL (spiked buffer)	Y_2O_2S:Yb,Er[a] (PAA, Ø 260 nm)	[104]

LbL layer-by-layer coating, *PAA* poly(acrylic acid) coating
[a]Ground UCP bulk material

Generally, the smaller particles resembling molecular labels are more practical, but the thermodynamic instability of the nanoparticles increases with decreasing size, leading to particle aggregation.

The very first papers introducing the UCPs in bioanalytical application were published by the researchers working for SRI International (California, USA) in the late 1990s. Wright et al. [128] carried out a sandwich immunoassay for a food poisoning Staphylococcal enterotoxin B (SEB) both in a glass capillary providing miniature binding regions and on magnetic glass beads. The washing steps in capillary were realized with a peristaltic pump creating a liquid flow. Magnetic beads, in turn, are easy to control with a magnetic field during the removal of unbound components. It was documented that the LOD of the SEB assay (35 fmol in capillary or 180 fmol on beads) was limited only by the nonspecific binding of the UCPs. Magnetic beads in combination with UCP labels have also been utilized for detection of single-stranded DNA [110, 129, 130] with LODs reaching the femtomole range. SRI International has further developed bead-based immunoassays to detect biological warfare agents from environmental samples with a flow cytometer [131].

In a microtiter plate format, a sandwich immunoassay has been reported for a widely used cancer marker, the free prostate-specific antigen (f-PSA) [104]. The dynamic range of this relatively sensitive assay (LOD 0.0002 fmol for f-PSA) extended over three orders of magnitude, after which there were no more UCP conjugates left to form the sandwich complexes. A similar sandwich assay in dual-parametric format was constructed to recognize both IgM and IgG antibodies against cytomegalovirus in order to differentiate the early and the secondary immune response [110]. Green-emitting Yb^{3+}–Er^{3+} doped UCPs and blue-emitting Yb^{3+}–Tm^{3+} doped UCPs were utilized to discriminate between the two analytes in the same reaction.

The features of the ground UCP bulk material ($NaYF_4$:Yb^{3+},Er^{3+}, Ø 280 nm) in heterogeneous model assays carried out in standard microtiter wells were studied by Kuningas et al. [132]. The lowest detectable amount of these UCPs bound to a microtiter well through a strong biotin–streptavidin interaction was determined to be 0.75 ng. Actually, the focused laser beam excited only less than 1 % of the surface area of the well and probably only few picograms of UCPs were bound to that area, corresponding roughly to tens of individual particles. According to this result, the UCPs should enable highly sensitive assays if nonspecific binding is minimal. The luminescence intensity of the UCPs increased linearly over 4 orders of magnitude, demonstrating the high specific activity of the UCP labels, which allows a wide dynamic range in heterogeneous assays. A reflective solid surface (white-colored microtiter well) appears to enhance the anti-Stokes photoluminescence by about 100 times, from which only a fivefold increase was explained by the more efficient photon collection, while the basis of the phenomenon leading to the remaining 20-fold increase remained unclear [133]. The effect was discovered both in fluoride and oxysulfide hosts doped with Yb^{3+}–Er^{3+} pair and was even more pronounced at the red emission wavelengths compared to the green ones. Unfortunately, the LOD (1.5 fmol) of the model sandwich assay for biotinylated protein was not improved in white wells as the luminescence arising from the nonspecifically bound UCPs was enhanced equally.

The major obstacle limiting the LOD of the heterogeneous assays is the nonspecific binding of the UCPs, which is a problem shared by particle labels collectively. The fact that the UCP technology avoids all the other sources of background luminescence especially highlights the importance of minimizing this problem.

7.2 Array-Type Multiplexed Assays

If several analytes are connected somehow to the condition under investigation, it may be cost-effective to use multiplexed assays capable of analyzing them all simultaneously from one reaction mixture. If the detection of analytes is based on different-colored fluorophores, maximally 4–5 analytes may be simultaneously distinguished due to the limitations set by the overlapping fluorescence spectra. Computer algorithms are usually required to solve the relative proportions of slightly overlapping fluorophores. Instead, the analytes must be identified based on a binding position to open up the opportunities for infinite multiplexing.

Both oligonucleotides and proteins have been spotted on glass slides and detected with UCP conjugates. The simplest test involved spotting of biotinylated immunoglobulins on the slides and direct visualization of the spots (diameter 900 μm) with streptavidin-conjugated UCPs ($NaYF_4$:Yb^{3+},Er^{3+} with magnetic core, Ø 68 nm) [134]. A more practical nucleic acid microarray (spot diameter 150 μm) was constructed to measure the expression levels of 24 housekeeping genes of bladder carcinoma cells [135]. UCPs were detected with a modified fluorescence microscope, which had a Xenon lamp as an excitation source instead of more optimal laser diode. Nonetheless, the bright emission of UCPs (Y_2O_2S:Yb^{3+},Er^{3+}, Ø ~400 nm) allowed four times better LOD than an organic cyanine dye Cy5, which is commonly used in microarray applications.

Recently, the high-content capacity of microarrays has been transferred from glass slides to microtiter wells, which are widely used reaction vessels in high-throughput concepts. Ylihärsilä et al. [136] demonstrated genotyping of ten common adenovirus genotypes with an array-in-well platform and validated the assay with clinical samples. Eleven selective probe spots (diameter 375 μm) in three replicas and positive control oligonucleotide spots were printed on the bottom of standard microtiter wells. Extracted DNA was amplified using generic biotinylated primers, which allowed the detection of all adenovirus genotypes on the array with universal streptavidin-conjugated UCPs ($NaYF_4$:Yb^{3+},Er^{3+}, Ø 55 nm). Cross-hybridization of similar sequences creates a challenge when a large number of probes are combined in one array. Therefore, the identification of the genotype was based on a hybridization pattern (Fig. 6) rather than specific hybridization with only one type of probes. The UCPs were detected with a special microwell imager, which is simpler and the acquisition costs are lower compared to a confocal microscope scanner. Later, the assay was successfully applied for >200 patient samples to identify clinically relevant human adenovirus genotypes [137]. Array-in-well platform fits also to multiparameter immunoassays for protein detection,

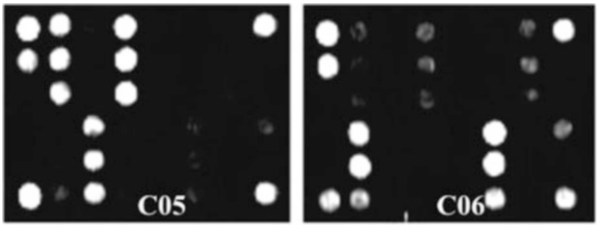

Fig. 6 Array-in-well platform for qualitative genotyping based on hybridization patterns [136]. The DNA probes were spotted in three replicas together with control spots in the corners. Reprinted with permission from *Anal Chem* (23:1456–1461). Copyright 2011 American Chemical Society

although possible cross-reactivity of antibodies limit the extent of multiplexing. Päkkilä and Ylihärsilä et al. [138] demonstrated simultaneous quantitative analysis of three protein biomarkers by utilizing an antibody array (spot diameter 1000 μm).

The repetitive scanning and long-lasting imaging of microarrays expose the fluorescent labels to the excitation radiation for an extended period of time and the stability of the label becomes relevant. The organic fluorophores tend to lose their fluorescent properties gradually under intense excitation. In UCPs, the emitting ions are located in a protective inorganic crystal lattice and, thus, no photodegradation is expected. In addition to the outstanding photostability of the UCPs, the high emission intensity renders the UCPs an attractive label option for microarray applications. Now that nano-sized UCPs are available, the dynamic range in the compact binding region is less limited by the size of UCPs and the diameter of the spots may be reduced to allow larger amounts of information per certain area of solid support.

7.3 Lateral Flow Tests

Lateral flow (LF) tests, also known as immunochromatographic tests, are typically carried out on nitrocellulose-based strips or other polymeric materials allowing capillary flow of the solution containing the sample and labels (Fig. 7). The LF platform is attractive due to its suitability for low-resource situations such as point-of-care and on-site testing. Colored particle labels (e.g., colloidal gold, latex beads) are used for qualitative applications utilizing visual readout. More sensitive and also quantitative results are obtained if an optical reader is used for detecting the label in question.

Examples of the UCP-based LF immunoassays have been collected in Table 2. They are mainly targeted at pathogen identification (food pathogens and possible biological warfare agents) or infection diagnostics. OraSure Technologies, Inc. (former STC Technologies; Pennsylvania, USA) with its research partners SRI International (California, USA) and Leiden University Medical Center (the

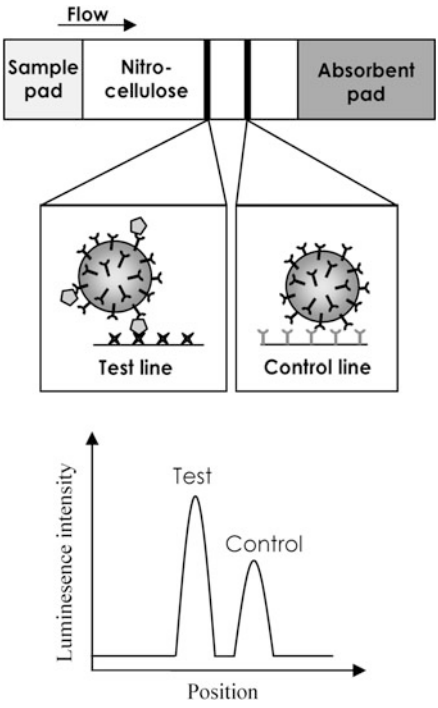

Fig. 7 Principle of the sandwich-type lateral flow test based on the UCP labels. Fluid sample together with the UCP conjugates flow through the nitrocellulose membrane toward the absorbent pad. UCP labels are captured on the test line via the analyte (*gray pentagon*), while binding to the control line occurs irrespective of the analyte and verifies the successful flow. The strip is optically scanned to record the UCP emission at capture lines

Netherlands) were the first to demonstrate the use of UCPs in lateral flow tests for various analytes. The first papers described immunoassays for the cardiac marker troponin T (sandwich-type assay for a protein), for a food pathogen (sandwich-type assay for a whole bacteria cell) and for several metabolites of drugs of abuse (competitive assay for small molecules) [139, 140]. The preliminary studies with UCP labels enabled a 10- to 100-fold improvement in the detection limit (LOD <1 mIU/mL of hCG hormone in a non-biological matrix) compared to gold and latex particles [141]. However, to roughly compare, modern hypersensitive pregnancy tests (hCG hormone) based on enzyme-catalyzed chemiluminescence of luminol may reach the LOD of even 1 nIU/mL [142], which is million times more sensitive than the UCP-based result. On the other hand, the technology based on chemiluminescence requires the addition of luminol substrate and the activity of the enzyme needs to be assured, which may be problematic in low-resource situations. Compared to another enzyme-based assay method, widely used ELISA tests (enzyme-linked immunosorbent assay), Corstjens et al. [143, 144] and Li et al. [145] have reported for UCP-based LF immunoassays 10- to 20-fold improvements in analytical sensitivities.

Nucleic acid detection on the LF platform has mainly been studied by Prof. Tanke's and Corstjens's research group in Leiden University Medical Center. The kinetic characteristics of nucleic acid hybridization between complementary

Table 2 Examples of lateral flow assays based on the UCP labels

Analyte	Special	Limit of detection	Sample volume	UCP material (coating, diameter)	Reference
Sandwich immunoassays					
Escherichia coli O157:H7 (food pathogen)	–	10^3 org./mL	100 µL (diluted culture)	Y_2O_2S:Yb,Er/Tm (silica, Ø 400 nm)	[139, 140]
Human chorionic gonadotropin (hCG) (pregnancy hormone)	–	0.4 fmol (~0.9 mIU/mL)	150 µL (spiked buffer)	Y_2O_2S:Yb,Er (silica, Ø 400 nm)	[141]
Anti-hepatitis C virus and anti-HIV or anti-tuberculosis antibodies (response to infection)	Multiplexed[a] strip, consecutive flow	Qualitative (not reported)	2 or 10 µL (diluted plasma)	Y_2O_2S:Yb,Er (silica, Ø 400 nm)	[153]
Respiratory syncytial virus (RSV) antigen (respiratory infection)	–	Semi-quantitative (not reported)	200 µL (naso-pharyngeal wash)	Y_2O_2S:Yb,Er (silica, Ø 400 nm)	[161]
Schistosoma sp. antigen (parasite)	–	~0.1 × 10^{-3} fmol	10 µL (diluted serum)	Y_2O_2S:Yb,Er (silica, Ø 400 nm)	[143]
Interferon gamma (cytokine)	–	<5 × 10^{-3} fmol	40 µL (stimulated cell culture)	Y_2O_2S:Yb,Er (silica, Ø 400 nm)	[144]
	Cyclo-olefin polymer strip, 2D scanning	0.3 fmol	100 µL (spiked buffer)	Y_2O_2S:Yb,Er (silica, Ø 400 nm)	[162]
Interleukin 10 combined with Interferon gamma or IgM (cellular and humoral immune response)	Multiplexed[a] strip, single and consecutive flow	Qualitative (not reported); 8.3 × 10^{-3} fmol for interleukin 10 alone	100 µL (spiked buffer or diluted serum)	Y_2O_2S:Yb,Er (silica, Ø 400 nm)	[163]
Yersinia pestis (pathogen, possible biological warfare agent)	–	10^4 CFU/mL	100 µL (diluted culture)	$NaYF_4$:Yb,Er (silica, Ø 400 nm)	[150]
Yersinia pestis F1 antigen (pathogen, possible biological warfare agent)	–	3 fmol	10 µL (spiked buffer)	$NaYF_4$:Yb,Er (silica, Ø 400 nm)	[151]
Anti-*Yersinia pestis* antibodies (response to infection)	Multiplexed[a] LF disk	From tens to thousands of fmol	10 µL/strip (serum)	$NaYF_4$:Yb,Er (silica, Ø 250 nm)	[164]
Anti-hepatitis B antibody (response to infection)	–	20 mIU/mL	70 µL (serum)	$NaYF_4$:Yb,Er (silica, Ø 250 nm)	[145]

Brucella (pathogen, possible biological warfare agent)	–	5×10^6 CFU/mL	70 µL (pure culture)	$NaYF_4$:Yb,Er (silica, Ø 400 nm)	[165]
Anti-HIV antibody (response to infection)	Automated[b] microfluidic system, consecutive flow	Qualitative (not reported)	10 µL (spiked plasma/spiked saliva)	Y_2O_2S:Yb,Er/Tm (silica, Ø 400 nm)	[159, 160]
Competitive immunoassays					
Drugs of abuse (for four drugs)	Multiplexed[a] strip	Hundreds of fmol (<5 ng/mL)	100 µL (spiked saliva)	Y_2O_2S:Yb,Er/Tm (silica, Ø 400 nm)	[139, 140]
Nucleic acid detection					
Human papilloma virus type 16 (HPV16; cause of cancer)	Separate PCR amplification	~30×10^{-3} fmol (10 pg)	2 µL (PCR solution)	Y_2O_2S:Yb,Er (silica, Ø 400 nm)	[147]
Streptococcus pneumoniae (pathogen)	No PCR amplification	<1,000 pg genomic DNA (10^6 bacteria)	10 µL (digestion solution)	Y_2O_2S:Yb,Er (silica, Ø 400 nm)	[148]
Emiliania huxleyi cDNA (phytoplancton)	No PCR amplification, no denaturation	0.1 fmol (3 pg ssDNA)	<10 µL	Y_2O_2S:Yb,Er (silica, Ø 400 nm)	[149]
Vibrio cholerae (pathogen)	Separate PCR amplification	0.3×10^{-3} fmol (0.1 pg)	5 µL (PCR dilution)	Y_2O_2S:Yb,Er (silica, Ø 400 nm)	[110]
Bacillus cereus (food pathogen)	Microfluidic system[c]	5 fmol (1,000 pg)	8 µL (PCR solution)	Y_2O_2S:Yb,Er (silica, Ø 400 nm)	[155]
	Microfluidic system[c]	0.5 fmol (100 pg)	10 µL (PCR solution)	Y_2O_2S:Yb,Er (silica, Ø 400 nm)	[160]
	Microfluidic system[c]	10^3–10^4 cells/mL	100 µL (spiked saliva)	Y_2O_2S:Yb,Tm (silica, Ø 400 nm)	[154]

The LF strips were constructed from a nitrocellulose membrane, and the single flow format was used if not stated otherwise

HIV human immunodeficiency virus, *2D* two-dimensional, *CFU* colony-forming unit (viable bacteria), *cDNA* complementary DNA, *ssDNA* single-stranded DNA

[a]Several test lines on the same strip one after the other or separate strips positioned in a multichannel LF disk

[b]Self-contained microfluidic cassette comprising a pumping system, reagents, mixer, and lateral flow strip

[c]Integrated DNA amplification (PCR), lateral flow, and UCP detection (optical scanning) combined with microfluidistics

sequences are more complicated at the solid–liquid interface (e.g., immobilized probe) compared to the hybridization of strands in solution [146]. In addition, the capillary flow on LF strip limits the contact time between the target sequence and the test line probes, therefore requiring a fast annealing rate. Consequently, Corstjens et al. did not use nucleic acid probes on LF test lines, but captured the pre-hybridized double-stranded complexes on the test line through haptens [147]. Two specific haptenized probes conjugated with either biotin or digoxigenin were hybridized with the amplified and heat-denatured target sequence (human papilloma virus type 16) in the solution phase. The formed sandwich complex can be captured and detected with universally adaptable LF strips containing an avidin test line and UCP conjugates recognizing digoxigenin hapten. The LF platform allowed detection of low attomole quantities of target DNA molecules, which translates into a 100- to 10,000-fold improvement in LOD compared to gold nanoparticle labels in an LF test and up to 10^5-fold compared to ethidium bromide-stained agarose gel electrophoresis [110]. It was anticipated that an ultrasensitive assay could possibly detect nucleic acid sequences without any amplification step, thus reducing the risk for false results caused by possible amplification artifacts or inhibition. In addition, the required thermal cycler and polymerase enzyme add the complexity and costs of the test. Based on a study, less than 1 ng of fragmented genomic *Streptococcus pneumoniae* DNA, corresponding to approximately 10^6 pathogenic bacterial cells, was required to detect the presence of one gene without any amplification step [148]. This LOD may be acceptable for applications where the sample availability is not limited. However, by multiplying the number of targets (e.g., additional probe sets, multi-copy gene, or abundant mRNA target), the amplification-free concept could be more widely applicable. Still, only single-stranded targets (e.g., RNA) can be quantified at ambient temperature because a thermal denaturation of the double-stranded genomic DNA at elevated temperature precedes the hybridization of haptenized probes [149]. In general, the amplification step is often included in nucleic acid detection.

Several variations of LF tests exist. The UCPs may be mounted on the LF strip in advance to allow a very simple assay procedure involving only addition of the sample (single flow format) [150, 151]. An alternative version is called the consecutive flow format, which involves a washing step to remove unbound sample material before addition of the UCP conjugate to the LF strip [152, 153]. Various analytes may be detected simultaneously from one sample by discriminating between the analytes on the basis of test line position [140, 141, 153].

The ambitious aim of combining immunoassays and nucleic acid detection into a same integrated microfluidic system provides, when successfully completed, extensive data for simultaneous identification of pathogen (based on antigens, DNA, and RNA) and evaluation of the host immunological responses (emerging antibodies) from a single noninvasive saliva sample [152–154]. The system is constructed on a disposable, self-contained microfluidic cassette comprising all reagents for upstream sample pretreatment and an LF strip for multiplexed analysis of the processed sample. All operations are carried out automatically by the analyzer [155–157], and the result is obtained in less than 1 h, which sets strict time limits

on each step [158]. Different versions of portable analyzers (manual, mechanical, or thermal actuations) with external LF strip scanner have been described [158–160].

Most of the commercial LF tests presently are based on colloidal gold as a label. The UCP labels provide improvements in the assay performance without any apparent disadvantages. However, if low detection limits are not required, the visual read-out of the colloidal gold is of course a simple and cost-effective option. In more demanding situations, the UCP label can be quantified with relatively simple instrumentation, which suits well the on-site testing usually associated with the LF platform.

7.4 Proximity-Based Homogeneous Assays

Simple automation can be achieved with homogeneous assay concepts, also termed "mix-and-read" protocols or separation-free assays. Energy transfer between closely situated fluorophore and absorbing species can be employed in bioanalytical assays to indicate specific binding events. Two different energy transfer mechanisms combined with the UCP donors have been reported: resonance energy transfer and evanescent wave coupling.

7.4.1 Upconversion Resonance Energy Transfer

The traditional resonance energy transfer (RET) discovered by Theodor Förster [166] was described between the singlet states of two fluorophores. The lanthanides producing long-lived luminescence from the triplet state mainly obey the same rules, but certain differences also exist and the term lanthanide (or luminescence) resonance energy transfer (LRET) is typically used. The energy is transferred over a short distance between the two resonant energy states through dipole–dipole interactions. The efficiency of RET strongly depends on the distance between the two molecules and it is typically quite inefficient over distances greater than 10 nm. As the dimensions of biomolecules in general are at the same range, RET can be utilized in the detection of biomolecules: if two biomolecules labeled with either a suitable donor or an acceptor are specifically bound to each other, the distance between the labels is short enough to facilitate the RET. Either the increase of sensitized acceptor emission intensity or decreasing donor emission intensity may be monitored. As RET is a close proximity process, the acceptors further away remain "invisible."

The upconversion RET (UC-RET) from a UCP donor shares the valuable characteristics of LRET [167] but also has some extra advantages mainly covered already above. First, the Förster radius R_0 (the distance at which 50 % of the energy is transferred) between the donor and the acceptor is longer for the lanthanides (even $>$7.5 nm) compared to conventional fluorophores and thus allows efficient energy transfer over extended distances. Second, the signal-to-background ratio of

luminescence intensity measurement is improved due to the elimination of autofluorescence (with spectral separation or temporal resolution), which enables detection of lower signal levels corresponding to relatively large distances (potentially four times the R_0). As a consequence, the distance between the donor and the bound acceptor may be a bit longer than is generally the case with non-lanthanide donors. Third, the NIR excitation source for the UCP donor is incapable of directly exciting the acceptor fluorophores, and the observed acceptor emission originates entirely from those acceptors excited through the UCPs.

Nano-sized UCPs (preferably <50 nm) should be favored over larger UCP donors in UC-RET applications as the emitting ions far away from the surface are not able to participate in the RET process. Instead, they increase the background emission mainly originating from the unbound acceptors reabsorbing the UCP emission through a photon-mediated way, which is especially prominent in the case of UCP particles having a relatively large volume compared to the surface area. Our research group concluded based on luminescence lifetime data that both nonradiative UC-RET and photon reabsorption were present in a system involving UCP donor with average diameter around 110 nm [168]. As the quantity of the photon reabsorption is concentration dependent, it is possible to maximize the signal-to-background ratio of the homogeneous RET-based assay by carefully optimizing the donor and acceptor concentrations. Additionally, the relevance of reaction volume in the UC-RET-based assays has been discussed in paper by Vuojola et al. [169]. The volume outside the excitation beam does not produce any signal specific for the analyte but increases the probability of photon reabsorption and thus causes elevated background.

Several studies exploiting the UCPs as RET donors have been published since 2005 (Table 3). Two research groups independently submitted their first reports of the UC-RET within a few weeks, both using the strong binding affinity of biotin and (strept)avidin [170, 171] to bring the donor and the acceptor into close proximity. Wang et al. [94] utilized the absorption properties of gold nanoparticles to quench the green emission of nano-sized β-$NaYF_4$:Yb^{3+},Er^{3+} crystals, and they were able to detect 0.5–370 nM avidin concentrations with a sandwich-type bioaffinity assay (Fig. 8a). The UCP emission was quenched as much as 70 % (corresponding to 3.3-fold change) in tandem with the increasing avidin concentration, but due to lacking control experiments it is unclear how strong are the nonspecific effects (e.g., inner filter effect). Kuningas et al. [75] measured the amount of biotin by following the sensitized emission intensity of a fluorescent B-phycoerythrin acceptor in a competitive bioaffinity assay (Fig. 8b). The submicrometer-sized UCP crystals were physically bead-milled from a bulk La_2O_2S:Yb^{3+},Er^{3+} or Y_2O_2S:Yb^{3+}, Er^{3+} material. Regardless of the less optimal UCPs, a similar detection limit (below 0.5 nM) was achieved. Increasing analyte concentration resulted in a greater than tenfold signal modulation.

Later, Kuningas et al. developed the previous proof-of-principle into a competitive immunoassay for estradiol hormone (17β-estradiol, E2) [172]. The assay was modified to be totally compatible with whole blood samples by introducing a far-red acceptor matching with the red emission band (~660 nm) of the UCP

Table 3 Examples of homogeneous bioaffinity assays based on UCP labels

Analyte	Type of assay	Acceptor	Limit of detection	UCP material (coating, diameter)	Reference
Ligand binding assays					
Avidin (model assay)	Sandwich-type	Colloidal gold (quencher)	0.5 nM	$NaYF_4$:Yb,Er (LbL, Ø 50 nm)	[94]
Biotin (model assay)	Competitive	B-phycoerythrin	<0.5 nM	La_2O_2S:Yb,Er[a] (PAA, Ø 300 nm)	[75]
Immunoassays					
17β-estradiol (hormone)	Competitive	Oyster 556	<0.5 nM	La_2O_2S:Yb,Er[a] (PAA, Ø 280 nm)	[172]
		AlexaFluor 680	<0.5 nM	La_2O_2S:Yb,Er[a] (PAA, Ø 390 nm)	[107]
IgG (immune response)	Sandwich-type	Colloidal gold (quencher)	5.9 nM	$NaYF_4$:Yb,Er (silica, Ø 47 nm)	[176]
Nucleic acid detection					
Target DNA (26 nt)	Sandwich hybridization	TAMRA	1.3 nM	$NaYF_4$:Er (silica)	[179]
Target DNA (30 nt)	Sandwich hybridization	TAMRA	10 nM	$NaYF_4$:Yb,Er (oleic acid, Ø 13 nm)	[187]
HLA-B27 allele (auto-immune disease) and β-actin gene (housekeeping)	Sandwich hybridization, dual-parameter	AlexaFluor 680, AlexaFluor 546	<0.35 nM (<28 fmol)	$NaYF_4$:Yb,Er (PAA, Ø 300 nm)	[180]
Mutant hemoglobin β chain (HBB) gene	Sandwich hybridization	TAMRA	0.6 nM (120 fmol)	$NaYF_4$:Yb,Er (silica, Ø 72 nm)	[178]
	Direct hybridization	SYBR Green I (intercalating dye)	0.1 nM (20 fmol)	$NaYF_4$:Yb,Tm (DTPA, Ø 45 nm)	[87]
Assays involving aptamer binders					
ATP (coenzyme)	Conformation change of aptamer	Graphene oxide (quencher)	80 nM	$NaYF_4$:Yb,Er (PAA, Ø 29 nm)	[182]
Thrombin (coagulation agent)	Conformational change of aptamer	Carbon nanoparticles (quencher)	0.18 nM	$NaYF_4$:Yb,Er (PAA, Ø 50 nm)	[184]
OTA and FB_1 (mycotoxins)	Conformation change of aptamer	Graphene oxide (quencher)	0.05 nM (OTA), 0.14 nM (FB_1)	$BaYF_5$:Yb,Er/Tm (silica, Ø 35 nm)	[183]

(continued)

Table 3 (continued)

Analyte	Type of assay	Acceptor	Limit of detection	UCP material (coating, diameter)	Reference
Enzyme activity assays					
Benzonase (endonuclease)	Enzymatic cleavage	AlexaFluor 680–BBQ 650 (internally quenched)	0.01 U	$NaYF_4$:Yb,Er (PAA, Ø 340 nm)	[97]
Matrix metalloproteinase-2 (degradation)	Enzymatic cleavage	Carbon nanoparticles (quencher)	1.4×10^{-4} nM	$NaYF_4$:Yb,Er (PEI, Ø 40 nm)	[185]
Caspase-3 (apoptosis mediator) inhibitor	Enzymatic cleavage	AlexaFluor680–BHQ-3 (internally quenched)	~10 nM	$NaYF_4$:Yb,Er (silica, Ø 80 nm)	[169]
Carbohydrate assays					
Mannose (sugar)	Competitive lectin recognition	Rhodamine	–	$NaGdF_4$:Yb,Er (dendrimer, Ø 25 nm)	[188]
Glucose (sugar)	Competitive lectin recognition	Graphene oxide (quencher)	25 nM	$NaYF_4$:Yb,Er (PAA, Ø 50 nm)	[189]
		Colloidal gold (quencher)	43 nM	$NaYF_4$:Yb,Er (PAA, Ø 30–60 nm)	[190]
Other assays					
Hg^{2+} (metal ion)	Metal-assisted nucleic acid pairing	SYBR Green I (intercalating dye)	0.06 nM	$NaYF_4$:Yb,Tm (DTPA, Ø 45 nm)	[181]
		Graphene oxide (quencher)	0.5 nM	$NaYF_4$:Yb,Er (PAA, Ø 29 nm)	[182]
Glutathione (antioxidant)	Switch	MnO_2 nanosheet (quencher)	900 nM	$NaYF_4$:Yb,Tm@ $NaYF_4$ (oxidized ligand, Ø 30 nm)	[191]

ATP adenosine triphosphate, *BHQ-3* Black Hole Quencher 3, *BBQ650* Black-Berry Quencher 650, *DTPA* diethylenetriaminepentaacetic acid, *FB_1* fumonisin B_1, *HLA-B27* human leukocyte antigen B27, *LbL* layer-by-layer coating, *OTA* ochratoxin A, *PAA* poly(acrylic acid) coating, *PEI* poly(ethylenimine)

[a]Ground UCP bulk material

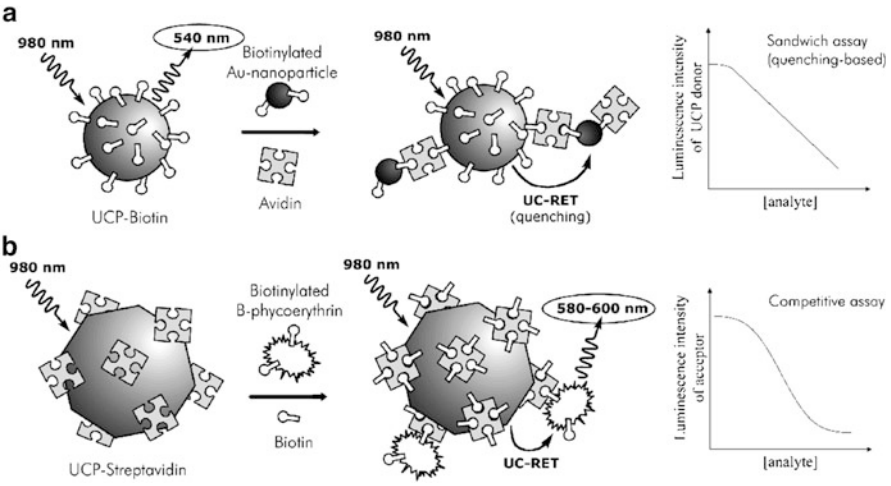

Fig. 8 Principles of the first upconversion RET-based assays. (**a**) Sandwich-type assay for detection of avidin [94]. Presence of avidin results in linearly decreasing UCP emission intensity due to quenching of close proximity gold nanoparticles. (**b**) Competitive assay for biotin [75]. Biotin blocks the binding of the biotinylated acceptor fluorophore, resulting in a sigmoidal inhibition curve with decreasing sensitized emission intensity along with increasing biotin concentration

[107]. No reduction of overall emission intensity was observed in strongly red-colored blood when compared to the colorless buffer solution, because wavelengths only above the absorption range of blood were utilized. The simple homogeneous assay principle and minimal sample pretreatment appears to be a smart combination for low-resource and fast-operating applications.

Sandwich-type assays can be utilized to quantify analytes capable of binding simultaneously with two specific biomolecules. Immunoassays based on RET between the components of the sandwich complex are almost nonexistent because the massive size of the antibodies (length around 10 nm [173]) prevents close proximity of the donor and the acceptor. However, surface energy transfer (SET) from dipole to a metallic surface (e.g., colloidal gold) enables efficient energy transfer up to 25-nm distance [174, 175] and allows detection of protein-sized molecules. The distance dependence of SET is R^{-4} while the Förster-type RET is more dependent on distance (R^{-6}). Wang et al. [176] demonstrated the quantification of immunoglobulin G with a sandwich-type immunoassay utilizing a UCP donor (diameter ~50 nm) and gold nanoparticle quenchers bridged by a sandwich complex, which was likely to have dimensions greater than typical LRET distance. Surprisingly successful quenching efficiency (maximally 80 %) was achieved, which is consistent with the similar avidin assay discussed above [94].

RET-based sandwich assays in nucleic acid detection are easier to realize than immunoassays, as the length of one nucleotide unit is only approximately 0.33 nm [177] and the distance between adjacent hybridization probes is in the range of typical RET. An oligonucleotide sensor detecting a point mutation associated with sickle cell disease [178] was developed based on an earlier proof-of-principle sandwich hybridization assay [179]. In the further advanced version, the rhodamine

(TAMRA) acceptor was replaced by a DNA-intercalating dye (SYBR Green I cyanine dye) [87]. The fluorescence quantum yield of the intercalating dye increases significantly when bound to a double-stranded DNA compared to a single-stranded one, and an increase in sensitized acceptor emission intensity was observed. The LOD (0.1 nM) of this simple sensor was close to that our group achieved with a traditional sandwich-type hybridization assay (LOD <0.35 nM) [180]. The SYBR Green I absorbs at blue wavelengths and, therefore, Yb^{3+}–Tm^{3+}-doped UCPs were used as donors. If the UCPs were omitted from the sensor system and the NIR excitation was replaced with visible light, the LOD was impaired by a factor of 3500, highlighting the advantages of the UCP labels. Another application based on UC-RET to SYBR Green I was constructed to detect the presence of Hg^{2+} ions [181]. A thymine-rich oligonucleotide conjugated with the UCP remains single stranded in the absence of mercury at 50 °C, but the thymine–Hg^{2+}–thymine coordination chemistry induces formation of a double-stranded hairpin structure, giving rise to the sensitized acceptor emission intensity. A detection limit for mercury was reported to be 0.06 nM.

Specifically selected oligonucleotides, aptamers, bind also targets other than complementary nucleic acid strands and may be used as binders instead of antibodies. Aptamer–UCP conjugates were utilized in detection of small molecules [182, 183] as well as larger proteins [184]. In addition to the target molecule, aptamers have affinity toward nano-sized carbon materials with sp^2 electronic structure (e.g., graphene oxide sheets, carbon nanoparticles) due to a strong π–π stacking effect. The carbon material absorbs strongly at visible wavelengths and quenches the emission of UCPs in proximity. The conformational change of an aptamer upon binding of the target molecule (e.g., adenosine triphosphate, thrombin, or mycotoxin) weakened the interaction between the carbon material and aptamer releasing the UCPs from influence of the quencher, which was observed as a recovered UCP emission.

Separation of the RET partners due to enzymatic cleavage provides a useful way to monitor enzyme activity. Double-labeled substrate molecule allows RET while in the intact form, but cleavage results in recovery of the donor luminescence. Enzyme activity assays utilizing both nucleic acid substrates and peptide substrates have been demonstrated. The carbon nanoparticle quenchers used by Wang et al. [185] utilized SET and were capable of quenching the emission of the nano-sized UCPs with a maximal efficiency of 80 %, which was an acceptable magnitude for the assay. Our group used organic quencher molecules, which unfortunately had no effect on the emission intensity of the submicrometer-sized UCPs and a chain-like energy transfer system was constructed to solve the quenching issue. The UCP donors were coupled with an additional fluorophore whose emission intensity was modulated by the presence of the quencher [97, 169]. Consequently, the sensitized emission of the fluorophore was quenched with high efficiency (>95 %).

To summarize, subnanomolar (<1 nM) detection limits are typical for the assay concepts based on the UC-RET. The analyte types vary from proteins and hormones to carbohydrates, oligonucleotides, toxins, enzymes, and even metal ions. Also multiparametric detection has been demonstrated to quantitatively identify two

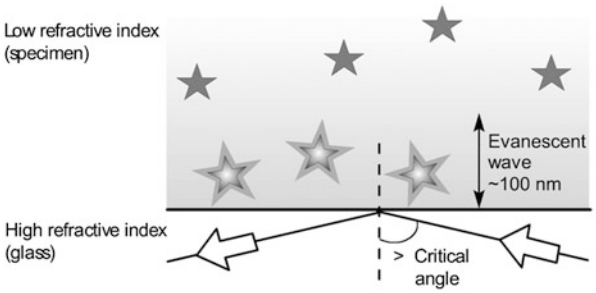

Fig. 9 Evanescent wave excitation. Only those fluorophores near the interface of the two materials are excited. The *white arrows* indicate incident and reflected light

analytes at the same time [180, 183]. Green-, red-, and blue-emitting Er^{3+} and Tm^{3+} activators have been utilized as energy donors and the selection of used acceptors is extensive: organic fluorophores, fluorescent proteins, intercalating dye, colloidal gold, and various nanostructures. The UC-RET to quantum dots has also been shown in heterostructures containing UCPs, but these specific examples did not involve a direct bioanalytical scope [95, 186].

7.4.2 Evanescent Wave Coupling

When light is totally internally reflected at the interface between the materials of high and low refractive index (e.g., glass and liquid), an electromagnetic field called an evanescent wave is formed at the interface. The wavelength of the evanescent wave is identical with the original light source, and its intensity decays exponentially when the distance to the interface increases. This phenomenon has been utilized in the total internal reflection fluorescence microscopy from the 1980s (for review see Fish [192]). The evanescent wave can transfer energy to fluorescent species that are typically within ~100 nm from the surface (Fig. 9) [193]. Morgan and Mitchell have modified the technique by introducing an upconverting glass-ceramic called "Yaglass" [120]. The Yb^{3+}–Er^{3+} doped optically transparent material is primarily based on a lead fluoride and enables the use of NIR radiation. The custom-made planar "Yaglass" waveguides are 200 μm thick and covered with a thin protective titanium dioxide layer (50 nm).

Evanescent wave excitation-mediated energy transfer from the upconverting glass to surface-bound fluorophores was first demonstrated with an amine-modified "Yaglass" and carboxylated fluorescent beads [120]. A straightforward bioaffinity assay can be carried out on the surface of the "Yaglass," in principle, without any washing steps. The presence of avidin was detected on the "Yaglass" by monitoring the fluorescence of the formed sandwich complex comprising a biotinylated fluorescent protein, R-phycoerythrin [121]. Response to different analyte concentrations was not shown, and no estimations about the detection limit have been reported.

The evanescent wave coupling allows longer distances (~100 nm) compared to the short-range interactions of RET (~10 nm); hence it is anticipated that this

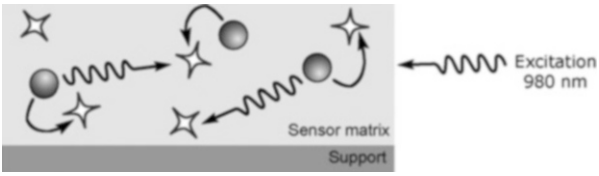

Fig. 10 Principle of optical sensors based on UCPs. The thin, reversible sensor matrix consisting of UCPs (*gray spheres*) and probes (*white stars*) is formed on the support material. The characteristics of the probe (e.g., absorption spectrum or fluorescence intensity) are affected by the surrounding environment (e.g., pH, O_2). The probe molecules, in turn, modulate the UCP emission somehow (e.g., quenching of UCP emission or emergence of sensitized acceptor emission). The *curly arrows* indicate photon-mediated processes and the *bent arrows* nonradiative UC-RET processes

technique could be utilized even in detection of large analytes (such as viruses) by sandwich-type assays. Based on Morgan and Mitchell, the final application could be a microplate format with an upconverting waveguide formed on the base of each well. Another option would be a non-planar assay format involving microsphere resonators or ring resonators. The main challenge for this technique is to find an easy route to produce low-cost upconverting surfaces.

7.5 Optical Sensors

Sensors reversibly respond to the presence of the analyte and convert the quantity into a measurable signal. Prof. Wolfbeis with his research group (University of Regensburg, Germany) has developed several sensor systems based on UCPs combined with compounds sensitive to either pH or oxygen. The UCP material ($NaYF_4$:Yb^{3+},Er^{3+}/Tm^{3+}) and the probe are both incorporated in a layer of suitable matrix to form a thin sensor film (typical thickness a few μm) (Fig. 10). The UCPs are acting as energy donors, but in this case the photon-mediated radiative energy transfer is exploited in addition to the close proximity RET.

Separate sensors for pH [194], ammonia [195], and carbon dioxide [196] were based on various pH-sensitive probes, whose absorption band shifts in line with the pH changes (Table 4). As a result, the UCP emission was either quenched or recovered when the analyte concentration increased. The CO_2 sensor was especially targeted at monitoring a low concentration range suitable for clinical and respiratory applications. The ammonia sensor was designed for environmental and industrial monitoring. A proton-impermeable polystyrene matrix was used in the ammonium and the CO_2 sensors to block the effects of environmental pH changes, while the sensor matrix for pH monitoring was constructed from a nonselective polyurethane hydrogel. Recently, a similar pH sensor with a proton selective matrix was developed in Nanjing University (China) [108]. This sensor operated also in diluted whole blood samples and served as a basis for other sensors responding to either Na^+ or Ca^{2+} ions.

Table 4 Examples of UCP-based sensors

Analyte	Probe	Way of action	Response range	Special	UCP material (diameter)	Reference
pH	Bromothymol blue (dark quencher)	pH-induced red shift of absorption quenches the green and red UCP emission	pH 6–10	–	$NaYF_4$:Yb,Er (50 nm × 950 nm)	[194]
	Nile Blue derivative (fluorophore)	pH-induced blue shift of absorption quenches the green and recovers the red UCP emission	pH 6–11	Ratiometric detection; operates in diluted whole blood	$NaYF_4$:Yb,Er (200 nm × 1,000 nm)	[108]
NH_3	Phenol red (dark quencher)	pH-induced red shift of absorption quenches green UCP emission	1–20 mM (40–800 ppm)	Ratiometric detection	$NaYF_4$:Yb,Er (200 nm × 1,000 nm)	[195]
CO_2	Bromothymol blue (dark quencher)	pH-induced blue shift of absorption recovers UCP emission	0.11 to <3 %	–	$NaYF_4$:Yb,Er (Ø 40–100 nm)	[196]
O_2	Iridium(III) complex (fluorophore)	Oxygen quenches the emission of Ir^{3+} complex	–	Ratiometric detection	$NaYF_4$:Yb,Er (200 nm × 1,000 nm)	[197]
Hg^{2+}	Ruthenium(II) complex (fluorophore)	Hg^{2+}-induced blue shift of absorption recovers the green UCP emission	0.1–45 μM (2–900 ppm)	Ratiometric detection; not reusable	$NaYF_4$:Yb,Er (200 nm × 1,000 nm)	[200]
CN^-	Iridium(III) complex (fluorophore)	CN^--induced drop in absorbance recovers the green UCP emission	0.18–100 μM	Ratiometric detection; not reusable	$NaYF_4$:Yb,Er (200 nm × 1,000 nm)	[198]
			38–600 μM	Ratiometric detection; not reusable	$NaYF_4$:Yb,Er (200 nm × 1,000 nm)	[199]
Temperature	UCP (luminescent)	Temperature affects the intensity ratios of the emission bands	25–45 °C	Ratiometric detection (I_{525nm}/I_{545nm}); intracellular sensing	$NaYF_4$:Yb,Er (200 nm × 1,000 nm)	[201]
			18–33 °C	Ratiometric detection (I_{539nm}/I_{651nm}); intracellular sensing	$NaYF_4$:Yb,Er (Ø ~100 nm)	[202]

Continuous monitoring of the analyte concentration is possible with these reversible sensors

The UC-RET-based oxygen sensor [197] involved a fluorescent iridium(III) complex, whose emission is sensitive to oxygen quenching. The presence of oxygen was detected based on decrease of UC-RET-induced iridium emission. The luminescent species were mounted in a thin oxygen-permeable ethyl cellulose matrix (2 μm). However, low response to oxygen was achieved probably due to the limited accessibility of oxygen and local heating. Chromophoric complexes were also exploited by the group of Prof. Li Fu-You (Fudan University, China). They have investigated several UCP-based sensor systems in solution phase without a polymer matrix (non-reusable sensors). The probe has been simply assembled on the surface of UCPs. Cyanide anion was detected with a system involving iridium(III) complex [198, 199] and Hg^{2+} ion with ruthenium(II) complex [200].

A completely different UCP-based sensor responds to temperature changes in physiological temperature range [201, 202]. No probes are involved, but the upconversion efficiency of the UCPs themselves is temperature dependent. The rate of nonradiative relaxations increases with the raising temperature and results in decreased luminescence intensity. Different transitions have a different dependence, and therefore a ratiometric reading can be used to rule out other variables affecting the emission intensity. The functionality of upconverting nanothermometers was demonstrated in intracellular temperature measurements [201, 202].

8 Instrumentation for Detecting the UCP Emission

The readers for the bioanalytical applications based on UCPs can generally be divided into four categories: optical scanners, imagers, spectrofluorometers, and plate readers. The *scanners* are used for reading the UCP emission from array-type platforms or across the LF strip either in a one-dimensional (progress longitudinally along the strip) or a two-dimensional (2D; raster scanning) manner. The *imagers* (including microscopes) are optional readers for the arrays that capture the UCP emission from a larger area without the need for scanning. Microscopes for small-animal imaging purposes are reviewed elsewhere [12]. The *spectrofluorometers* are applied for measuring the emission from a solution placed into a transparent cuvette (commonly 90° detection geometry), which limits the use only in homogeneous assays or in assays performed on magnetic beads. The *plate readers* typically collect the UCP emission from each microtiter well (e.g., standard 96- and 384-well plates) for a certain short period of time and enable fast data collection from a large number of individual samples. In addition to high throughput, the plate readers allow smaller sample volumes compared to standard cuvettes and due to epi-illumination also non-transparent plastic materials may be used.

Commercial readers for UCPs are not available at the moment, but several prototypes have been introduced in the literature (Table 5). Actually, the portable UP*link*™ analyzer from OraSure Technologies [161] was commercially launched, but the company has replaced the test platform designed for drugs of abuse with other products not related to the UCPs. Commonly, the research groups have

utilized standard spectrofluorometers equipped with an appropriate external excitation source (omitted from Table 5). Similarly, FluoroCount™ [139, 140] and Plate Chameleon™ fluorometers [136, 203] have been modified by changing certain components resulting in dedicated instrumentation for UCP detection. The cuvette-based multiparameter measurement apparatus developed at Chinese Academy of Sciences (Shanghai, China) has a special feature as it is has been designed to quantify the UCP concentration based on scattering in addition to luminescence measurement [204]. Both quantification modes were shown to provide more reliable results if transmittance of the sample was used for compensating the excitation source fluctuation.

The nonlinear relationship between the excitation power density and UCP emission intensity (Fig. 2) is worth consideration when choosing an excitation source. Laser diodes (LDs) provide a narrow, coherent excitation beam that is more easily focused on a small area compared to broad-area excitation sources such as Xenon lamps, and thus LDs can provide a significantly higher power density. The emission bandwidth of an LD is typically only a few nanometers, which could be a limiting factor, but as suitable LDs emitting at ~980 nm are available, it may be regarded solely as an advantage in this case. The compact light emitting diodes (LEDs) also provide fairly narrow emission bandwidths (around tens of nanometers), and they operate with low power consumption, but the beam quality is not competitive with the LDs due to low spatial coherence [205]. Therefore, the LDs predominate in the instrumentation constructed for the UCPs. Affordable continuous wave LDs are commonly available from various commercial suppliers. They are offered with different output powers, and one may also choose a fiber-coupled diode or a diode equipped with a cooler (e.g., peltier element). A respectable LD for the UCP-based bioanalytical applications can be purchased with only a few hundred Euros, and portable laser pointers for the on-site applications are in the same price category. The decentralized analyzers intended for POCT are a special market segment particularly calling for reasonable pricing.

The PlateChameleon Imager [136] has a significantly more powerful LD compared to the other instruments in Table 5. The high power is required to compensate the low power density due to a relatively large illumination area covering a standard microwell bottom. A more valid value in Table 5 would be the power density (W/cm^2) instead of the laser output power, but unfortunately that information is not available.

The detector for the UCP emission is more commonly a photomultiplier tube (PMT) than a silicon-based detector [e.g., a charge-coupled device (CCD) or photodiode (PD)], due to its superior sensitivity, marginal noise level, and lower response toward NIR radiation [162, 205]. The continuous NIR excitation is much more intense compared to the visible emission of the UCPs, and although optical filters are used for blocking the NIR radiation from the detector, it is an advantageous feature that the detector itself naturally filters out unwanted wavelengths originating from the excitation source. The silicon-based detectors are approximately 100 times more responsive to NIR photons than the PMTs. However, the most significant feature of the PMT is the signal amplification, which allows

Table 5 List of some instruments used for reading the UCP emission in bioanalytical applications

Instrument	Manufacturer[a]	Max. excitation power output	Detector	Measurement time	Resolution	CV	Ref.
Optical scanners for LF strips							
Modified FluoroCount™	Packard Instruments	1.2 W (LD)	PMT	–	91 μm	<7 %	[110, 139, 140]
Portable UP*link*™	OraSure Technologies	1 W (LD)	PMT	–	–	–	[161]
Handheld sensor, battery-operated	(Research group)	1.5 W (LD)	PMT	–	–	–	[131]
Portable scanner	(Research group)	0.05 W (LD)	PMT	1 min per strip	20 μm	<5 %	[150, 151]
2D scanner	(Research group)	1.2 W (LD)	PMT	8 min per strip	20 μm 500 μm	<2 %	[162]
Instrumentation for reading arrays							
Modified DM epifluorescence microscope	Leica	75 W (Xenon lamp)	CCD camera	5 min	–	–	[110, 135]
Biochip Scanner	(Research group)	0.25 W (LD)	CCD camera	–	–	–	[134]
Modified PlateChameleon™ microwell imager	Hidex	8 W (LD)	CCD camera	1–30 s per well	–	–	[136]
Optical reading of UCP concentration from cuvette							
Multiparameter measurement apparatus	(Research group)	0.08 W (LD)	PMT (luminescence), PD (scattering and transmittance)	–	n/a	<15 %	[204]
Plate readers							
Modified PlateChameleon™ reader	Hidex	0.2 W (LD)	PMT	2 s per well	n/a (500 μm)	–	[203]

LD laser diode, *CV* coefficient of variation, *LF* lateral flow, *2D* two-dimensional, *PD* photodiode, *PMT* photomultiplier tube, *CCD* charge-coupled device, *n/a* not applicable, – not reported

[a]Industrial manufacturer of the original instrument (without modifications)

detection of minute amounts of photons. Conspicuously, all instruments aimed for array platforms in Table 5 are equipped with CCD cameras. A 2D image may be produced either by scanning the desired area point by point or by utilizing a two-dimensional matrix of detector elements (e.g., CCD), of which the latter usually operates quicker.

The measurement time per single sample varies according to the number of data points collected. Scanning the LF strips takes some time, rendering the LF assays therefore more suitable for individual testing, while the microtiter plate-based assays fit well with the high-throughput applications providing results rapidly. The substantially long time required for 2D raster scanning of the LF strips provides a large number of data points and allows therefore more sophisticated data analysis for the subtraction of the background signal and for the reduction of the random errors resulting from an inhomogeneous UCP distribution on each strip [162]. However, the 8-min data acquisition time for one LF strip is acceptable only for occasional testing—it is inconvenient for other applications.

The technological solutions for the anti-Stokes photoluminescence readers have been existing for a long time. It provides a lead over the other merging labels producing conventional fluorescence upon NIR excitation (e.g., molecular Yb^{3+} complexes and inorganic Yb^{3+}-doped nanocrystals [206–208]), because good detectors for such high wavelengths are still in the development stage. Solid-state NIR detectors are available, but the sensitivity of, for example, PMTs is not adequate at NIR wavelengths.

9 Conclusions

The UCP technology with its special photoluminescent features theoretically provides an opportunity for ultrasensitive detection of analyte molecules with simple instrumentation. The potential of the UCPs has already been demonstrated in various proof-of-principle studies. Today, one of the major problems related to UCP technology has been solved, as the recent development in the synthesis of the nanocrystalline UCPs has enabled the replacement of the bulk materials. Although the surface functionalization of the UCPs remains a challenge, as with other inorganic labels (e.g., quantum dots), several optional coating methods have been reported providing a broad selection for various applications. Instrumentation for reading the UCP emission is not yet commonly available, but the elements and the technological solutions exist to enable the potential commercial exploitation of the UCP technology.

The demands for the UCPs utilized in *in vivo* intracellular applications (e.g., particle size <10 nm, non-toxicity, intensive emission) are even higher than those required in *in vitro* bioanalytical assays described in this review. Undoubtedly, the future research in material sciences will aim to ever brighter UCPs that form stable colloids in aqueous solutions. Discovery of new UCP materials is pursued and the materials known today are extensively studied to find controlled ways for tuning

the optical properties, structure, and size of the UCPs. In addition, cooperation with bioscience expertise is needed to transform the UCP material into biocompatible label conjugates—the tools for analyte detection and visualization.

Acknowledgments The authors wish to thank Dr. Paul Corstjens and Jan Slats (Leiden University Medical Center, the Netherlands) for microscopy examination of the PTIR550/F material. Financial support from the Research Executive Agency (REA) of the European Union under Grant Agreement number PITN-GA-2010-264772 (ITN CHEBANA) is gratefully acknowledged.

References

1. Ekins R (1998) Ligand assays: from electrophoresis to miniaturized microarrays [Review]. Clin Chem 44(9):2015–2030
2. Junker R, Schlebusch H, Luppa PB (2010) Point-of-care testing in hospitals and primary care [Review]. Dtsch Arztebl Int 107(33):561–567
3. Ouellette AL, Li JJ, Cooper DE, Ricco AJ, Kovacs GTA (2009) Evolving point-of-care diagnostics using up-converting phosphor bioanalytical systems [Review]. Anal Chem 81(9):3216–3221
4. He GS, Tan LS, Zheng Q, Prasad PN (2008) Multiphoton absorbing materials: molecular designs, characterizations, and applications [Review]. Chem Rev 108(4):1245–1330
5. Hänninen P, Soukka J, Soini JT (2008) Two-photon excitation fluorescence bioassays. Ann NY Acad Sci 1130:320–326
6. Auzel F (2004) Upconversion and anti-Stokes processes with *f* and *d* ions in solids [Review]. Chem Rev 104(1):139–173
7. Kaiser W, Garrett C (1961) Two-photon excitation in CaF_2: Eu^{2+}. Phys Rev Lett 7(6):229–231
8. Franken P, Hill A, Peters C, Weinreich G (1961) Generation of optical harmonics. Phys Rev Lett 7(4):118–119
9. Armstrong J, Bloembergen N, Ducuing J, Pershan P (1962) Interactions between light waves in a nonlinear dielectric [Review]. Phys Rev 127(6):1918–1939
10. Denk W, Strickler JH, Webb WW (1990) Two-photon laser scanning fluorescence microscopy. Science 248(4951):73–76
11. Haase M, Schäfer H (2011) Upconverting nanoparticles [Review]. Angew Chem Int Ed 50(26):5808–5829
12. Gnach A, Bednarkiewicz A (2012) Lanthanide-doped up-converting nanoparticles: merits and challenges [Review]. Nano Today 7(6):532–563
13. Mita Y (2007) Infrared up-converting phosphors. In: Yen WM, Shionoya S, Yamamoto H (eds) Phosphor handbook. CRC, Boca Raton, FL, p 775
14. Gamelin DR, Güdel HU (2001) Upconversion processes in transition metal and rare earth metal systems [Review]. Top Curr Chem 214:1–56
15. Bloembergen N (1959) Solid-state infrared quantum counters. Phys Rev Lett 2:84–85
16. Auzel F (1966) Compteur quantique par transfert d'energie entre de Yb^{3+} a Tm^{3+} dans un tungstate mixte et dans verre germanate. C R Acad Sci (Paris) 163:819–821
17. Auzel F (1966) Compteur quantique par transfert d'energie entre deux ions de terres reres dans un tungstate mixte et dans un verre. C R Acad Sci (Paris) 262:1016–1019
18. Chivian JS, Case WE, Eden DD (1979) The photon avalanche: a new phenomenon in Pr^{3+}-based infrared quantum counters. Appl Phys Lett 35:124–125
19. Joubert M, Guy S, Jacquier B (1993) Model of the photon-avalanche effect. Phys Rev B 48(14):10031–10037

20. Morgan CG, Dad S, Mitchell AC (2008) Present status of, and future prospects for, upconverting phosphors in proximity-based bioassay [Review]. J Alloys Compd 451(1–2):526–529
21. Suyver JF, Aebischer A, García-Revilla S, Gerner P, Güdel HU (2005) Anomalous power dependence of sensitized upconversion luminescence [Review]. Phys Rev B 71(12):125123
22. Pollnau M, Gamelin D, Lüthi S, Güdel H, Hehlen M (2000) Power dependence of upconversion luminescence in lanthanide and transition-metal-ion systems [Review]. Phys Rev B 61(5):3337–3346
23. Wang F, Liu X (2009) Recent advances in the chemistry of lanthanide-doped upconversion nanocrystals [Review]. Chem Soc Rev 38(4):976–989
24. Riedener T, Krämer K, Güdel HU (1995) Upconversion luminescence in Er^{3+}-doped $RbGd_2Cl_7$ and $RbGd_2Br_7$. Inorg Chem 34(10):2745–2752
25. Suyver JF, Aebischer A, Biner D, Gerner P, Grimm J, Heer S et al (2005) Novel materials doped with trivalent lanthanides and transition metal ions showing near-infrared to visible photon upconversion. Opt Mater 27(6):1111–1130
26. Zarling DA, Rossi MJ, Peppers NA, Kane J, Faris GW, Dyer MJ (1994) Up-converting reporters for biological and other assays using laser excitation techniques. US Patent PCT/US93/08712
27. Güdel HU (1998) New light-emitting inorganic materials. Chimia 52:561–565
28. Ong LC, Gnanasammandhan MK, Nagarajan S, Zhang Y (2010) Upconversion: road to El Dorado of the fluorescence world [Review]. Luminescence 25(4):290–293
29. Cotton S (2006) Lanthanide and actinide chemistry. Wiley, West Sussex
30. Bünzli JC, Piguet C (2005) Taking advantage of luminescent lanthanide ions [Review]. Chem Soc Rev 34(12):1048–1077
31. Wybourne BG (1965) Spectroscopic properties of rare earths. Interscience Publishers, New York
32. Zhang L, Hu H, Qi C, Lin F (2001) Spectroscopic properties and energy transfer in Yb^{3+}/Er^{3+}-doped phosphate glasses. Opt Mater 17(3):371–377
33. Suyver JF, Grimm J, van Veen MK, Biner D, Krämer KW, Güdel HU (2006) Upconversion spectroscopy and properties of $NaYF_4$ doped with Er^{3+}, Tm^{3+} and/or Yb^{3+}. J Lumin 117(1):1–12
34. Suyver JF, Grimm J, Krämer KW, Güdel HU (2005) Highly efficient near-infrared to visible up-conversion process in $NaYF_4:Er^{3+}$, Yb^{3+}. J Lumin 114(1):53–59
35. Wei Y, Lu F, Zhang X, Chen D (2007) Synthesis and characterization of efficient near-infrared upconversion Yb and Tm codoped $NaYF_4$ nanocrystal reporter. J Alloy Compd 427(1–2):333–340
36. Wang F, Deng R, Wang J, Wang Q, Han Y, Zhu H et al (2011) Tuning upconversion through energy migration in core–shell nanoparticles. Nat Mater 10:968–973
37. Wang J, Wang F, Wang C, Liu Z, Liu X (2011) Single-band upconversion emission in lanthanide-doped $KMnF_3$ nanocrystals. Angew Chem Int Ed 50(38):10369–10372
38. Tian G, Gu Z, Zhou L, Yin W, Liu X, Yan L et al (2012) Mn^{2+} dopant-controlled synthesis of $NaYF_4$:Yb/Er upconversion nanoparticles for *in vivo* imaging and drug delivery. Adv Mater 24(5):1226–1231
39. Zeng JH, Su J, Li ZH, Yan RX, Li YD (2005) Synthesis and upconversion luminescence of hexagonal-phase $NaYF_4:Yb^{3+}$, Er^{3+} phosphors of controlled size and morphology. Adv Mater 17(17):2119–2123
40. Zhang H, Li Y, Lin Y, Huang Y, Duan X (2011) Composition tuning the upconversion emission in $NaYF_4$:Yb/Tm hexaplate nanocrystals. Nanoscale 3(3):963–966
41. Lu W, Cheng L, Zhong H, Sun J, Wan J, Tian Y et al (2010) Dependence of upconversion emission intensity on Yb^{3+} concentration in Er^{3+}/Yb^{3+} co-doped flake shaped $Y_2(MoO_4)_3$ phosphors. J Phys D 43(8):085404
42. Chen G, Ohulchanskyy TY, Kumar R, Ågren H, Prasad PN (2010) Ultrasmall monodisperse $NaYF_4:Yb^{3+}/Tm^{3+}$ nanocrystals with enhanced near-infrared to near-infrared upconversion photoluminescence. ACS Nano 4(6):3163–3168

43. Krämer KW, Biner D, Frei G, Güdel HU, Hehlen MP, Lüthi SR (2004) Hexagonal sodium yttrium fluoride based green and blue emitting upconversion phosphors. Chem Mater 16(7):1244–1251
44. Wang F, Liu X (2008) Upconversion multicolor fine-tuning: visible to near-infrared emission from lanthanide-doped $NaYF_4$ nanoparticles. J Am Chem Soc 130(17):5642–5643
45. Liang L, Wu H, Hu H, Wu M, Su Q (2004) Enhanced blue and green upconversion in hydrothermally synthesized hexagonal $NaY_{1-x}Yb_xF_4:Ln^{3+}$ (Ln^{3+}= Er^{3+} or Tm^{3+}). J Alloys Compd 368(1–2):94–100
46. Boyer JC, van Veggel FC (2010) Absolute quantum yield measurements of colloidal $NaYF_4$: Er^{3+}, Yb^{3+} upconverting nanoparticles. Nanoscale 2(8):1417–1419
47. Page RH, Schaffers KI, Waide PA, Tassano JB, Payne SA, Krupke WF et al (1998) Upconversion-pumped luminescence efficiency of rare-earth-doped hosts sensitized with trivalent ytterbium. J Opt Soc Am B 15(3):996–1008
48. Bril A, Sommerdijk JL, de Jager AW (1975) On the efficiency of Yb^{3+}–Er^{3+} activated up-conversion phosphors. J Electrochem Soc 122(5):660
49. Nyk M, Kumar R, Ohulchanskyy TY, Bergey EJ, Prasad PN (2008) High contrast in vitro and in vivo photoluminescence bioimaging using near infrared to near infrared up-conversion in Tm^{3+} and Yb^{3+} doped fluoride nanophosphors. Nano Lett 8(11):3834–3838
50. Svenmarker P, Xu CT, Andersson-Engels S (2010) Use of nonlinear upconverting nanoparticles provides increased spatial resolution in fluorescence diffuse imaging. Opt Lett 35(16):2789–2791
51. Xu CT, Svenmarker P, Liu H, Wu X, Messing ME, Wallenberg LR et al (2012) High-resolution fluorescence diffuse optical tomography developed with nonlinear upconverting nanoparticles. ACS Nano 6(6):4788–4795
52. Zou W, Visser C, Maduro JA, Pshenichnikov MS, Hummelen JC (2012) Broadband dye-sensitized upconversion of near-infrared light. Nat Photon 6(8):560–564
53. Aebischer A, Hostettler M, Hauser J, Krämer K, Weber T, Güdel HU et al (2006) Structural and spectroscopic characterization of active sites in a family of light-emitting sodium lanthanide tetrafluorides. Angew Chem Int Ed 45(17):2802–2806
54. Yi GS, Chow GM (2007) Water-soluble $NaYF_4$:Yb, Er(Tm)/$NaYF_4$ polymer core/shell/shell nanoparticles with significant enhancement of upconversion fluorescence. Chem Mater 19(3):341–343
55. Hyppänen I, Hölsä J, Kankare J, Lastusaari M, Pihlgren L, Soukka T (2009) Preparation and up-conversion luminescence properties of $NaYF_4:Yb^{3+}$, Er^{3+} nanomaterials. Terrae Rarae 16:1–6
56. Schäfer H, Ptacek P, Eickmeier H, Haase M (2009) Synthesis of hexagonal Yb^{3+}, Er^{3+}-doped $NaYF_4$ nanocrystals at low temperature. Adv Funct Mater 19(19):3091–3097
57. Harju E, Hyppänen I, Hölsä J, Kankare J, Lahtinen M, Lastusaari M et al (2011) Polymorphism of $NaYF_4:Yb^{3+},Er^{3+}$ up-conversion luminescence materials. Zeitschrift für Kristallographie 381–387
58. Renero-Lecuna C, Martín-Rodríguez R, Valiente R, González J, Rodríguez F, Krämer KW et al (2011) Origin of the high upconversion green luminescence efficiency in β-$NaYF_4$:2% Er^{3+},20%Yb^{3+}. Chem Mater 23(15):3442–3448
59. Liang S, Liu Y, Tang Y, Xie Y, Sun H, Zhang H et al (2011) A user-friendly method for synthesizing high-quality $NaYF_4$:Yb,Er(Tm) nanocrystals in liquid paraffin. J Nanomater [Article ID 302364]
60. Li C, Lin J (2010) Rare earth fluoride nano-/microcrystals: synthesis, surface modification and application [Review]. J Mater Chem 20:6831–6847
61. Yi GS, Lu H, Zhao S, Ge Y, Yang W, Chen D et al (2004) Synthesis, characterization, and biological application of size-controlled nanocrystalline $NaYF_4$:Yb,Er infrared-to-visible up-conversion phosphors. Nano Lett 4(11):2191–2196
62. Mathews M, Ambekar BR, Tyagi AK, Köhler J (2004) High temperature X-ray diffraction studies on sodium yttrium fluoride. J Alloy Compd 377(1–2):162–166

63. Yi GS, Chow GM (2006) Synthesis of hexagonal-phase $NaYF_4$:Yb, Er and $NaYF_4$:Yb,Tm nanocrystals with efficient up-conversion fluorescence. Adv Funct Mater 16(18):2324–2329
64. Wang F, Han Y, Lim CS, Lu Y, Wang J, Xu J et al (2010) Simultaneous phase and size control of upconversion nanocrystals through lanthanide doping. Nature 463(7284):1061–1065
65. Ostrowski AD, Chan EM, Gargas DJ, Katz EM, Han G, Schuck PJ et al (2012) Controlled synthesis and single-particle imaging of bright, sub-10 nm lanthanide-doped upconverting nanocrystals. ACS Nano 6(3):2686–2692
66. Heer S, Kömpe K, Güdel HU, Haase M (2004) Highly efficient multicolour upconversion emission in transparent colloids of lanthanide-doped $NaYF_4$ nanocrystals. Adv Mater 16(23–24):2102–2105
67. Wang Y, Tu L, Zhao J, Sun Y, Kong X, Zhang H (2009) Upconversion luminescence of β-$NaYF_4$: Yb^{3+}, Er^{3+}@β-$NaYF_4$ core/shell nanoparticles: excitation power density and surface dependence. J Phys Chem C 113(17):7164–7169
68. Bogdan N, Vetrone F, Ozin GA, Capobianco JA (2011) Synthesis of ligand-free colloidally stable water dispersible brightly luminescent lanthanide-doped upconverting nanoparticles. Nano Lett 11(2):835–840
69. Yu X, Li M, Xie M, Chen L, Li Y, Wang Q (2010) Dopant-controlled synthesis of water-soluble hexagonal $NaYF_4$ nanorods with efficient upconversion fluorescence for multicolor bioimaging. Nano Res 3(1):51–60
70. Dou Q, Zhang Y (2011) Tuning of the structure and emission spectra of upconversion nanocrystals by alkali ion doping. Langmuir 27:13236–13241
71. Cheng Q, Sui J, Cai W (2012) Enhanced upconversion emission in Yb^{3+} and Er^{3+} codoped $NaGdF_4$ nanocrystals by introducing Li^+ ions. Nanoscale 4(3):779–784
72. Sui Y, Tao K, Tian Q, Sun K (2012) Interaction between Y^{3+} and oleate ions for the cubic-to-hexagonal phase transformation of $NaYF_4$ nanocrystals. J Phys Chem C 116(2):1732–1739
73. Zhang C, Sun L, Zhang Y, Yan C (2010) Rare earth upconversion nanophosphors: synthesis, functionalization and application as biolabels and energy transfer donors [Review]. J Rare Earth 28(6):807–819
74. Lin M, Zhao Y, Wang S, Liu M, Duan ZF, Chen YM et al (2012) Recent advances in synthesis and surface modification of lanthanide-doped upconversion nanoparticles for biomedical applications [Review]. Biotechnol Adv 30(6):1551–1561
75. Kuningas K, Rantanen T, Ukonaho T, Lövgren T, Soukka T (2005) Homogeneous assay technology based on upconverting phosphors. Anal Chem 77(22):7348–7355
76. Sanjuro A, Lau KH, Lowe D, Canizales A, Jiang N, Schneider LV et al (2000) Production of substantially monodisperse phosphor particles. Patent 08/986196
77. Li S, Feindt H, Giannaras G, Scarpino R, Salamone S, Niedbala SR (2002) Preparation, characterization, and fabrication of uniform coated $Y_2O_2S:RE^{3+}$ up-converting phosphor particles for biological detection applications. Proc SPIE 4809:100
78. Mai HX, Zhang YW, Si R, Yan ZG, Sun LD, You LP et al (2006) High-quality sodium rare-earth fluoride nanocrystals: controlled synthesis and optical properties. J Am Chem Soc 128(19):6426–6436
79. Boyer JC, Vetrone F, Cuccia LA, Capobianco JA (2006) Synthesis of colloidal upconverting $NaYF_4$ nanocrystals doped with Er^{3+}, Yb^{3+} and Tm^{3+}, Yb^{3+} via thermal decomposition of lanthanide trifluoroacetate precursors. J Am Chem Soc 128(23):7444–7445
80. Boyer JC, Cuccia LA, Capobianco JA (2007) Synthesis of colloidal upconverting $NaYF_4$: Er^{3+}/Yb^{3+} and Tm^{3+}/Yb^{3+} monodisperse nanocrystals. Nano Lett 7(3):847–852
81. Ye X, Collins JE, Kang Y, Chen J, Chen DTN, Yodh AG et al (2010) Morphologically controlled synthesis of colloidal upconversion nanophosphors and their shape-directed self-assembly. Proc Natl Acad Sci USA 107(52):22430–22435
82. Cheng L, Yang K, Shao M, Lee ST, Liu Z (2011) Multicolor in vivo imaging of upconversion nanoparticles with emissions tuned by luminescence resonance energy transfer. J Phys Chem C 115(6):2686–2692

83. Shan J, Ju Y (2009) A single-step synthesis and the kinetic mechanism for monodisperse and hexagonal-phase $NaYF_4$:Yb, Er upconversion nanophosphors. Nanotechnology 20(27):275603
84. Rufaihah AJ, Zhang Y (2008) Biocompatibility of silica coated $NaYF_4$ upconversion fluorescent nanocrystals. Biomaterials 29:4122–4128
85. Zhang SZ, Sun LD, Tian H, Liu Y, Wang JF, Yan CH (2009). Reversible luminescence switching of $NaYF_4$:Yb,Er nanoparticles with controlled assembly of gold nanoparticles. Chem Commun (18):2547–2549
86. Ma DK, Huang SM, Yu YY, Xu YF, Dong YQ (2009) Rare-earth-ion-doped hexagonal-phase $NaYF_4$ nanowires: controlled synthesis and luminescent properties. J Phys Chem C 113(19):8136–8142
87. Kumar M, Zhang P (2009) Highly sensitive and selective label-free optical detection of DNA hybridization based on photon upconverting nanoparticles. Langmuir 25(11):6024–6027
88. Vetrone F, Naccache R, Morgan CG, Capobianco JA (2010) Luminescence resonance energy transfer from an upconverting nanoparticle to a fluorescent phycobiliprotein. Nanoscale 2(7):1185
89. Shan J, Qin X, Yao N, Ju Y (2007) Synthesis of monodisperse hexagonal $NaYF_4$:Yb, Ln (Ln = Er, Ho and Tm) upconversion nanocrystals in TOPO. Nanotechnology 18(44):445607
90. Li Z, Zhang Y (2006) Monodisperse silica-coated polyvinylpyrrolidone/$NaYF_4$ nanocrystals with multicolor upconversion fluorescence emission. Angew Chem Int Ed 45(46):7732–7735
91. Haase M, Haubold S, Ibarra F, Meysamy H, Riwotzky C, Weller H (2002) Synthesis of nanoparticles. Patent PCT/DE01/03433
92. Lehmann O, Meyssamy H, Kömpe K, Schnablegger H, Haase M (2003) Synthesis, growth, and Er^{3+} luminescence of lanthanide phosphate nanoparticles. J Phys Chem B 107(30):7449–7453
93. Heer S, Lehmann O, Haase M, Güdel HU (2003) Blue, green, and red upconversion emission from lanthanide-doped $LuPO_4$ and $YbPO_4$ nanocrystals in a transparent colloidal solution. Angew Chem Int Ed 42(27):3179–3182
94. Wang L, Yan R, Huo Z, Wang L, Zeng J, Bao J et al (2005) Fluorescence resonant energy transfer biosensor based on upconversion-luminescent nanoparticles. Angew Chem Int Ed 44(37):6054–6057
95. Li Z, Zhang Y, Jiang S (2008) Multicolor core/shell-structured upconversion fluorescent nanoparticles. Adv Mater 20:4765–4769
96. Chan EM, Xu C, Mao AW, Han G, Owen JS, Cohen BE et al (2010) Reproducible, high-throughput synthesis of colloidal nanocrystals for optimization in multidimensional parameter space. Nano Lett 10:1874–1885
97. Rantanen T, Järvenpää ML, Vuojola J, Kuningas K, Soukka T (2008) Fluorescence-quenching-based enzyme-activity assay by using photon upconversion. Angew Chem Int Ed 47(20):3811–3813
98. Siitari H, Hemmilä I, Soini E, Lövgren T, Koistinen V (1983) Detection of hepatitis B surface antigen using time-resolved fluoroimmunoassay. Nature 301(5897):258–260
99. Hemmilä I, Dakubu S, Mukkala V, Siitari H, Lövgren T (1984) Europium as a label in time-resolved immunofluorometric assays. Anal Biochem 137(2):335–343
100. Waynant RW, Ilev IK, Gannor I (2001) Mid-infrared laser applications in medicine and biology. Philos Trans R Soc Lond A 359:635–644
101. Simpson CR, Kohl M, Essenpreis M, Cope M (1998) Near-infrared optical properties of *ex vivo* human skin and subcutaneous tissues measured using the Monte Carlo inversion technique. Phys Med Biol 43(9):2465–2478
102. Gaigalas AK, Wang L, Vogt RF (2007) Frequency-domain measurement of the photodegradation process of fluorescein. Photochem Photobiol 76(1):22–28
103. Eggeling C, Widengren J, Rigler R, Seidel CAM (1998) Photobleaching of fluorescent dyes under conditions used for single-molecule detection: evidence of two-step photolysis. Anal Chem 70(12):2651–2659

104. Ukonaho T, Rantanen T, Jämsen L, Kuningas K, Päkkilä H, Lövgren T et al (2007) Comparison of infrared-excited up-converting phosphors and europium nanoparticles as labels in a two-site immunoassay. Anal Chim Acta 596(1):106–115
105. Duan C, Meyerhoff ME (1994) Separation-free sandwich enzyme immunoassays using microporous gold electrodes and self-assembled monolayer/immobilized capture antibodies. Anal Chem 66:1369–1377
106. Meyerhoff ME, Duan C, Meusel M (1995) Novel nonseparation sandwich-type electrochemical enzyme immunoassay system for detecting marker proteins in undiluted blood. Clin Chem 41(9):1378–1384
107. Kuningas K, Päkkilä H, Ukonaho T, Rantanen T, Lövgren T, Soukka T (2007) Upconversion fluorescence enables homogeneous immunoassay in whole blood. Clin Chem 53(1):145–146
108. Xie L, Qin Y, Chen HY (2012) Polymeric optodes based on upconverting nanorods for fluorescent measurements of pH and metal ions in blood samples. Anal Chem 84(4):1969–1974
109. Soukka T, Rantanen T, Kuningas K (2008) Photon upconversion in homogeneous fluorescence-based bioanalytical assays. Ann NY Acad Sci 1130:188–200
110. Corstjens PL, Li S, Zuiderwijk M, Kardos K, Abrams WR, Niedbala RS et al (2005) Infrared up-converting phosphors for bioassays [Review]. IEE Proc Nanobiotechnol 152(2):64–72
111. Hu M, Yan J, He Y, Lu H, Weng L, Song S et al (2010) Ultrasensitive, multiplexed detection of cancer biomarkers directly in serum by using a quantum dot-based microfluidic protein chip. ACS Nano 4(1):488–494
112. Peng C, Li Z, Zhu Y, Chen W, Yuan Y, Liu L et al (2009) Simultaneous and sensitive determination of multiplex chemical residues based on multicolor quantum dot probes. Biosens Bioelectron 24(12):3657–3662
113. Soini E, Kojola H (1983) Time-resolved fluorometer for lanthanide chelates–a new generation of nonisotopic immunoassays. Clin Chem 29(1):65–68
114. Bazin H, Trinquet E, Mathis G (2002) Time resolved amplification of cryptate emission: a versatile technology to trace biomolecular interactions. J Biotechnol 82(3):233–250
115. Selvin PR (2002) Principles and biophysical applications of lanthanide-based probes [Review]. Annu Rev Biophys Biomol Struct 31:275–302
116. Eliseeva SV, Bünzli JC (2010) Lanthanide luminescence for functional materials and bio-sciences [Review]. Chem Soc Rev 39(1):189–227
117. Sun LD, Gu JQ, Zhang SZ, Zhang YW, Yan CH (2009) Luminescence resonance energy transfer based on β-$NaYF_4$:Yb,Er nanoparticles and TRITC dye. Sci China Ser B 52(10):1590–1595
118. Bednarkiewicz A, Nyk M, Samoc M, Strek W (2010) Up-conversion FRET from Er^{3+}/Yb^{3+}: $NaYF_4$ nanophosphor to CdSe quantum dots. J Phys Chem C 114(41):17535–17541
119. Wang F, Banerjee D, Liu Y, Chen X, Liu X (2010) Upconversion nanoparticles in biological labeling, imaging, and therapy [Review]. Analyst 135(8):1839–1854
120. Morgan CG, Mitchell AC (2006) Total internal reflection fluorescence imaging using an upconverting cover slip for multicolour evanescent excitation. J Microsc 222(Pt 1):48–57
121. Morgan CG, Mitchell AC (2007) Prospects for applications of lanthanide-based upconverting surfaces to bioassay and detection. Biosens Bioelectron 22(8):1769–1775
122. Zeng SM, Yankowitz J, Widness JA, Strauss RG (2001) Etiology of differences in hematocrit between males and females: sequence-based polymorphisms in erythropoietin and its receptor. J Gend Specif Med 4(1):35–40
123. Davies C (2005) Introduction to immunoassay principles. In: Wild DG (ed) The immunoassay handbook. Elsevier, Oxford, p 3
124. (2012) Description of analytical methods and results. http://www.clinchem.org/site/info_ar/info_authors.xhtml#anal_meth. Accessed 25 Aug 2012
125. Mader HS, Kele P, Saleh SM, Wolfbeis OS (2010) Upconverting luminescent nanoparticles for use in bioconjugation and bioimaging [Review]. Curr Opin Chem Biol 14(5):582–596

126. Wang M, Abbineni G, Clevenger A, Mao C, Xu S (2011) Upconversion nanoparticles: synthesis, surface modification and biological applications [Review]. Nanomed Nanobiotechnol 7(6):710–729
127. Zhou J, Liu Z, Li F (2012) Upconversion nanophosphors for small-animal imaging [Review]. Chem Soc Rev 41:1323–1349
128. Wright WH, Mufti NA, Tagg NT, Webb RR, Schneider LV (1997) High-sensitivity immunoassay using a novel upconverting phosphor reporter. Proc SPIE 2985:248–255
129. Wollenberger LV, Yao YMM, Mufti NA, Schneider LV (1997) Detection of DNA using upconverting phosphor reporter probes. Proc SPIE 2985:100–111
130. Wang L, Li Y (2006) Green upconversion nanocrystals for DNA detection. Chem Commun 24(24):2557–2559
131. Cooper DE, D'Andrea A, Faris GW, MacQueen B, Wright WH (2006) Upconverting phosphors for detection and identification using antibodies. In: Van Emmon JM (ed) Immunoassay and other bioanalytical techniques. CRC, Boca Raton, FL, p 217
132. Kuningas K, Rantanen T, Karhunen U, Lövgren T, Soukka T (2005) Simultaneous use of time-resolved fluorescence and anti-stokes photoluminescence in a bioaffinity assay. Anal Chem 77(9):2826–2834
133. Kuningas K, Rantanen T, Lövgren T, Soukka T (2005) Enhanced photoluminescence of up-converting phosphors in a solid phase bioaffinity assay. Anal Chim Acta 543(1–2):130–136
134. Lu H, Yi G, Zhao S, Chen D, Guo LH, Cheng J (2004) Synthesis and characterization of multi-functional nanoparticles possessing magnetic, up-conversion fluorescence and bio-affinity properties. J Mater Chem 14(8):1336–1341
135. van de Rijke F, Zijlmans H, Li S, Vail T, Raap AK, Niedbala RS et al (2001) Up-converting phosphor reporters for nucleic acid microarrays. Nat Biotechnol 19(3):273–276
136. Ylihärsilä M, Valta T, Karp M, Hattara L, Harju E, Hölsä J et al (2011) Oligonucleotide array-in-well platform for detection and genotyping human adenoviruses by utilizing upconverting phosphor label technology. Anal Chem 83:1456–1461
137. Ylihärsilä M, Harju E, Arppe R, Hattara L, Hölsä J, Saviranta P et al (2013) Genotyping of clinically relevant human adenoviruses by array-in-well hybridization assay. Clin Microbiol Infect 19(6):551–557
138. Päkkilä H, Ylihärsilä M, Lahtinen S, Hattara L, Salminen N, Arppe R et al (2012) Quantitative multianalyte microarray immunoassay utilizing upconverting phosphor technology. Anal Chem 84(20):8628–8634
139. Niedbala RS, Vail TL, Feindt H, Li S, Burton JL (2000) Multiphoton up-converting phosphors for use in rapid immunoassays. Proc SPIE 3913:193–203
140. Niedbala RS, Feindt H, Kardos K, Vail T, Burton J, Bielska B et al (2001) Detection of analytes by immunoassay using up-converting phosphor technology. Anal Biochem 293(1):22–30
141. Hampl J, Hall M, Mufti NA, Yao YM, MacQueen DB, Wright WH et al (2001) Upconverting phosphor reporters in immunochromatographic assays. Anal Biochem 288(2):176–187
142. Kim HS, Pyun JC (2009) Hyper sensitive strip test with chemi-luminescence signal band. Proc Chem 1(1):1043–1046
143. Corstjens PL, van Lieshout L, Zuiderwijk M, Kornelis D, Tanke HJ, Deelder AM et al (2008) Up-converting phosphor technology-based lateral flow assay for detection of *Schistosoma* circulating anodic antigen in serum. J Clin Microbiol 46(1):171–176
144. Corstjens PL, Zuiderwijk M, Tanke HJ, van der Ploeg-van Schip JJ, Ottenhoff TH, Geluk A (2008) A user-friendly, highly sensitive assay to detect the IFN-gamma secretion by T cells. Clin Biochem 41(6):440–444
145. Li L, Zhou L, Yu Y, Zhu Z, Lin C, Lu C et al (2009) Development of up-converting phosphor technology-based lateral-flow assay for rapidly quantitative detection of hepatitis B surface antibody. Diagn Microbiol Infect Dis 63(2):165–172

146. Levicky R, Horgan A (2005) Physicochemical perspectives on DNA microarray and biosensor technologies. Trends Biotechnol 23(3):143–149
147. Corstjens PL, Zuiderwijk M, Brink A, Li S, Feindt H, Niedbala RS et al (2001) Use of up-converting phosphor reporters in lateral-flow assays to detect specific nucleic acid sequences: a rapid, sensitive DNA test to identify human papillomavirus type 16 infection. Clin Chem 47(10):1885–1893
148. Zuiderwijk M, Tanke HJ, Sam NR, Corstjens PL (2003) An amplification-free hybridization-based DNA assay to detect Streptococcus pneumoniae utilizing the up-converting phosphor technology. Clin Biochem 36(5):401–403
149. Corstjens PL, Zuiderwijk M, Nilsson M, Feindt H, Niedbala RS, Tanke HJ (2003) Lateral-flow and up-converting phosphor reporters to detect single-stranded nucleic acids in a sandwich-hybridization assay. Anal Biochem 312(2):191–200
150. Yan Z, Zhou L, Zhao Y, Wang J, Huang L, Hu K et al (2006) Rapid quantitative detection of Yersinia pestis by lateral-flow immunoassay and up-converting phosphor technology-based biosensor. Sens Actuators B Chem 119(2):656–663
151. Huang L, Zhou L, Zhang Y, Xie C, Qu J, Zeng A et al (2009) A simple optical reader for upconverting phosphor particles captured on lateral flow strip. IEEE Sens J 9(10):1185–1191
152. Malamud D, Bau H, Niedbala SR, Corstjens PL (2005) Point detection of pathogens in oral samples. Adv Dent Res 18(1):12–16
153. Corstjens PL, Chen Z, Zuiderwijk M, Bau HH, Abrams WR, Malamud D et al (2007) Rapid assay format for multiplex detection of humoral immune responses to infectious disease pathogens (HIV, HCV, and TB). Ann NY Acad Sci 1098:437–445
154. Chen D, Mauk M, Qiu X, Liu C, Kim J, Ramprasad S et al (2010) An integrated, self-contained microfluidic cassette for isolation, amplification, and detection of nucleic acids. Biomed Microdevices 12(4):705–719
155. Wang J, Chen Z, Corstjens PL, Mauk MG, Bau HH (2006) A disposable microfluidic cassette for DNA amplification and detection. Lab Chip 6(1):46–53
156. Chen Z, Wang J, Qian S, Bau HH (2005) Thermally-actuated, phase change flow control for microfluidic systems. Lab Chip 5(11):1277–1285
157. Chen Z, Mauk MG, Wang J, Abrams WR, Corstjens PL, Niedbala RS et al (2007) A microfluidic system for saliva-based detection of infectious diseases. Ann NY Acad Sci 1098:429–436
158. Qiu X, Chen D, Liu C, Mauk MG, Kientz T, Bau HH (2011) A portable, integrated analyzer for microfluidic-based molecular analysis. Biomed Microdevices 13(5):809–817
159. Qiu X, Thompson JA, Chen Z, Liu C, Chen D, Ramprasad S et al (2009) Finger-actuated, self-contained immunoassay cassettes. Biomed Microdevices 11(6):1175–1186
160. Liu C, Qiu X, Ongagna S, Chen D, Chen Z, Abrams WR et al (2009) A timer-actuated immunoassay cassette for detecting molecular markers in oral fluids. Lab Chip 9:768–776
161. Mokkapati VK, Niedbala SR, Kardos K, Perez RJ, Guo M, Tanke HJ et al (2007) Evaluation of UPlink-RSV: prototype rapid antigen test for detection of respiratory syncytial virus infection. Ann NY Acad Sci 1098:476–485
162. Li JJ, Ouellette AL, Giovangrandi L, Cooper DE, Ricco AJ, Kovacs GTA (2008) Optical scanner for immunoassays with up-converting phosphorescent labels. IEEE T Bio-Med Eng 55(5):1560–1571
163. Corstjens PL, de Dood CJ, van der Ploeg-van Schip JJ, Wiesmeijer KC, Riuttamäki T, van Meijgaarden KE et al (2011) Lateral flow assay for simultaneous detection of cellular- and humoral immune responses. Clin Biochem 44(14–15):1241–1246
164. Hong W, Huang L, Wang H, Qu J, Guo Z, Xie C et al (2010) Development of an up-converting phosphor technology-based 10-channel lateral flow assay for profiling antibodies against Yersinia pestis. J Microbiol Methods 83(2):133–140
165. Qu Q, Zhu Z, Wang Y, Zhong Z, Zhao J, Qiao F et al (2009) Rapid and quantitative detection of Brucella by up-converting phosphor technology-based lateral-flow assay. J Microbiol Methods 79(1):121–123

166. Förster T (1948) Zwischenmoleculare energiewanderung und fluoreszenz. Ann Phys 2:55–75
167. Selvin PR (1996) Lanthanide-based resonance energy transfer [Review]. IEEE J Sel Top Quant Electr 2(4):1077–1087
168. Riuttamäki T, Hyppänen I, Kankare J, Soukka T (2011) Decrease in luminescence lifetime indicating nonradiative energy transfer from upconverting phosphors to fluorescent acceptors in aqueous suspensions. J Phys Chem C 115(36):17736–17742
169. Vuojola J, Riuttamäki T, Kulta E, Arppe R, Soukka T (2012) Fluorescence-quenching-based homogeneous caspase-3 activity assay using photon upconversion. Anal Chim Acta 725:67–73
170. Wilchek M, Bayer EA, Livnah O (2006) Essentials of biorecognition: the (strept)avidin-biotin system as a model for protein-protein and protein-ligand interaction [Review]. Immunol Lett 103(1):27–32
171. Diamandis EP, Christopoulos TK (1991) The biotin-(strept)avidin system: principles and applications in biotechnology [Review]. Clin Chem 37(5):625–636
172. Kuningas K, Ukonaho T, Päkkilä H, Rantanen T, Rosenberg J, Lövgren T et al (2006) Upconversion fluorescence resonance energy transfer in a homogeneous immunoassay for estradiol. Anal Chem 78(13):4690–4696
173. Harris LJ, Skaletsky E, McPherson A (1998) Crystallographic structure of an intact IgG1 monoclonal antibody. J Mol Biol 275(5):861–872
174. Ling J, Huang CZ (2010) Energy transfer with gold nanoparticles for analytical applications in the fields of biochemical and pharmaceutical sciences. Anal Methods 2(10):1439–1447
175. Yun CS, Javier A, Jennings T, Fisher M, Hira S, Peterson S et al (2005) Nanometal surface energy transfer in optical rulers. Breaking the FRET barrier. J Am Chem Soc 127(9):3115–3119
176. Wang M, Hou W, Mi CC, Wang WX, Xu ZR, Teng HH et al (2009) Immunoassay of goat antihuman immunoglobulin G antibody based on luminescence resonance energy transfer between near-infrared responsive $NaYF_4$:Yb,Er upconversion fluorescent nanoparticles and gold nanoparticles. Anal Chem 81(21):8783–8789
177. Mandelkern M (1981) The dimensions of DNA in solution. J Mol Biol 152(1):153–161
178. Kumar M, Guo Y, Zhang P (2009) Highly sensitive and selective oligonucleotide sensor for sickle cell disease gene using photon upconverting nanoparticles. Biosens Bioelectron 24(5):1522–1526
179. Zhang P, Rogelj S, Nguyen K, Wheeler D (2006) Design of a highly sensitive and specific nucleotide sensor based on photon upconverting particles. J Am Chem Soc 128(38):12410–12411
180. Rantanen T, Järvenpää ML, Vuojola J, Arppe R, Kuningas K, Soukka T (2009) Upconverting phosphors in a dual-parameter LRET-based hybridization assay. Analyst 134(8):1713–1716
181. Kumar M, Zhang P (2010) Highly sensitive and selective label-free optical detection of mercuric ions using photon upconverting nanoparticles. Biosens Bioelectron 25(11):2431–2435
182. Liu C, Wang Z, Jia H, Li Z (2011) Efficient fluorescence resonance energy transfer between upconversion nanophosphors and graphene oxide: a highly sensitive biosensing platform. Chem Commun 47(16):4661–4663
183. Wu S, Duan N, Ma X, Xia Y, Wang H, Wang Z et al (2012) Multiplexed fluorescence resonance energy transfer aptasensor between upconversion nanoparticles and graphene oxide for the simultaneous determination of mycotoxins. Anal Chem 84(14):6263–6270
184. Wang Y, Bao L, Liu Z, Pang DW (2011) Aptamer biosensor based on fluorescence resonance energy transfer from upconverting phosphors to carbon nanoparticles for thrombin detection in human plasma. Anal Chem 83(21):8130–8137
185. Wang Y, Shen P, Li C, Wang Y, Liu Z (2012) Upconversion FRET-based biosensor for ultrasensitive detection of matrix metalloproteinases-2 (MMP-2) in blood. Anal Chem 84(3):1466–1473

186. Yan C, Dadvand A, Rosei F, Perepichka DF (2010) Near-IR photoresponse in new up-converting CdSe/$NaYF_4$:Yb,Er nanoheterostructures. J Am Chem Soc 132(26): 8868–8869
187. Chen Z, Chen H, Hu H, Yu M, Li F, Zhang Q et al (2008) Versatile synthesis strategy for carboxylic acid-functionalized upconverting nanophosphors as biological labels. J Am Chem Soc 130(10):3023–3029
188. Bogdan N, Vetrone F, Roy R, Capobianco JA (2010) Carbohydrate-coated lanthanide-doped upconverting nanoparticles for lectin recognition. J Mater Chem 20:7543–7550
189. Zhang C, Yuan Y, Zhang S, Wang Y, Liu Z (2011) Biosensing platform based on fluorescence resonance energy transfer from upconverting nanocrystals to graphene oxide. Angew Chem Int Ed 50(30):6851–6854
190. Peng J, Wang Y, Wang J, Zhou X, Liu Z (2011) A new biosensor for glucose determination in serum based on up-converting fluorescence resonance energy transfer. Biosens Bioelectron 28(1):414–420
191. Deng R, Xie X, Vendrell M, Chang YT, Liu X (2011) Intracellular glutathione detection using MnO_2-nanosheet-modified upconversion nanoparticles. J Am Chem Soc 133(50): 20168–20171
192. Fish KN (2009) Total internal reflection fluorescence (TIRF) microscopy. Curr Protoc Cytom 50:12.18.1–12.18.13
193. Axelrod D, Hellen EH, Fulbright RM (2002) Total internal reflection fluorescence. In: Lakowicz JR (ed) Topics in fluorescence spectroscopy. Plenum, New York, p 289
194. Sun LN, Peng H, Stich MI, Achatz D, Wolfbeis OS (2009) pH sensor based on upconverting luminescent lanthanide nanorods. Chem Commun (33):5000–5002
195. Mader HS, Wolfbeis OS (2010) Optical ammonia sensor based on upconverting luminescent nanoparticles. Anal Chem 82(12):5002–5004
196. Ali R, Saleh SM, Meier RJ, Azab HA, Abdelgawad II, Wolfbeis OS (2010) Upconverting nanoparticle based optical sensor for carbon dioxide. Sens Actuators B Chem 150(1): 126–131
197. Achatz DE, Meier RJ, Fischer LH, Wolfbeis OS (2011) Luminescent sensing of oxygen using a quenchable probe and upconverting nanoparticles. Angew Chem Int Ed 50(44):260–263
198. Liu J, Liu Y, Liu Q, Li C, Sun L, Li F (2011) Iridium(III) complex-coated nanosystem for ratiometric upconversion luminescence bioimaging of cyanide anions. J Am Chem Soc 133(39):15276–15279
199. Yao L, Zhou J, Liu J, Feng W, Li F (2012) Iridium-complex-modified upconversion nanophosphors for effective LRET detection of cyanide anions in pure water. Adv Funct Mater 22(13):2667–2672
200. Liu Q, Peng J, Sun L, Li F (2011) High-efficiency upconversion luminescent sensing and bioimaging of Hg(II) by chromophoric ruthenium complex-assembled nanophosphors. ACS Nano 5(10):8040–8048
201. Vetrone F, Naccache R, Zamarron A, de la Fuente AJ, Sanz-Rodriguez F, Martinez ML et al (2010) Temperature sensing using fluorescent nanothermometers. ACS Nano 4(6): 3254–3258
202. Fischer LH, Harms GS, Wolfbeis OS (2011) Upconverting nanoparticles for nanoscale thermometry [Review]. Angew Chem Int Ed 50(20):4546–51
203. Soukka T, Kuningas K, Rantanen T, Haaslahti V, Lövgren T (2005) Photochemical characterization of up-converting inorganic lanthanide phosphors as potential labels. J Fluoresc 15(4):513–528
204. Feng C, Huang L, Wang J, Huang H (2012) Development of multi-parameter measurement apparatus for up-conversion phosphor particles. IEEE Sens J 12(6):2150–2156
205. Demchenko AP (2009) Introduction to fluorescence sensing. Springer, New York
206. Zhang J, Petoud S (2008) Azulene-moiety-based ligand for the efficient sensitization of four near-infrared luminescent lanthanide cations: Nd^{3+}, Er^{3+}, Tm^{3+}, and Yb^{3+}. Chemistry 14(4):1264–1272

207. Zucchi G, Maury O, Thuéry P, Gumy F, Bünzli JC, Ephritikhine M (2009) 2,2′-Bipyrimidine as efficient sensitizer of the solid-state luminescence of lanthanide and uranyl ions from visible to near-infrared. Chemistry 15(38):9686–9696
208. Zhang J, Shade CM, Chengelis DA, Petoud S (2007) A strategy to protect and sensitize near-infrared luminescent Nd^{3+} and Yb^{3+}: organic tropolonate ligands for the sensitization of Ln^{3+}-doped $NaYF_4$ nanocrystals. J Am Chem Soc 129(48):14834–14835

BIOREV (2014) 1: 205–236
DOI: 10.1007/11663_2013_7

Published online: 14 November 2013

Periplasmic Binding Proteins in Biosensing Applications

Felix S. Grünewald

Abstract Periplasmic binding proteins (PBPs) of gram-negative bacteria have been widely used as recognition elements for the development of biosensors for small molecule analytes owing to their intrinsically high selectivity and affinity towards their cognate ligands. Analyte binding is accompanied by a large hinge motion that can readily be transduced to a detectable signal. While fundamental work demonstrating the versatility of PBPs as scaffolds for biosensors dates back to the 1990s, recent years have seen more subtle improvements in detection strategies. Measurement of cellular metabolites with PBP-based biosensors has allowed significant contributions to basic research, and a first functional sensor for continuous blood glucose monitoring with glucose-binding protein as biological recognition element was tested in preclinical trials. In this chapter, strategies and applications of biosensors using PBPs as specifiers will be reviewed.

Keywords Periplasmic binding proteins · Affinity based biosensors · Solvatochromism · Fluorescence biosensors

Contents

F.S. Grünewald (✉)
Department of Chemistry Development, Roche Diabetes Care, Roche Diagnostics GmbH, Sandhofer Str. 116, 68305 Mannheim, Germany

Department of Biotechnology Development, Roche Professional Diagnostics, Roche Diagnostics GmbH, Nonnenwald 2, 82377 Penzberg, Germany

Abbreviations

$[Ru(bpy)3]^{2+}$	Ruthenium tris(2,2′-bipyridine)dichloride
5-IAF	5-Iodoacetamidofluorescein
ABP	Allose-binding protein
Acrylodan	6-Acryloyl-2-(dimethylamino)naphthalene
AF488	Alexa Fluor 488
AF680	Alexa Fluor 680
AF750	Alexa Fluor 750
ANS	2-(4′-Iodoacetamidoanilino)naphtalene-6-sulphonic acid
BADAN	2-Bromo-1-[6-(dimethylamino)-2-naphthalenyl]-ethanone
BLA	β-Lactamase
BP	Binding protein
BRET	Bioluminescence resonance energy transfer
cpGFP	Circularly permuted GFP
ECFP	Enhanced cyan fluorescent protein
EDC	1-Ethyl-3-(3-dimethylaminopropyl)carbodiimide
EYFP	Enhanced yellow fluorescent protein
FLIP	Fluorescent indicator proteins
FP	Fluorescent protein
FRET	Förster resonance energy transfer
GBP	Glucose-/galactose-binding protein
GFP	Green fluorescent protein
GlnBP	Glutamine-binding protein
IAEDANS	5-(Iodoacetamidoethyl)aminonaphthalene-1-sulfonic acid
IANBD	4-[*N*-(2-(iodoacetoxy)ethyl)-*N*-methylamino]-7-nitrobenz-2-oxa-1,3-diazole
K_d	Dissociation constant
LIVBP	Branched-chain (leucine, isoleucine, valine) amino acid-binding protein
MBP	Maltose-binding protein
MDCC	*N*-[2-(l-maleimidyl)ethyl]-7-(diethylamino)coumarin-3-carboxamide
NBD	7-Nitrobenz-2-oxa-1,3-diazole
NHS	*N*-Hydroxysuccinimide
Ni-NTA	Nickel nitrilotriacetic acid
NIR	Near infrared
NMR	Nuclear magnetic resonance
PBP	Periplasmic binding protein
PEG	Polyethylene glycol
PEGDMA: MAA	PEG-dimethacrylate/methacrylic acid copolymer
PRE	Paramagnetic resonance enhancement
PDB	Protein Data Bank
RBP	Ribose-binding protein

RR	Rhodamine red
S/N	Signal-to-noise
SWV	Squarewave voltammetry
TMR	Tetramethyl rhodamine
ΔF	Fluorescence intensity change
τ	Fluorescence lifetime

1 Introduction

Ligand recognition lies at the basis of a multitude of biological processes, such as enzymatic conversion of substrates, transport of nutrients, metabolites, and toxins, recognition and neutralization of antigens, communication between adjacent and distant cells, or the reception of external stimuli. Similarly, specific recognition of a selected substance is an essential feature of an analytical sensor. Therefore, the inherent recognition capabilities of biological entities have been widely utilized in the design of sensitive elements for the construction of biosensors. Periplasmic binding proteins (PBPs) are a family of proteins from the periplasmic space of gram-negative bacteria, where they participate in transport and sensing processes [1]. Their high intrinsic selectivity, the availability of structurally similar receptors for a broad range of ligands, and a large ligand-induced conformational change that can readily be transduced to a detectable signal have made them popular subjects of biosensor research [2]. In order to develop a universal biosensing platform for a multitude of potential analytes, and to prototype general concepts of biosensor design, PBPs have been subjected to exhaustive protein engineering. In this article, different strategies to monitor analyte binding to PBPs by detection of spectroscopic changes or an electrochemical response and selected applications that have emerged from these endeavors will be reviewed. To facilitate the understanding of strategies for the transduction of recognition events, the structure and function of PBPs will be discussed with special focus on aspects relevant to biosensor design.

2 Structure and Function of PBPs

In gram-negative bacteria, solute binding by PBPs is the key recognition step initiating two processes that interface the bacterial environment with the intracellular compartment: nutrient transport across the inner membrane and solute sensing as a trigger for chemotaxis and transcriptional regulation of downstream effectors [1, 3].

The intriguing diversity of ligands for PBPs includes carbohydrates (mono- and oligosaccharides), amino acids, opines and oligopeptides, organic (e.g., citrate and dicarboxylate) and inorganic (e.g., phosphate and sulfate) anions, organic acids like taurine, polyamines, such as spermidine and putrescine, metal ions and their

chelates, and vitamins (reviewed in [3]). The size of recognized ligands spans almost three orders of magnitude – from 1.5 Å for metal cations to 1,000 Å for oligopeptides [4]. An individual PBP can either stringently select one single substrate species (e.g., phosphate- or sulfate-binding proteins, respectively), tolerate a narrow set of structurally related compounds (e.g., the galactose-/glucose-binding protein (GBP) or branched-chain amino acid-binding protein (LIVBP)), or show affinity to a wide range of substances (e.g., oligopeptide-binding protein) [3, 5]. PBPs generally exhibit high affinities for their cognate ligands with K_d values ranging from 5 nM to 10 μM [1, 4], allowing highly sensitive analyte detection. Rational design or random mutagenesis can be applied in order to adjust the binding constant to shift the dynamic range towards a suitable range of analyte concentrations if needed for a given analyte [6]. Likewise, the spectrum of analytes has been extended beyond the range of natural ligands by introducing artificial functionalities using rational design [7, 8]. Although the introduction of novel functionalities is subject to critical reinvestigation [9], the broad ligand spectrum clearly makes PBPs an attractive target for biosensor design.

A plethora of structural information about many members of the PBP superfamily has been acquired by spectroscopic methods, X-ray crystallography, small-angle X-ray scattering, nuclear magnetic resonance (reviewed in [4]), or, more recently, paramagnetic relaxation enhancement [10]. More than 150 PBP structures have been submitted to the Protein Data Bank (PDB [11]) and comparison of apoprotein structures with their ligand-engaged counterparts has led to a detailed understanding of the molecular mechanisms governing substrate recognition and binding. A number of highly authoritative review articles [1–4, 12] have covered this area; therefore, the emphasis here will be on aspects relevant to biosensor design.

PBPs are monomeric polypeptides sized between 25 and 60 kDa with an elliptical shape and a maximum diameter along the longitudinal axis of 50–70 Å [13]. All PBPs share a common structural architecture. In their canonical form, they consist of two globular domains of similar topology with a single-ligand binding site located in a deep cleft between the two lobes. Each domain is formed by a central β-sheet framed by α-helical regions [4, 14]. Additional secondary structure elements or even complete domains are present in the larger PBPs, e.g., oligopeptide and nickel BPs [15]. A peculiarity of glucose-binding protein is a calcium binding site in the C-terminal domain remote from the actual ligand binding site [16] that is supposed to stabilize the protein structure [17].

While the tertiary structure is conserved across species, reflecting a common general function, the primary amino acid sequence homology can be below 20%. This is a result of specific structural features that have evolved in order to accommodate and recognize ligands from diverse chemical classes [1, 4, 12].

The two ligand binding lobes are thought to have arisen from genetic fusion of a hypothetical dimeric evolutionary ancestor [4, 12]. They are connected by two or three usually elongated polypeptide segments that confer a considerable degree of flexibility to the hinge region and allow for large-scale interdomain movements.

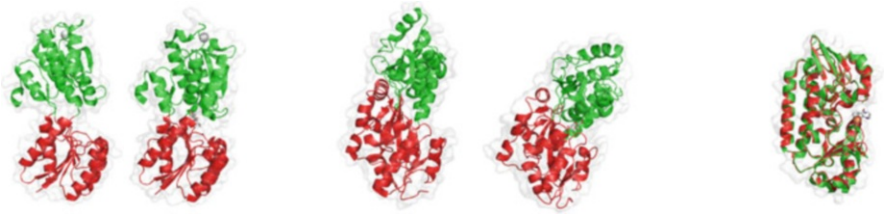

Fig. 1 Side-by-side comparison of the ligand-induced hinge-bending motions of class I, II, and III PBPs. While GBP (a class I PBP, *left*) and MBP (a class II PBP, *middle*) undergo a significant conformational change, an overlay of the liganded and unliganded siderophore CeuE (class III PBP, *right*) reveals only minor structural rearrangements. Figure was generated with PyMOL [18] using PDB accession codes 2FW0/2FVY (GBP, [19]), 1JW4/1ANF (MBP [20, 21]), and 3ZK3/3ZKW (CeuE [22]), respectively

Three classes (I, II, and III) of PBPs can be distinguished based on the topology of the secondary structure elements in the two ligand binding lobes [4, 12].

A distinct feature of PBP classes I and II is a significant hinge motion upon binding of their cognate ligand. The two lobes reorient with respect to each other in a rigid body movement, with minimal changes of the internal structure of each domain (Fig. 1). Thus, both domains close around the ligand in a motion resembling the venus flytrap plant capturing its prey, hence the pictorial designation of the mechanism [23]. In most PBPs, the ligand is bound deep within the binding crevice and is for the most part sequestered from the solvent by the two protein lobes. Ligand binding thus goes along with a significant change of overall protein shape, presumed to facilitate interaction with the transmembrane proteins that mediate signal transduction or transport through the inner membrane in vivo [1, 4].

Crystal structures of leucine bound to the surface of the N-terminal lobe of LIVBP in its open conformation suggested that initial interaction of the ligand with the interior of the groove would eventually lead to domain closure [24]. Although this notion suggests a mechanism in which the two lobes remain well separated until engagement of the ligand entails domain closure in an "induced fit" mechanism, this is probably not the case for all PBPs alike. Several groups have investigated the question whether ligand binding precedes and initiates the conformational change or if a population shift occurs by selection from preexisting conformations. Using time-resolved fluorescence studies Döring et al. [25] observed considerable flexibility of maltose-binding protein (MBP) in the absence of ligand. The flexibility was reduced in the presence of either maltose or β-cyclodextrin, an MBP ligand that occupies the binding site but prevents domain closure. Paramagnetic resonance enhancement (PRE) NMR data of MBP suggest that in the absence of ligand as much as 5% of the population assume the closed conformation that rapidly (20 ns–20 μs) interchanges with the open form [10]. In contrast, there was no indication for a closed population of glutamine-binding protein (GlnBP) in similar PRE experiments [26]. Recently, Ortega et al. [27] have reported NMR data suggesting that the behavior of GBP is best described by a population shift model, whereas ribose-binding protein (RBP) follows an induced fit mechanism. These

differences appear to be governed by the mobility of the hinge regions, since reciprocal grafting of hinge residues effectively inverts the phenotypes [27].

For the design of PBP-based biosensors, it is important to note the dimension and heterogeneity of the interdomain movements: The amino- and carboxy-termini of GBP [19], MBP, and RBP [13] are separated by distances of 35–50 Å. In the closed conformation, the termini of RBP approach by approximately 7 Å, while they move apart by 2 Å in MBP [13]. In contrast, the distance between the N- and C-termini of GBP hardly changes upon closure of the structure, despite a considerable 14 Å lateral movement of the C-terminal lobe with respect to the N-terminal domain (determined by comparison of PDB codes 2FW0 and 2FVY [19]).

Angles of opening for those proteins with both the open and the closed structures available were determined to be between 26° and 64° [4]. A detailed analysis of the hinge segments that undergo changes in torsion angles upon domain closure has been performed for RBP, for which not only open and closed but also intermediate structures have been determined by X-ray crystallography [28]. Structures opened by 43°, 50°, and 64° with respect to the liganded, closed form lie along a single opening trajectory, tracking back to bond rotations around a small set of amino acids in each hinge segment. Similar results were obtained for allose-binding protein (ABP) [29], LIVBP [30], and GBP [19] with only 1–2 residues per hinge strand undergoing significant torsional movement. Two comparative analyses [19, 29] of the motions of GBP, ABP, and RBP, all members of class I PBPs, demonstrate that the reorientation axes of the three proteins are distinct by as much as 40°. These differences were demonstrated to result from rotation around different sets of bonds in and close to the hinge regions [19]. A detailed inspection of these movements can give important information about possible attachment sites for reporter molecules. For example, identification of sites with a maximal distance change can indicate suitable locations for anchorage of FRET pairs.

In a number of PBPs, additional surface features can be identified that stabilize the open conformation in the absence of ligand. In MBP (but not in, e.g., GBP [19]), a crevice opposite of the maltose binding site termed “balancing interface” is tightly packed in the open state and intramolecular interactions stabilize this conformation [31]. In order for the venus flytrap to close, the interface needs to unfurl and an energetic barrier has to be overcome to break the interactions. Based on the assumption that the overall free energy gain for ligand binding to PBPs is composed of the individual contributions of the binding event itself and the interconversion between open and closed forms, Marvin and Hellinga [6] sought to manipulate the affinity of MBP towards maltose by interfering with the intrinsic equilibrium between both states. The introduction of bulky residues to the balancing interface indeed destabilized the open conformation, thereby allosterically increasing the overall affinity for maltose, whereas smaller residues had the opposite effect [6]. Allosteric modulation of affinities has since become an important tool for design of biosensors with tailor-made affinities.

The large interdomain movement and the concomitant changes in overall shape, intramolecular distances, and specific microenvironments lie at the basis of the attractiveness to use PBPs as recognizing elements in biosensors. Multiple strategies have been developed to transduce the ligand-induced motions into signals amenable to exterior detection. However, despite the apparent similarity among the PBP family, subtle differences complicate the transfer of technical developments from one member to another one. In fact, the identification and positioning of a functional transducer for bioanalytical applications is still a usually empirical process for any given PBP. Allosteric manipulation of binding affinities has been a powerful tool to develop biosensors with altered or enhanced concentration ranges and has been substantially aided by the wealth of structural information available [2].

3 Biosensing with PBPs

3.1 General Aspects

Biological macromolecules are extensively used as recognition elements for diagnostic purposes. The exquisite specificity of antibodies is at the basis of countless analytical procedures [32], but many common analytes are inherently non-immunogenic because they play pivotal roles in normal physiology, and generation of antibodies against these metabolites continues to be challenging. Frequently, specific enzymes can be used to detect and quantify small molecule analytes. Enzymatic conversion can be followed by the generation or consumption of a chromophore, or the transfer of redox equivalents, and highly specific enzymes are available for many applications. Effects inherent to substrate turnover, such as substrate or product inhibition at high analyte concentrations, depletion of analyte at low concentrations, or temperature dependence, are frequent sources of error for enzymatic sensors [33]. In addition, many common enzymatic tests are based on monitoring multistep reactions or require mediators as electron shuttles to transfer redox equivalents, which introduces additional complexity to these systems [34]. Monitoring the binary associations of PBPs with their cognate ligands promises to circumvent many of the problems associated with enzymatic biosensors.

Historically, the first attempts to utilize the specific binding of PBPs for quantification of analytes used histidine- [35], cystine- [36], glutamine- [37], or galactose- [38] binding proteins adsorbed to nitrocellulose membranes. The assays were based on competition of the analyte with a radiolabeled ligand that allowed for a sensitive detection of small quantities of the respective amino acid or carbohydrate. While these assays exploited the specific and tight binding characteristic of PBPs, they took no advantage of the reporter capabilities of the concomitant hinge motion. Similarly, a number of assays detect the displacement of the fluorescently labeled MBP ligand β-cyclodextrin from the binding site [39]. These approaches

are not generally applicable to other PBP family members because they require a suitable binding site competitor – a condition that is frequently not fulfilled due to the PBP's high selectivity.

3.2 Fluorescence-Based Detection Strategies

3.2.1 General Concepts

Most technologies developed to perform biosensing with PBPs rely on the detection of changes in certain well-defined spectroscopic properties in response to the biochemical stimulus. Among these, fluorescence has been most widely employed due to its outstanding sensitivity, the availability of highly developed tools for genetic or chemical attachment of reporter groups to almost arbitrary sites of the PBP structure, and readily available instrumentation. Two principal approaches have been taken to transduce the hinge motions to a fluorescent signal: Solvatochromic fluorophores attached to specific sites on the protein surface report changes in the polarity of their environment to altered emission spectra, quantum yields, or fluorescence lifetimes. When attached to PBPs, changes in the dye's microenvironment can be the result of direct interaction between fluorophore and ligand, altered solvent accessibility or the protein surface due to the conformational change, or a combination of these contributions [40]. The second line of research employs Förster resonance energy transfer (FRET), a phenomenon relying on radiationless transfer of energy between two fluorophores. Since this effect is highly distance and orientation dependent, it can be used as a highly sensitive means to detect subtle changes in molecular spacing [41].

3.2.2 Sensing with Solvatochromic Fluorophores

The simplest case of monitoring solvatochromic effects on PBP fluorescence is the observation of tryptophan fluorescence, a natural amino acid with weak solvatochromic properties. Boos et al. [42] realized a 13.5% increase in fluorescence and a 2 nm blue shift of the emission maximum upon galactose binding to *E. coli* GBP. However, monitoring tryptophan fluorescence for analytical applications suffers from the low intrinsic fluorescence and weak solvatochromism. The first experiments to report the conformational change of a PBP by attachment of an organic fluorophore were performed by Zukin et al. [43] who labeled *S. typhimurium* GBP, then believed to contain a single tryptophan as fluorescence donor, with the FRET acceptor 5-iodoacetamidofluorescein (5-IAF). A 10% quenching of fluorescein emission intensity in the presence of galactose could not be explained by the interaction between ligand and fluorophore alone, but indicated contribution of a conformational change [43]. Similar experiments were carried out with the environment-sensitive naphthalene derivative 5-(iodoacetamidoethyl)

aminonaphthalene-1-sulfonic acid (IAEDANS) conjugated to *E. coli* MBP [44]. By monitoring energy transfer from tryptophan to the dye as a function of maltose concentration, a dissociation constant of 1 μM could be determined that was in good agreement with other methods. In these experiments the position of the conjugated fluorophores was determined by the repertoire of functional groups accessible to the coupling chemistry that were present in the wild-type protein. A more stringent control over the attachment site can be achieved by the introduction of artificial cysteine residues to binding proteins otherwise devoid of sulfhydryl functions, such that thiol-reactive dyes can be attached at sites selected by the researcher. First sensors with attachments of solvatochromic dyes at selected positions were constructed by introducing the mutation S337C to *E. coli* MBP, at a position lining the border of the binding cleft [45, 46]. Conjugation with 4-[*N*-(2-(iodoacetoxy)ethyl)-*N*-methylamino]-7-nitrobenz-2-oxa-1,3-diazole (IANBD) and 6-acryloyl-2-(dimethylamino)naphthalene (acrylodan) yielded sensors with fluorescence intensity increases by 160% and 50%, respectively, upon saturation with maltose [46].

Hellinga's group has elaborated the potential of PBPs by pointing out important design strategies for manipulation of different surface features of biosensor proteins. Solvatochromic dyes can be attached to three distinct areas relative to the binding site [2, 47]: Endosteric attachment within the binding site offers the potential for direct interaction between ligand and label, thereby potentially inducing a strong change in the chemical environment of the dye and generating a large signal. Dyes attached to peristeric sites at the margins of the binding cleft are likely to form additional contacts with the opposite lobe upon closure of the structure. Changes in hydration and novel direct interaction with groups from previously distant residues will report to changes in spectroscopic properties. The third option is allosteric placement of the reporter group. By inspection of the open and closed conformations of a binding protein, residues distant from the binding site that undergo changes in solvent accessibility or pairs of residues that change their relative distances can be identified [2, 40].

Since allosteric placement of the reporter group spatially uncouples signal generation from ligand binding, effects of the protein modification on the binding event are expected to be minimal. Furthermore, additional amino acid substitutions that alter affinity or selectivity can be independently introduced without affecting signal transduction. In contrast, manipulation of the active site or adjacent regions may entail unpredictable changes in the affinity and selectivity towards the desired analyte due to inactivation of residues directly involved in ligand binding, subtle changes in the structure of the binding site, direct interaction between ligand and fluorophore, or steric hindrance by the bulky reporter group. Despite the wealth of available structural information, a detailed prediction of the interactions between protein, ligand, and fluorophore exceeds current possibilities of molecular modeling, so that sensing proteins with sufficiently large signal changes still need to be identified empirically [2].

A second parameter that usually needs to be adjusted is the affinity of the produced sensor towards its ligand. Only in rare cases the dynamic range of measurement of a sensor with sufficiently large change in fluorescence intensity (ΔF) will happen to

overlap with expected analyte concentrations. As the nature and position of the reporter group may influence the affinity, it is often beneficial to adjust the dissociation constant (K_d) of a sensor with suitable signal intensity in a second step by mutations in the "balancing interface" or the binding site. An instructive example is the optimization of the glucose sensor GBP-H152C labeled with 2-bromo-1-[6-(dimethylamino)-2-naphthalenyl]-ethanone (BADAN), which carries the fluorophore at an endosteric position. This construct shows a 400% fluorescence increase at saturating concentrations of glucose, but its K_d is only 5 μM, making it unsuitable for measurements at physiological glucose concentrations of 4–10 mM. Introduction of two additional point mutations (A213R and L238S) that had previously been identified to lower the affinity in wild-type GBP [48] increased the K_d of this construct to 11 mM so that concentrations of 1–100 mM can readily be covered [49]. Likewise, three tryptophan to alanine substitutions in the binding site of MBP decrease the affinity towards maltose in the wild-type protein and similarly in a construct labeled with IANBD at the rear of the globular protein (mutant D95C) [6].

The efforts to explore the potential of solvatochromic dyes as transducers of PBP ligand binding culminated in a seminal paper reporting biosensors generated from combinations of 11 PBPs with 8 solvatochromic fluorophores [47]. This paper highlights the use of a common design strategy for various PBPs as a toolbox for biosensor design. An important lesson learned from this systematic work is that for any given PBP, a suitable combination of attachment site and dye has to be empirically determined. A given fluorophore may exhibit a large fluorescence intensity or any other spectroscopic observable in response to an analyte at a specific position, while another dye, even of similar chemical structure, changes its spectroscopic properties only negligibly. Similarly, the readout produced by the same dye will vary dramatically, depending on the specific attachment location [47]. Prediction of suitable attachment sites is complicated by the fact that not only the overall polarity of a dye's environment but also specific hydrogen bonds formed with the protein environment affect the observed fluorescence [50].

Initial studies on PBP biosensors were generally performed with commercially available dyes. Commonly implemented solvatochromic fluorophores and their use have recently been reviewed in [40]. Practical application of these fluorophores, in particular in biological fluids, is frequently limited by the wavelengths of their absorption and emission maxima. Absorption of tissues and serum components and autofluorescence of biological material interfere with detection at wavelengths below 600 nm. The repertoire of environment-sensitive dyes for biomedical applications has therefore recently been extended by dyes allowing measurement in the near-infrared (NIR) light spectrum. Additional solvatochromic phenoxazine [51] benzothiazolium squaraine [52] and coumarin [53] derivatives have been synthesized with the explicit intention to be used in PBP-based biosensors [54]. Such sensing elements were incorporated to GBP and MPB, embedded into cross-linked polyethylene glycol (PEG) disks and their response to maltose and glucose measured through explanted rabbit skin. Transdermal fluorescence increase in

response to the analyte was as high as 111% and 96% for the best PEG disk embedded sensors for maltose and glucose, respectively [54].

Ratiometric Detection

A particular challenge for the implementation of solvatochromic fluorescence readout is the need for proper referencing and calibration. A fluorescence intensity signal measured at a given wavelength and time will depend on the concentration of PBP, the degrees of labeling and photobleaching, absorption or scattering by the surrounding tissue or fluid, temperature, pH, excitation intensity, and other optical parameters of the instrument [55]. Depending on the intended use of the biosensor, calibration prior to use can be inconvenient or impossible. While occasional calibration of a subcutaneously implanted meter for continuous blood glucose monitoring with a sample obtained by finger pricking is a nuisance to the patient at best, calibration against a reference sample may not be feasible at all for a single-use sensor immobilized on a test strip matrix.

A number of internal referencing strategies have been developed to overcome the difficulties associated with intensometric fluorometry. A technically straightforward approach exploits the property of some solvatochromes, such as PRODAN and its derivatives acrylodan and BADAN, to exhibit large spectral shifts when the polarity of their environment changes. Self-referencing is feasible, when the intensities at two different wavelengths change relative to each other. The ratio of both intensities should then be largely independent of fluorophore concentration, excitation intensity, and photobleaching. Robust ratiometric detection of glucose with different variants of GBP conjugated to the NIR emitting aza-coumarin dye ICOPOC was recently reported [53]. More recently, an advanced sensor for continuous glucose monitoring with robust performance in preclinical trials was presented. It relies on the ratiometric readout of acrylodan fluorescence coupled to position 183 (W183C) of a thermostable variant of *E. coli* GBP [56].

An alternative to self-referencing based on the intrinsic spectral shifts of a single dye is the inclusion of a second fluorophore that is unresponsive to ligand binding. GlnBP was modified with acrylodan as the reporter dye at an artificial cysteine at position 179 and additional ruthenium [57] or europium [58] complexes at the amino-terminus. While the fluorescence emission stemming from the lanthanide complexes measured at 600–640 nm was unaffected by glutamine addition, acrylodan emission at 515 nm was quenched by increasing concentrations of glutamine. These internal references are supposed to account for fluctuations in total protein concentration and excitation intensity, whereas differences in labeling efficiency between batches cannot be accounted for, since the coupling efficiencies can vary independently for each fluorophore. Similarly, differential photobleaching or pH dependence of the dyes and wavelength-dependent absorption are likely to be insufficiently accounted for by these approaches. In addition, similar experiments from the same laboratory with dual-emitting GBP indicated a strong temperature dependence of the intensity ratios [59].

Fluorescence Lifetime

Measurement of fluorescence decay times allows to compensate for interference resulting from various sources, such as fluctuating intensities of the light source, instrumental parameters, length of the emission path, local concentration, background fluorescence or color, sample absorption or scattering, and inhomogeneous dye loading or the loss thereof due to leaching, bleaching, or decomposition [55]. The technology therefore is able to account for many of the drawbacks of intensometric observation of an environment-sensitive fluorophore. In addition, time-resolved measurements can provide information about the structure and environment of a fluorophore that is not accessible by simple intensometric measurements. Contributions of different fluorophores, or discrete conformations or microenvironments of otherwise identical fluorophores present, in a sample can be dissected by analytically separating individual lifetime components [41].

Gilardi et al. [60] reported on the lifetime distribution of the MBP variant S337C labeled with IANBD. In the absence of maltose a broad distribution of lifetimes with a center at $\tau = 2.71$ ns stemming from the nitrobenzoxadiazole (NBD) group was observed. Concomitant with a 150% intensity change in response to maltose, the distribution split up into two lifetime components of $\tau = 1.3$ ns and $\tau = 4.34$ ns, respectively, associated with the distribution of NBD to two conformational populations [60]. Multifrequency phase and modulation data were also collected for an MDCC (*N*-[2-(l-maleimidyl)ethyl]-7-(diethylamino)coumarin-3-carboxamide)-conjugated phosphate BP. Both the absolute values and the relative contributions of two lifetime components were found to be strongly dependent on the presence of phosphate [61]. While the focus of these investigations was the elucidation of structural and mechanistic details of the respective binding protein conjugate, the results already suggest that time-resolved measurement is a suitable means of generating interference-reduced PBP biosensors.

Fluorescence lifetime measurement as a readout for a biosensor was explored by Dattelbaum and Lakowicz [62]. GlnBP-S179C-acrylodan lifetime decreased from 2.28 to 0.97 ns upon binding of glutamine. Frequency-domain lifetime measurements revealed a maximum phase angle change of 18° at an excitation frequency of 110 MHz. Titration of the sensor with glutamine allowed the authors to plot the phase angle shift as a function of the concentration with a nonlinear response in a concentration range between 0.03 μM and 5 μM glutamine [62]. Recently, the group of John Pickup has undertaken efforts to develop a fluorescence lifetime-based glucose sensor by labeling variants of *E. coli* GBP with the PRODAN derivative BADAN at position H152C [49, 63, 64]. Global analysis of the decay times in the presence of nine different glucose concentrations revealed a short ($\tau = 0.8$ ns) and a long ($\tau = 3.1$ ns) lifetime component. The fractional contribution of the long lifetime component increased from 10% in the absence to 95% in the presence of 310 μM glucose [63]. By introducing two additional mutations (A213R/L238S) the dynamic range of the sensor could be adjusted to the physiologically more relevant region between 1 and 100 mM in both buffer and human serum [49]. From this construct, a fiber-optic glucose sensor was constructed by attaching the

hexahistidine-tagged protein to nickel nitrilotriacetic acid (Ni-NTA) functionalized polystyrene or agarose beads and positioning the beads in a glass chamber at the tip of a fiber-optic detector. A nylon mesh was used to allow the passage of glucose while retaining the functionalized beads. Dose-response curves for these devices indicated a hyperbolic response to glucose concentrations from 1 to 100 mM, with a maximum lifetime change of $\tau = 0.6$ ns and $\tau = 0.25$ ns for functionalized agarose and polystyrene beads, respectively [64]. This compares to a change of approximately 1 ns for the free labeled protein [49]. As the sensor response to glucose is reversible, the authors propose their approach to be applicable to devices for continuous glucose monitoring [64].

Fluorescence Modulation

The fluorescence lifetime sensor for glutamine described by Dattelbaum and Lakowicz [62] operated at a frequency of 110 MHz. Conventional measurement of fluorescence lifetimes in this frequency range requires sophisticated equipment, which is frequently incompatible with miniaturization and cost-efficient manufacturing. Therefore, strategies to reduce the excitation frequency have been devised that allow measurement of fluorescence modulation with simpler and less expensive optoelectronics, while retaining the accuracy and robustness of lifetime sensing (reviewed in [65]).

Lakowicz et al. [66] employed the combination of a short-lifetime (nanosecond scale) solvatochromic fluorophore that reports the analyte concentration by changes to its spectral properties with a long-lived fluorophore, such as a ruthenium complex ($\tau \sim 1$ μs), that is unresponsive to the analyte. In this setting, the relative intensities of the short- and long-lived fluorophore report as a change in fluorescence modulation at low frequencies in the range of 1–10 MHz. With a constant intensity of the long-lived dye, an intensity change of the nanosecond dye directly reports to a change in fluorescence modulation [66]. Importantly, the analyte-sensing fluorophore does not have to change its lifetime so that a wider choice of dyes with large intensity changes in response to analyte can be applied [66]. The two fluorophores can be either attached to different sites of a BP, simply be mixed in solution, or even spatially separated. However, the relative amounts of both fluorophores have to remain constant, so that preferential photobleaching of decay of one dye or divergent temperature dependence will affect the measurement.

The concept of low-frequency fluorescence modulation has been applied to PBPs in order to construct sensors for glucose and glutamine. GBP Q26C was labeled with 2-(4′-iodoacetamidoanilino)naphtalene-6-sulphonic acid (ANS). The fluorescence of this construct decreases by more than 50% upon the addition of 8 μM glucose, whereas the lifetime of ~5 ns remained largely unchanged. However, when the measurements were performed in a cuvette covered with a painted film of polyvinyl alcohol embedded ruthenium tris(2,2′-bipyridine) dichloride ($[Ru(bpy)3]^{2+}$), modulation at 2.1 MHz was responsive to changes in glucose concentrations. With this construct, glucose concentrations from 0 to

8 μM could be measured with an accuracy of 0.2 μM [67]. Similar sensors operating at 1.58 and 2.5 MHz were constructed with dual-labeled variants of GBP L255C [59] and GlnBP S179C [57], respectively, that were conjugated to acrylodan and ruthenium bis(2,2′-bipyridyl)-1,10-phenanthroline-9-isothiocyanate.

Additional referencing to eliminate interference from ambient light can be accomplished by performing an auxiliary measurement at a lower frequency, where modulation is practically unresponsive to ligand binding [57]. The ruthenium- and acrylodan-labeled GBP-L255C were used to construct a low-cost glucose sensor operating at two frequencies [68]. At an excitation frequency of 2.1 MHz, the pulses are too short for efficient excitation of ruthenium so that fluorescence will originate only from acrylodan in an analyte-dependent manner. In contrast, excitation at 30 kHz excites both acrylodan and ruthenium. Alternating measurement of intensities at both modulation frequencies allows to separate the contribution of both fluorophores without the use of attenuating band-pass filters [68]. By replacing the ruthenium label of GlnBP S179-acrylodan for a europium complex with a significantly longer lifetime of >300 μs, the operating frequencies could be further decreased to 320 Hz and 10 kHz, respectively [58].

Lanthanide Fluorescence

A variation on the theme of reporting conformational changes by solvatochromic fluorophores has been applied to GBP, which contains a natural calcium binding site in the C-terminal domain, believed to be important to stabilize the tertiary structure [16, 17]. Wenner et al. [69] stripped GBP of its natural calcium ligand by dialysis against an EDTA-containing buffer and reconstituted the apoprotein with either of the three lanthanides europium (Eu^{3+}), terbium (Tb^{3+}), and dysprosium (Dy^{3+}). These lanthanides exhibit environment-sensitive luminescence in that their decay times respond to the number of coordinated water molecules [41]. All three lanthanides have been used as optical reporters of glucose binding to GBP, with terbium showing as much as 85 and 92 % signal increase upon saturation with glucose and galactose, respectively [69]. These results are somewhat surprising as comparison of open and closed states of GBP suggests that the presumed binding site for the lanthanides does not alter its conformation sufficiently to induce such a strong signal. The use of lanthanides as optical reporters for GBP occupancy might benefit from their long decay times in the range of milliseconds that are easily amenable to detection by cost-efficient instrumentation. Furthermore, luminescence lifetime measurement is insensitive to a number of interferences as outlined above and would therefore facilitate referencing [65].

3.2.3 Förster Resonance Energy Transfer (FRET)

Förster resonance energy transfer (FRET) is a powerful tool to obtain information about the relative distance of a fluorescence donor/acceptor pair. Non-radiative

energy transfer from an excited donor fluorophore to an acceptor requires both fluorophores to be in close proximity of typically several nanometers and a spectral overlap of the donor emission spectrum with the excitation spectrum of the acceptor. FRET results in a decrease of donor fluorescence and, if the acceptor is itself fluorescent, an increasing intensity of the acceptor so that the response is inherently ratiometric [70]. Due to the strong distance and orientation dependence of FRET, it has been extensively employed in the biological sciences to gather information about molecular interactions and conformational changes of biomolecules. Given the large conformational changes of PBPs in response to their ligand it is not surprising that several groups have devised strategies to report these movements by modulation of FRET.

In principle, introduction of a single fluorophore as an acceptor for FRET from exited tryptophan residues would be sufficient to detect a conformational change and has been utilized to probe movements in *S. typhimurium* GBP [43]. However, due to the low tryptophan fluorescence and the requirement for excitation in the UV range this approach is not feasible for biosensing applications. FRET-based strategies are therefore based on genetic fusion of fluorescent proteins (FPs) or conjugation of organic fluorophores as both FRET donors and acceptors to PBPs.

Fluorescent Indicator Proteins

A large array of FRET sensors with PBPs as sensory elements has been constructed, mainly by the Frommer Lab, by genetic fusion of two different spectral variants of green fluorescent protein (GFP) to the polypeptide chain of the sensory protein. These constructs were termed fluorescent indicator proteins (FLIP). This strategy has been especially advantageous to construct sensors for intracellular detection of metabolites as the expressed biosensor can be used in situ without any chemical modification. Furthermore, by fusing specific sorting tags to the N-terminus of such constructs, the expressed biosensor can be directed to a desired subcellular compartment or membrane. Advances in microscopy technology allow for the analysis of metabolite concentrations with high spatiotemporal resolution [71].

The most obvious approach to combine a PBP and a FRET pair is a linear fusion of two GFP variants to the N- and C-termini of a PBP displaying a large closing movement. For sensors based on MBP and other class I PBPs, the two termini will approach each other upon hinge closure resulting in increased FRET, whereas the termini of GBP and other class II PBPs separate and FRET is expected to decrease [72]. However, it became clear that besides the distance of the fluorophores, additional factors contribute to a FRET response. In several instances, optimization of the linker length between the fluorescent proteins and the PBP was crucial for obtaining a FRET response. For example, the deletion of five amino acids from the amino-terminus of MBP sandwiched between ECFP and EYFP was required to obtain a measurable FRET change in response to maltose [73]. In a subsequent investigation, the rigidity was increased by the systematic deletion

of linker regions and terminal sequences of MBP and FPs not required for folding and function, with a resulting threefold increase in FRET response [74]. The signal intensity of an ECFP-MBP-EYFP construct could be further increased by an order of magnitude by introducing rationally designed linkers that adopt a more rigid helical structure to improve coupling of the conformational change of MBP to the fluorescent proteins [75]. These results suggest that, much more than distance, the relative dipole orientation of the two fluorophores provides a significant contribution to the observed FRET response in this system [71]. The strong orientation dependence of FRET has also been employed to design biosensors in which the relative distance of both fluorophores is not expected to undergo a significant change: Hybrid proteins were constructed by linear fusion of two FPs to phosphate-binding protein whose termini reside on the same lobe [76] or by internal fusion to selected sites of both opposing or the same lobe of glutamate- [74] and glucose-binding proteins [77]. In these setups, ligand binding is expected to restrict the rotational freedom of the fluorophores with concomitant changes in FRET [71, 74]. A different strategy to improve the dynamic range of amino acid-binding PBPs was devised by Okada et al. [78]. By circular permutation of six PBPs, their N- and C-termini were relocated with respect to the tertiary structure in order to spatially separate both fluorophores. As a result, the ligand-induced FRET change of all PBPs increased as compared to the respective linear fusion protein [78].

FLIPs have been employed to measure analyte concentrations in complex solutions such as beer [73], soy sauce [79], calf serum [79], and yeast culture medium [78]. However, the most significant applications of FLIPs were in the field of real-time noninvasive monitoring of metabolites in tissues, cells, or subcellular compartments. FLIPs were used to analyze glucose levels in the cytosol [80] and nuclei [81] of COS-7 cells, epidermal cells and roots of Arabidopsis plants [82], and yeast [83]. In neurobiology, glutamate release from rat neuronal cells was detected by a surface-exposed FLIP in cell culture [79] or by diffusion of an isolated FLIP into whole brain slices [84], to mention just a few exemplary applications of FLIPs. The Frommer Lab has ideally exploited the possibilities of PBPs as recognition elements for a modular system and constructed a vast array of FLIPs with distinct specificities, affinities, subcellular locations, and expression hosts and published standard protocols for intracellular metabolite monitoring in bacteria [85], yeast [83], and mammalian cells [86]. As a number of excellent reviews have been published on this topic [71, 72, 86, 87], details will not be reiterated here.

One shortcoming of the genetically encoded FRET-based biosensors is the fairly small intensity change, which results in low signal-to-noise (S/N) ratios. While averaging over multiple measurements can account for this drawback, prolonged measurement times are impractical for monitoring rapid analyte changes [71]. Alternative strategies to construct genetically encoded sensors with improved S/N ratios aim at modulating FP brightness directly instead on relying on FRET (see below).

Chemical FRET Labels

As an alternative to the genetic fusion of fluorescent proteins to the PBP scaffold, chemical labeling with low molecular weight fluorophores as donor/acceptor pairs has been employed. Chemical attachment of the labels offers the opportunity to strategically position the dyes at precisely defined sites within the three-dimensional structure of the sensor protein. The large number of available crystal structures potentially allows selection of attachment sites with maximal distance changes in response to ligand binding for many PBPs. Furthermore, dyes can be specifically selected for their absorption or emission ranges, large Stokes shifts, or minimal susceptibility to interferences, such as pH dependence [88]. However, orthogonal conjugation of two dyes to different sites is not trivial and has hampered the wide application of this methodology. A few reports, however, have highlighted the potential of organic dye FRET pairs coupled to PBPs.

Dual labeling of MBP at orthogonally reactive thiol groups was performed by carboxy-terminal genetic fusion of a Cys_2His_2 zinc-finger domain. The two cysteines present in this motif can be protected by disulfide formation in oxidizing conditions or by coordinating zinc with high affinity. After conjugation of a single unprotected cysteine group with a label, the zinc-finger thiols can be deprotected by reducing the disulfide bond or by chelating the coordinated zinc, respectively, to release two equally reactive sulfhydryl groups. An additional, truncated version of the zinc finger lacking the two characteristic histidines can be orthogonally protected by disulfide bond formation only [89]. Using this approach, Smith et al. [89] labeled MBP with the FRET pair Cy5 and tetramethyl rhodamine (TMR) in both possible arrangements and demonstrated the maltose dependence of the donor/acceptor ratio. Resonance transfer decreased by 0.1-fold in case of the carboxy-terminal $(TMR)_2$ and threefold in case of the carboxy-terminal $(Cy5)_2$ label. Since the unprotected cysteine is located in the C-terminal lobe and is therefore not expected to change its distance to the carboxy-terminus dramatically, the authors suggest relative orientation effects to be responsible for this strong change in intensities [89]. Combination of the complete zinc finger at the C-terminus with the truncated version fused to the amino-terminus permitted orthogonal triple labeling with 5-IAF, TMR, and Cy5. Transfer of energy via a FRET relay did not improve the change in donor/acceptor ratios, but increases the wavelength separation of donor and acceptor emission which reduces spectral bleed-through [89].

A different approach to specifically label the amino-terminus in a cysteine-independent reaction eliminates the requirement to install differentially reactive thiol groups. Crochet et al. [88] specifically labeled the N-termini of *E. coli* GlnBP and two amino acid-binding proteins isolated from thermophilic organisms with Alexa Fluor 488 (AF488) in a pyridoxal phosphate-mediated reaction. Standard maleimide coupling was used to install the FRET acceptor (TMR) at single cysteines introduced at selected positions of the PBP sequence. Relatively low donor/acceptor ratio changes were observed in response to ligand binding. Surprisingly, of nine double-labeled GlnBP constructs, the one with the smallest predicted donor/acceptor distance change exhibited the highest change in FRET,

which indicates an additional contribution of orientation effects. As a consequence, the selection of appropriate attachment sites might prove equally difficult for FRET labels as for the solvatochromic fluorophores [88].

In an effort to develop a FRET sensor suitable for continuous glucose monitoring in vivo, the NIR dyes Alexa Fluor 680 (AF680) and Alexa Fluor 750 (AF750) were attached to glucose-binding protein [90]. While the FRET acceptor AF750 was specifically attached to a cysteine residue at position 175 in the bottom third of the C-terminal lobe, the donor AF680 was nonspecifically coupled to lysine residues. A decrease in donor/acceptor ratio was reported in response to glucose in solution; however, the data do not allow fitting due to insufficient data points in the dynamic range of this specific construct. Interestingly, the authors could introduce the FRET construct into erythrocytes by hypoosmotic dialysis and analyze the response of the encapsulated NIR sensor to addition of glucose. Although the results of this experiment were inconsistent with data from solution measurements, site-specific attachment of both dyes might provide biosensors with improved performance that cover applications in which interference from biomolecules is expected [90].

Reporting Conformational Change with Excimers

Some fluorophores can form non-covalent dimers (excimers) through stacking interactions that entail changes in their absorption and fluorescence spectra. The fluorescence decrease of rhodamine dyes upon dimer formation has been linked to the conformational changes of PBPs in two instances to report ligand binding. Dual labeling with two identical dyes circumvents the difficulty of introducing orthogonal functionality required for FRET labeling, while maintaining the possibility to rationally position the labels.

Five different double cysteine mutants of phosphate-binding protein were labeled with three different thiol-reactive rhodamines. The best performing combination exhibited an impressive 18-fold increase of fluorescence upon phosphate addition due to the dissociation of the dimer. In an interesting application, the release of inorganic phosphate from ATP by the action of a helicase could be monitored with this construct [91].

A similar strategy was employed to use molecular exciton quenching to report glucose binding to GBP [92]. Several combinations of attachment sites appropriately spaced to permit rhodamine dimer formation were identified by examination of the crystal structure of GBP. After labeling with either rhodamine red (RR) or TMR, responsiveness to glucose was observed for most of these combinations. However, the observed signal change was significantly smaller than in the reported phosphate sensor [91], not exceeding a 43% increase. Additional mutations in the binding pocket of GBP were introduced to enhance the range of measurable glucose concentrations to several orders of magnitude by altering the dissociation constants [92].

Reporting PBP conformational changes by forming or breaking of excimers offers several potential advantages over detection with solvatochromic dyes.

First, the favorable spectral characteristics of rhodamine dyes permit measurements at longer wavelengths (>575 nm) than many of the commercially available environment-sensitive dyes. Second, the detection does not rely on the polarity of the solvent, which eliminates a potential source of error when measuring in complex samples [92]. On the other hand, any unpaired rhodamines introduce high background fluorescence. Indeed, a strong dependence of signal change on the coupling efficiency of TMR to phosphate-binding protein was reported [91]. The difficulty to account for this variable by referencing might limit the potential applications of this approach in routine measurements.

Bioluminescence Resonance Energy Transfer

A variation of the well-characterized FLIPs has recently been described, in which the fluorescence donor is functionally replaced by a variant of the bioluminescent Renilla luciferase. Bioluminescence resonance energy transfer (BRET) enables better spectral separation of the donor and acceptor emission peaks and has larger Förster distances which better agree with typical distances between N- and C-termini of PBPs. Furthermore, there is no requirement for an excitation light source, which simplifies the necessary instrumentation. An MBP-based BRET sensor was recently reported as proof of principle [93]. However, the requirement for supplying coelenterazine as a luciferase substrate limits the broad applicability of this concept.

3.3 Protein Complementation

Protein complementation assays have found wide application in the biological sciences to monitor binary protein interactions in vivo. In the classical implementation, two fragments of a reporter protein are tethered to the potential interaction partners and reconstitute to a functional assembly when brought into close proximity [94, 95]. In variations of this approach, hybrid proteins have been created by attachment of both reporter protein fragments to a single PBP polypeptide chain in order to report ligand binding to the PBP recognition element. Reconstitution of the functional reporter proteins is accomplished by structural rearrangement of the PBP element upon ligand binding. Alternatively, PBP conformational changes can allosterically modulate the activity of linear or circularly permuted enzymes or FPs by inducing subtle steric rearrangements. In several independent approaches, the use of enzymes, transcription factors, and fluorescent proteins as transducing elements has been explored.

Amplification of signals of biological detection systems is frequently achieved by coupling to a secondary enzymatic reaction. Complementation of functional enzymes from inactive fragments, modulation of enzyme activity, and transcriptional activation of an enzyme in response to PBP conformational changes have

been reported. One drawback for routine practical applications with enzymes as diagnostic tools is the requirement for an exogenous agent as substrate for the enzyme, which needs to be supplemented before use.

A glucose sensor with unusually broad dynamic range was constructed by inserting glucose-binding protein in a flexible surface loop of the bioluminescent protein aequorin [96]. Aequorin creates a bioluminescent signal through oxidation of its substrate coelenterazine in the presence of molecular oxygen and calcium ions. A concentration-dependent increase of bioluminescence from the GBP-aequorin fusion protein was recorded, covering an analyte concentration range of 4–5 orders of magnitude. Although a priori the interaction of GBP with its ligand is not expected to be significantly changed compared to the free binding protein, the apparent affinity of the biosensor towards glucose was only in the high micromolar range, indicating subtle disturbances of GBP structure or flexibility [96]. A bioluminescent glucose sensor was similarly constructed by alternating the small and large domains of firefly luciferase with stretches from the GBP sequence. The apparent affinity of this construct towards glucose better reflects that of wild-type GBP [97]. Indirect bioluminescent reporting of intracellular glucose concentrations was recently achieved by functional coupling of ligand binding to GBP to transcriptional activation of luciferase expression. GBP was fused between the DNA binding and oligomerization domains of the LacI transcription repressor. Binding of glucose to the hybrid protein triggers release of the repressor from its operator region and transcription of a downstream luciferase gene [98].

The Ostermeier Lab has developed a technology which allows to screen for sensors with strong signal gains from a library of bacterial clones. A combinatorial approach was used to identify sites within the sequence of MBP that tolerate insertion of linear or circularly permuted TEM-1 β-lactamase (BLA). Screening for variants that retain both maltose binding and BLA activity followed by extensive optimization of linker and insertion sites finally identified protein switches that respond to maltose by a 600-fold alteration of BLA activity [99–101]. Structural analysis and molecular modeling of one of these sensors suggest that physical strain imposed to a β-strand region of BLA by the MBP scaffold prevents productive assembly of the binding site. After binding of maltose, relaxation of the substructure is thought to allow for restoration of the catalytic activity [102]. The virtue of this approach lies in the use of β-lactamase as transducer which combines two functions: it allows for screening of large libraries for antibiotic-resistant clones and provides the readout of the sensor by hydrolysis of the chromogenic substrate nitrocefin. The efficiency of the screening approach was demonstrated by identifying MBP mutants from a binding site library that respond to a different substrate, i.e. to glucose [101]. Although the screening technology should be applicable to virtually all members of the PBP family, only recently a ribose sensor was constructed by recombination of RBP and β-lactamase [103].

Fluorescence complementation was achieved by sandwiching MBP between the N- and C-terminal halves of GFP. MBP closure induced by maltose binding reconstitutes GFP and switches on fluorescence. However, this sensor requires

further optimization due to its low signal change and long response time in the order of at least tens of minutes [104].

In an effort to create a family of high S/N fluorescent sensors, Marvin et al. [105] designed a similar construct by allosterically inserting circularly permuted GFP (cpGFP) into the backbone of MBP. In the absence of ligand, fluorescence is minimal, but maltose binding alters the microenvironment of the chromophore molecule within the GFP barrel such that an appreciably bright sensor is obtained. In this study, taking advantage of allosteric coupling, the authors independently altered the affinity of the recognition element to the ligand and the spectral parameters of the transducing fluorophore to construct an array of maltose sensors covering different concentration ranges. The combination of all four sensors in one solution allowed to measure maltose concentrations over three orders of magnitude [105]. While the strategy of inserting circularly permuted FPs into the PBP scaffold has the potential to design high S/N sensors for various substrates, subsequent work on a phosphonate sensor with cpGFP as reporting element shows that each sensor still needs to be optimized individually [106].

3.4 Electrochemical PBP Sensors

A direct electrochemical readout of ligand binding events without an intermediate optical step could simplify the development of miniaturized and inexpensive devices. However, while electrochemical reporting of hinge-bending motions of nucleic acid aptamers is an established technique [107], the conformational changes of PBPs appear less amenable to electrochemical detection. Compared to the large body of data documenting the efforts to generate optical transducers of PBP-ligand binding, relatively few groups have reported electrochemical biosensors based on periplasmic binding proteins.

Similar to optical probes that change their spectral properties in function of the polarity of their microenvironment, solvatochromism has been described for redox active complexes of transition metals. Trammell et al. synthesized a cysteine reactive redox probe, $[Ru(II)(NH_3)_4(1,10\text{-phenanthroline-5-maleimide})](PF_6)_2$, and demonstrated that the formal potential of the Ru(II/III) redox couple in this complex is sensitive to the polarity of the solvent [108]. Subsequently, the complex was conjugated to two MBP variants (D95C and S233C, respectively), previously shown to be maltose responsive when analogously labeled with the fluorophores IANBD or acrylodan [109]. Cyclic voltammetry measurements of the modified MBPs in aqueous solutions demonstrated a clear response of the formal redox potential to maltose for ruthenium-conjugated D95C MBP. The shift in electrochemical potential upon maltose saturation varies between 6 and 14 mV, depending on protein concentration and solvent. In contrast, the S233C variant, where the label is supposed to reside partially within the binding site, is unresponsive to maltose [108].

The same redox probe was utilized in a different setup, where four different PBPs (MBP, GBP, GlnBP, and an engineered zinc-sensitive MBP derivative) were

tethered with their respective carboxy-termini to a Ni-NTA-coated gold electrode through an oligohistidine tag. The ruthenium label was attached to residues estimated to face towards the electrode surface and probed by AC voltammetry. In this setup, the attachment sites were not selected to undergo a change in solvent accessibility upon hinge closure. Therefore, the observable in this experiment is a current difference that is supposed to depend on the average distance of the redox label from the electrode surface, rather than a variation in redox potential. In all four instances, the observed AC current decreased upon titration of the respective ligand and binding isotherms could be readily fitted [110]. This concept was further elaborated by direct attachment of labeled MBP to a gold electrode surface through a metallothionein domain. In the absence of a surface-modifying linker layer, electron transfer to the electrode is improved and squarewave voltammetry (SWV) can be used to characterize the redox system [111]. SWV reduces the sensitivity of the system to capacitive background current and diffusion processes, which makes the response less complex and data analysis generally simpler and more quantitative.

Direct, orientation-specific deposition of a binding protein on a bare gold electrode surface through a Au-S bond was similarly accomplished by engineering a cysteine residue at the N-terminus of GBP [112, 113]. The protein monolayer covering the electrode surface governs the impedance of the system in response to an AC current without the need to attach a redox probe to the protein. In the presence of glucose, a maximum change in the magnitude of the impedance of 4.5% [113] reflects alterations in the thickness and rigidity of the protein film [114]. The concentration-dependent impedance change is readily fitted to a Langmuir isotherm and indicates a dramatic loss of GBP affinity, probably due to steric restrictions imposed by the linkerless attachment to the surface [113].

More recently, label-free GBP was deposited by sulfhydryl linkage to gold nanoparticles coated to a glassy carbon electrode. Cyclic voltammetry (CV) was used to detect electron transfer to the ferrocyanide/ferricyanide redox couple in solution. Upon addition of glucose the peak potential increased with a concomitant decrease of current, indicating impeded charge transfer of the redox probe by the adsorbed surface layer. Application of CV in this system permits the use of standard instrumentation and facilitates the interpretation of the data since it eliminates the requirement to create the detailed circuit models necessary for impedance spectroscopy. Instead, a linear correlation between glucose concentration and peak current can be observed. Further advantages of the improved electrode surface are a lower detection limit, faster response times, and enhanced signal stability [115].

4 Towards PBP-Based Sensor Devices

Considerable efforts have been undertaken to transduce the conformational changes of PBPs to an observable that can be easily detected and quantified and many valuable proof-of-principle experiments were reported. The majority of these experiments

were performed in aqueous solution, with the notable exceptions of genetically encoded sensors observed in situ in the cellular environment of their hosts, and electrochemical detection schemes, where immobilization to the electrode is a necessary condition to monitor sensor performance. However, simple solution phase measurements are practical only for relatively few applications. In order to permit efficient transport and storage of the sensor, its durable implementation into a dedicated device, or facile positioning in a test object or sample, it is usually desired that the sensor be trapped into a solid matrix or immobilized to a surface. A substantial challenge for the construction of immobilized PBP-based biosensors is the requirement to retain (or instantaneously restore) the conformational flexibility of the immobilized protein. Many common immobilization strategies, such as copolymerization with a biopolymer or immobilization to a carrier through amine coupling, are prone to imposing conformational stress on the immobilized protein [116]. Fluorescent detection schemes are furthermore susceptible to interferences by background fluorescence or, in the case of solvatochromic fluorophores, to unspecific interactions between dye and matrix that may alter its spectroscopic properties [117]. The most suitable immobilization technique will depend not only on the chemical and optical properties of the sensors but also on the intended application: steady state measurements, in which an analyte is sampled prior to measurement and its concentration determined at a single point in time, allow the investigator to manipulate the sample, e.g., by dilution, temperature control, or placement into a dedicated device, before the measurement is performed. In contrast, when an analyte is to be continuously monitored over a period of time, sample manipulation is infeasible.

Microtiter plate-based optical sensing systems for high-throughput measurements were developed by orientation-specific attachment of labeled PBPs to plastic surfaces. Glutamine-binding protein was directionally immobilized to microplates by hydrophobic interaction through a carboxy-terminal fusion with a tandem repeat of a hydrophobic peptide sequence derived from the structural protein elastin. IANBD-labeled GlnBP adsorbed to polystyrene microplates through a 12-mer elastin repeat retained its responsiveness to glutamine in fluorescence assays [118]. An alternative to the potentially labile adhesion by hydrophobic interactions is the covalent attachment to the support. Because the protein requires a unique reactive functionality for site-specific attachment, this is a challenging task, especially, if a reporter fluorophore is to be conjugated to a sulfhydryl group. Directional attachment of fluorescently labeled PBPs has been achieved using strategies developed for orthogonal labeling with two different dyes: Coupling of fluorescently labeled GBP and RBP from thermophilic organisms to maleimide-activated microplates was performed using a zinc-finger deprotection strategy [119] similar to the protocol used for orthogonal labeling with a FRET pair [89]. Both N- and C-terminal attachments of the zinc finger slightly altered affinity and brightness of the sensor without compromising the applicability of the sensor [119]. A pyridoxal phosphate-mediated amino-terminal biotinylation of TAMRA labeled GlnBP, and its immobilization to streptavidin-coated plates, was demonstrated, but the response to glutamine was not analyzed [88].

Research directed towards the development of continuous measurement devices was mainly driven by the desire to develop systems for continuous monitoring of blood glucose in diabetes management. Therefore, the most advanced sensor prototypes so far are based on GBP as recognition element. Initially, solutions of fluorescent biosensors were encapsulated in hollow dialysis membranes and analytes allowed to access the detection chamber by diffusion [120, 121]. More recently, adsorption to $CaCO_3$ particles and microencapsulation in alternating layers of poly-L-lysine and heparin [63] or capture of hexahistidine-tagged GBP with Ni-NTA functionalized agarose and polystyrene beads [64] was proposed to immobilize the sensors. Beads labeled with GBP-BADAN were placed in a chamber made up of a porous nylon mesh at the tip of an optical fiber and immersed in an organ bath. Fluorescence lifetimes changed by 40% and 10% in response to saturating concentrations of glucose for the agarose and polystyrene-immobilized sensor, respectively [64]. Despite its beneficial reference-free detection technique and fast response times of only 10 min, possible leaking of nickel from the support is a concern for in vivo application.

Immobilization of labeled protein to a two-dimensional surface limits the amount of available biosensor and consequently the attainable S/N ratio. Embedding the sensor into three-dimensional matrices greatly enhances the available space for biosensor deposition. The most sophisticated sensors reported so far utilize labeled GBP embedded into hydrogel matrices positioned at the tip of an optical fiber. Hydrogels can be engineered to exhibit excellent biocompatibility and resistance to biofouling and provide a hydrophilic environment [122] that supports hydration and thus maintains the functionality of PBPs. For initial experiments, binding proteins labeled with NIR solvatochromic dyes were infused into disks of cross-linked polyethylene glycol (PEG), and glucose- or maltose-dependent signals read across skin explants with fiber optics. These sensors showed a ligand-dependent signal increase of up to 111% when observed through the skin, and response times were within a few minutes, limited by the diffusion of sugar into the PEG disks [54]. Later implementations used GBP functionalized with MDCC embedded in a poly-acrylamide hydrogel [123] or with acrylodan in a copolymer of PEG-dimethacrylate and methacrylic acid (PEGDMA:MAA) [56]. For this most recent implementation, immobilization of a thermostability enhanced GBP-acrylodan to the PEGDMA: MAA matrix by amine coupling with EDC/NHS was performed in an independent reaction after polymerization of the hydrogel. The performance of a subcutaneously implanted sensor device was demonstrated in a preclinical trial in a Yucatan swine model over a period of 7 days. While the absolute fluorescence intensity decreases over time, supposedly through a combination of biofouling and photobleaching effects, a ratiometric determination of acrylodan fluorescence allowed for accurate glucose determination using single daily reference measurements for sensor recalibration [56].

A common feature of the matrix materials successfully employed for fluorescent biosensor embedding is their hydrophilic character, which indicates that hydration of the labeled protein is required to maintain its structure, flexibility, or the micro-environment of the solvatochrome. This is supported by studies with NBD-labeled

MBP that was embedded in a diglycerolsilane-derived mesoporous sol gel [117]. PEGylation increased the maltose-induced fluorescence change of this conjugate when embedded in the matrix, but not in solution. Improved hydration of the protein is thought to be responsible for this effect. Embedment into hydrophilic matrices with high water content has shown significant potential for applications in continuous monitoring where stabilities over periods of days or weeks are envisaged and regular recalibration is feasible to account for loss of activity. However, protein inactivation by high water content is a serious obstacle for applications requiring storage stability over prolonged periods of time, such as disposable test strip formats for home glucose monitoring. Numerous diagnostic procedures are based on enzymes or antibodies that are embedded in dry matrices without significant loss of activity. In contrast, immobilization and dehydration of PBPs or their respective conjugates have only been reported in a few instances. Weidemaier et al. [56] mention drying GBP-acrylodan in microplates in the presence of trehalose and reconstitution of the protein with sample solution within minutes. A thermostable, IAANS-labeled sugar-binding protein from *Pyrococcus horikoshii* was immobilized to aldehyde-functionalized quartz slides and retained weak responsiveness to glucose when observed in front-face fluorescence measurements after drying [124]. Development of support materials that allow for long-term storage and efficient rehydration of PBP biosensors and minimally interfere with fluorescence detection by auto-fluorescence or light scattering will be of critical importance to extend the application range of PBP biosensors.

Acknowledgments I would like to thank Stacy DuVall for helpful discussions on electrochemical topics and critical reading of the draft. Thomas Meier is acknowledged for valuable suggestions to the draft. This work was promoted by the European Union under grant agreement number 264772 (ITN CHEBANA).

References

1. Tam R, Saier MH Jr (1993) Structural, functional, and evolutionary relationships among extracellular solute-binding receptors of bacteria. Microbiol Rev 57:320–346
2. Dwyer MA, Hellinga HW (2004) Periplasmic binding proteins: a versatile superfamily for protein engineering. Curr Opin Struct Biol 14:495–504
3. Felder CB, Graul RC, Lee AY et al (1999) The Venus flytrap of periplasmic binding proteins: an ancient protein module present in multiple drug receptors. AAPS PharmSci 1:E2
4. Wilkinson AJ, Verschueren KHG (2003) Crystal structures of periplasmic solute-binding proteins in ABC transport complexes illuminate their function. In: Holland IB, Susan PCC, Karl K, Higgins CF (eds) ABC proteins. Academic, London
5. Quiocho FA, Ledvina PS (1996) Atomic structure and specificity of bacterial periplasmic receptors for active transport and chemotaxis: variation of common themes. Mol Microbiol 20:17–25
6. Marvin JS, Hellinga HW (2001) Manipulation of ligand binding affinity by exploitation of conformational coupling. Nat Struct Biol 8:795–798
7. Marvin JS, Hellinga HW (2001) Conversion of a maltose receptor into a zinc biosensor by computational design. Proc Natl Acad Sci U S A 98:4955–4960

8. Allert M, Rizk SS, Looger LL et al (2004) Computational design of receptors for an organophosphate surrogate of the nerve agent soman. Proc Natl Acad Sci U S A 101: 7907–7912
9. Schreier B, Stumpp C, Wiesner S et al (2009) Computational design of ligand binding is not a solved problem. Proc Natl Acad Sci U S A 106:18491–18496
10. Tang C, Schwieters CD, Clore GM (2007) Open-to-closed transition in apo maltose-binding protein observed by paramagnetic NMR. Nature 449:1078–1082
11. Berman HM, Westbrook J, Feng Z et al (2000) The Protein Data Bank. Nucleic Acids Res 28:235–242
12. Davidson AL, Dassa E, Orelle C et al (2008) Structure, function, and evolution of bacterial ATP-binding cassette systems. Microbiol Mol Biol Rev 72:317–364
13. Deuschle K, Fehr M, Hilpert M et al (2005) Genetically encoded sensors for metabolites. Cytometry A 64A:3–9
14. Quiocho FA, Higgins CF (1990) Atomic structures of periplasmic binding proteins and the high-affinity active transport systems in bacteria [and discussion]. Philos Trans R Soc Lond B Biol Sci 326:341–352
15. Heddle J, Scott DJ, Unzai S et al (2003) Crystal structures of the liganded and unliganded nickel-binding protein NikA from *Escherichia coli*. J Biol Chem 278:50322–50329
16. Vyas NK, Vyas MN, Quiocho FA (1987) A novel calcium binding site in the galactose-binding protein of bacterial transport and chemotaxis. Nature (Lond) 327:635–638
17. Stepanenko OV, Povarova OI, Stepanenko OV et al (2010) Structure and stability of D-galactose/D-glucose-binding protein. The role of D-glucose binding and Ca ion depletion. Spectroscopy 24:355–359
18. Schrödinger, LLC (2010) The PyMOL molecular graphics system, Version 1.3.
19. Borrok MJ, Kiessling LL, Forest KT (2007) Conformational changes of glucose/galactose-binding protein illuminated by open, unliganded, and ultra-high-resolution ligand-bound structures. Protein Sci 16:1032–1041
20. Duan X, Quiocho FA (2001) Structural evidence for a dominant role of nonpolar interactions in the binding of a transport/chemosensory receptor to its highly polar ligands. Biochemistry 41:706–712
21. Quiocho FA, Spurlino JC, Rodseth LE (1997) Extensive features of tight oligosaccharide binding revealed in high-resolution structures of the maltodextrin transport/chemosensory receptor. Structure (London) 5:997–1015
22. Raines DJ, Moroz OV, Wilson KS et al (2013) Interactions of a periplasmic binding protein with a tetradentate siderophore mimic. Angew Chem 52:4595–4598
23. Mao B, Pear MR, McCammon JA et al (1982) Hinge-bending in L-arabinose-binding protein. The "Venus's-flytrap" model. J Biol Chem 257:1131–1133
24. Sack JS, Saper MA, Quiocho FA (1989) Periplasmic binding protein structure and function: refined X-ray structures of the leucine/isoleucine/valine-binding protein and its complex with leucine. J Mol Biol 206:171–191
25. Döring K, Surrey T, Nollert P et al (1999) Effects of ligand binding on the internal dynamics of maltose-binding protein. Eur J Biochem 266:477–483
26. Bermejo GA, Strub M-P, Ho C et al (2010) Ligand-free open−closed transitions of periplasmic binding proteins: the case of glutamine-binding protein. Biochemistry 49:1893–1902
27. Ortega G, Castaño D, Diercks T et al (2012) Carbohydrate affinity for the glucose-galactose binding protein is regulated by allosteric domain motions. J Am Chem Soc 134:19869
28. Björkman AJ, Mowbray SL (1998) Multiple open forms of ribose-binding protein trace the path of its conformational change. J Mol Biol 279:651–664
29. Magnusson U, Chaudhuri BN, Ko J et al (2002) Hinge-bending motion of D-Allose-binding protein from *Escherichia coli*. J Biol Chem 277:14077–14084
30. Trakhanov S, Vyas NK, Luecke H et al (2005) Ligand-free and -bound structures of the binding protein (LivJ) of the *Escherichia coli* ABC Leucine/Isoleucine/Valine transport system: trajectory and dynamics of the interdomain rotation and ligand specificity. Biochemistry 44:6597–6608

31. Telmer PG, Shilton BH (2003) Insights into the conformational equilibria of maltose-binding protein by analysis of high affinity mutants. J Biol Chem 278:34555–34567
32. Conroy PJ, Hearty S, Leonard P et al (2009) Antibody production, design and use for biosensor-based applications. Semin Cell Dev Biol 20:10–26
33. Bergmeyer HU, Bergmeyer J, Grassl M (1983) Methods of enzymatic analysis. Verlag Chemie, Weilheim (Vol. Bd. 1)
34. Hönes J, Müller P, Surridge N (2008) The technology behind glucose meters: test strips. Diabetes Technol Ther 10:S-10–S-26
35. Lever JE (1972) Quantitative assay of the binding of small molecules to protein: comparison of dialysis and membrane filter assays. Anal Biochem 50:73–83
36. Oshima RG, Willis RC, Furlong CE et al (1974) Binding assays for amino acids. J Biol Chem 249:6033–6039
37. Willis RC, Seegmiller JE (1976) A filtration assay specific for the determination of small quantities of l-glutamine. Anal Biochem 72:66–77
38. Zukin RS, Strange PG, Heavey LR et al (1977) Properties of the galactose binding protein of Salmonella typhimurium and *Escherichia coli*. Biochemistry 16:381–386
39. Medintz IL, Deschamps JR (2006) Maltose-binding protein: a versatile platform for prototyping biosensing. Curr Opin Biotechnol 17:17–27
40. Loving GS, Sainlos M, Imperiali B (2010) Monitoring protein interactions and dynamics with solvatochromic fluorophores. Trends Biotechnol 28:73–83
41. Lakowicz JR (2006) Principles of fluorescence spectroscopy. Springer, New York
42. Boos W, Gordon AS, Hall RE et al (1972) Transport properties of the Galactose-binding protein of *Escherichia coli*. J Biol Chem 247:917–924
43. Zukin RS, Hartig PR, Koshland DE (1977) Use of a distant reporter group as evidence for a conformational change in a sensory receptor. Proc Natl Acad Sci 74:1932–1936
44. Zhou LQ, Cass AEG (1991) Periplasmic binding protein based biosensors. 1. Preliminary study of maltose binding protein as sensing element for maltose biosensor. Biosens Bioelectron 6:445–450
45. Sohanpal K, Watsuji T, Zhou LQ et al (1993) Reagentless fluorescence sensors based upon specific binding proteins. Sens Actuators B Chem 11:547–552
46. Gilardi G, Zhou LQ, Hibbert L et al (1994) Engineering the maltose binding protein for reagentless fluorescence sensing. Anal Chem 66:3840–3847
47. de Lorimier RM, Smith JJ, Dwyer MA et al (2002) Construction of a fluorescent biosensor family. Protein Sci 11:2655–2675
48. Amiss TJ, Sherman DB, Nycz CM et al (2007) Engineering and rapid selection of a low-affinity glucose/galactose-binding protein for a glucose biosensor. Protein Sci 16:2350–2359
49. Khan F, Saxl TE, Pickup JC (2010) Fluorescence intensity- and lifetime-based glucose sensing using an engineered high-Kd mutant of glucose/galactose-binding protein. Anal Biochem 399:39–43
50. Dattelbaum JD, Looger LL, Benson DE et al (2005) Analysis of allosteric signal transduction mechanisms in an engineered fluorescent maltose biosensor. Protein Sci 14:284–291
51. Sherman DB, Pitner JB, Ambroise A et al (2006) Synthesis of thiol-reactive, long-wavelength fluorescent phenoxazine derivatives for biosensor applications. Bioconjug Chem 17:387–392
52. Thomas J, Sherman DB, Amiss TJ et al (2007) Synthesis and biosensor performance of a near-IR thiol-reactive fluorophore based on Benzothiazolium Squaraine. Bioconjug Chem 18:1841–1846
53. Thomas J, Cash MT (2008) Preparation of coumarin containing dyes having ratiometric fluorescence response for biosensor in detecting metabolites. Patent number WO2008147805A2
54. Thomas J, Ambroise A, Birchfield K et al (2006) Long wavelength fluorescence based biosensors for in vivo continuous monitoring of metabolites. Proc SPIE-Int Soc Opt Eng 6078:60781Y-1–60781Y-9
55. Borisov SM, Wolfbeis OS (2008) Optical biosensors. Chem Rev 108:423–461

56. Weidemaier K, Lastovich A, Keith S et al (2011) Multi-day pre-clinical demonstration of glucose/galactose binding protein-based fiber optic sensor. Biosens Bioelectron 26:4117–4123
57. Tolosa L, Ge X, Rao G (2003) Reagentless optical sensing of glutamine using a dual-emitting glutamine-binding protein. Anal Biochem 314:199–205
58. Lam H, Kostov Y, Rao G et al (2008) Low-cost optical lifetime assisted ratiometric glutamine sensor based on glutamine binding protein. Anal Biochem 383:61–67
59. Ge X, Tolosa L, Rao G (2004) Dual-labeled glucose binding protein for ratiometric measurements of glucose. Anal Chem 76:1403–1410
60. Gilardi G, Mei G, Rosato N et al (1997) Spectroscopic properties of an engineered maltose binding protein. Protein Eng 10:479–486
61. Brune M, Hunter JL, Howell SA et al (1998) Mechanism of inorganic phosphate interaction with phosphate binding protein from *Escherichia coli*. Biochemistry 37:10370–10380
62. Dattelbaum JD, Lakowicz JR (2001) Optical determination of glutamine using a genetically engineered protein. Anal Biochem 291:89–95
63. Saxl T, Khan F, Matthews DR et al (2009) Fluorescence lifetime spectroscopy and imaging of nano-engineered glucose sensor microcapsules based on glucose/galactose-binding protein. Biosens Bioelectron 24:3229–3234
64. Saxl T, Khan F, Ferla M et al (2011) A fluorescence lifetime-based fibre-optic glucose sensor using glucose/galactose-binding protein. Analyst 136:968–972 (Cambridge, UK)
65. Tolosa L (2009) On the design of low-cost fluorescent protein biosensors. Adv Biochem Eng Biotechnol 116:143–157
66. Lakowicz JR, Castellano FN, Dattelbaum JD et al (1998) Low-frequency modulation sensors using nanosecond fluorophores. Anal Chem 70:5115–5121
67. Tolosa L, Gryczynski I, Eichhorn LR et al (1999) Glucose sensor for low-cost lifetime-based sensing using a genetically engineered protein. Anal Biochem 267:114–120
68. Ge X, Lam H, Modi SJ et al (2007) Comparing the performance of the optical glucose assay based on glucose binding protein with high-performance anion-exchange chromatography with pulsed electrochemical detection: efforts to design a low-cost point-of-care glucose sensor. J Diabetes Sci Technol 1:864–872
69. Wenner BR, Douglass P, Shrestha S et al (2001) Genetically designed biosensing systems for high-throughput screening of pharmaceuticals, clinical diagnostics, and environmental monitoring. Proc SPIE-Int Soc Opt Eng 4252:59–70
70. Frommer WB, Davidson MW, Campbell RE (2009) Genetically encoded biosensors based on engineered fluorescent proteins. Chem Soc Rev 38:2833–2841
71. Okumoto S, Takanaga H, Frommer WB (2008) Quantitative imaging for discovery and assembly of the metabo-regulome. New Phytol 180:271–295
72. Galbán J, Sanz-Vicente I, Ortega E et al (2012) Reagentless fluorescent biosensors based on proteins for continuous monitoring systems. Anal Bioanal Chem 402:3039–3054
73. Fehr M, Frommer WB, Lalonde S (2002) Visualization of maltose uptake in living yeast cells by fluorescent nanosensors. Proc Natl Acad Sci 99:9846–9851
74. Deuschle K, Okumoto S, Fehr M et al (2005) Construction and optimization of a family of genetically encoded metabolite sensors by semirational protein engineering. Protein Sci 14:2304–2314
75. Ha J-S, Song JJ, Lee Y-M et al (2007) Design and application of highly responsive fluorescence resonance energy transfer biosensors for detection of sugar in living Saccharomyces cerevisiae cells. Appl Environ Microbiol 73:7408–7414
76. Gu H, Lalonde S, Okumoto S et al (2006) A novel analytical method for in vivo phosphate tracking. FEBS Lett 580:5885–5893
77. Takanaga H, Chaudhuri B, Frommer WB (2008) GLUT1 and GLUT9 as major contributors to glucose influx in HepG2 cells identified by a high sensitivity intramolecular FRET glucose sensor. Biochim Biophys Acta 1778:1091–1099
78. Okada S, Ota K, Ito T (2009) Circular permutation of ligand-binding module improves dynamic range of genetically encoded FRET-based nanosensor. Protein Sci 18:2518–2527

79. Okumoto S, Looger LL, Micheva KD et al (2005) Detection of glutamate release from neurons by genetically encoded surface-displayed FRET nanosensors. Proc Natl Acad Sci U S A 102:8740–8745
80. Fehr M, Lalonde S, Lager I et al (2003) In Vivo imaging of the dynamics of glucose uptake in the Cytosol of COS-7 cells by fluorescent nanosensors. J Biol Chem 278:19127–19133
81. Fehr M, Lalonde S, Ehrhardt DW et al (2004) Live imaging of glucose homeostasis in nuclei of COS-7 cells. J Fluoresc 14:603–609
82. Deuschle K, Chaudhuri B, Okumoto S et al (2006) Rapid metabolism of glucose detected with FRET glucose nanosensors in epidermal cells and intact roots of Arabidopsis RNA-Silencing mutants. Plant Cell 18:2314–2325
83. Bermejo C, Haerizadeh F, Takanaga H et al (2011) Optical sensors for measuring dynamic changes of cytosolic metabolite levels in yeast. Nat Protoc 6:1806–1817
84. Dulla C, Tani H, Okumoto S et al (2008) Imaging of glutamate in brain slices using FRET sensors. J Neurosci Methods 168:306–319
85. Kaper T, Lager I, Looger LL et al (2008) Fluorescence resonance energy transfer sensors for quantitative monitoring of pentose and disaccharide accumulation in bacteria. Biotechnol Biofuels 1:11
86. Hou B-H, Takanaga H, Grossmann G et al (2011) Optical sensors for monitoring dynamic changes of intracellular metabolite levels in mammalian cells. Nat Protoc 6:1818–1833
87. Bermejo C, Ewald JC, Lanquar V et al (2011) In vivo biochemistry: quantifying ion and metabolite levels in individual cells or cultures of yeast. Biochem J 438:1–10
88. Crochet AP, Kabir MM, Francis MB et al (2010) Site-selective dual modification of periplasmic binding proteins for sensing applications. Biosens Bioelectron 26:55–61
89. Smith JJ, Conrad DW, Cuneo MJ et al (2005) Orthogonal site-specific protein modification by engineering reversible thiol protection mechanisms. Protein Sci 14:64–73
90. Dweik M, Milanick M, Grant S (2007) Development of a glucose binding protein biosensor. Proc SPIE-Int Soc Opt Eng 6759:67590I-1–67590I-8
91. Okoh MP, Hunter JL, Corrie JET et al (2006) A biosensor for inorganic phosphate using a rhodamine-labeled phosphate binding protein. Biochemistry 45:14764–14771
92. Der BS, Dattelbaum JD (2008) Construction of a reagentless glucose biosensor using molecular exciton luminescence. Anal Biochem 375:132–140
93. Dacres H, Michie M, Anderson A et al (2013) Advantages of substituting bioluminescence for fluorescence in a resonance energy transfer-based periplasmic binding protein biosensor. Biosens Bioelectron 41:459–464
94. Shekhawat SS, Ghosh I (2011) Split-protein systems: beyond binary protein-protein interactions. Curr Opin Chem Biol 15:789–797
95. Stynen B, Tournu H, Tavernier J et al (2012) Diversity in genetic in vivo methods for protein-protein interaction studies: from the yeast two-hybrid system to the mammalian split-luciferase system. Microbiol Mol Biol Rev 76:331–382
96. Teasley Hamorsky K, Ensor CM, Wei Y et al (2008) A bioluminescent molecular switch for glucose. Angew Chem 120:3778–3781
97. Taneoka A, Sakaguchi-Mikami A, Yamazaki T et al (2009) The construction of a glucose-sensing luciferase. Biosens Bioelectron 25:76–81
98. Sakaguchi-Mikami A, Taniguchi A, Sode K et al (2011) Construction of a novel glucose-sensing molecule based on a substrate-binding protein for intracellular sensing. Biotechnol Bioeng 108:725–733
99. Guntas G, Ostermeier M (2004) Creation of an allosteric enzyme by domain insertion. J Mol Biol 336:263–273
100. Guntas G, Mitchell SF, Ostermeier M (2004) A molecular switch created by in vitro recombination of nonhomologous genes. Chem Biol 11:1483–1487
101. Guntas G, Mansell TJ, Kim JR et al (2005) Directed evolution of protein switches and their application to the creation of ligand-binding proteins. Proc Natl Acad Sci U S A 102:11224–11229

102. Ke W, Laurent AH, Armstrong MD et al (2012) Structure of an engineered beta-Lactamase maltose binding protein fusion protein: insights into heterotropic allosteric regulation. PLoS One 7:e39168
103. Tullman J, Guntas G, Dumont M et al (2011) Protein switches identified from diverse insertion libraries created using S1 nuclease digestion of supercoiled-form plasmid DNA. Biotechnol Bioeng 108:2535–2543
104. Jeong J, Kim SK, Ahn J et al (2006) Monitoring of conformational change in maltose binding protein using split green fluorescent protein. Biochem Biophys Res Commun 339:647–651
105. Marvin JS, Schreiter ER, Echevarria IM et al (2011) A genetically encoded, high-signal-to-noise maltose sensor. Proteins 79:3025–3036
106. Alicea I, Marvin JS, Miklos AE et al (2011) Structure of the *Escherichia coli* phosphonate binding protein PhnD and rationally optimized phosphonate biosensors. J Mol Biol 414: 356–369
107. Vallée-Bélisle A, Plaxco KW (2010) Structure-switching biosensors: inspired by nature. Curr Opin Struct Biol 20:518–526
108. Trammell SA, Goldston HM, Tran PT et al (2001) Synthesis and characterization of a Ruthenium(II)-based redox conjugate for reagentless biosensing. Bioconjug Chem 12: 643–647
109. Marvin JS, Corcoran EE, Hattangadi NA et al (1997) The rational design of allosteric interactions in a monomeric protein and its applications to the construction of biosensors. Proc Natl Acad Sci 94:4366–4371
110. Benson DE, Conrad DW, de Lorimier RM et al (2001) Design of bioelectronic interfaces by exploiting hinge-bending motions in proteins. Science 293:1641–1644
111. Morón C, Tremps E, Garcia A et al (2012) Development of an electrochemical maltose biosensor. Key Eng Mat 495:116–119
112. Wang J, Carmon KS, Luck LA et al (2005) Electrochemical impedance biosensor for glucose detection utilizing a periplasmic *E. coli* receptor protein. Electrochem Solid St 8:H61–H64
113. Wang J, Luck LA, Suni II (2007) Immobilization of the Glucose-Galactose receptor protein onto a Au electrode through a genetically engineered cysteine residue. Electrochem Solid St 10:J33–J36
114. Sokolov I, Subba-Rao V, Luck LA (2006) Change in rigidity in the activated form of the Glucose/Galactose receptor from *Escherichia coli*: a phenomenon that will be key to the development of biosensors. Biophys J 90:1055–1063
115. Andreescu S, Luck LA (2008) Studies of the binding and signaling of surface-immobilized periplasmic glucose receptors on gold nanoparticles: a glucose biosensor application. Anal Biochem 375:282–290
116. Costa SA, Azevedo HS, Reis RL (2005) Enzyme immobilization in biodegradable polymers for biomedical applications. In: Reis RL, Roman JS (eds) Biodegradable systems in tissue engineering and regenerative medicine. CRC, Boca Raton, pp 301–323. doi:10.1201/9780203491232.ch17
117. Dattelbaum AM, Baker GA, Fox JM et al (2009) PEGylation of a maltose biosensor promotes enhanced signal response when immobilized in a Silica Sol-Gel. Bioconjug Chem 20: 2381–2384
118. Wada A, Mie M, Aizawa M et al (2003) Design and construction of glutamine binding proteins with a self-adhering capability to unmodified hydrophobic surfaces as reagentless fluorescence sensing devices. J Am Chem Soc 125:16228–16234
119. de Lorimier RM, Tian Y, Hellinga HW (2006) Binding and signaling of surface-immobilized reagentless fluorescent biosensors derived from periplasmic binding proteins. Protein Sci 15:1936–1944
120. Ye K, Schultz JS (2003) Genetic engineering of an allosterically based glucose indicator protein for continuous glucose monitoring by fluorescence resonance energy transfer. Anal Chem 75:3451–3459

121. Salins LLE, Deo SK, Daunert S (2004) Phosphate binding protein as the biorecognition element in a biosensor for phosphate. Sens Actuators B B97:81–89
122. Heo YJ, Takeuchi S (2012) Hydrogel microbeads for implantable glucose sensors. In: Ramalingam M, Tiwari A, Ramakrishna S, Kobayashi H (eds) Integrated biomaterials for biomedical technology. Scrivener Publishing LLC, Beverly MA
123. Siegrist J, Kazarian T, Ensor C et al (2010) Continuous glucose sensor using novel genetically engineered binding polypeptides towards in vivo applications. Sens Actuators B 149:51–58
124. Staiano M, Sapio M, Scognamiglio V et al (2004) A thermostable sugar-binding protein from the Archaeon Pyrococcus horikoshii as a probe for the development of a stable fluorescence biosensor for diabetic patients. Biotechnol Prog 20:1572–1577

BIOREV (2014) 1: 237–260
DOI: 10.1007/11663_2013_6

Published online: 7 December 2013

Hyphenation of Electrochemistry with Mass Spectrometry for Bioanalytical Studies

Marija Cindric and Frank-Michael Matysik

Abstract Hyphenation of electrochemistry (EC) and mass spectrometry (MS) is a growing research field with particular importance for bioanalytical applications. It opens the way for studying reaction mechanisms and metabolic pathways of biological compounds and drugs. Electrochemical conversion of sample molecules prior to MS analysis gives rise to short-lived intermediates and products naturally occurring in biological systems, which leads to better understanding of physiological processes. Numerous interesting and attractive studies in this field have been published so far demonstrating potential of EC–MS coupling. The combination with separation system such as liquid chromatography or capillary electrophoresis widens the scope of application providing additional information about compounds of interest. The combination of EC with liquid chromatography has been the most frequently used hyphenated system due to the simplicity of coupling to mass spectrometric detection. In terms of bioanalytical applications capillary electrophoresis offers some advantages and is a complementary technique to liquid chromatography. This review summarizes recent developments in this field from both instrumental and application perspectives. A rather new approach of coupling electrochemistry–capillary electrophoresis–mass spectrometry and its potential for bioanalysis is presented.

Keywords Bioanalysis · Capillary electrophoresis · Electrochemistry · Liquid chromatography · Mass spectrometry

Contents

M. Cindric and F.-M. Matysik (✉)
Institute of Analytical Chemistry, Chemo- and Biosensors, University of Regensburg, 93040 Regensburg, Germany
e-mail: Frank-Michael.Matysik@chemie.uni-regensburg.de

Abbreviations

APAP	Acetaminophen
AQ	Amodiaquine
Arg	Arginine
BDD	Boron-doped diamond
CE	Capillary electrophoresis
CEM	Chain ejection model
CLZ	Clozapine
CRM	Charge residue model
DEMS	Differential electrochemical mass spectrometry
DESI	Desorption electrospray ionization
DNA	Deoxyribonucleic acid
EAI	Electrochemically assisted injection
EC	Electrochemistry
ESI	Electrospray ionization
FTICR	Fourier transform ion cyclotron resonance
GAL	Galantamine
GMP	Guanosine monophosphate
GSH	Glutathione
ICP–MS	Inductively coupled plasma mass spectrometry
IDA	Interdigitated array
IEM	Ion evaporation model
IR	Infrared
LC	Liquid chromatography
LYC	Lycorine
MALDI	Matrix-assisted laser desorption/ionization
MEKC	Micellar electrokinetic chromatography
MS	Mass spectrometry
NACE	Nonaqueous capillary electrophoresis
NMR	Nuclear magnetic resonance
RNA	Ribonucleic acid
SECM	Scanning electrochemical microscopy
SPE	Screen-printed electrode

TCC	Triclocarban
TOF	Time-of-flight
Trp	Tryptophan
Tyr	Tyrosine
β-LGA	β-lactoglobulin

1 Introduction

Electrochemistry (EC) is a complex and well-developed field, known for its sensitivity and wide scope of application. However, the ability for structural elucidation and the inherent selectivity make mass spectrometry (MS) as detection technique irreplaceable. Therefore hyphenation of these two attractive techniques was a logical step. Coupling of electrochemistry to mass spectrometry dates back to 1970s when Gadde and Bruckenstein [1] applied porous membrane as an EC–MS interface for studying gaseous and volatile products and intermediates of electrochemical reactions. This technique termed differential electrochemical mass spectrometry (DEMS) was established and described by Wolter and Heitbaum in 1984 [2].

The breakthrough of EC–MS coupling in bioanalytics happened in 1992 when Volk et al. [3] applied this concept for studying oxidation pathway of uric acid. Owing to its excellent time resolution and ability to efficiently monitor reactants, short-lived intermediates and reaction products this has become a favorable approach for mimicking processes occurring in vivo. By varying conditions (electrode potential, electrode material, pH, and buffer composition) it is possible to simulate metabolic pathways of biomolecules and pharmaceuticals without unwanted interferences with complex matrix components. The significant advantage of the electrochemical generation of metabolites over other methods is the simple integration of the oxidation reaction into the instrumental system [4]. Combination with separation technique such as liquid chromatography or capillary electrophoresis widens its scope of application and provides additional information about compounds of interest. Recently, a few groups of scientists developed novel approaches for EC–MS coupling.

2 Electrochemical Cell

Electrochemical conversion of target analytes is performed in an electrochemical cell which contains a three-electrode setup as the main part – working, counter (auxiliary), and reference electrodes. The working electrode, where the reaction of interest takes place, is made of glassy carbon, graphite, platinum, gold, or other materials (Table 1). The appropriate potential is adjusted between the working and

Table 1 List of recent bioanalytical applications of EC–MS coupling

Compound	Technique	Electrode material	References
Mitoxantrone	Microchip ESI–MS	Pt	[5]
Guanosine, adenosine, cytidine, uridine, GMP	EC–MS	Conductive diamond	[10]
Paracetamol	EC–MS	Glassy carbon	[12]
Tetrazepam	EC–MS EC–LC–MS	Glassy carbon, Au, Pt	[13]
Verapamil	EC–MS EC–LC–MS	BDD	[14]
Galantamine, lycorine	EC–MS EC–LC–MS	BDD	[15]
Amodiaquine	EC–MS EC–LC–MS	Porous graphite	[16]
Triclocarban	EC–LC–MS	BDD	[17]
Paracetamol, amodiaquine, clozapine	EC–LC–MS	Glassy carbon	[18, 20]
Amiodarone	EC–LC–MS	Glassy carbon	[19]
Diclofenac	EC–MS EC–LC–MS	BDD	[21]
Toremifene	EC–LC–MS	Glassy carbon	[22]
Isatin	EC–MS	Au	[23]
Aniline	EC–MS EC–LC–MS	BDD	[24]
p-Phenylenediamine	EC–MS EC–LC–MS	BDD	[25, 26]
Haloperidol	EC–MS EC–LC–MS	Porous graphite	[28]
4-Chloroaniline	EC–MS	Glassy carbon	[29]
Boscalid	EC–MS EC–LC–MS	Glassy carbon	[30]
Lidocaine	EC–LC–MS	Glassy carbon, Pt, Au	[31, 32]
Catechin, resveratrol, kaempferol, quercetin, quercetin glucosides	EC–MS EC–LC–MS	Glassy carbon	[33]
Roscovitine	EC–LC–MS	Porous glassy carbon	[34]
Zotepine	EC–MS	Porous graphite	[35]
Acebutolol	EC–LC–MS	Glassy carbon	[36]
Methabenzthiazuron, ethidimuron, propanil, PCBs, PAHs	EC–MS	Conductive diamond	[37]
Phenacetin	EC–LC–MS	Pt	[39]
Cyanidin-3-galactoside chloride, cyanidin-3,5-diglucoside chloride	EC–MS	Pt	[40]
α-Tocopherol	EC–LC–MS	Porous graphite	[41]
Guanosine	EC–LC–MS	Conductive diamond	[42]
dGMP, dAMP, dCMP, dTMP, dUMP	EC–MS	Glassy carbon, BDD	[43]

(continued)

Table 1 (continued)

Compound	Technique	Electrode material	References
Uric acid	EC–MS	Stainless steel	[44]
Guanine, adenine, xanthine, hypoxanthine	EC–MS	Stainless steel	[45]
Dopamine, cysteine	EC–MS	Stainless steel	[46, 47]
Guanosine	EC–LC–MS	Conductive diamond	[48]
Gd-based contrast agents Gd-DTPA, Gd-BT-DO3A, Gd-DTPA-BMA, Gd-BOPTA	EC–MS EC–LC–MS EC–CE–MS	BDD	[49]
Tyr- and Trp-containing tripeptides	EC–MS EC–LC–MS	Porous graphite	[51]
Ubiquitin, lysozyme, apomyoglobin	EC–MS EC–LC–MS	Porous graphite, BDD	[53]
Organothiols homocysteine, cysteine, methionine, mercaptoacetic acid, biotin–avidin	EC–MS	Pt	[54]
Cysteine, glutathione disulfide, insulin, β-lactoglobulin A	EC–DESI–MS	Glassy carbon, amalgam	[59]
Apamin, endothelin, flunitrazepam, clonazepam, chlorpromazine hydrochloride	EC–DESI–MS	BDD, amalgam	[60]
β-Lactoglobulin A, lysozyme	EC–DESI–MS	BDD, amalgam	[61]
[Arg^8]-conopressin G, somatostatin 1-14, insulin, α-lactalbumin, L-glutathione disulfide	EC–DESI–MS	Amalgam	[62]
Dopamine, flunitrazepam, clonazepam, chlorpromazine	EC–nanoDESI–MS	Glassy carbon	[63]
Picric acid, alkaline phosphatase	SECM–MS	Carbon	[65]

the reference electrode, while the current generated during oxidation or reduction flows through the counter electrode.

Commercially available EC flow cells have been implemented in most of the studies (Fig. 1). There are two basic types of such cell: amperometric and coulometric [4]. In an amperometric cell the solution either flows over the working electrode surface (thin-layer design) or impinges perpendicularly to the working electrode (wall-jet design). In an amperometric cell only 5–10% analyte is oxidized or reduced

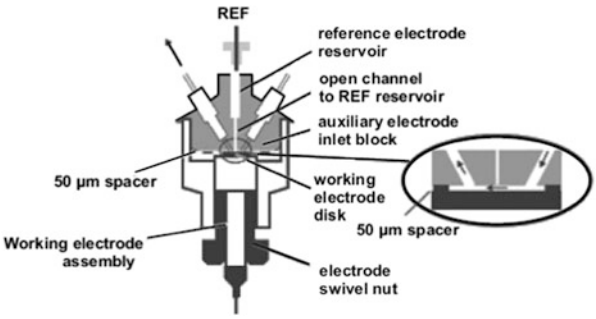

Fig. 1 Schematic diagram of an electrochemical flow cell. Reprinted from [42], with permission from Wiley

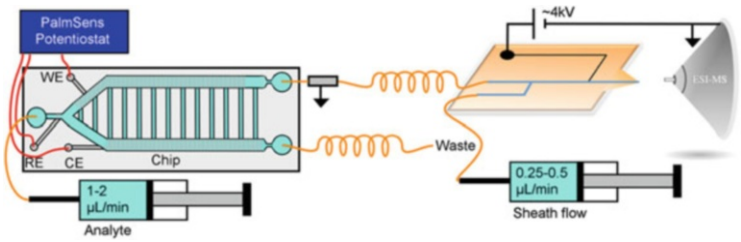

Fig. 2 Schematic overview of a microchip-based setup used for drug metabolism studies. Reprinted from [5], Copyright (2012) American Chemical Society

unless the flow is very low. In a coulometric cell the solution passes through a large porous working electrode, resulting in nearly 100% conversion efficiency. Coulometric cell exhibits high efficiency, good reproducibility and longer maintenance intervals. However, a wider range of electrode materials, easier cleaning procedure and replacement of electrodes make amperometric cells widely used.

Odijk et al. [5] presented a miniaturized electrochemical cell with significantly improved conversion efficiency. The working and the counter electrode are placed in two separated channels to isolate the reaction products generated at both electrodes. The novel design includes connecting channels between these two electrodes to provide a uniform distribution of the current density over the entire working electrode. In addition, the effect of ohmic drop is decreased. A syringe pump introduces the analyte into the electrochemical chip. Electrode potentials are controlled by a potentiostat. The outlet of the working electrode channel is connected to the microchip ESI using a grounded metal union and a fused-silica tubing to provide sufficient electrical resistance. Two flow resistors are included to ensure an equal flow of analyte through both electrode channels (Fig. 2). Using this setup metabolism of mitoxantrone by microchip electrospray ionization mass spectrometry was studied.

3 Electrospray Ionization (ESI)

Electrospray ionization (ESI) invented by John Fenn is currently the most commonly used ionization technique for liquid phase studies due to its ability to detect both small molecules (drugs, metabolites) and large species (proteins, oligonucleotides) and easy online coupling to separation systems. ESI belongs to soft ionization techniques, i.e. little or no fragmentation occurs in the ionization source [6]. Even noncovalent complexes can remain intact. Since analytes are separated according to their mass-to-charge ratio, formation of multiply charged ions enables analysis of very large molecules.

The ESI process comprises the formation of highly charged nanodroplets from analyte solution [7]. At atmospheric pressure the solution is infused through the narrow metal capillary which is held at the potential of some kV vs. counter electrode. Therefore, the ESI source can be considered as an electrochemical cell itself [6, 8]. In order to prevent unwanted electrochemical reactions in the ESI source, redox buffers can be employed [8]. A cone-shaped mist of charged droplets is emitted from the capillary tip (Taylor cone). In case of positive ionization mode, the capillary is set at positive voltage vs. a counter electrode. Excess of cationic species such as H^+, NH_4^+, Na^+, and K^+ leads to the formation of positively charged droplets (Fig. 3). The opposite is applied for negative ionization mode. Initially formed droplets in μm radii range shrink due to further solvent evaporation until an increasing charge density is balanced by Coulombic repulsion. At this critical stage, called Rayleigh limit, droplet fission occurs and even smaller, highly charged offspring droplets in the nm range are formed. This process continues until gaseous analyte ions are released.

The mechanism of final ion formation is still under debate. Different theories have been summarized as three proposed models depending on the structure and molecular weight of the analytes: (1) ion evaporation model (IEM), for low molecular weight analytes; (2) charge residue model (CRM), for large globular species; and (3) chain ejection model (CEM), for disordered polymers [9].

4 Coupling of Electrochemistry, Mass Spectrometry and Liquid Chromatography

4.1 Conventional Approach

In a common EC–MS setup an electrochemical flow cell is directly coupled to the ESI source. Interferences between the electrospray potential and the potential applied at the electrochemical cell must be taken into account. Such interferences can be sometimes beneficial (e.g. they can decrease oxidation potential of certain analytes) [10]. However, decoupling of these two potentials is desirable in order to

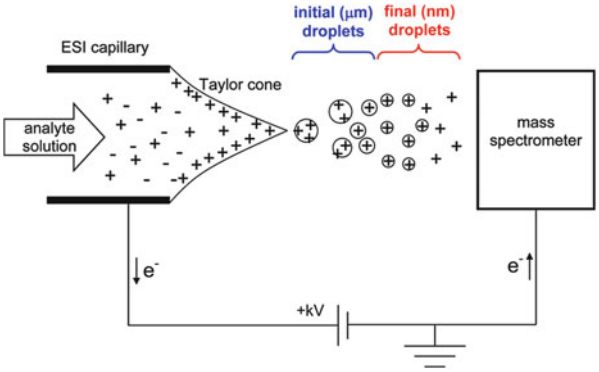

Fig. 3 Schematic depiction of an ESI source operated in positive ion mode. From [9], Copyright (2012) American Chemical Society

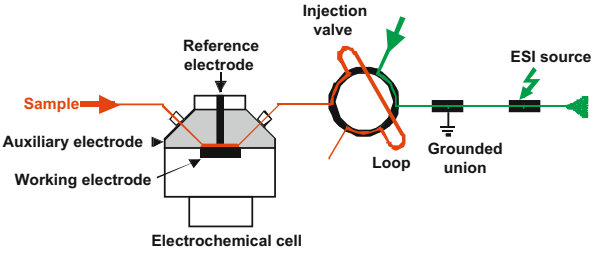

Fig. 4 Experimental EC–MS setup used for the simulation of oxidation processes of nucleic acid. From [10], with permission from Springer

obtain fully controllable conditions. This can be achieved by introducing an injection loop and a grounded union between the EC cell and the ESI source (Fig. 4) or using an instrument with a grounded ESI emitter. This setup allows for sweeping the potential of the EC cell and simultaneous recording of mass spectra, thus obtaining the so-called mass voltammogram – a plot of ion abundance (as an equivalent of voltammetric current) vs. mass-to-charge ratio as a function of EC potential (Fig. 5).

There are two possible arrangements for EC–MS coupling with LC (Fig. 6). The LC–EC–MS setup is implemented when electrochemical conversion of each single compound present in a complex mixture is required [11]. In this way, only the reaction products of one single compound are detected at one time (Fig. 6, route a). In the case of an EC–LC–MS arrangement the pure starting material is first oxidized or reduced electrochemically. The products are subsequently separated by liquid chromatography and detected by mass spectrometry (Fig. 6, route b).

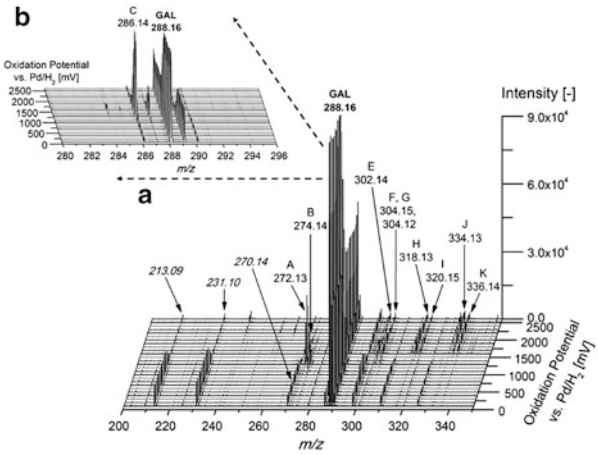

Fig. 5 Mass voltammogram of galantamine obtained by direct EC–MS online coupling (**a**) overview on the mass range *m*/*z* 200–350 and (**b**) enlargement of the mass range close to galantamine from *m*/*z* 280–296. The given *m*/*z* data corresponds to the $[M+H]^+$ ions of detected oxidation products (lettered) and galantamine fragment ions (italics), respectively. From [15], with permission from Elsevier

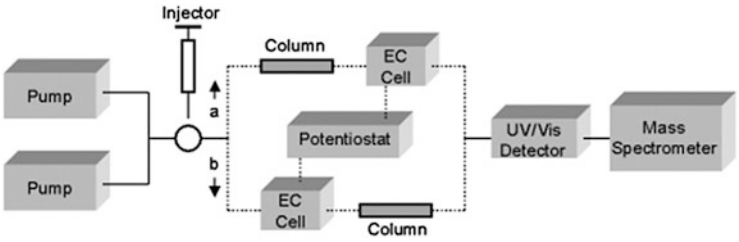

Fig. 6 Schematic setup of LC/EC/MS (route *a*) and EC/LC/MS (route *b*), including an optional UV/Vis detector prior to the mass spectrometer. From [11], with permission from Wiley

4.2 Main Applications

4.2.1 Drug Metabolism

Understanding metabolism of pharmaceuticals is the crucial step within a drug discovery process, since biochemical transformations in the cell may lead to their deactivation or formation of toxic intermediates. Enzymatically driven changes of drugs and xenobiotics occurring mostly in liver are divided into three steps or phases. In phase I polar functional groups are introduced by the so-called cytochrome P450 group of enzymes. These reactive intermediates are trapped in the

phase II metabolism by nucleophiles such as peptides or small proteins. Phase III involves further modifications and final excretion from the cell.

Findings in this field are still based on in vitro experiments like incubation with liver microsomes or in vivo studies, e.g. analyses of urine after the treatment with the drug of interest. However, this is often a time-consuming process which does not provide enough information about short-lived intermediates and reaction mechanism.

Electrochemistry is a fast and accurate technique that can successfully be used for studying drug metabolism. As already mentioned, different concepts can be employed for studying processes in living cells and organisms – each with corresponding advantages and drawbacks. However, it must be pointed out that none of them can completely simulate the complexity of biological systems. Taking into account different parameters and aspects they can lead to different results. Nevertheless, performed under carefully chosen conditions, such experiments are of great importance for better understanding of reaction pathways and mechanisms.

Online coupling of electrochemistry to mass spectrometry for the simulation of drug metabolism was first reported in 1989 when Getek et al. [12] studied the electrochemical oxidation of paracetamol to *N*-acetyl-*p*-quinoneimine in a commercially available flow-through cell equipped with a glassy carbon working electrode. Quinoneimine was subsequently trapped with the bioavailable thiols glutathione and cysteine. Baumann et al. [13] applied this approach for studying tetrazepam metabolism using wall-jet amperometric cell with exchangeable electrode material and widened the potential range. Obtained results were compared to microsomal incubations and in vivo experiments by analysing urine samples from a patient after tetrazepam delivery. In a verapamil study, a widely prescribed calcium channel blocker, a boron-doped diamond (BDD) electrode was employed due to its extraordinary properties – large potential window, ability to generate hydroxyl radicals and fouling resistance [14]. A similar comparison study for alkaloids galantamine (GAL) and lycorine (LYC) was reported by Jahn et al. [15]. Electrochemical oxidation of the antimalarial agent amodiaquine was performed by Jurva et al. [16]. Reactive metabolites as well as their conjugates with the nucleophiles cysteine and glutathione were subsequently characterized by MS/MS, NMR, and IR spectroscopy. In order to obtain deeper insight into the potentially reactive metabolites of triclocarban (TCC), widely used antibacterial agent in personal care products, their reactivity toward glutathione (GSH) and the model protein β-lactoglobulin (β-LGA) was studied [17]. It was proved for the first time that the oxidative metabolism of TCC might lead to formation of quinone imine species, which are reactive toward cellular nucleophiles. Modification site of the protein can be localized using FTICR mass spectrometry [18]. Metabolites of antiarrhythmic agent amiodarone were quantified by EC–LC–ICPMS [19]. Tagging biologically important species, e.g. peptides or proteins with ferrocenyl entity, was presented in 2012 by Karst's group [20]. In order to obtain an overview of the possible reaction products EC–ESI–MS experiments without chromatographic separation were performed. The pharmaceuticals amodiaquine (AQ), an antimalarial reagent, and clozapine (CLZ), an antipsychotic drug used in the treatment of refractory

schizophrenia, served as model compounds. In the second step reactive metabolites are trapped with ferrocenyl-modified glutathione and products analyzed by LC–MS, thus elucidating phase II of drug metabolism. Using a similar approach oxidative metabolism of the anti-inflammatory drug diclofenac [21] and toremifene [22], used for breast cancer treatment, was investigated. Lohmann and Karst [4] discussed the differences, advantages and limitations between three different nonenzymatic models for simulation of cytochrome P450 catalyzed reactions – metalloporphyrins as surrogates of the active center of cytochrome P450, Fenton's reagent, and the electrochemical oxidation of drug compounds. Potential oxidative metabolites of the radiotracer isatin determined by EC coupled to MS were compared to in vitro and in vivo experiments [23]. Karst's group was concerned with metabolic pathways of skin sensitizers that can be released from cosmetic products such as hair dyes. Both aniline (phenylamine) [24] and *p*-phenylenediamine (1,4-diaminobenzene) [25, 26] were oxidized electrochemically and trapped with various nucleophiles such as peptides or proteins. Tong et al. [27] reported a novel approach for indirect quantification of parent drug and its unstable metabolites by complete online coulometric conversion. Mali'n et al. [28] commented the difference between P450-catalyzed and electrochemical oxidation of haloperidol, a potent antipsychotic agent. Reactive intermediates were trapped by KCN and then analyzed by ultra-performance liquid chromatography–electrospray ionization mass spectrometry. Zettersten et al. [29] employed two electrochemical flow cells of different design in 4-chloroaniline oxidation study. By introducing the second electrochemical cell into the EC–LC–MS setup valuable information on the regioselectivity of the pesticide boscalid oxidation were obtained [30]. In the first cell, the oxidative metabolism was simulated, while in the second one the quinoid oxidation products were reduced. Nouri-Nigjeh et al. [31] were concerned with oxidative metabolism of lidocaine, a common anesthetic drug. Using a two-compartment electrochemical cell they showed that direct oxidation of lidocaine at the gold anode resulted in *N*-dealkylation, whereas reaction with H_2O_2, generated at the cathode, produced the N-oxide, both known lidocaine metabolites formed in vivo. They also suggested that electrocatalytic oxidation of H_2O_2 on the Pt electrode involved surface-bound platinum-oxo species. These were capable of oxygen insertion through a mechanism reminiscent of the reaction of oxo-ferryl radical cations during the aromatic hydroxylation of substrates by P450, thus leading to the formation of 3- and 4-hydroxylidocaine [32]. Zettersten et al. [33] employed the LC–EC–MS/MS concept for screening antioxidant activity (i.e. oxidation potential) and capacity (i.e. amount) of polyphenols catechin, kaempferol, resveratrol, quercetin and quercetin glucosides. By applying a suitable electrode potential antioxidant behavior of individual compounds present in the mixture can be assessed unlike traditional chemical methods where only information about total antioxidant capacity can be obtained. Both online coupling setups (LC–EC–MS and EC–LC–MS) were employed by Karady et al. [34] for studying oxidative metabolism of potential anticancer drug R-roscovitine. For the system optimization the EC cell was placed between the LC column and the ESI interface. An EC–LC–MS/MS setup was used for the separation and identification of metabolites. Oxidation of R-roscovitine in an electrochemical cell equipped with a glassy carbon electrode resulted in the

appearance of six major products. Nozaki et al. [35] reported a simple, rapid and sensitive online LC–EC–MS/MS method for the determination of zotepine in human serum using a new fragment ion generated electrochemically. The fate of wide range polarity environmental pollutants was successfully elucidated. Selected examples include acebutolol [36], methabenzthiazuron, ethidimuron, propanil [37] and sulfadiazine [38]. Nouri-Nigjeh et al. [39] simulated phenacetin to acetaminophen biotransformation by applying square-wave potential pulses consisting of consecutive sub-second oxidation and reduction steps. Due to the fast hydrolysis of the reactive intermediates, this transformation could not be achieved by oxidation at constant potential. Jirovsky´et al. [40] performed the electrochemical oxidation of anthocyanins cyanidin-3-galactoside (ideain) and cyanidin-3,5-diglucoside (cyanin) using a porous graphite coulometric electrode and subsequent online mass spectrometric identification of the products formed. The successful detection of a pair of chiral stereoisomers generated by electrochemical oxidation of α-tocopherol on a porous graphite electrode was described [41]. In addition to MS, circular dichroism detection was employed, since chiral stereoisomers show identical MS spectra.

4.2.2 Biomolecule Modification

Another field where electrochemistry coupled to a separation technique and MS detection gives promising results is protein and DNA research. Main applications include protein tagging, disulfide bond cleavage and simulation of oxidative stress. The latter is mainly focused on electrochemical generation of well-known biomarkers for DNA and RNA damage.

Erb et al. [42] studied oxidative transformation of guanosine. They performed thorough method development and optimization considering electrode material, flow rate, solvent and mobile phase composition. 8-Hydroxyguanosine and (guanosine-H)$_2$ were identified as primary oxidation products. Baumann et al. [43] characterized oxidation pathways of DNA and RNA nucleotides employing an electrochemical flow cell equipped with a BDD working electrode. Oxidation pathways of uric acid were investigated by Mautjana et al. [44]. They showed that a low online electrochemical cell voltage floating on the ESI source high voltage significantly improved ionization efficiency. Unlike common cylindrical ESI–MS capillary inlet they introduced a new configuration with a cone-shaped capillary inlet enabling enhanced sensitivity in EC–ESI–MS analysis of all purine bases [45] as well as dopamine and cysteine [46]. This study was extended to guanine–tyrosine and guanine–glutathione cross-links formation [47].

Plattner et al. [48] investigated the mechanism of covalent adduct formation between guanosine and acetaminophen (APAP). Radical species of both APAP and guanosine were generated via one electron–one proton reactions. These subsequently reacted with each other. The same mechanism was confirmed for other nucleosides and nucleotides [10]. Telgmann et al. [49] investigated metabolic pathways of Gd-based contrast agents, commonly used in magnetic resonance

imaging. Electrochemically generated oxidation products were separated by either CE or LC and detected by ESI–MS and ICP–MS.

Electrochemically generated modifications of proteins were reviewed by Roeser et al. [50]. Electrochemical oxidation of peptides and proteins combined with mass spectrometry (MS) has revealed specific cleavage of the peptide bond at the C-terminal side of Tyr and Trp residues [51]. Basile and Hauser [52] combined online microwave heating acid hydrolysis at aspartic acid residue and electrochemical oxidation at tryptophan and tyrosine residues. Peptides with an average sequence length of 10 amino acids were well suited for collision-induced dissociation tandem mass spectrometry experiments.

An interesting application of electrochemistry in combination with liquid chromatography and mass spectrometry in proteomic research was reported by McClintock et al. [53]. They employed electrochemical modification of proteins under both non-native and native-like conditions for probing higher order protein structure. Namely, in native-like conditions (aqueous buffer, pH ~7), proteins keep their compact structure; thus amino acid residues exposed to the solvent are more readily oxidized; more buried residues were found to be oxidized in "non-native" solution. Oxidized proteins were collected offline for proteolytic digestion followed by LC–MS/MS analysis.

Gutkin et al. [54] presented a novel concept for online preconcentration of analytes and their subsequent electrochemically induced delivery to an electrospray mass spectrometer. After electrodeposition of a silver layer on the Pt working electrode and subsequent accumulation of the target analyte by electrochemical or chemical means onto the active layer, electrostripping of the conductive layer along with the analyte is performed. Dissolved silver ions promoted ionization, and its characteristic isotopic pattern assisted in the identification of the target analyte. Homocysteine and other organothiols were chosen as test compounds. This approach was extended to the conjugation of the target analyte avidin to a thiolated ligand biotin which was electrodeposited on the silver-coated surface.

4.3 DESI–MS

Type and design of the interface is an important aspect of EC–MS coupling. In desorption electrospray ionization (DESI), charged droplets are directed from an electrosonic spray ionization source toward a surface with a proximal atmospheric pressure mass spectrometer inlet. In this way little or no sample pretreatment is required [55]. An enhanced version, nanoDESI–MS was applied for tissue imaging such as rat brain and human kidney tissue [56]. A solvent bridge formed between the primary and nanospray capillaries contacts the analysis surface. Analyte-containing solvent is removed from the surface by a self-aspirating nanospray [57]. Miao and Chen [58] introduced the concept of coupling

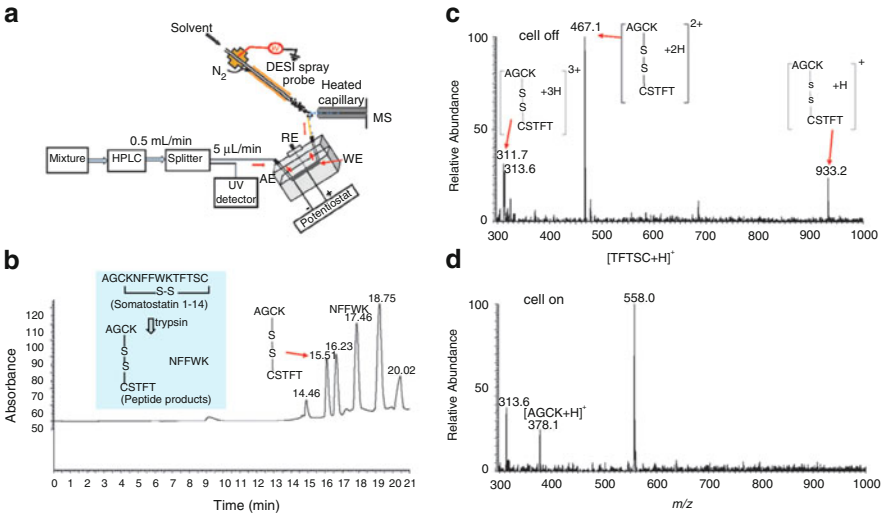

Fig. 7 (**a**) Apparatus for LC–EC–DESI–MS; (**b**) acquired UV chromatogram (254 nm) showing the separation of the tryptic digest of a peptide; DESI–MS mass spectra of AGCK/TFTSC peptides with a cell potential of (**c**) 0.0 V and (**d**) 1.5 V. From [64], Copyright (2011) The Royal Society of Chemistry

EC with DESI–MS enabling the detection of a perylene radical cation generated by electro-oxidation in a nonaqueous solution in a tubular cell. Li et al. [59] improved this approach by removing the sample surface and directing the DESI spray to the capillary tip from which sample solution flowed out. They examined several electrochemical reactions such as dopamine and thiol oxidation and reduction of disulfide bonds in glutathione disulfide and bovine pancreas insulin. In the same study they investigated online derivatization of peptides and proteins. Cysteine residue of β-lactoglobulin A was tagged by electro-oxidized dopamine. Oxidation of chlorpromazine and reduction of nitroaromatic drugs flunitrazepam and clonazepam to corresponding amines via *N*-hydroxyl intermediates provided insight into a mechanism of important reactions involved in carcinogenesis [60]. Disulfide bond reduction in apamin and endothelin showed an alternative way for peptide sequencing unlike traditional approach which involved an excess amount of reagents such as dithiothreitol or tris(2-carboxyethyl)phosphine. Zhang et al. [61] performed sequencing of *β*-lactoglobulin A and lysozyme. In another study an enhanced sequence elucidation of biologically active peptides (containing both intra- and inter-disulfide bonds), intact proteins and protein/peptide digest mixtures was achieved [62]. Selected examples were trypsin digested [Arg8]-conopressin G and somatostatin 1-14, pepsin-digested insulin, [Arg8]-vasopressin, glutathione disulfide and proteins α-lactalbumin and ebselen. Liu et al. [63] demonstrated the first online and offline coupling of EC with MS using nanospray desorption electrospray ionization for dopamine and chlorpromazine oxidation, flunitrazepam and clonazepam reduction and electrochemical derivatization of thiols. In the first

approach they used a conventional electrochemical flow cell. Another setup employed an interdigitated array electrode (IDA) enabling chemical analysis of electrolyzed samples directly from the electrode surfaces. Zhang et al. [64] demonstrated the first coupling of LC with DESI–MS. A mixture consisting of three neurotransmitter compounds – norepinephrine, normetanephrine and dopamine – first underwent LC separation, flowed through the UV detector and then was ionized by DESI. Furthermore, they combined the concept with electrochemistry by placing the electrochemical cell between the LC column and the DESI source. As a proof of concept disulfide-containing peptide somatostatin was digested by trypsin and peptide mixture analyzed by LC–EC–DESI–MS (Fig. 7). Tandem MS analysis was performed for the determination of electrogenerated ion structures, establishing the disulfide bond position and elucidation of peptide sequence.

4.4 SECM–MS

Coupling of scanning electrochemical microscopy (SECM) with mass spectrometry detection was introduced by Momotenko et al. [65]. A specially designed SECM probe contained a working microelectrode, an integrated counter/reference electrode and two microchannels maintaining a nanoliter droplet at the probe tip by pushing redox mediator toward and pulling extracted analyte solution from the substrate (Fig. 8). The fabrication of the so-called push–pull scanner was previously described [66]. This arrangement enabled imaging over dry horizontal, tilted or even vertical surfaces by performing electrochemical measurements in a single droplet [67]. The potential of the concept was demonstrated by imaging latent human fingerprints contaminated by explosives and parallel chemical/electrochemical characterization of the activity of an immobilized enzyme. In the former arrangement SECM was coupled offline with matrix-assisted laser desorption ionization mass spectrometry (MALDI–MS). Liquid aspirated from the push−pull probe was collected and a small fraction deposited on a MALDI target plate. In order to assay the activity of surface spotted enzymes the push−pull electrochemical scanner was coupled with electrospray ionization mass spectrometry (ESI–MS). Alkaline phosphatase was immobilized on polyvinylidene difluoride membrane and laterally scanned under a thick layer of deionized water. Buffer solution containing *p*-aminophenyl phosphate and lysine which served as internal standard was continuously pumped through the inlet microfluidic channel to the probe tip. The enzyme catalyzed the conversion of *p*-aminophenyl phosphate to *p*-aminophenol generating the current which was simultaneously monitored. Electrolyte solution was aspirated in small portions with air bubbles in between in order to prevent loss of spatiotemporal resolution and then driven to the polyimide microchip ESI emitter first implemented by Qiao et al. [68] The chip contained three microchannels and an integrated micro-carbon electrode which was in contact with the microchannel and served as a high voltage supply for ESI. Supporting buffer consisting of water, methanol and acetic acid

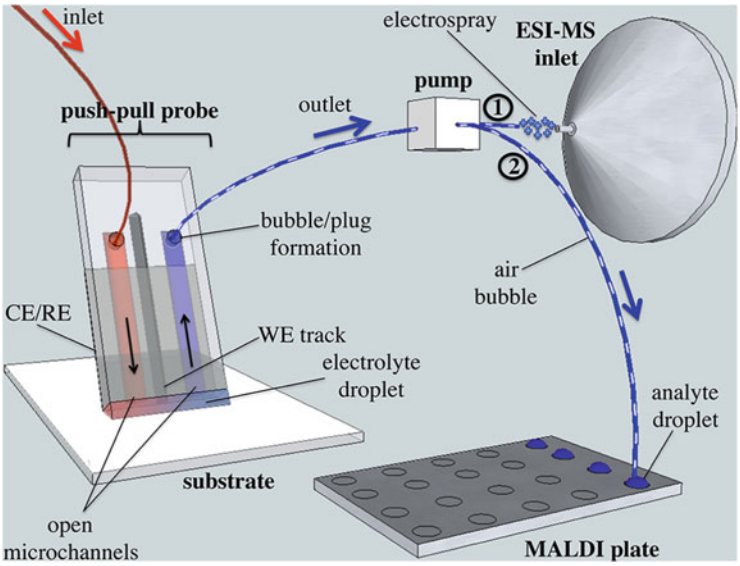

Fig. 8 Schematic view of the general operation principle of the push−pull probe. From [65], Copyright (2012) American Chemical Society

was infused via another microchannel. The two flow streams were mixed just before arriving at the microelectrode; therefore, the microelectrode was always in contact with an acidic medium leading to a relatively stable ESI, regardless of the air bubbles collected in a capillary.

5 Coupling of EC–MS with CE

5.1 CE–MS Interface

Capillary electrophoresis is a separation technique complementary to liquid chromatography. Although it provides excellent efficiency and resolution, short analysis time and low sample and solvent consumption, LC has been by far the most frequently used separation technique due to easy coupling with MS. Capillary electrophoresis can successfully separate analytes which are very difficult to handle by LC. For the analysis of ionic species, CE is always a method of choice. Use of CE is particularly attractive for bioanalysis. The main advantage of CE over LC in terms of bioanalytical applications is the ability to perform analysis under near physiological conditions, i.e. using only aqueous buffer solutions without organic solvents (methanol, acetonitrile) commonly employed for LC separations. This important feature enables studies of processes that occur in a comparable environment in living cells and organisms. Artifacts originating from the presence of organic solvents are therefore avoided.

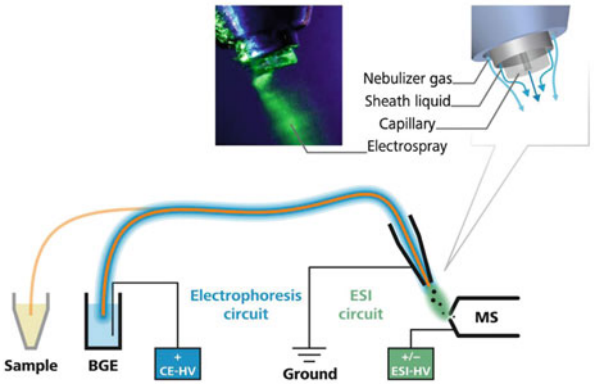

Fig. 9 CE–MS coupling – schematic representation. From [72]

After Smith et al. [69] had introduced a sheath-flow CE–MS interface in 1988, interest in this approach started to increase. Maxwell and Chen [70] and most recently Bonvin et al. [71] reviewed CE–MS interface development. The commonly employed CE–MS interface design refers to a commercially available coaxial sheath-liquid ESI sprayer [72]. A schematic representation is given in Fig. 9. The sheath liquid serves as an electrolytic bridge enabling the grounding of the electrophoretic current via the stainless steel tubing. In addition, the sheath liquid provides a sufficient flow needed for spray formation. The ESI sprayer is usually also grounded in the electrospray circuit. In this way interference between two high voltage circuits (CE and ESI circuit) is avoided.

5.2 EAI–CE–MS

According to its separation principle, capillary electrophoresis is applicable to analytes that carry a charge under the given pH conditions. Neutral analytes can be separated only with the help of additives (e.g. surfactants) – employing micellar electrokinetic chromatography (MEKC). However, the large amount of nonvolatile additives has negative effects on ionization efficiency of analytes and deteriorates MS performance.

In 2003 Matysik [73] introduced a new concept for CE separation of neutral analytes termed electrochemically assisted injection (EAI). In a specially designed electrochemical cell, electroactive neutral analytes are oxidized or reduced during the injection into the separation capillary. The capillary inlet is in close proximity to the working electrode (50 ± 10 μm). After the injection step the capillary inlet is placed in a vial containing the separation buffer and the separation voltage is applied. Any transfer from the generation to the separation system is avoided, thus preventing contact with oxygen and delays in the analytical process. EAI–CE enables the identification of the parent compounds based on differences in the electrophoretic mobilities of the ionic products. Initial studies involved electrochemical or UV detection.

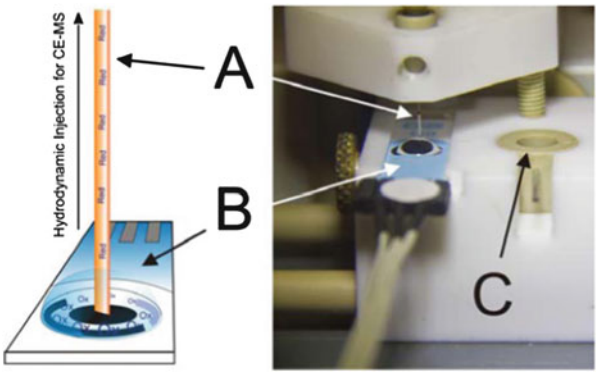

Fig. 10 Fully automated injection device for EAI–CE–MS experiments. Main components: fixed separation capillary (A), screen-printed electrode with drop of sample (B) and CE buffer reservoir with high voltage electrode (C). From [77], with permission from Wiley

Scholz and Matysik [74] combined EAI and nonaqueous capillary electrophoretic (NACE) separations with ESI–MS detection. Ferrocene species were successfully separated and detected showing much better ionization efficiency.

Palatzky and Matysik [75] developed amperometric capillary probes with an integrated microwire electrode for the characterization and optimization of EAI cell arrangements. A scanning electrochemical microscope (SECM) was used for the precise positioning of the capillary probes. This led to the construction of semiautomated arrangement for electrochemically assisted injection in combination with capillary electrophoresis and time-of-flight mass spectrometry [76]. The EAI cell arrangement consisted of an integrated buffer reservoir for CE separations and a compartment holding screen-printed electrodes. A drop of sample solution (50 μL) was sufficient to cover the three-electrode structures. A piezo motor provided a fast and precise capillary positioning over the screen-printed electrode assembly. Preliminary studies of the EAI–CE–MS setup involved the analysis of nitroaromatic compounds. The formation of corresponding hydroxylamines and amines paved the way for selective and sensitive CE–MS determinations without the need of adding surfactants to the electrophoresis buffer. Further on a fully automated EAI injection device was developed and applied to mechanistic and quantitative studies of the reduction of 4-nitrotoluene [77] (Fig. 10). The change in 4-hydroxylaminotoluene and 4-aminotoluene concentrations was determined in dependence on electrode potential and electrode material. Three different carbon-based screen-printed electrodes (SPEs) were used including unmodified carbon, carbon nanofiber and reduced graphene oxide SPEs. Ongoing research of EAI–CE–MS is mainly directed toward bioanalytical studies.

6 Conclusions

Hyphenation of electrochemistry and mass spectrometry is a powerful and versatile tool for the simulation of metabolic processes occurring in living organisms. Additional offline and especially online combination with a separation system is

a promising, fully instrumental approach which has a good potential to surpass time-consumable in vitro and in vivo experiments. However, based on numerous studies in this field, it can be concluded that there is no universal approach which can completely simulate complex physiological conditions. Since several parameters influence electrochemical conversion/separation/MS detection, the various concepts may lead to different results. It is important to select suitable tools from the toolbox and to adjust experimental conditions appropriately. In this context valuable insights into physiological processes can be gained.

Capillary electrophoresis shows some advantages over liquid chromatography, especially in terms of bioanalytical applications. The separation of ions can be achieved under near physiological conditions, employing only aqueous buffers.

A new approach for CE separation of neural analytes without using additives is termed electrochemically assisted injection (EAI). In a specially designed automated injection cell, electroactive analytes are converted during the injection into the CE capillary. Coupled to mass spectrometry detection, the EAI–CE concept represents a valuable means for studying complex processes. An important issue of this concept is the use of disposable screen-printed (disposable) electrodes, which provides reliability of results. In that respect the EAI–CE–MS approach is a promising technique for bioanalytical applications.

Acknowledgments This work was supported by the European Union under Grant Agreement number 264772 (ITN CHEBANA).

References

1. Bruckenstein S, Gadde RR (1971) Use of a porous electrode for in situ mass spectrometric determination of volatile electrode reaction products. J Am Chem Soc 93:793–794
2. Wolter O, Heitbaum J (1984) Differential electrochemical mass-spectroscopy (DEMS) – a new method for the study of electrode processes. Berichte der Bunsengesellschaft für physikalische Chemie 88:2–6
3. Volk KJ, Yost RA, Brajter-Toth A (1992) Electrochemistry on line with mass spectrometry, insight into biological redox reactions. Anal Chem 64:21A–26A
4. Lohmann W, Karst U (2008) Biomimetic modeling of oxidative drug metabolism. Anal Bioanal Chem 391:79–96
5. Odijk M, Olthuis W, Van den Berg A, Qiao L, Girault H (2012) Improved conversion rates in drug screening applications using miniaturized electrochemical cells with frit channels. Anal Chem 84:9176–9183
6. De la Mora JF, Van Berkel GJ, Enke CG, Cole RB, Martinez-Sanchez M, Fenn JB (2000) Electrochemical processes in electrospray ionization mass spectrometry. J Mass Spectrom 35:939–952
7. Crotti S, Seraglia R, Traldi P (2011) Some thoughts on electrospray ionization mechanism. Eur J Mass Spectrom 17:85–100
8. Plattner S, Erb R, Chervet JP, Oberacher H (2012) Ascorbic acid for homogenous redox buffering in electrospray ionization–mass spectrometry. Anal Bioanal Chem 404:1571–1579
9. Konermann L, Ahadi E, Rodriguez AD, Vahidi S (2013) Unraveling the mechanism of electrospray ionization. Anal Chem 85:2–9

10. Pitterl F, Chervet JP, Oberacher H (2010) Electrochemical simulation of oxidation processes involving nucleic acids monitored with electrospray ionization–mass spectrometry. Anal Bioanal Chem 397:1203–1215
11. Karst U (2004) Electrochemistry/mass spectrometry (EC/MS) — a new tool to study drug metabolism and reaction mechanisms. Angew Chem Int Ed 43:2476–2478
12. Getek TA, Korfmacher WA, McRae TA, Hinson JA (1989) Utility of solution electrochemistry mass spectrometry for investigating the formation and detection of biologically important conjugates of acetaminophen. J Chromatogr A 474:245–256
13. Baumann A, Lohmann W, Schubert B, Oberacherb H, Karst U (2009) Metabolic studies of tetrazepam based on electrochemical simulation in comparison to in vivo and in vitro methods. J Chromatogr A 1216:3192–3198
14. Jahn S, Baumann A, Roscher J, Hense K, Zazzeroni R, Karst U (2011) Investigation of the biotransformation pathway of verapamil using electrochemistry/liquid chromatography/mass spectrometry – a comparative study with liver cell microsomes. J Chromatogr A 1218:9210–9220
15. Jahn S, Seiwert B, Kretzing S, Abraham G, Regenthal R, Karst U (2012) Metabolic studies of the Amaryllidaceous alkaloids galantamine and lycorine based on electrochemical simulation in addition to in vivo and in vitro models. Anal Chim Acta 756:60–72
16. Jurva U, Holmén A, Grönberg G, Masimirembwa C, Weidolf L (2008) Electrochemical generation of electrophilic drug metabolites: characterization of amodiaquine quinoneimine and cysteinyl conjugates by MS, IR, and NMR. Chem Res Toxicol 21:928–935
17. Baumann A, Lohmann W, Rose T, Ahn KC, Hammock BD, Karst U, Schebb NH (2010) Electrochemistry-mass spectrometry unveils the formation of reactive triclocarban metabolites. Drug Metabolism Disposition 38:2130–2138
18. Lohmann W, Hayen H, Karst U (2008) Covalent protein modification by reactive drug metabolites using online electrochemistry/liquid chromatography/mass spectrometry. Anal Chem 80:9714–9719
19. Lohmann W, Meermann B, Moller I, Scheffer A, Karst U (2008) Quantification of electrochemically generated iodine-containing metabolites using inductively coupled plasma mass spectrometry. Anal Chem 80:9769–9775
20. Jahn S, Lohmann W, Bomke S, Baumann A, Karst U (2012) A ferrocene-based reagent for the conjugation and quantification of reactive metabolites. Anal Bioanal Chem 402:461–471
21. Faber H, Melles D, Brauckmann C, Wehe C, Wentker K, Karst U (2012) Simulation of the oxidative metabolism of diclofenac by electrochemistry/(liquid chromatography/)mass spectrometry. Anal Bioanal Chem 403:345–354
22. Lohmann W, Karst U (2009) Electrochemistry meets enzymes: instrumental on-line simulation of oxidative and conjugative metabolism reactions of toremifene. Anal Bioanal Chem 394:1341–1348
23. Baumann A, Faust A, Law M, Michael T, Kuhlmann M, Kopka K, Scheafers M, Karst U (2011) Metabolite identification of a radiotracer by electrochemistry coupled to liquid chromatography with mass spectrometric and radioactivity detection. Anal Chem 83:5415–5421
24. Melles D, Vielhaber T, Baumann A, Zazzeroni R, Karst U (2012) Electrochemical oxidation and protein adduct formation of aniline: a liquid chromatography/mass spectrometry study. Anal Bioanal Chem 403:377–384
25. Jahn S, Faber H, Zazzeroni R, Karst U (2012) Electrochemistry/liquid chromatography/mass spectrometry to demonstrate irreversible binding of the skin allergen *p*-phenylenediamine to proteins. Rapid Commun Mass Spectrom 26:1415–1425
26. Jahn S, Faber H, Zazzeroni R, Karst U (2012) Electrochemistry/mass spectrometry as a tool in the investigation of the potent skin sensitizer *p*-phenylenediamine and its reactivity toward nucleophiles. Rapid Commun Mass Spectrom 26:1453–1464
27. Tong W, Chowdhury SK, Su A, Alton KB (2010) Quantitation of parent drug and its unstable metabolites by in situ coulometric oxidation and liquid chromatography-tandem mass spectrometry. Anal Chem 82:10251–10257

28. Mali'n TJ, Weidolf L, Castagnoli N, Jurva J, Jurva U (2010) P450-catalyzed vs. electrochemical oxidation of haloperidol studied by ultra-performance liquid chromatography/electrospray ionization mass spectrometry. Rapid Commun Mass Spectrom 24:1231–1240
29. Zettersten C, Sjoberg P, Nyholm L (2009) Oxidation of 4-chloroaniline studied by on-line electrochemistry electrospray ionization mass spectrometry. Anal Chem 81:5180–5187
30. Lohmann W, Dötzer R, Gütter G, Van Leeuwen S, Karst U (2009) On-line electrochemistry/liquid chromatography/mass spectrometry for the simulation of pesticide metabolism. J Am Soc Mass Spectrom 20:138–145
31. Nouri-Nigjeh E, Permentier H, Bischoff R, Bruins A (2010) Lidocaine oxidation by electrogenerated reactive oxygen species in the light of oxidative drug metabolism. Anal Chem 82:7625–7633
32. Nouri-Nigjeh E, Bruins A, Bischoff R, Permentier H (2012) Electrocatalytic oxidation of hydrogen peroxide on a platinum electrode in the imitation of oxidative drug metabolism of lidocaine. Analyst 137:4698
33. Zettersten C, Co M, Wende S, Turner C, Nyholm L, Sjoberg P (2009) Identification and characterization of polyphenolic antioxidants using on-line liquid chromatography, electrochemistry and electrospray ionization tandem mass spectrometry. Anal Chem 81:8968–8977
34. Karady M, Novk O, Horna A, Strnad M, Dolez K (2011) High performance liquid chromatography-electrochemistry-electrospray ionization mass spectrometry (HPLC/EC/ESI-MS) for detection and characterization of roscovitine oxidation products. Electroanalysis 23(12):2898–2905
35. Nozaki K, Osaka I, Kawasaki H, Arakawa R (2009) Application of online electrochemistry/electrospray/tandem mass spectrometry to a quantification method for the antipsychotic drug zotepine in human serum. Anal Sci 25:1197–1201
36. Bussy U, Ferchaud-Roucher V, Tea I, Krempf M, Silvestre V, Boujtita M (2012) Electrochemical oxidation behavior of Acebutolol and identification of intermediate species by liquid chromatography and mass spectrometry. Electrochim Acta 69:351–357
37. Chen L, Hofmann D, Klumpp E, Xiang X, Chen Y, Küppers S (2012) Bottom-up approach for the reaction of xenobiotics and their metabolites with model substances for natural organic matter by electrochemistry–mass spectrometry (EC–MS). Chemosphere 89:1376–1383
38. Hoffmann T, Hofmann D, Klumpp E, Küppers S (2011) Electrochemistry-mass spectrometry for mechanistic studies and simulation of oxidation processes in the environment. Anal Bioanal Chem 399:1859–1868
39. Nouri-Nigjeh E, Bischoff R, Bruins A, Permentier H (2011) Electrochemical oxidation by square-wave potential pulses in the imitation of phenacetin to acetaminophen biotransformation. Analyst 136:5064
40. Jirovsky D, Bednar P, Myjavcova R, Bartosova Z, Skopalova J, Tvrdonova M, Lemr K (2011) Study of electrochemical oxidation of cyanidin glycosides by online combination of electrochemistry with electrospray ionization tandem mass spectrometry. Monatsh Chem 142:1211–1217
41. Tahara K, Makii E, Iijima S, Abe Y, Mochizuki M (2008) On-line liquid chromatography and circular dichroism detection of stereo-isomers of α-tocopherol derivatives generated by an electrochemical reaction. Anal Sci 24
42. Erb R, Plattner S, Pitter F, Brouwer H, Oberacher H (2012) An optimized electrochemistry-liquid chromatography-mass spectrometry method for studying guanosine oxidation. Electrophoresis 33:614–621
43. Baumann A, Lohmann W, Jahn S, Karst U (2010) On-line electrochemistry/electrospray ionization mass spectrometry (EC/ESI-MS) for the generation and identification of nucleotide oxidation products. Electroanalysis 22(3):286–292
44. Mautjana N, Estes J, Eyler J, Brajter-Toth A (2008) One-electron oxidation and sensitivity of uric acid in on-line electrochemistry and in electrospray ionization mass spectrometry. Electroanalysis 20(23):2501–2508

45. Mautjana N, Looi D, Eyler J, Brajter-Toth A (2009) Sensitivity of positive ion mode electrospray ionization mass spectrometry (ESI MS) in the analysis of purine bases in ESI MS and on-line electrochemistry ESI MS (EC/ESI MS). Electrochim Acta 55:52–58
46. Mautjana N, Estes J, Eyler J, Brajter-Toth A (2008) Antioxidant pathways and one-electron oxidation of dopamine and cysteine in electrospray and on-line electrochemistry electrospray ionization mass spectrometry. Electroanalysis 20(18):1959–1967
47. Looi D, Eyler J, Brajter-Toth A (2011) Electrochemistry-electrospray ionization FT ICR mass spectrometry (EC ESI MS) of guanine–tyrosine and guanine–glutathione crosslinks formed on-line. Electrochim Acta 56:2633–2640
48. Plattner S, Erba R, Pitterl F, Brouwerb H, Oberacher H (2012) Formation and characterization of covalent guanosine adducts with electrochemistry—liquid chromatography–mass spectrometry. J Chromatogr B 883–884:198–204
49. Telgmann L, Faber H, Jahn S, Mellesa D, Simon H, Sperling M, Karst U (2012) Identification and quantification of potential metabolites of Gd-based contrast agents by electrochemistry/separations/mass spectrometry. J Chromatogr A 1240:147–155
50. Roeser J, Bischoff R, Bruins A, Permentier H (2010) Oxidative protein labeling in mass-spectrometry-based proteomics. Anal Bioanal Chem 397:3441–3455
51. Roeser J, Permentier H, Bruins A, Bischoff R (2010) Electrochemical Oxidation and Cleavage of Tyrosine- and Tryptophan-Containing Tripeptides. Anal Chem 82:7556–7565
52. Basile F, Hauser N (2011) Rapid online nonenzymatic protein digestion combining microwave heating acid hydrolysis and electrochemical oxidation. Anal Chem 83:359–367
53. McClintock C, Kertesz V, Hettich R (2008) Development of an electrochemical oxidation method for probing higher order protein structure with mass spectrometry. Anal Chem 80:3304–3317
54. Gutkin V, Gun J, Lev O (2009) Electrochemical deposition-stripping analysis of molecules and proteins by online electrochemical flow cell/mass spectrometry. Anal Chem 81:8396–8404
55. Takats Z, Wiseman JM, Gologan B, Cooks R (2004) Graham Sci. (Washington, DC) 306 (5695):471–473
56. Laskin J, Heath BS, Roach PJ, Cazares L, Semmes OJ (2012) Tissue imaging using nanospray desorption electrospray ionization mass spectrometry. Anal Chem 84(1):141–148
57. Roach P, Laskin J, Laskin A (2010) Nanospray desorption electrospray ionization: an ambient method for liquid-extraction surface sampling in mass spectrometry. Analyst 135:2233–2236
58. Miao Z, Chen H (2009) Direct analysis of liquid samples by desorption electrospray ionization-mass spectrometry (DESI-MS). J Am Soc Mass Spectrom 20:10–19
59. Li J, Dewald H, Chen H (2009) Online coupling of electrochemical reactions with liquid sample desorption electrospray ionization-mass spectrometry. Anal Chem 81:9716–9722
60. Lu M, Wolff C, Cui W, Chen H (2012) Investigation of some biologically relevant redox reactions using electrochemical mass spectrometry interfaced by desorption electrospray ionization. Anal Bioanal Chem 403:355–365
61. Zhang Y, Cui W, Zhang H, Dewald H, Chen H (2012) Electrochemistry-assisted top-down characterization of disulfide-containing proteins. Anal Chem 84:3838–3842
62. Zhang Y, Dewald H, Chen H (2011) Online mass spectrometric analysis of proteins/peptides following electrolytic cleavage of disulfide bonds. J Proteome Res 10:1293–1304
63. Liu P, Lanekoff I, Laskin J, Dewald H, Chen H (2012) Study of electrochemical reactions using nanospray desorption electrospray ionization mass spectrometry. Anal Chem 84:5737–5743
64. Zhang Y, Yuan Z, Dewald H, Chen H (2011) Coupling of liquid chromatography with mass spectrometry by desorption electrospray ionization (DESI). Chem Commun 47:4171–4173
65. Momotenko D, Qiao L, Rodriguez A, Cortes-Salazar F, Lesch A, Wittstock G, Girault H (2012) Electrochemical push−pull scanner with mass spectrometry detection. Anal Chem 84:6630–6637

66. Momotenko D, Cortes-Salazar F, Lesch A, Wittstock G, Girault H (2011) Microfluidic push-pull probe for scanning electrochemical microscopy. Anal Chem 83:5275–5282
67. Cortes-Salazar F, Lesch A, Momotenko D, Busnel J, Wittstock G, Girault H (2010) Fountain pen for scanning electrochemical microscopy. Anal Methods 2:817–823
68. Qiao L, Lu Y, Liu B, Girault H (2011) Copper-catalyzed tyrosine nitration. J Am Chem Soc 133:19823–19831
69. Smith RD, Barinaga CJ, Udseth HR (1988) Improved electrospray ionization interface for capillary zone electrophoresis-mass spectrometry. Anal Chem 60:1948–1952
70. Maxwell E, Chen D (2008) Twenty years of development for capillary electrophoresis-electrospray ionization-mass spectrometry. Anal Chim Acta 627:25–33
71. Bonvin G, Schappler J, Rudaz S (2012) Capillary electrophoresis-electrospray ionization-mass spectrometry interfaces: fundamental concepts and technical developments. J Chromatogr A 1267:17–31
72. Grundmann M (2012) PhD Thesis, University of Regensburg
73. Matysik FM (2003) Electrochemically assisted injection – a new approach for hyphenation of electrochemistry with capillary-based separation systems. Electrochem Commun 5:1021–1024
74. Scholz R, Matysik FM (2011) A novel approach for the separation of neutral analytes by means of electrochemically assisted injection coupled to capillary electrophoresis-mass spectrometry. Analyst 136:1562–1565
75. Palatzky P, Matysik FM (2011) Development of capillary-based SECM probes for the characterization of cell arrangements for electrochemically assisted injection. Electroanalysis 23:50–54
76. Palatzky P, Matysik FM (2012) Development and characterization of a novel semiautomated arrangement for electrochemically assisted injection in combination with capillary electrophoresis time-of-flight mass spectrometry. Electrophoresis 33:2689–2694
77. Palatzky P, Zöpfl A, Hirsch T, Matysik FM (2013) Electrochemically assisted injection in combination with capillary electrophoresis-mass spectrometry (EAI-CE-MS) – mechanistic and quantitative studies of the reduction of 4-nitrotoluene at various carbon-based screen-printed electrodes. Electroanalysis 25:117–122

Index